MICHIGAN STATE UNIVERSITY LIBRARIES
3 1293 01420 3354

THESIS
3
(1996)

This is to certify that the

dissertation entitled

DYNAMIC ANALYSIS OF MULTI-LAYERED PAVEMENT SYSTEMS UNDER MOVING ARBITRARY LOADS

presented by

Kyong Ku Yun

has been accepted towards fulfillment of the requirements for

Ph.D. degree in Civil Engineering

Major professor

Date 11/13/95

MSU is an Affirmative Action/Equal Opportunity Institution

O-12771

LIBRARY
Michigan State
University

PLACE IN RETURN BOX to remove this checkout from your record.
TO AVOID FINES return on or before date due.

DATE DUE	DATE DUE	DATE DUE

MSU Is An Affirmative Action/Equal Opportunity Institution
c:\circ\datedue.pm3-p.1

DYNAMIC ANALYSIS OF MULTI-LAYERED PAVEMENT SYSTEMS UNDER MOVING ARBITRARY LOADS

By

Kyong Ku Yun

A DISSERTATION

Submitted to
Michigan State University
in partial fulfillment of the requirements
for the degree of

DOCTOR OF PHILOSOPHY

Department of Civil and Environmental Engineering

1995

ABSTRACT

DYNAMIC ANALYSIS OF MULTI-LAYERED PAVEMENT SYSTEMS UNDER MOVING ARBITRARY LOADS

By

Kyong Ku Yun

A new solution for the dynamic analysis of multi-layered asphalt concrete pavement systems under moving arbitrary loads has been developed. The method builds on an existing model for stationary loads, SAPSI, which uses the complex response method of transient analysis with a continuum solution in the horizontal direction and a finite-element solution in the vertical direction. The structural model is a n-layered damped-elastic medium. The subgrade can be modeled as either a rigid base or a semi-infinite halfspace. The loads are surface circular loads which may be constant in magnitude or may vibrate as an arbitrary time function, and the analysis is under axisymmetric conditions. The moving loads are modeled as a series of pulses with a duration equal to the time required for the wheel to pass by a fixed point in the pavement.

The proposed method of analysis in the new version of the program, SAPSI-M, is an improvement over the existing methods because: (1) it treats moving arbitrary loads on a n-layered damped-elastic system; (2) it incorporates such important factors as wave propagation, inertia and damping effects of the medium as well as frequency-dependent

asphalt concrete properties; (3) it can handle any load configurations, thus making it possible to model multiple wheel configurations of truck axles and airplane landing gears.

The moving load solution of the developed program SAPSI-M has been validated with the PACCAR full-scale field truck tests, which was conducted on an instrumented asphalt concrete section on a test track at the PACCAR Technical Center in Mount Vernon, Washington. The transient analysis of the original SAPSI program has been validated using the PACCAR's results for Falling Weight Deflectometer (FWD) tests. Further, an approach based on energy dissipation and visco-elastic properties of an asphalt concrete pavement for predicting the fatigue life of asphalt concrete pavements has been presented using the moving load solution in SAPSI-M computer program. The effect of truck speed on the response of asphalt concrete pavements is significant, and the frequency-dependent properties of the asphalt are a major contributor to the speed effect. A simplified solution where the moving loads are assumed to be non-vibrating seems to be sufficient for accurately predicting the pavement response. Static analysis using statically back-calculated layer moduli seems to be sufficient in analyzing FWD field tests.

Dedicated to

the memory of my father

ACKNOWLEDGMENTS

I would like to express my sincere gratitude to Dr. Karim Chatti for providing the research topic to me, for his guidance, critique and discussion during this research project.

I also wish to thank Dr. Ronald Harichandran for being a Ph.D. committee member and my academic advisor in the M.S. program. Appreciation is extended to Dr. Gilbert Baladi and Dr. Harvey Davis for being on my Ph.D. guidance committee.

Financial support for this research was provided by the Great Lakes Center for Truck and Transit Research and the Research Excellence Fund of the State of Michigan. Their support is gratefully acknowledged.

An expression of immeasurable gratitude is given to my mother, parents-in-law, brother and sisters, brothers and sisters-in-law for their understanding, encouragement and support through the years of my studies.

Finally, but not least, I wish to express my sincere appreciation to my wife, Jung, for her continuous understanding, patience and love, and to my son, Byong-Wook, for having been a source of joy.

TABLE OF CONTENTS

LIST OF TABLES xi

LIST OF FIGURES xii

CHAPTER 1. INTRODUCTION 1

1.1 Problem Statement 1

1.2 Dynamics of Pavements 2

1.3 Research Objectives and Organization 3

1.3.1 Objectives 3

1.3.2 The Proposed Model 3

1.3.3 Organization 4

CHAPTER 2. LITERATURE REVIEW 8

2.1 Introduction 8

2.2 Closed-Form Solutions 9

2.2.1 Static Analysis 10

2.2.2 Dynamic Analysis 10

2.2.3 Moving Load Solutions 11

2.3 Numerical Solutions 13

2.3.1 Layer Theory 13

2.3.1.1 Static Analysis Models 14

2.3.1.2 Dynamic Analysis Models 16

2.3.2 Finite Element Method 19

2.4 Summary 21

CHAPTER 3. RESPONSE OF VISCO-ELASTIC MULTI-LAYERED SYSTEM TO STATIONARY DYNAMIC LOADS 23

3.1 Introduction 23

3.2 Equation of Motion 23

3.3 Multi-Layered Model 24

3.4 Simulation of Half Space 26

3.5 Complex Modulus Representation 29

3.6 Method of Analysis 33

3.6.1 Complex Response Method 33

3.6.2 Dynamic Analysis 33

3.7 Steady-State Solution 34

3.7.1 Introduction 34

3.7.2 Stiffness Matrix Approach 35

3.7.3 Layer Stiffness Matrix 38

3.7.4 Eigenvalue Problem 39

3.7.5 Green's Functions 41

3.7.6 Validation of Steady State Solution 46

3.8 Transient Solution 47

3.8.1 Introduction 47

3.8.2 Interpolation Scheme 48

3.8.3 Algorithm and Validation of Transient Analysis 50

3.9 SAPSI Computer Program 51

CHAPTER 4. DYNAMIC RESPONSE OF VISCO-ELASTIC MULTI-LAYERED SYSTEM TO MOVING ARBITRARY LOADS ... 54

4.1 Introduction 54

4.2 Assumptions 55

4.2.1 Material Properties 55

4.2.2 Geometry 56

4.2.3 Loads 57

4.3 Moving Load Representation 57

4.3.1 Response to Moving Loads 58
4.3.2 Response to Moving Constant Loads 62
4.3.3 Response to Moving Arbitrary Loads 64
4.4 SAPSI-M Computer Program 65
4.4.1 Program Layout 65
4.4.2 Algorithm 70
4.4.2.1 Steady-State Solution 70
4.4.2.2 Moving Load Solution 72
4.4.3 Uses and Limitations 75
4.4.3.1 Capabilities 75
4.4.3.2 Limitations 75

CHAPTER 5. FIELD VERIFICATION 77
5.1 Introduction 77
5.2 Previous Full-Scale Field Test Studies 77
5.2.1 Test Facilities 77
5.2.2 Previous Flexible Pavement Tests 78
5.3 Description of PACCAR Field Test 84
5.3.1 Test Section 84
5.3.2 Instrumentation 84
5.3.3 Test Procedure 86
5.3.4 Load Measurements 89
5.3.5 Strain Measurements 89
5.3.6 Correcting for the Effect of Lateral Offset 93
5.4 Material Characterization of Cores 94
5.4.1 Pavement Layer Characterization 94
5.4.2 Back-calculation of Layer Moduli 94
5.4.3 Frequency-dependent AC Properties 97
5.5 Verification of Moving Constant Load Solution 99
5.5.1 Modeling of the Moving Wheel Load 99
5.5.2 Modeling of Pavement Cores 99
5.5.3 Results of SAPSI-M Analysis 101

5.5.3.1 Typical Response Curves of Moving Constant Loads 101
5.5.3.2 The Effect of Frequency-Dependent AC Properties 104
5.5.3.3 Effect of Truck Speed 106
5.6 Verification of Moving Arbitrary Load Solution 109
5.6.1 Moving Arbitrary Load Time History 109
5.6.2 Typical Response Curves of Moving Arbitrary Loads 111
5.7 Verification of SAPSI Transient Analysis Using FWD Tests 114
5.7.1 Characteristics of FWD Field Data 114
5.7.1.1 Linearity of FWD Field Data 114
5.7.1.2 Isotropy of FWD Field Data 116
5.7.2 Static and Dynamic Predictions of Strains 116
5.7.2.1 October 1991 FWD Tests 119
5.7.2.2 June 1992 FWD Tests 119
5.7.2.3 February 1993 FWD Tests 125
5.8 Summary 126

CHAPTER 6. APPLICATION OF SAPSI-M PROGRAM TO PREDICTING FATIGUE DAMAGE 128

6.1 Introduction 128
6.2 Review of Fatigue Laws in Flexible Pavements 129
6.2.1 Prediction of Fatigue Life 129
6.2.2 Accelerated Performance Tests 130
6.2.3 Factors Affecting Fatigue Life 131
6.2.4 Existing Fatigue Models 133
6.3 Review of Energy-Based Fatigue Damage Models 136
6.3.1 Road Damage Prediction 136
6.3.2 Energy Concepts for Fatigue Damage 139
6.3.3 Previous Studies 141
6.3.4 Dissipated Energy versus Fatigue Life 144

6.4 Prediction of Pavement Fatigue Damage Using SAPSI-M Program 147
6.4.1 Calculation of Dissipated Energy in SAPSI-M 148
6.4.1.1 Derivation of Energy Dissipation in 1-D 148
6.4.1.2 Derivation of Energy Dissipation in 3-D 150
6.4.2 Strain, Dissipation Energy and Fatigue Life 152
6.4.3 The Effect of Speed on Energy Dissipation 156
6.4.4 Load Equivalency Factors from Energy Dissipation 157
6.5 Summary 165

CHAPTER 7. CONCLUSION 167
7.1 Summary and Conclusion 167
7.2 Recommendations for Future Research 171

LIST OF REFERENCES 172

APPENDIX A: PARAMETRIC STUDY 182

APPENDIX B: SAPSI-M USER GUIDE 199

LIST OF TABLES

TABLE 2.1 Computer Program used in Asphalt Pavement Analysis 22

TABLE 3.1 Comparison of Transient Analysis.....51

TABLE 5.1 Summary of Various Instrumented Flexible Pavement Tests 79

TABLE 5.2 Range of Experimental Conditions from Various Instrumented Flexible Pavement Tests.....83

TABLE 5.3 Effective Pavement Layer Thickness of Axial Cores 95

TABLE 5.4 Layer Properties for October 1991 FWD Testing.....96

TABLE 5.5 Layer Properties for February 1993 FWD Testing 96

TABLE 5.6 Comparison of Measured and Calculated Strains - October 1991 FWD Testing.....123

TABLE 5.7 Comparison of Measured and Calculated Strains - June 1992 FWD Testing 123

TABLE 5.8 Comparison of Measured and Calculated Strains - February 1993 FWD Testing.....124

TABLE 6.1 Estimated Fatigue Life of FHWA-ALF Section using Elastic Analysis 154

TABLE 6.2 Fatigue Life based on Dissipated Energy from Moving Load Solution ..155

TABLE 6.3 Observation of Speed Effect by Energy Dissipation.....156

TABLE 6.4 Load Equivalency Factor by Dissipated Energy 164

LIST OF FIGURES

FIGURE 1.1 Schematic View of the SAPSI-M Model 5

FIGURE 3.1 Orientation of Stress Components in Cylindrical Coordinate 25

FIGURE 3.2 Layer System Subjected to Uniform Circular Load 25

FIGURE 3.3 Simulation of Halfspace.....27

FIGURE 3.4 Representation of Stress and Strain for Linear Elastic Material 30

FIGURE 3.5 Representation of Stress and Strain for Linear Visco-Elastic Material 30

FIGURE 3.6 Boundary Condition at Layered Interfaces due to Rayleigh Wave.....37

FIGURE 3.7 Assembling of Submatrices of Each Layer.....37

FIGURE 3.8 Validation of Interpolation Scheme by Maple 52

FIGURE 4.1 Interpretation of Stationary Loading Condition.....59

FIGURE 4.2 Interpretation of Moving Load Condition.....60

FIGURE 4.3 Response Pulses at a Specific Location of AC Bottom as the Load Approach.....61

FIGURE 4.4 Discretized Moving Loads.....63

FIGURE 4.5 The Flow Chart of SAPSI-M Program 66

FIGURE 4.6 Algorithm for Steady-State Solution 71

FIGURE 4.7 Algorithm for Moving Load Solution.....73

FIGURE 5.1 Plane View of PACCAR Technical Center 85

FIGURE 5.2 Cross Section of the PACCAR Test Section 85

FIGURE 5.3 Instrumentation Layout of the PACCAR Pavement Test Track 87

FIGURE 5.4 The Peterbilt 359 Test Truck 88

FIGURE 5.5 Effect of Truck Speed on Axle Load 90

FIGURE 5.6 Effect of Pressure on Axle Load 91

FIGURE 5.7 Typical Time Histories of Measured Strain at the Bottom of AC Layer ... 92

FIGURE 5.8 Asphalt Concrete Properties Versus Frequency 98

FIGURE 5.9 SAPSI-M Model Used in the Analysis 100

FIGURE 5.10 Typical Response of Longitudinal Strain for Moving Constant Loads ... 102

FIGURE 5.11 Typical Response of Transverse Strain for Moving Constant Loads 103

FIGURE 5.12 Comparison of Calculated and Measured Strains at Different Speeds Core-1 105

FIGURE 5.13 Comparison of Calculated and Measured Strains at Different Speeds Core-3 107

FIGURE 5.14 Comparison of Calculated and Measured Strains at Different Speeds Core-4 108

FIGURE 5.15 Measured Wheel Loads 110

FIGURE 5.16 Comparison of Measured and Predicted Response Curves of Moving Arbitrary Dynamic Solution 112

FIGURE 5.17 Comparison of Measured and Predicted Curves of Moving Arbitrary Quasi-Dynamic Solution 113

FIGURE 5.18 Linearity of Strain Measurement in FWD Tests 115

FIGURE 5.19 Ratio of Transverse to Longitudinal Strains in FWD Tests 117

FIGURE 5.20 Actual and Simulated FWD Load Pulses 118

FIGURE 5.21 Comparison of Measured to Calculated Strains - Oct. 1991 FWD Tests 120

FIGURE 5.22 Comparison of Measured to Calculated Strains - June 1992 FWD Tests..... 121

FIGURE 5.23 Comparison of Measured to Calculated Strains - Feb. 1993 FWD Tests 122

FIGURE 6.1 Comparison of Fatigue Models at Various Test Methods.....137

FIGURE 6.2 Typical Stress-Strain Hysteresis Loop 140

FIGURE 6.3 Typical Curve of Dissipated Energy versus Number of Cycles.....142

FIGURE 6.4 In Situ FHWA-ALF Fatigue Test for Surface Cracking 154

FIGURE 6.5 Types of Axle Configuration for Load Equivalency Factor.....158

FIGURE 6.6 Stress-Strain Hysteresis Loop -Axle Type-1.....159

FIGURE 6.7 Stress-Strain Hysteresis Loop -Axle Type-3.....160

FIGURE 6.8 Stress-Strain Hysteresis Loop -Axle Type-4.....162

FIGURE 6.9 Stress-Strain Hysteresis Loop -Axle Type-7.....163

CHAPTER 1
INTRODUCTION

1.1 PROBLEM STATEMENT

Over the past thirty years, developments in both analysis techniques and material testing procedures have made it possible to better simulate the response of asphalt concrete pavements to traffic loads and environmental conditions. This has allowed the use of mechanistically based design methodologies in the form of design charts, computer solutions and catalogues of design. Numerous pavement response models have been generated since the early sixties, ranging from an infinite beam on a Winkler foundation to a multi-layered system over an infinite half space. Current analytically-based procedures, however, assume that the load is applied statically. In recent years, there have been some analyses which study the response of pavements to dynamic loads. Dynamic models vary in complexity according to the structure analyzed (finite or infinite beam/plate; elastic or damped-elastic Winkler foundation, or damped-elastic layers) and the loading (stationary, moving, constant, harmonic, random).

A number of methods have been used to account for the moving effect of the load. They range from using the Dirac function or the Kronecker delta operator to pre-multiplying the load by time dependent deflection shape functions (finite element analysis) or applying a pulse load with a duration equal to the time taken to travel one tire contact length.

There is only a small number of studies which have considered the validation of these models by comparison with field measurements. The agreement between experiment and theory has been qualitative and for low speed [40, 105] because of the difficulties in

measuring the response of roads accurately and the fluctuation of wheel loads, if they are not measured [40].

1.2 DYNAMICS OF PAVEMENTS

Most current models of pavement analysis assume static loads. However, peak dynamic vehicle loads may be considerably higher than static loads, and thus dynamic loading may have a considerable impact on pavement performance. The following is a list of reasons for considering dynamic methods of pavement analysis [18]:

(1) Traffic loads are inherently dynamic since they move over the pavement and vibrate.

(2) The pavement may respond "dynamically" if either inertial or viscous forces are significant.

(3) Propagation of waves induced by dynamic wheel loads from the pavement surface through the different pavement layers may significantly affect the response.

(4) Dynamic interactions between truck axles and the pavement surface could be significant.

(5) Materials may respond differently to static and dynamic stresses if the effect of rate or frequency of loading is important.

(6) Field observations may be strongly influenced by dynamic factors, as in the cases of strain gauge measurements, accelerometer readings, non-destructive testing, and weigh-in-motion measurements.

All of the above considerations lead to the conclusion that it may be necessary to use dynamic methods in analyzing pavement structures. Fluctuations in wheel loads due to axle vibrations may cause a significant increase in the damage incurred by pavements system. In order to quantify this effect, it is necessary to accurately predict the primary responses of pavements (stresses, strains and deflections) due to moving arbitrary loads.

1.3 RESEARCH OBJECTIVES AND ORGANIZATION

1.3.1 Objectives

The objectives of the research are as follows:

(1) To develop a model for the response of multi-layered system subjected to moving arbitrary dynamic loads applied on the surface.

(2) To develop an efficient computer program to evaluate the response of a general multi-layered system over a half space excited by dynamic surface loads.

(3) To verify the model and the corresponding computer code against full-scale field truck tests.

(4) To verify the stationary transient analysis against FWD (Falling Weight Deflectometer) tests.

(5) To investigate possible applications of fatigue damage models for asphalt concrete pavements.

1.3.2 The Proposed Model

The proposed model and the related computer program SAPSI-M allows for a realistic dynamic analysis of general multi-layered system. The following is a list of its capabilities:

(1) Considers dynamic loads.

(2) Simulates multiple surface moving arbitrary loads.

(3) Uses of linear visco-elastic theory.

(4) Analyzes a multi-layered system.

(5) Obtains a continuum solution in the horizontal direction.

(6) Obtains a finite element solution in the vertical direction.

The proposed method of analysis in the new version of the program, SAPSI-M, is an improvement over the existing methods because: (1) it treats moving fluctuating loads on a n-layered damped-elastic system; (2) it incorporates such important factors as wave

propagation, inertia and damping effects of the medium as well as frequency-dependent asphalt concrete properties; (3) it can handle any load configuration, thus making it possible to model multiple wheel configurations of truck axles and airplane landing gears.

When modeling a moving wheel load as a stationary haversine pulse with a duration equal to the time it takes the wheel to roll over a fixed point in the pavement, the pressure exerted by the tire is applied only when the tire is in direct contact with the point. This means that the effect from the wheel load as it approaches (and leaves) the response point is not accounted for. In reality, the moving wheel load sends stress waves as it approaches the fixed point, and theses waves (in the form of body and surface waves) propagate so that the effect of the load is felt by the fixed point in the pavement before and after the load is directly on top of it. These waves could be a combination of direct waves from the moving load and reflected waves from a layer boundary below the surface such that the net pavement response may be amplified or de-amplified, depending on radiation damping, relative to the stationary response. Thus, in general, a moving load cannot be modeled by a stationary transient haversine pulse. The SAPSI-M computer program computes the response of the multi-layered asphalt concrete pavement to moving transient loads. Figure 1.1 shows the schematic view of the proposed model.

1.3.3 Organization

An introduction with the objective of this research is presented in Chapter 1. After reviewing the related literature and discussing the existing methods of analyses, the remaining chapters of this dissertation describe in detail the theoretical formulations, implementation, field verifications and applications.

In chapter 2, the review of relevant literature on closed-form and numerical solutions for the analysis of asphalt concrete pavements is presented. The currently available

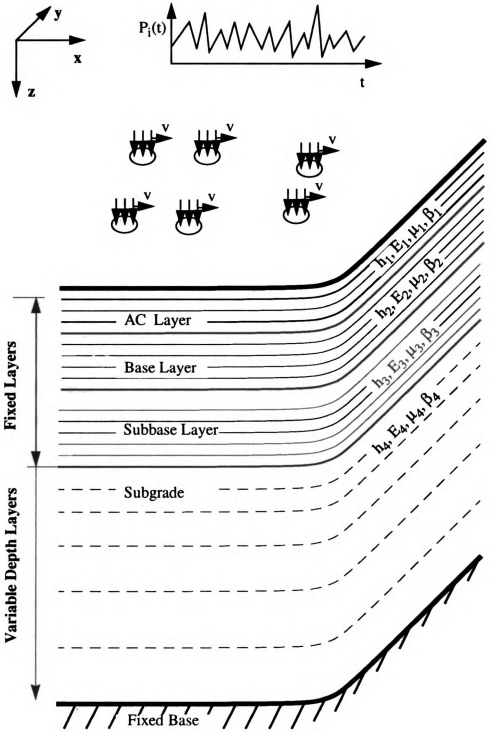

FIGURE 1.1 Schematic View of the SAPSI-M Model

closed-form solutions are mostly static and based on an elastic multi-layer system. Most of the numerical solutions involve the static analysis of a beam or plate supported by a Winkler foundation or a layered structure supported by a half-space based on the finite method or layer theory, respectively. However, no analysis was found in the literature for the dynamic response of a realistic layered pavement system to moving steady or random forces.

In chapter 3, the theoretical back ground for calculating the response of a visco-elastic multi-layered system subjected to stationary loads is presented. It is developed for the axisymmetric coordinate system, and is based on the linear visco-elastic layer theory in the horizontal direction and the finite element method in the vertical direction. The model consists of subdividing the natural layers within the pavement profile into sublayers supported by a rigid base or a half-space.

In chapter 4, a new method for the analysis of multi-layered pavement systems subjected to moving loads is presented. Assumptions for the new proposed model are listed, and the moving load representation is described. Then, the response to moving constant and arbitrary loads is presented in detail. Finally, the implementation of the proposed method is described by presenting the layout and algorithm of the SAPSI-M computer program.

In chapter 5, the validation of SAPSI-M computer program against full-scale field data is presented. First, the PACCAR field test program is described including instrumentation, measurements and material characterization. Then, the validation of SAPSI-M is presented for both the moving constant and arbitrary load solutions. The verification of SAPSI transient analysis is also presented with a Falling Weight Deflectometer (FWD) tests.

In chapter 6, the application of SAPSI-M program into the prediction of pavement fatigue damage using the dissipated energy concept is described. The comparison of fatigue lives from the conventional fatigue damage law using peak strain only and from the dissipated energy law using the entire time history of the response due to moving loads is made. This chapter also includes a section on the development of load equivalency factors using the dissipated energy approach.

In chapter 7, the results of the research are summarized and a number of conclusion are put forward. Finally, some recommendations for future work are suggested.

CHAPTER 2

LITERATURE REVIEW

2.1 INTRODUCTION

An asphalt pavement may consist of a thin covering surface course over a base course, subbase course, and compacted roadbed soil. Thus, the term pavement herein implies all the layers in the pavement structures. The load carrying capacity of a flexible pavement is brought about by the load distribution characteristics of the layered system. The highest quality layer is placed at or near the surface. Hence, the strength of the pavement is the result of building up thick layers and, thereby, distributing the load over the relative weak road bed soil [124].

The design and analysis of the pavement system have been approached from two main different points of view: Empirical and mechanistic. Initially, design engineers have approached the problem from the empirical method. As theory, researchers started analyzing the problem using mechanistic concepts.

Empirical procedures in pavement design greatly rely the past experience and laboratory or field tests. Empirical relationships have also been used to assess the structural capacity of pavements and to predict pavement strength from simple field tests. Empirical and semi-empirical procedures can be advantageous because they are usually simple and are derived from actual field data. On the other hand, the disadvantage of the empirical approach is that it can be applied only to a given set of environmental, material, and loading conditions. If these conditions are changed, the design is no longer valued and a new method should be developed through a new trial to account for a new set of conditions. AASHTO, NSA (National Stone Association), and Califonia Design methods may be the most popular empirical design methods for flexible pavements.

Mechanistic flexible pavement design procedures are typically based on the assumption that a pavement can be modeled as a multi-layered elastic or visco-elastic structure on an elastic or visco-elastic foundation. Assuming that pavements can be modeled in this manner, it is possible to calculate stresses, strains, or deflections due to traffic loading and environmental conditions at any point in the structure. An important advantage of this design method is the ability to analyze a pavement for several different distress modes such as cracking and permanent deformation. This allows the engineer to adjust the pavement design and produce a cost-effective pavement section that does not fail prematurely. The main disadvantage of this design method is that it requires more comprehensive and sophisticated data than empirical design methods. Extensive laboratory and field testing may be required to determine the design parameters such as the resilient modulus, creep compliance, and others.

During the past few decades, a significant improvement in the area of pavement design and analysis has been established using theoretical mechanics. The development of theoretical methods, especially the layer theory and its numerical development, are reviewed and discussed in the subsequent sections.

2.2 CLOSED-FORM SOLUTIONS

Civil engineers have traditionary considered the structures of road surface to behave as continua, and have used the methods of continuum mechanics. The first such analysis was performed in 1926 by Westergaard who modeled a rigid pavement as a elastic plate supported by a Winkler foundation [120]. In the 1940's the theory of elastic layered systems was published by Burmister [12], which established the analysis of system with a 2 or 3 layers of infinite extent and accounted for the effects of the interface conditions between layers.

2.2.1 Static Analysis

The currently available closed-form solutions mostly use static analysis and are based on an elastic multi-layer system.

Burmister [12] developed the first general equations and solution to obtain deflections and stresses in two and three-layer systems based on the theory of elasticity. The solution assumed a uniform vertical static load distributed over a circular area and each layer is continuous in the lateral direction. Burmister obtained his solution by assuming a stress function involving Bessel functions and the exponential. Comprehensive tables and charts of influence values for two and three-layer systems subjected to uniform circular loading were produced [13]. To use these solutions easily, he developed charts for practical pavement design applications.

The application of the theory of elasticity in the design and analysis of flexible pavements raises some questions such as whether a flexible pavement is an elastic body and Hooke's law is in fact satisfied. Considerable research and theoretical studies have been done on this point by several authors who considered the effects of visco-elasticity or non-linearity.

2.2.2 Dynamic Analysis

The inertia effect in pavement analysis has been modeled using single and multi-degree of freedom systems. When a dynamic load is applied at the surface of a homogeneous half-space, three main types of waves are formed; primary (compression), secondary (shear), and surface (Rayleigh) waves. Waves result in three-dimensional states of stress, strain, and deflection at various points in the half space.

Kausel and Peek [56] presented an explicit and closed-form solution for the Green's functions (displacements due to unit loads) corresponding to dynamic loads acting on layered system. These functions embody all the essential mechanical properties of the medium and can be used to derive solutions to problems of elasto-dynamics, such as scattering of waves by rigid inclusions, soil-structure interaction, seismic sources, etc. The solution is based on a discretization of the medium in the vertical direction.

One method of dynamic analysis is based on Fourier transformation. To simplify the analysis, a transient mode of loading can be represented by a series of harmonic loads with different frequencies and magnitudes using Fourier transformation. Once the response to steady-state loading is obtained as a function of frequency and magnitude, the response to a transient load in the time domain can be obtained through the inverse Fourier transform. The governing equation for steady-state elastodynamics is the Helmholtz equation [45].

2.2.3 Moving Load Solutions

The moving problem was investigated by Cole and Huth [25] for the special case of a vertical line load moving at constant velocity over the surface of a uniform elastic half space. They found that the major effect of load movement is an increase in the maximum stresses that occur in the pavement. Unfortunately, the above result is not directly applicable to pavement structures, which behave like layered systems.

Pister and Westmann [81] modeled an asphalt pavement as a visco-elastic beam, infinite in extent, supported on a Winkler foundation subjected to a concentrated moving load at constant velocity. The solution, which was written as the product of a number of constants and a dimensionless coefficient dependent upon the space and the time variables, was obtained with the initial and boundary conditions through the use of iterated

Laplace and Fourier transform. They observed the deflection and curvature occurring directly under the moving load for different velocities and relaxation time. They concluded that the relaxation time of the material is quite important. The lower relaxation times tend to extend the viscous behavior of the beam over a larger range of velocities as compared to higher relaxation times. For lower velocities, the visco-elastic effects are more important so there is a considerable difference obtained by elastic and visco-elastic analysis.

The computer program MOVE was developed by Chen [21], for dynamic analysis of a linear elastic layered system resting on a rigid base subjected to a vertical line load that moves with a constant velocity over the surface of the system. In MOVE, the wave equation of displacement potentials is converted to an equivalent Laplace's equation by the Galilean transformation. The general solution of the equivalent Laplace's equation is then solved by specifying appropriate boundary conditions and transforming the load into a Fourier integral. It should be noted that both Cole and Huth [25] and MOVE [21] solutions assume elastic properties of materials. Therefore, the response increases with an increase in velocity. Under actual field conditions, internal damping in the materials as well as radiation damping in the structure will cause the response to decrease as the velocity of the load is increased [18].

Fryba [34] solved the problem of an infinite beam on an elastic foundation subjected to a constant force moving at constant speed. He calculated the covariance of the response of a beam on a Winkler foundation that had statically varying stiffness to a statically stationary force moving along it at constant velocity. However, Fryba did not extend the model to two or three dimensional problems.

Cebon [14] presented a numerical convolution method of the applied loads with a field of road surface impulse response functions, for calculating the time domain response

of an infinite beam on a damped Winkler foundation subjected to moving random loads. The impulse response can be calculated for an idealized road response model, or determined by field measurements subjected to an impulse. He also validated his model by comparing theoretical results with fields measurements.The model, however, is restricted to two-dimensional models.

Chatti [17] extended an existing solution for a moving harmonic load on a finite beam resting on an elastic Winkler foundation, published by Boquenet [11]. The improved solution allows for a load of arbitrary time history through the use of complex number representation and the Fast Fourier Transform algorithm, and accounts for energy dissipation through the foundation.

2.3 NUMERICAL SOLUTIONS

The currently available methods of pavement analysis are mostly based on static analysis and may be subdivided into two main groups: Layer theory based on continuum mechanics and the finite-element method. A few analytical methods for solving dynamic problems in pavements are now available.

2.3.1 Layer Theory

Flexible pavements are layered system with better materials on top and cannot be represented by a homogeneous mass, thus the use of Burmister's layered theory is more appropriate [49]. The basic assumptions for layer theory to be satisfied are:

(1) Each layer is homogeneous, isotropic and elastic or visco-elastic.

(2) Each layer is infinite in the horizontal direction.

(3) Each layer has a finite thickness, but the lowest layer is a half-space having infinite thickness.

(4) Continuity conditions are satisfied at the layer interface, as indicated by the same vertical stress, shear stress, vertical displacement, and radial displacement. For a frictionless interface, the continuity of shear stress and radial displacement is replaced by zero shear stress at each side of the interface.

The use of a layer theory in modeling pavements has been quite extensive and many presently available design methods for flexible pavements are based on this theory. These models are based upon the assumption of linear elastic or visco-elastic material properties. A brief literature review on the numerical solution with layer theory will be made in the following sections.

2.3.1.1 Static Analysis Models

Elastic layer theory has been used successfully for the analysis of flexible pavements since the 1940's, when it was introduced by Burmister [12]. Initially, the use of the method was restricted to systems with two or three layers that extend to infinity in the horizontal directions [13]. More recently, a number of computer models have been developed to handle more layers [6, 30, 57]. Surprisingly, there is only a small number of studies which have considered the validation of these models by comparison with field measurements.

The elastic multi-layer system solution and some of its modified versions such as CHEV [117] and ELSYM5 [6] have been extensively used in the area of pavement evaluation. The program CHEV can be applied only to linear elastic materials but was modified by the Asphalt Institute in the DAMA program to account for nonlinear elastic granular materials [52]. ELSYM5 was originally developed at the University of California, Berkeley, for analyzing five-layer systems under multiple wheel loads [6]. The response of the multi-layer pavement system to uniform circular loading was analyzed by Michelow [69]. The model characterized the pavement as a semi-infinite solid with n-layers with their

elastic characteristics being different from one layer to another. Another well known program is BISAR [30], developed by the Shell company, which considers both vertical loads and horizontal loads. Based on the nonlinear theory, Finn et al. [33] developed a computer program named PDMAP (Probabilistic Distress Model for Asphalt Pavements) for predicting the fatigue cracking and rutting in asphalt concrete pavements.

The VESYS II computer program was developed at the Massachusetts Institute of Technology by Soussou [103] in 1973. The program models a three layer system; the upper two layers have finite thicknesses over one infinite layer. All Layers have infinite dimension in the horizontal direction and have visco-elastic properties. The VESYS model consists of a primary response model, a damage model, and a serviceability model. A closed-form probability solution of the response of the layered system to an axisymmetric stationary load applied at the surface is obtained. The probabilistic estimates of stress, strain and deflection, the loading characteristics, and the temperature history are used as inputs to the damage model to obtain the extent of cracking. The distress indicators obtained from the damage model are combined using the AASHTO equation to provide a subjective measure of the present serviceability index (PSI).

The computer program, KENLAYER, was developed by Huang [49], based on Burmister's layer theory. It solves the response for a elastic multi-layered system under stationary single or multiple circular loads. The AC layer can be treated as linear elastic or visco-elastic. The moduli vary in the vertical direction but remain constant along the horizontal plane for each sublayer. The base and the subgrade can be divided into several sublayers and the stress-dependent moduli can be estimated for each sublayer through an iterative procedure.

Both the linear and non-linear visco-elastic material properties have been modeled in an effort to recognize the time-dependent response of the asphaltic materials. The use of

non-linear visco-elastic theory has been very limited because of the complexity of material characterization. The validity of using a linear visco-elastic analysis to evaluate the pavement response was thoroughly studied by Nair et al. [77]. Their investigation consisted of performing laboratory tests on paving materials to determine the degree of linearity in the response function. The study concluded that linear visco-elastic theory can be acceptably used in pavement evaluation analysis; in order to reduce the influence of stress level, stress state, anisotropy and other effects to a level that will make linear isotropic visco-elasticity an acceptable characterization of asphalt concrete, a limit must be placed on the strain level that can occur in the asphalt concrete.

2.3.1.2 Dynamic Analysis Models

Loading from a truck consists of a set of moving, time-varying surface stresses. These stresses represent the static load carried by each wheel as well as the dynamic fluctuations generated by the roughness of the pavement surface profile. A number of truck simulation models for predicting dynamic wheel loads have been developed by several research organizations, including MIT [44], UMTRI [31] and the University of Cambridge [14]. These models are planar, with pitch (rotation along the longitudinal direction of the truck) being the only form of rotation allowed. Key factors affecting the accuracy of these models include the proper modeling of non-linear properties of the suspension springs, kinematics of tandem axles and the sequential input of the road profile into the different axles [34]. Truck simulation models have by-in-large been validated by comparison with full-scale tests [30].

Many dynamic models have been developed for the analysis of pavements and can be largely classified into two main categories as follows [14]:

(1) A beam or plate supported by massless springs (Winkler foundation) [11, 14, 17, 34, 42, 51, 59, 60, 125] or supported by a half-space [3, 17]. The foundation may be modified to include inertial effects [48, 96].

(2) A layered structure of elastic or visco-elastic solids [21, 34, 54, 97, 126].

Harr [42] presented a simple model for the dynamic response of a pavement subjected to a rectangular uniform pulse of duration t_1 seconds required for the passage of the vehicle. His model consists of a mass, spring and damping to consider the inertia, elastic deformation and time-dependent deformation of the pavement, respectively. By suitable selection of model parameters, he was able to achieve close results with the AASHTO road test [1].

Moavenzadeh and Elliott [72] presented a solution technique for the investigation of the stresses and displacements induced in a three layer visco-elastic system subjected to uniformly distributed normal loads. A steady localized load is made to move at a constant velocity in a straight line on the initially flat surface of a three layer system. They investigated the response of the system to a load that is repeatedly applied to the same region on the surface at a specified frequency. Actually, they extended Burmister's elastic solution to visco-elastic material and a moving load by using the Heaviside step function and Duhamel superposition/integral, respectively.

Chen [21] developed the SAPSI computer program in 1987. SAPSI is a PC-based FORTRAN computer program which calculates the dynamic response of a n-layered visco-elastic system to multiple surface loads. Material properties for each layer may be varied with frequency. Chen verified the program against analytical solutions [21], and Tabatabaie validated it by comparison with field measurements [105].

Sebaaly [91] modified a computer program DYNAMIC which was developed by Kausel [56] to compute stresses and strains in addition to displacements due to both har-

monic and impulse loadings using the Fourier transform. Peak theoretical vertical pavement deflections were validated by comparison with field data from the AASHTO road test. He could not, however, validate the speed effect on strain under a moving load because he simulated the response of the road to a falling weight rather than to a moving load.

Zafir et al. [127] developed a computer program DYNPAVE to evaluate dynamic pavement strains under moving traffic load based on a continuum-based finite-layer approach. The model is based on a modified plane-strain model, in which three-dimensional effects are taken into account by using two special viscous boundaries (front and back) connected to the two-dimensional plane-strain model. The dynamic material properties of the asphalt concrete layer can be varied as a function of the loading frequency. They concluded that the pavement strains are strongly functions of the pavement thickness and the vehicle speed, and they reduce substantially with the increase in the speed of the vehicle. Also, a substantial compressive strain component is present at the bottom of AC layer that may be important for any realistic fatigue life estimation of the pavement.

A new numerical method was introduced by Hanazato et al. [38] to analyze moving traffic-induced ground vibrations three-dimensionally on the basis of a dynamic elastic finite element method. Moving load is expressed to be composed of a constant static component and dynamic component, which is expanded into the Fourier series as the sum of harmonic motions. This is a new prismatic model combining the finite element method and visco-elastic layer theory. The finite element formulation is used to model an irregular region which includes the pavement structure and the soils underneath it. The visco-elastic layer theory is used to model the far-field region via semi-infinite thin-layered elements. The two regions are joined by energy-transmitting boundaries. This model applies only to

continuous flexible pavements because of its prismatic nature and its inability to handle discontinuity.

2.3.2 Finite Element Method

The finite element method has also been used extensively and is particularly useful for analysis of jointed rigid pavements which is not continuous in the horizontal direction and can be prone to be thermal warping as well as being subjected to vehicle loads. Almost all of the models assume linear material properties, although some of model include visco-elastic effects [9, 53, 121]. The finite element method in pavement analysis offers the capability of modeling joints in rigid pavements and incorporates the effect of slab dimensions on the rigid pavement response. The pavement is represented by a grid of small elements where the layers need not be infinite in the lateral direction. The method provides solutions for stresses, strains and deformations based on numerical evaluations which makes its accuracy very much dependent on the fineness of the initial grid and the means of conducting computations.

Three kinds of finite element models may be used in the analysis of flexible pavements: Two-dimensional plane strain, three-dimensional and axisymmetric models. Using the two-dimensional plane strain model of the pavement cross section, the wheel loading would have to be considered as a line loading, infinitely long in the longitudinal direction. This would be unrealistic because of the truck's configuration and loading condition.The most comprehensive approach would be one that uses three-dimensional finite element analysis. In a three dimensional model, suitable boundary conditions must be considered at some reasonable distance away from the loaded region in all three directions. The most commonly used two-dimensional model is the axisymmetric one. This model assume that the pavement geometry and loading are both axisymmetric. With these assumptions, a three dimensional problem can be reduced to a two-dimensional problem. However, the

asphalt surface must be assumed to be infinitely wide and therefore the edge effect cannot be considered. Non-axisymmetric multiple loads can be analyzed by superposition for linear elastic or visco-elastic materials.

Duncan et al. [31] first applied the finite element method in 1968 for the analysis of flexible pavements. The method was later incorporated in the ILLI-PAVE computer program by Raad and Figueroa in 1980 [83], which included a non-linear finite element program to analyze the pavement system. Raad and Figueroa used the Mohr-Coulomb failure criterion to modify the stress calculated using a finite element method at the end of each iteration.

Harichandran et al. [41] developed in 1989 a non-linear finite element program called MICH-PAVE for use on a personal computer to analyze flexible pavements. The program computes the primary responses within the pavement system subjected to a single circular wheel load. Useful design information such as fatigue life and rut depth are also estimated through empirical equations. In the MICH-PAVE program, the pavement is represented by an axisymmetric finite element model, and the resilient modulus model together with the Mohr-Coulomb failure criterion is used to characterize the non-linear material response of granular and cohesive soils.

Chatti [17] developed the DYNA-SLAB computer program in 1992, which calculates the dynamic response of a concrete slab system to moving fluctuating loads using the finite-element method of analysis. The underlying soils can be modeled either as a damped Winkler foundation or as a layered visco-elastic system. Chatti validated the model by comparison with theoretical results as well as field measurements.

2.4 SUMMARY

In this chapter, the review of relevant literature on closed-form and numerical solutions for the analysis of asphalt concrete pavements is presented. The currently available closed-form solutions are mostly static and use an elastic multi-layered system based on Burmister's solution [12]. Considerable research in theoretical studies have been done by several authors using visco-elasticity or non-linearity. Most numerical solutions are for the static analysis of a beam or plate supported by Winkler foundation or a layered structure. A few moving load solutions were presented, ranging from a beam on a damped Winkler foundation to a simplified plane strain layered visco-elastic system. The finite element method has also been used extensively and is particularly useful for analysis of jointed rigid pavements which is not continuous in the horizontal direction. The pavement system is represented by a grid of small elements where the layers need not be infinite in the lateral direction. Because of the numerical nature of discretization systems, the accuracy is greatly dependent on the fineness of the initial grid and the means of conducting computations.

Hardy and Cebon [40] pointed out that no analysis was found in the literature of the dynamic response of a realistic layered road model to moving steady or random forces and that very few pavement response models have been validated by comparison with field measurements. Table 2.1 lists some of the available computer programs applicable to flexible pavement analysis, and briefly describes their source, availability and theory.

TABLE 2.1 Computer Program used in Asphalt Pavement Analysis

Name	Source [Reference]	Year	Loads	Theory
CHEV	Chevron Company [117]	1963	Static	Elastic layer theory
ELSYM5	U.C. Berkeley [6]	1972	Static	Elastic layer theory
BISAR	Shell Company [30]	1973	Static	Elastic layer theory
VESYS II	M.I.T. [103]	1973	Static	Visco-elastic layer theory
DAMA	Asphalt Institute [52]	1979	Static	Nonlinear elastic layer theory
ILLI-PAVE	U. of Illinois [83]	1980	Static	Linear FEM
VESYS3A	FHWA		Static	Linear Visco-elastic
PDMAP	U.C. Berkeley	1986	Static, probabilistic	Elastic layer theory
DYNAMIC	Arizonan State U. [91]	1987	Stationary Dynamic	Visco-elastic layer theory
SAPSI	U.C. Berkeley [21]	1987	Dynamic	Visco-elastic layer theory
MICH-PAVE	Michigan State U. [41]	1989	Static	Nonlinear FEM
KENLAYER	U. of Kentucky [49]	1993	Static	Visco-elastic layer theory
DYNPAVE	U. of Nevada, Reno [127]	1994	Moving DynamicLoads	Plane strain, layer theory
SAPSI-M	Current study		Moving Dynamic Loads	Axisymmetric, layer theory

CHAPTER 3

RESPONSE OF VISCO-ELASTIC MULTI-LAYERED SYSTEM TO STATIONARY DYNAMIC LOADS

3.1 INTRODUCTION

Chen [21] developed a computer program, termed SAPSI, which can be used to calculate the response of visco-elastic multi-layered systems subjected to multiple circular surface loads. Material properties for each layer may be varied with frequency. SAPSI was developed for the axisymmetric case, which enables the reduction of three-dimensional problems to two-dimensions. The analysis in SAPSI is based on the theory of linear visco-elastic layer theory in the horizontal direction and the finite element method in the vertical direction. The theoretical background for the solution in SAPSI is described in the following sections.

3.2 EQUATION OF MOTION

The equilibrium conditions for an infinitesimal element together with the strain-displacement relations and the stress-strain relations yield to the equation of motion in terms of the displacements. Using the axisymmetric coordinate system, the governing differential equation of motion for the homogeneous case becomes as follows [61]:

$$
\begin{aligned}
&(\lambda + 2G)\left(\frac{\partial^2 u_r}{\partial r^2} + \frac{1}{r}\frac{\partial u_r}{\partial r} - \frac{u_r}{r^2} + \frac{\partial^2 u_z}{\partial z \partial r}\right) + G\left(\frac{\partial^2 u_r}{\partial z^2} - \frac{\partial^2 u_z}{\partial z \partial r}\right) = \rho\left(\frac{\partial^2 u_r}{\partial t^2}\right) \\
&(\lambda + 2G)\left(\frac{\partial^2 u_r}{\partial z \partial r} + \frac{1}{r}\frac{\partial u_r}{\partial z} + \frac{\partial^2 u_z}{\partial z^2}\right) + G\left(\frac{\partial^2 u_z}{\partial r^2} + \frac{1}{r}\frac{\partial u_r}{\partial r} - \frac{\partial^2 u_r}{\partial z \partial r} - \frac{1}{r}\frac{\partial u_r}{\partial z}\right) = \rho\left(\frac{\partial^2 u_z}{\partial t^2}\right)
\end{aligned}
\qquad (3\text{-}1)
$$

where, u_r and u_z are the displacements in the horizontal and vertical directions, respectively, ρ is the mass density, and λ and G are Lame's constants.

The strain-displacement relations for an axisymmetric loading are derived from the theory of elasticity as:

$$\begin{aligned} \varepsilon_r &= \frac{\partial u_r}{\partial r} \\ \varepsilon_\theta &= \frac{u_r}{r} \\ \varepsilon_z &= \frac{\partial u_z}{\partial z} \\ \gamma_{rz} &= \frac{\partial u_r}{\partial z} + \frac{\partial u_z}{\partial r} \end{aligned} \tag{3-2}$$

The stress-displacement relationships can be expressed by:

$$\begin{aligned} \sigma_r &= (\lambda + 2G)\frac{\partial u_r}{\partial r} + \lambda\left(\frac{\partial u_z}{\partial z} + \frac{u_r}{r}\right) \\ \sigma_\theta &= (\lambda + 2G)\frac{u_r}{r} + \lambda\left(\frac{\partial u_r}{\partial r} + \frac{\partial u_z}{\partial z}\right) \\ \sigma_z &= (\lambda + 2G)\frac{u_z}{z} + \lambda\left(\frac{\partial u_r}{\partial r} + \frac{u_r}{r}\right) \\ \tau_{rz} &= G\left(\frac{\partial u_r}{\partial z} + \frac{\partial u_z}{\partial r}\right) \end{aligned} \tag{3-3}$$

where, ε_r, ε_θ and ε_z are the radial, tangential and vertical strains, respectively, and γ_{rz} and τ_{rz} are the shear strain and shear stress as defined in Figure 3.1.

3.3 MULTI-LAYERED MODEL

The model consists of subdividing the natural layers within the pavement profile into thin sublayers which are assumed to extend to infinity in the horizontal direction as depicted in Figure 3.2. The axisymmetric condition enables the reduction of the three-dimensional problem into a two-dimensional one. The displacements within each sublayer are assumed to vary linearly in the vertical direction; however in the horizontal direction,

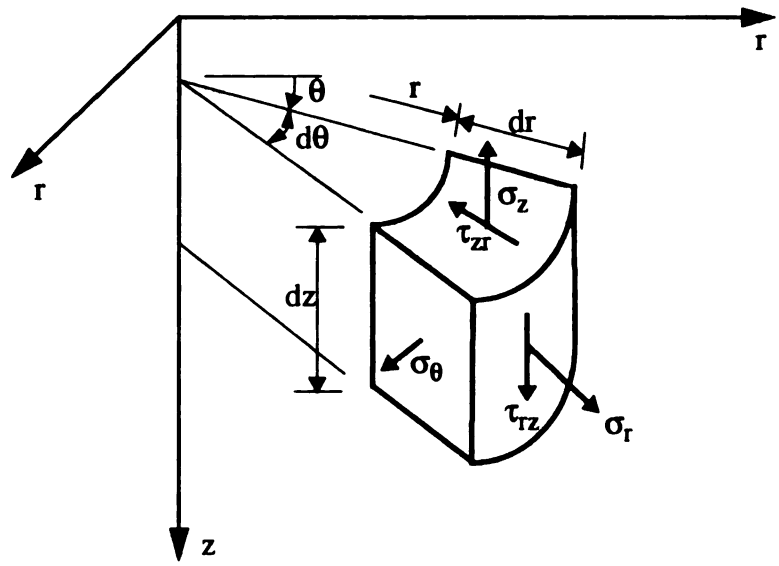

FIGURE 3.1 Orientation of Stress Components in Cylindrical Coordinate

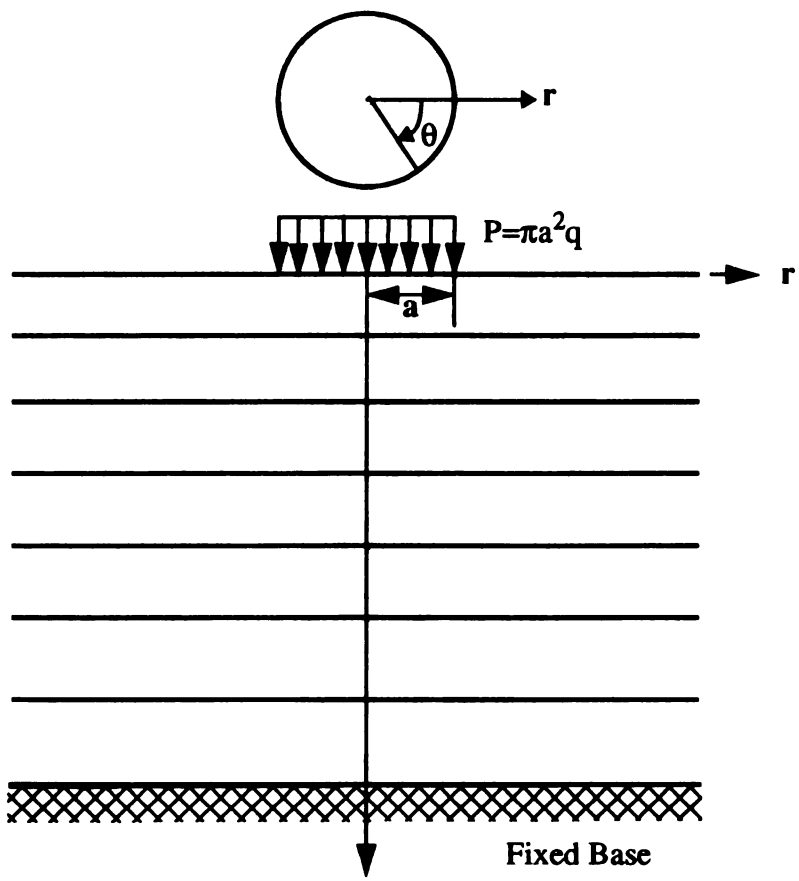

FIGURE 3.2 Layer System Subjected to Uniform Circular Load

the displacements are required to satisfy the pertinent ordinary differential equations which are obtained from Equation (3-1) by discretizing the medium into finite layers.

With the above discretization, the free motion at a given frequency consists of a finite number of wave modes which are obtained by solving an algebraic eigenvalue problem. These wave modes are used as shape functions to expand the displacements in the layered medium in terms of mode participation factors. Given the displacement field, the strains for each layer are determined by differentiation. The stresses in each layer are obtained assuming linear visco-elasticity. Finally, the layer effective stiffness matrix is obtained using the principle of virtual work, and the contributions from the individual layers are assembled to form the global stiffness matrix. The dynamic stiffness matrix is complex, symmetric and frequency-dependent [21].

3.4 SIMULATION OF HALF SPACE

The approach described above was originally developed for a layered system resting on a rigid base. In many practical cases the site is a layered system which extended to such great depth that it becomes necessary to introduce an artificial rigid boundary at some depth. This boundary will reflect some energy back into the system and will cause the site to have some erroneous natural frequencies which will affect the overall response. This becomes especially critical for sites with low material damping. To remedy this problem, the simulation of a semi-infinite halfspace was introduced by the Variable Depth Method which was developed by Chen [20].

The Variable Depth Method is used to simulate a site which is composed of soft materials extending to a great depth. Figure 3.3 shows the schematic view for simulating a halfspace [90]. According to this method, the layered system is extended by n additional layers having properties equal to those of the half space. At each frequency, the total depth

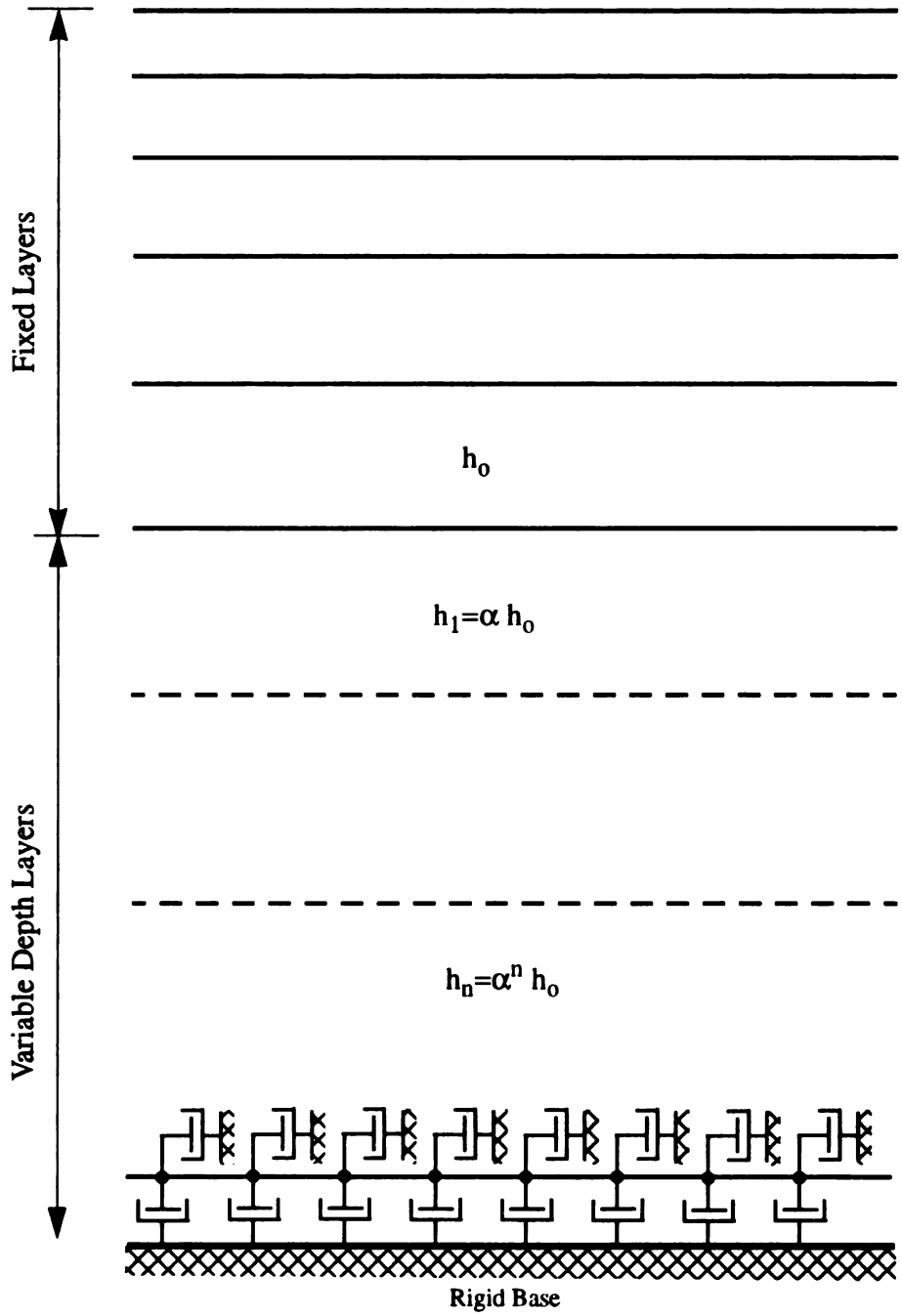

FIGURE 3.3 Simulation of Halfspace [90]

of the extended layers is set to equal 1.5 times the shear wave length, λ_s, of the half space. The choice of this depth is made on the observation that fundamental mode Rayleigh waves in a halfspace decay rapidly with depth and essentially vanish at a depth corresponding to one and a half wave length. The thickness of each extended layer is set to be a function of the excitation frequency and to increase as the term of a quotient series such that:

$$\alpha h_o + \alpha^2 h_o + \ldots\ldots + \alpha^n h_o = H = 1.5\frac{V_s}{f} \qquad (3\text{-}4)$$

where, h_o is the thickness of the last top layer, α is a constant factor, V_s is the shear wave velocity of the half-space, and f is the frequency.

Based on the above method of subdivision, the layer thickness will increase with depth and decrease with frequency. This means that the layer thickness becomes very large at low frequency and remains small as compared to the wave length. At zero frequency (static case) the method ceases to be valid. The choice of n=10 was found to be adequate for most practical problems [90].

The site model may be further improved by replacing the rigid boundary with a viscous boundary. For a site with very small material damping, the contribution of higher modes to the response may produce some artificial peaks that should not appear. This problem is handled by the use of Lysmer-Kuhlmeyer [63] viscous boundary dashpots at the bottom of the layered system. This boundary consists of two (vertical and horizontal) dashpots per unit area of the boundary. The dashpots will translate into the addition of an extra stiffness matrix, $[K]_H$ which is defined as:

$$[K]_H = \begin{bmatrix} i\omega\rho V_s & 0 \\ 0 & i\omega\rho V_p \end{bmatrix} \qquad (3\text{-}5)$$

where, ρ, V_s and V_p are the mass density, s-wave and p-wave velocities of the half-space, respectively, and ω is the circular frequency.

3.5 COMPLEX MODULUS REPRESENTATION

Consider a problem of one-dimensional wave propagation in a linear elastic material. The stress-strain relationship follows Hook's law as:

$$\sigma(x, t) = E \cdot \varepsilon(x, t) \tag{3-6}$$

where, σ and ε are the stress and strain components, respectively, and the constant value E is the modulus of elasticity.

For a harmonic motion of frequency ω the stress and strain are also harmonic with the frequency ω. Using the complex representation for harmonic oscillations the stress and strain can be written as:

$$\begin{aligned} \sigma(x, t) &= \sigma^*(x)e^{i\omega t} \\ \varepsilon(x, t) &= \varepsilon^*(x)e^{i\omega t} \end{aligned} \tag{3-7}$$

where, ω is circular frequency, σ^* and ε^* are the complex amplitudes of stress and strain, respectively, and i is $\sqrt{-1}$. They can be interpreted as a pair of vectors rotating at frequency ω about the origin of the complex plane, as shown in Figure 3.4 (a). Substitution of Equation (3-7) into Equation (3-6) yields:

$$\sigma^*(x) = E \cdot \varepsilon^*(x) \tag{3-8}$$

The above equation implies that the stress and strain vectors are in phase, as shown in Figure 3.4 (b), and therefore all the strain energy is stored in a recoverable form as would be expected for elastic materials.

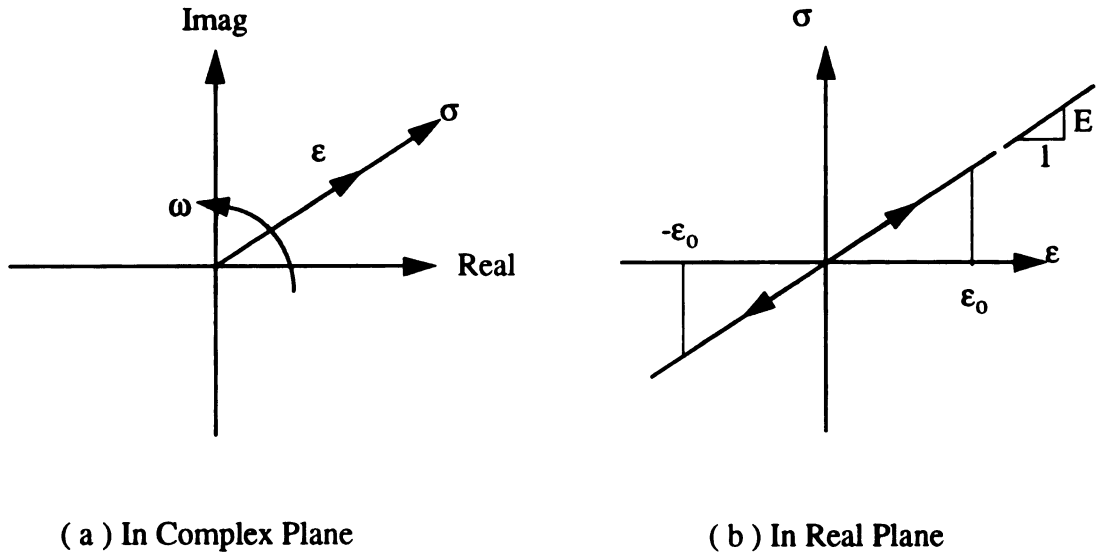

FIGURE 3.4 Representation of Stress and Strain for Linear Elastic Material [106]

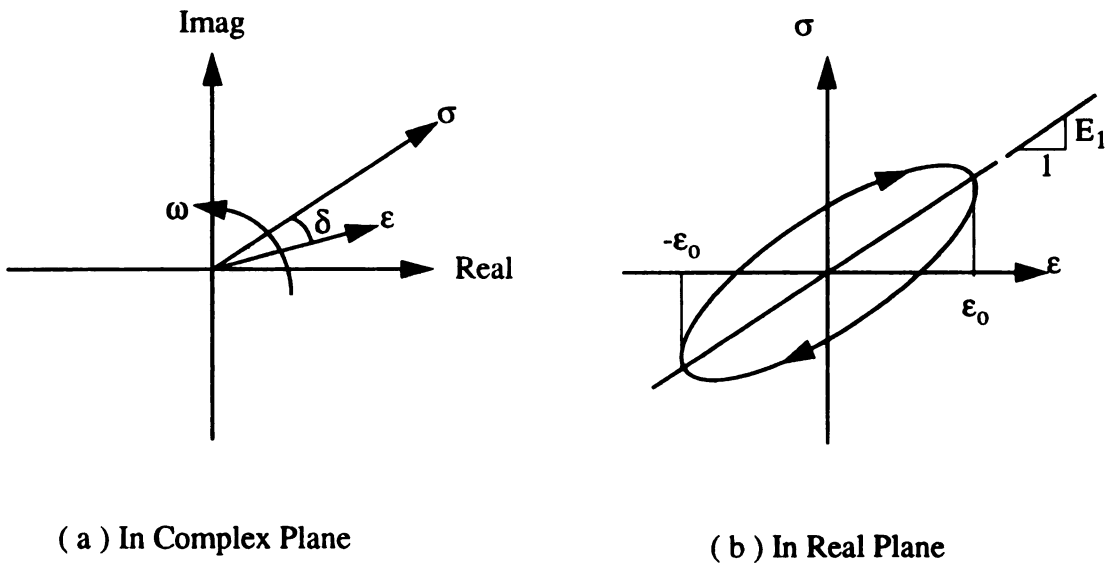

FIGURE 3.5 Representation of Stress and Strain for Linear Visco-Elastic Material [106]

However, most materials, including soils and asphalt concrete mixtures, do not behave in this manner and some of the energy is dissipated through various mechanisms which are collectively called internal damping. The internal damping in soil is not considered to be caused by viscosity, the stress-strain behavior of soils under vibratory loading is similar to that of visco-elastic materials. Asphalt concrete, on the other hand, is a visco-elastic material in large due to the viscosity of the asphalt. This permits the use of complex moduli in representing the stress-strain behavior of soils and asphalt concrete that are subjected to loads varying harmonically in time.

The stress-strain relation under uniaxial conditions can be expressed by:

$$\sigma^* e^{i\omega t} = E^* \varepsilon^* e^{i\omega t} \tag{3-9}$$

where E^* the is complex modulus which, in general, is frequency dependent. Due to the viscous effect and consequently the complex nature of E^*, the strain vector is no longer in phase with the stress vector and lags behind it by an angle δ, as shown in Figure 3.5 (a). This angle is often called the loss angle and is defined as follows:

$$\tan\delta = \frac{\mathrm{imag}(E^*)}{\mathrm{real}(E^*)} = \frac{E_2}{E_1} \tag{3-10}$$

Therefore,

$$E^* = E_1(\omega) + iE_2(\omega) = |E^*|e^{-i\delta} \tag{3-11}$$

The above equation implies that the real component of E^* is associated with elastic phenomena in which the energy is stored in a recoverable form while the imaginary component of E^* is associated with viscous phenomena in which energy is dissipated, and δ is a measure of this dissipation.

Laboratory tests seem to indicate that the stress-strain curve for most soils and for asphalt concrete mixtures under harmonic vibration form closed loops as shown in Figure 3.5 (b). The shape of these loops, for soils, are found to be substantially independent of the frequency of vibration and dependent on the strain amplitude involved [106], while they are dependent on the frequency of vibration in the case of asphalt concrete. The elastic modulus is expressed as the secant modulus determined by the extreme points on the hysteresis loop while damping is proportional to the area inside the hysteresis loop. This behavior is represented by the constant hysteresis model. According to this model E^* can be written as follows:

$$E^* = E(1 + i\tan\delta) \tag{3-12}$$

The loss angle δ can be related to the fraction of critical damping β as follows:

$$\tan\delta \approx 2 \cdot \beta \qquad \text{if} \qquad \beta \ll 1 \tag{3-13}$$

Substitution of Equation (3-13) into Equation (3-12) yields:

$$E^* = E_1(1 + i2\beta) \tag{3-14}$$

Equation (3-14) is valid at any frequency of vibration. The modulus and damping ratio are independent of frequency in soils, whereas they are dependent of frequency in the case of asphalt concrete. The use of a complex modulus implies that the actual hysteresis loops are approximated by elliptical hysteresis loops which are equivalent with respect to the slope of the principal axes and the areas enclosed by the loops. Thus the secant modulus equals the real component of the corresponding complex modulus. The energy losses per cycle which are proportional to the area of the hysteresis loops are also matched.

3.6 METHOD OF ANALYSIS

3.6.1 Complex Response Method

The complex response method uses the notation of complex algebra to express the response to a harmonic excitation force. This method is based on the assumption that if the forcing function is expressed in the complex form then the steady-state response to the driving force should have the same frequency as the excitation force. From this method, the complex amplitude is obtained as a function of frequency. The complex response method is very convenient in solving linear continuum mechanics problems.

Fourier series are used in the complex response method because they allow for the study of the frequency content of time dependent data in linear system. The development of the Fast Fourier Transform (FFT) algorithm by Cooley and Tukey [27] in 1965 and the availability of high speed computers have greatly increased the use of complex Fourier analysis.

The advantages of the complex response method in analyzing engineering problems are: First, it can handle damping very effectively; damping can be introduced via a complex stiffness and can be added easily where needed. Additional damping created by a semi-infinite medium can be modeled by complex dampers. Second, the transient solutions can be obtained from the steady-state solutions using the inverse Fast Fourier Transform algorithm.

3.6.2 Dynamic Analysis

Stationary dynamic analysis is performed in the frequency domain using the complex response method; transient loading is handled by Fourier transform techniques. An efficient interpolation scheme in the frequency domain is used to reduce the computational

effort. Material damping is introduced by the use of complex moduli. Multiple loadings can be applied at the surface and each loading can have a different radius and a different time history. Static loads can be simulated by specifying a harmonic input with zero excitation frequency.

The computation steps used to calculate the response of the multi-layered system subjected to stationary surface circular loads are as follows: (1) The dynamic loads are decomposed into harmonic components using the Fast Fourier Transform (FFT) algorithm; (2) Green's functions for displacements, stresses and strains are derived in the frequency domain from the solution of the eigenvalue problem. The response at each discretized frequency can thus be obtained by multiplying the Green's function by the complex amplitude of the loading at that frequency; and (3) the response computed in the frequency domain is then converted back to the time domain using the inverse Fast Fourier Transform. This technique has the advantage that the Green's functions in the wave-number domain are algebraic rather than transcendental. Thus, the Hankel transforms required for an evaluation of the Green's functions in the spatial domain can be computed in closed-form [54]. A computer program, SAPSI, was implemented following these procedures by Chen [21]. Details of the above solution techniques are described in the following sections.

3.7 STEADY-STATE SOLUTION

3.7.1 Introduction

If an impulse of short duration is created at the surface of an elastic half-space, the body waves travel into the medium with hemispherical wave fronts, and the Rayleigh waves will propagate radially outward along a cylindrical wave front. The ground displacement due to Rayleigh wave arrival is much greater than that for body waves. Also,

the attenuation of the amplitude of the Rayleigh wave is slower than that for the body waves. Hence Rayleigh wave is considered as the dominant wave near the surface.

If horizontal layering occurs in a half-space some energy originating at the surface and traveling into the half space will return to the surface. Multiple total reflections within the upper layer can generate a second type of surface wave called the Love wave. But a Love wave will not occur if the superficial layer is the higher velocity layer. Hence, the effect of Love wave is not considered in this research because the surface pavement layer is denser and has a higher velocity than the lower layer in the pavement system.

3.7.2 Stiffness Matrix Approach

The pavement loading problem can be characterized as a wave propagation problem, because the motion in the pavement and the layered system underneath at is dominated by propagating waves. The waves are generated at the surface by the moving wheel loads, and from there they propagate into the underlying medium. The effect of the propagating waves is to disperse energy into the infinite medium and at the same time to carry disturbance a long distance away from the source. Due to the energy dissipation by the waves, the pavement response to dynamic loads is damped.

The layered system can be treated by the finite element method in the horizontal direction; however it is numerically more efficient to use continuum theory in the horizontal direction because each layer can be assumed to be homogeneous and of infinite extent. The natural layers are subdivided into thin sublayers and it is assumed that the displacements within each sublayer vary linearly in the vertical direction. In the horizontal direction, the displacements are required to satisfy the pertinent ordinary differential equations which are obtained from the governing, partial differential equations.

At a given frequency, the free motion in the discretized layered region consists of a finite number of wave modes which are obtained by an algebraic eigenvalue solution. These wave modes serve as shape functions for expanding the displacements in terms of mode participation factors. These nodal forces which have to be applied at the boundary are derived from the displacement expansion by observing the strain-displacement and stress-strain relations. The nodal forces are uniquely related to the simultaneous nodal displacements at the boundary through a dynamic stiffness matrix. The dynamic stiffness matrix is complex, symmetric, and frequency-dependent.

Referring to Figure 3.6, consider the jth layer and consider the equilibrium equation at the interface. Since the system is linear, the relationship between the forces and the displacements at the top and bottom of each layer may be written in the frequency domain as:

$$\left[K_j\right]\{\bar{v}_j\} = \{\bar{P}_j\} \tag{3-15}$$

where, $\left[K_j\right]$ is the effective stiffness matrix for the jth layer, $\{\bar{v}_j\}$ and $\{\bar{P}_j\}$ are displacement and load vectors in the frequency domain, respectively. The displacement and load matrices, as shown in Figure 3.6, are expressed at the layer interfaces as:

$$\begin{aligned} \{v_j\}^T &= \{v_x^{\,j} \quad iv_z^{\,j} \quad v_x^{\,j+1} \quad iv_z^{\,j+1}\}^T \\ \{P_j\}^T &= \{P_x^{\,j} \quad iP_z^{\,j} \quad P_x^{\,j+1} \quad iP_z^{\,j+1}\}^T \end{aligned} \tag{3-16}$$

where the factor $i = \sqrt{-1}$ in the front of v_z and P_z has the advantage that the stiffness matrices thus defined are symmetric. In the case of a multi-layered system, the global stiffness matrix $\left[K\right] = \left\{\left[K_j\right]\right\}$ is constructed by overlapping the contribution of the layer matrices at each interface of the system as depicted in Figure 3.7. The global load vector

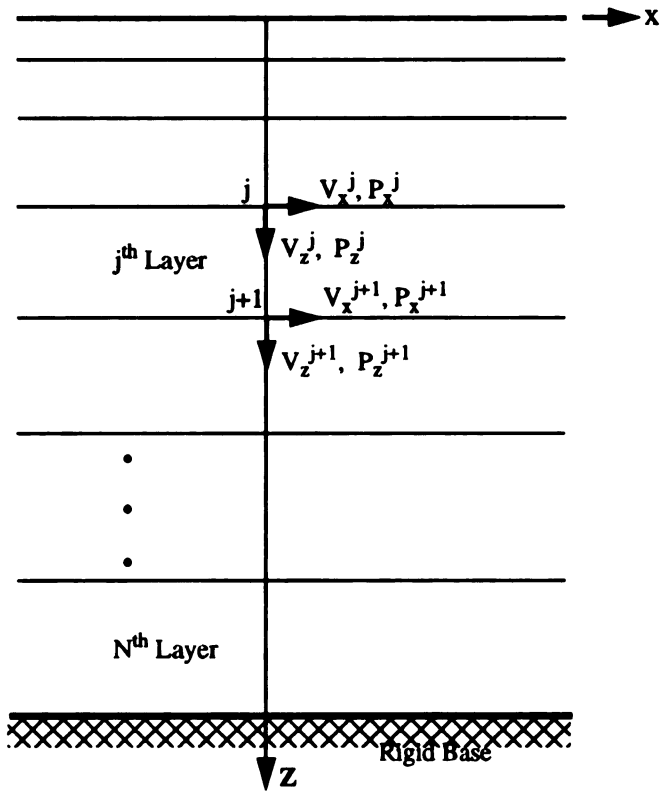

FIGURE 3.6 Boundary Condition at Layered Interfaces due to Rayleigh Wave

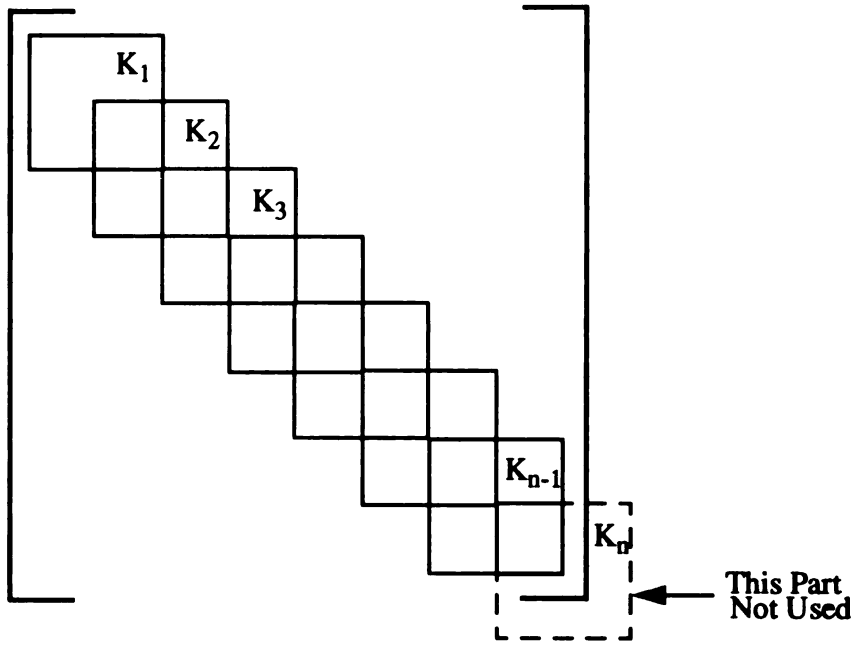

FIGURE 3.7 Assembling of Submatrices of Each Layer

corresponds to the prescribed external tractions at the interface. Thus, the assemblage of stiffness and load matrices are similar to that of structural dynamic problems in the frequency domain.

3.7.3 Layer Stiffness Matrix

Assuming that the displacement is the exponential function exp(-ikx) in the x-direction, Waas [118] expressed the element stiffness matrix as;

$$\left[K_j\right] = [A_j]k^2 + [B_j]k + [G_j] - \omega^2[M_j] \tag{3-17}$$

where, k is the wave number of a generated surface wave which decays or propagates energy in the positive x-direction, and ω the is excitation angular frequency. Each submatrix corresponds to a pavement layer. Denoting the thickness of the jth layer from the top by h_j, the mass density by ρ_j, the shear modulus by G_j, and the Lame's constant by λ_j, the layer submatrix is [55]:

$$\left[A_j\right] = \frac{h_j}{6}\begin{bmatrix} 2(2G_j+\lambda_j) & 0 & (2G_j+\lambda_j) & 0 \\ 0 & 2G_j & 0 & G_j \\ (2G_j+\lambda_j) & 0 & 2(2G_j+\lambda_j) & 0 \\ 0 & G_j & 0 & 2G_j \end{bmatrix}$$

$$\left[B_j\right] = \frac{1}{2}\begin{bmatrix} 0 & (\lambda_j-G_j) & 0 & (-\lambda_j-G_j) \\ (\lambda_j-G_j) & 0 & (\lambda_j+G_j) & 0 \\ 0 & (\lambda_j+G_j) & 0 & (-\lambda_j+G_j) \\ (-\lambda_j-G_j) & 0 & (-\lambda_j+G_j) & 0 \end{bmatrix} \tag{3-18}$$

$$\left[G_j\right] = \frac{1}{h_j}\begin{bmatrix} G_j & 0 & (-G_j) & 0 \\ 0 & (2G_j+\lambda_j) & 0 & -(2G_j+\lambda_j) \\ -G_j & 0 & G_j & 0 \\ 0 & -(2G_j+\lambda_j) & 0 & (2G_j+\lambda_j) \end{bmatrix}$$

$$\left[M_j\right] = \frac{\rho_j h_j}{6}\begin{bmatrix} 2 & 0 & 1 & 0 \\ 0 & 2 & 0 & 1 \\ 1 & 0 & 2 & 0 \\ 0 & 1 & 0 & 2 \end{bmatrix} \qquad (3\text{-}19)$$

The displacements within the layer are obtained by linear interpolation between the interfaces:

$$v = \zeta v_1 + (1-\zeta)v_2 \qquad 0 \le \zeta \le 1 \qquad (3\text{-}20)$$

As described in the previous section, the assemblage may be understood in the sense of the finite element method, with each thin layer constituting a linear element. The global stiffness matrix is obtained by overlapping the matrices for each layer and the same is done for the global load and displacement vectors. For prescribed loadings, the displacements are obtained by formal inversion of the stiffness matrix.

$$\{P\} = \left[K\right]\{v\} \qquad \text{then} \qquad \{v\} = \left[K\right]^{-1}\{P\} \qquad (3\text{-}21)$$

In practice, this inversion is not necessary since the spectral decomposition would be employed. This necessitates solving the quadratic eigenvalue problem which will be described in the following section.

3.7.4 Eigenvalue Problem

It was shown [118] that the eigenvalue problem and its solutions are the same for the plane and symmetric case. Thus, the eigensolutions obtained from the plane case may

be directly applied in seeking the response of the layered system for the axisymmetric case.

To solve the site response problem for surface waves, it is necessary to form and solve the eigenvalue problem for the pavement profile model. Based on the horizontally layered system and the linear variations of displacement within each layer, Wass [118] has formulated the eigenvalue problem for the plane strain condition. The free vibrations that may occur in the layered system consist of a displacement field of generalized Rayleigh waves of the form:

$$\{v\} = \{\phi\}\exp(i\omega k - ikx) \tag{3-22}$$

The mode shape $\{\phi\}$ and associated wave numbers, k, can be determined from an algebraic eigenvalue problem. The natural modes of wave propagation in the stratum are obtained from the eigenvalue problem that follows from setting the load vector equal to zero.

$$([A]k^2 + [B]k + [C])\{\phi\} = \{0\} \tag{3-23}$$

where, $[A] = \sum[A_j]$, $[B] = \sum[B_j]$, $[C] = \sum\{[G_j] - \omega^2[M_j]\}$, and ω is the excitation circular frequency, k is the eigenvalue known as the wave number, and $\{\phi\}$ is the associated eigenvector with 2n components. The matrices $[A]$, $[B]$, and $[C]$ are of order $2n \times 2n$ that are assembled from submatrices for the pavement layers according to the scheme shown in Figure 3.7. The equation constitutes a quadratic eigenvalue problem, with eigenvalues k_j and modal shapes ϕ_j. In this model there are 2 degree of freedom associated with each layer interface with total of 2n degree of freedom for a n-layer system. The solution yields 2n Rayleigh modes and 2n wave numbers.

While a quadratic eigenvalue problem may always be solved as a linear eigenvalue problem, this is not necessary here because of the special form of the matrices involved. After rearranging rows and columns by degree of freedom, Equation (3-23) can be witten in the partioned form:

$$\begin{bmatrix} k^2A_x + C_x & B_{xz} \\ k^2B_{xz}^T & k^2A_z + C_z \end{bmatrix} \begin{Bmatrix} \phi_x \\ k\phi_z \end{Bmatrix} = \begin{Bmatrix} 0 \\ 0 \end{Bmatrix} \tag{3-24}$$

The eigenvalue problems represented by the above equation yield the eigenvalues and produce the following eigenvectors [54]:

$$\boxed{Y} = \begin{bmatrix} \boxed{E}[\Phi_x] \\ [\Phi_z] \end{bmatrix} \text{ and } \boxed{Z} = \begin{bmatrix} [\Phi_x] \\ [E][\Phi_z] \end{bmatrix} \tag{3-25}$$

where, $\boxed{E}$ is a diagonal matrix of modulus and $[\Phi_x]$ and $[\Phi_z]$ are defined by eigenvectors $\{\phi_x\}_s$ and $\{\phi_z\}_s$ as follows:

$$[\Phi_x] = \langle \{\phi_x\}_1, \{\phi_x\}_2, \ldots, \{\phi_x\}_{2N} \rangle \text{ and } [\Phi_z] = \langle \{\phi_z\}_1, \{\phi_z\}_2, \ldots, \{\phi_z\}_{2N} \rangle \tag{3-26}$$

The matrices $\boxed{Y}$ and $\boxed{Z}$ were shown to be orthogonal to each other such that [54]:

$$[Y]^T[\bar{A}][Z] = [E] \quad \text{and} \quad [Y]^T[\bar{C}][Z] = -[E]^3 \tag{3-27}$$

$$\text{where } [\bar{A}] = \begin{bmatrix} A_x & 0 \\ B^T_{xz} & A_z \end{bmatrix} \quad \text{and} \quad [\bar{C}] = \begin{bmatrix} C_x & B_{xz} \\ 0 & C_z \end{bmatrix} \tag{3-28}$$

3.7.5 Green's Functions

According to Kausel [54] and Waas [118], the effective stiffness matrix and the corresponding eigenvalue problem are the same for the plane and axisymmetric cases.

Therefore, the equilibrium equation in the spatial domain may be derived from the results of Section 3.7.3 and Section 3.7.4.

For a distributed vertical pressure with intensity q acting over a circular area with radius a, as shown in Figure 3.2, the load vector in the axisymmetric spatial domain may be expressed by:

$$\{p\} = \begin{Bmatrix} p_r \\ p_z \end{Bmatrix} = q\begin{Bmatrix} 0 \\ 1 \end{Bmatrix} \qquad 0 \le r \le a \tag{3-29}$$

and, $\{p\}$ may also be expanded into its Hankel transform as:

$$\left(\begin{Bmatrix} P_r \\ P_z \end{Bmatrix} = \int_0^\infty k\begin{bmatrix} 1 & 0 \\ 0 & 1 \end{bmatrix}\begin{bmatrix} -J_1(kr) & 0 \\ 0 & -J_0(kr) \end{bmatrix}\begin{Bmatrix} \bar{P}_r \\ \bar{P}_z \end{Bmatrix} dk\right) \tag{3-30}$$

and by its inverse transform [99]:

$$\begin{aligned} \begin{Bmatrix} \bar{P}_r \\ \bar{P}_z \end{Bmatrix} &= \int_0^\infty r\begin{bmatrix} 1 & 0 \\ 0 & 1 \end{bmatrix}\begin{bmatrix} -J_1(kr) & 0 \\ 0 & -J_0(kr) \end{bmatrix} q\begin{Bmatrix} 0 \\ 1 \end{Bmatrix} dr \\ &= \int_0^a (-q) r J_o(kr)\begin{Bmatrix} 0 \\ 1 \end{Bmatrix} dr \\ &= \frac{qa}{k} J_1(ka)\begin{Bmatrix} 0 \\ 1 \end{Bmatrix} \end{aligned} \tag{3-31}$$

where k is the wave number and J_m is the Bessel function of the first kind and m^{th} order.

For the same layered system as shown in Figure 3.2, the displacement vector $\{u\}$ may be written in terms of cylindrical coordinates as:

$$\{u\} = \begin{Bmatrix} u_r \\ u_z \end{Bmatrix} \tag{3-32}$$

It should be noted that $\{u\}$ can be expanded into a Hankel transform in the spatial domain [55]:

$$\begin{Bmatrix} u_r(r,\theta,z) \\ u_z(r,\theta,z) \end{Bmatrix} = \int_0^\infty k \begin{bmatrix} 1 & 0 \\ 0 & 1 \end{bmatrix} \begin{bmatrix} -J_1(kr) & 0 \\ 0 & -J_0(kr) \end{bmatrix} \begin{Bmatrix} \bar{u}_r \\ \bar{u}_z \end{Bmatrix} dk \tag{3-33}$$

and the inverse Hankel transform:

$$\begin{Bmatrix} \bar{u}_r(k,z) \\ \bar{u}_z(k,z) \end{Bmatrix} = \int_0^\infty r \begin{bmatrix} 1 & 0 \\ 0 & 1 \end{bmatrix} \begin{bmatrix} -J_1(kr) & 0 \\ 0 & -J_0(kr) \end{bmatrix} \begin{Bmatrix} u_r \\ u_z \end{Bmatrix} dr \tag{3-34}$$

Now consider the force equilibrium in the spatial domain. The equilibrium equation may be derived from equations (3-15), (3-24), and (3-28), which give:

$$\left(\left[\bar{A}\right] k^2 + [\bar{C}] \right) \{\bar{V}\} = \{\bar{P}\} \tag{3-35}$$

where, $\{\bar{V}\} = \{\bar{V}_r \quad k\bar{V}_z\}^T \qquad \{\bar{P}\} = \{\bar{P}_r \quad k\bar{P}_z\}^T$.

After some handling of the above equation, the displacements in the frequency domain are described in terms of inverse Hankel transform as follows:

$$\begin{Bmatrix} \bar{V}_r \\ k\bar{V}_z \end{Bmatrix} = \begin{Bmatrix} [\Phi_x] \\ [\Phi_z][E] \end{Bmatrix} (k^2[E] - [E]^3)^{-1} \begin{Bmatrix} [E][\Phi_x] \\ [\Phi_z] \end{Bmatrix} \begin{Bmatrix} \bar{P}_r \\ k\bar{P}_z \end{Bmatrix} \tag{3-36}$$

which can be reduced to

$$\begin{Bmatrix} \bar{V}_r \\ \bar{V}_z \end{Bmatrix} = \begin{Bmatrix} [\Phi_x][D][\Phi_x]^T & k[\Phi_x][E]^{-1}[D][\Phi_z]^T \\ k[\Phi_z][D][E]^{-1}[\Phi_x]^T & [\Phi_z][D][\Phi_z]^T \end{Bmatrix} \begin{Bmatrix} \bar{P}_r \\ \bar{P}_z \end{Bmatrix} \tag{3-37}$$

where $[D] = (k^2[I] - [E]^2)^{-1}$.

The displacements at the mth layer due to a vertical circular load acting at the nth layer may then be obtained by substituting Equation (3-31) and (3-37) into equation (3-33), which gives:

$$
\begin{aligned}
u_r &= qa \sum_{s=1}^{2N} \phi^m_{x,s}\ \phi^n_{z,s}\ I_{2s}/k_s \\
u_\theta &= 0 \\
u_z &= qa \sum_{s=1}^{2N} \phi^m_{z,s}\ \phi^n_{z,s}\ I_{1s}/k_s
\end{aligned}
\qquad (3\text{-}38)
$$

where:

$$
I_{1s} = \int_0^\infty \frac{1}{(k^2 - k_s^2)} J_o(kr) J_1(ka) dk
$$

$$
\begin{cases}
= \dfrac{\pi}{2ik_s}\ J_0(k_s r)\ H_1^{(2)}(k_s a) - \dfrac{1}{k_s{}^2 a} & \text{for} \quad 0 \le r \le a \\[2ex]
= \dfrac{\pi}{2ik_s}\ J_1(k_s a)\ H_o^{(2)}(k_s r) & \text{for} \quad r \ge a
\end{cases}
$$

$$
I_{2s} = \int_0^\infty \frac{1}{(k^2 - k_s^2)} J_1(kr) J_1(ka) dk
$$

$$
\begin{cases}
= \dfrac{\pi}{2i}\ J_1(k_s r)\ H_1^{(2)}(k_s a) & \text{for} \quad 0 \le r \le a \\[2ex]
= \dfrac{\pi}{2i}\ J_1(k_s a)\ H_1^{(2)}(k_s r) & \text{for} \quad r \ge a
\end{cases}
$$

and J_m are the Bessel functions of the first kind with the mth order, and $H_m{}^{(2)}$ are the Hankel functions of the second kind and m^{th} order.

The stresses at the center of the mth layer due to a vertical circular load applied at the nth layer may be obtained by substituting Equation (3-38) into Equation (3-3), as follows;

$$\sigma_r = (\lambda + 2G)\frac{\partial u_r}{\partial r} + \lambda\left(\frac{\partial u_z}{\partial z} + \frac{u_r}{r}\right)$$

$$= qa\sum_{s=1}^{2N}\left(\frac{\phi_{x,s}^{m+1} + \phi_{x,s}^{m}}{2}\right)\phi_{z,s}^{n}\left[(\lambda + 2G)\frac{\partial I_{2s}}{\partial r} + \lambda\frac{I_{2s}}{r}\right]\frac{1}{k_s} \qquad (3\text{-}39)$$

$$+qa\sum_{s=1}^{2N}\lambda\left(\frac{\phi_{z,s}^{m+1} - \phi_{z,s}^{m}}{h_m}\right)\phi_{z,s}^{n} I_{1s}$$

$$\sigma_\theta = (\lambda + 2G)\frac{u_r}{r} + \lambda\left(\frac{\partial u_r}{\partial r} + \frac{\partial u_z}{\partial z}\right)$$

$$= (\lambda + 2G)\left[qa\sum_{s=1}^{2N}\left(\frac{\phi_{x,s}^{m+1} + \phi_{x,s}^{m}}{2}\right)\phi_{z,s}^{n}\frac{I_{2s}}{k_s r}\right] \qquad (3\text{-}40)$$

$$+\lambda qa\left[\sum_{s=1}^{2N}\left(\frac{\phi_{x,s}^{m+1} + \phi_{x,s}^{m}}{2}\right)\phi_{z,s}^{n}\ \frac{\partial I_{2s}}{\partial r}\ \frac{1}{k_s} + \sum_{s=1}^{2N}\left(\frac{\phi_{z,s}^{m+1} - \phi_{z,s}^{m}}{h_m}\right)\phi_{z,s}^{n} I_{1s}\right]$$

$$\sigma_z = (\lambda + 2G)\frac{\partial u_z}{\partial r} + \lambda\left(\frac{\partial u_r}{\partial r} + \frac{u_r}{r}\right)$$

$$= (\lambda + 2G)\left[qa\sum_{s=1}^{2N}\left(\frac{\phi_{z,s}^{m+1} - \phi_{z,s}^{m}}{h_m}\right)\phi_{z,s}^{n}\ I_{1s}\right] \qquad (3\text{-}41)$$

$$+\lambda qa\left[\sum_{s=1}^{2N}\left(\frac{\phi_{x,s}^{m+1} + \phi_{x,s}^{m}}{2}\right)\phi_{z,s}^{n}\ \left(\frac{\partial I_{2s}}{\partial r} + \frac{I_{2s}}{r}\right)\frac{1}{k_s}\right]$$

$$\tau_{rz} = G\left(\frac{\partial u_r}{\partial z} + \frac{\partial u_z}{\partial r}\right)$$

$$= Gqa\left[\sum_{s=1}^{2N}\left(\frac{\phi_{x,s}^{m+1} - \phi_{x,s}^{m}}{h_m}\right)\phi_{z,s}^{n}\frac{I_{2s}}{k_s} + \sum_{s=1}^{2N}\left(\frac{\phi_{z,s}^{m+1} + \phi_{z,s}^{m}}{2}\right)\phi_{z,s}^{n}\ (-I_{2s})\right] \qquad (3\text{-}42)$$

If Green's function in cylindrical coordinates is defined as the response of the system due to a load of unit intensity, the Green's functions for the displacements and stresses induced by the vertical circular load can be obtained by setting the load, q, to equal 1.0 in the above equations. The displacements and stresses in the frequency domain may then be computed by multiplying Green's function by the complex Fourier amplitudes of the load.

3.7.6 Validation of Steady State Solution

The accuracy of the SAPSI program has been verified against available "exact" solutions for the cases of a single-layered system, a homogeneous halfspace, and a two-layered system. Tabatabaie compared SAPSI predictions with experimental results from non-destructive tests [105]. Chatti et al. compared SAPSI results with data from FWD and truck tests at the PACCAR Test Track [19].

A single-layered system subjected to a static uniform circular load was utilized to compare the SAPSI solutions with those obtained by Harr [43], Ueshita and Meyerhof [112], and Milovic [70]. The static load was simulated by specifying a zero excitation frequency. The comparisons showed that the static responses of the single-layered system computed by SAPSI are very close to those obtained by others.

The half space solution of SAPSI was verified against the solution by Sung [104]. The halfspace was simulated by frequency dependent layers and dashpots attached to the bottom of the layered system. The vertical surface displacements at the center of the loaded area for the two cases were computed and compared with those obtained by Sung. The comparison showed that the static response could be approximated by calculating the response at a very small frequency.

A two-layered system with different properties for each layer was analyzed. The system was subjected to a surface circular load. The static results were compared, and

indicated that the static responses of the two-layered system computed by SAPSI are very close to the solution by Burmister [13].

3.8 TRANSIENT SOLUTION

3.8.1 Introduction

The complex response method is formulated for steady state vibrations. However, transient motions such as impulse loads may be analyzed using discrete Fourier transform techniques. Using these techniques the basic input is specified at N points uniformly distributed over the period T. The given function values are:

$$P_s(t) = P(s \cdot \Delta t) \qquad ; \quad s = 1, 2 \ldots N-1 \tag{3-43}$$

where, Δt is the time interval T/N. The input can be expressed using the exponential functions:

$$P_s(t) = \mathrm{Re} \sum_{s=0}^{N/2} P_s \exp(i\omega_s t) \tag{3-44}$$

where the frequencies are defined as $\omega_s = 2\pi s/(N\Delta t)$, and P_s are complex load amplitudes defined as follows:

$$\begin{aligned} P_s &= \frac{1}{N} \sum_{n=0}^{N-1} P(n\Delta t) \exp(-i\omega_s n\Delta t) \qquad \text{for} \qquad s = 0 \text{ and } N/2 \\ P_s &= \frac{2}{N} \sum_{n=0}^{N-1} P(n\Delta t) \exp(-i\omega_s n\Delta t) \qquad \text{for} \qquad s = 1, 2 \ldots N/2 - 1 \end{aligned} \tag{3-45}$$

If N is chosen as a power of 2, the complex amplitude can be computed by the Fast Fourier Transform (FFT) algorithm, developed by Cooley and Tukey [27]. Since Equation (3-44) is a truncated Fourier series, the function $P_s(t)$ should be periodic over

the period T. Actual moving pulse loads are not periodic. However, by the addition of a "quiet zone" consisting of a limited number of trailing zeroes to the input, both of the above requirements can be satisfied. The quiet zone should be chosen sufficiently long such that the response occurring at the beginning of the next cycle is very small due to the system damping. In this case, the response within each cycle is not influenced by the previous cycle.

Discrete values of the response, $U(t)$, in the time domain at interval Δt may be computed using the inverse Fourier transform on $\{U_s\}$ which is the solution for a single harmonic input.

To obtain a complete solution, the system of linear equations must be solved for all of the following FFT frequencies.

$$f_s = \frac{\omega_s}{2\pi} = \frac{s}{T} \text{ , } s=1, 2, \ldots, N/2 \qquad (3\text{-}46)$$

This is a formidable computation task. To minimize the computational cost, a cut-off frequency is introduced whereby the response for frequencies above a given frequency, f_{max}, are set to zero. Also, an efficient interpolation scheme is used so that the complex response amplitudes in the frequency domain are computed for a certain number of selected frequencies and the values for the rest of the FFT frequencies are obtained by interpolation. The interpolation method is described in the next section.

3.8.2 Interpolation Scheme

The interpolation technique was developed by Tajirian [107] to interpolate the response for all frequencies in-between the calculated frequencies. The technique is based on the frequency response function of a two degree of freedom system. This technique is general in that it works for multi degree of freedom system, and it is possible to choose the

computed frequencies at wider intervals to further reduce the cost of analysis. The total response of a two-degree-of freedom system subjected to a harmonic load for each degree-of-freedom has the following general form:

$$U(\omega) = \frac{c_1\omega^4 + c_2\omega^2 + c_3}{\omega^4 + c_4\omega^2 + c_5} \tag{3-47}$$

where, $U(\omega)$ is the response at frequency ω and c_1, c_2, c_3, c_4 and c_5 are constants. Thus, if the response of the system is known at five frequencies, the five constants may be obtained from:

$$\begin{bmatrix} \omega_1^4 & \omega_1^2 & 1 & -\omega_1^2 U_1 & -U_1 \\ \omega_2^4 & \omega_2^2 & 1 & -\omega_2^2 U_2 & -U_2 \\ \omega_3^4 & \omega_3^2 & 1 & -\omega_3^2 U_3 & -U_3 \\ \omega_4^4 & \omega_4^2 & 1 & -\omega_4^2 U_4 & -U_4 \\ \omega_5^4 & \omega_5^2 & 1 & -\omega_5^2 U_5 & -U_5 \end{bmatrix} \begin{Bmatrix} c_1 \\ c_2 \\ c_3 \\ c_4 \\ c_5 \end{Bmatrix} = \begin{Bmatrix} \omega_1^4 U_1 \\ \omega_2^4 U_2 \\ \omega_3^4 U_3 \\ \omega_4^4 U_4 \\ \omega_5^4 U_5 \end{Bmatrix} \tag{3-48}$$

Following the computation of the five constants from the above equation, Equation (3-47) can be used to obtain the interpolated responses for all the frequencies in the range from ω_1 to ω_5.

The interpolation techniques described above may be used for interpolating transfer functions for multi-degree-of freedom when the transfer functions behave like those of the two-degree-of-freedom system within small frequency regions. By interpolating the transfer function in each range so as to cover the entire range, the transfer function values are computed for all FFT frequencies shown in Equation (3-46).

3.8.3 Algorithm and Validation of Transient Analysis

Transient dynamic analysis (sometime called time-history analysis) is a technique used to determine the dynamic response of a structure under the action of any general time-dependent loads. This type of analysis may be used to determine the time-varying displacements, strains, and stresses. SAPSI uses the following procedures for transient analysis;

(1) Decompose the dynamic load into harmonic components to obtain complex amplitudes using the Fast Fourier Transform (FFT) algorithm.

(2) Obtain the steady-state response due to a unit harmonic load at a fixed number of frequencies.

(3) Interpolate the steady-state response for all FFT frequencies using the obtained interpolation function as described in the previous section.

(4) Calculate the actual response by multiplying the complex load amplitudes with the unit response.

(5) Finally, obtain the transient response in time domain using the inverse FFT algorithm.

The first procedures are well known and established; the second procedure is the steady-state solution which was verified by Chen as described in Section 3.7.6. Thus, only procedure (3) and (4) are required to be verified for the transient analysis in SAPSI.

To verify the coding of transient analysis, the results from SAPSI were compared with those obtained outside the program. First, the transient solution was obtained using SAPSI. Then, steady-state solutions at five frequencies were obtained using the SAPSI program. With these solutions, the transient response was calculated using the mathematical program Maple (a system for mathematical computation in symbol, numerical, and graphical) following the procedures above.

Figure 3.8 summarizes the algorithm of transient analysis, which was used in Maple. Figure 3.8(a) shows the complex load amplitudes in the frequency domain. The 16 points in Figure 3.8(b) show the steady-state response as obtained from SAPSI's steady-state solution. Only five points among 16 points were chosen for interpolation. The solid line in Figure 3.8(b) shows the extended steady-state solution at 512 points by using the interpolation function. The difference between the solid line and the 16 points is very small. Thus, the interpolation function which is based on the frequency response function of a two-degree-of freedom system is suitable to apply in the layered pavement system. Figure 3.8(c) shows the steady-state solution multiplied by the complex load amplitude at each corresponding frequency. Figure 3.8(d) is the final transient solution in the time domain, obtained using the inverse FFT algorithm.

Table 3.1 is a comparison of the transient analysis in SAPSI and the results using Maple. The differences between the results are within 2%. This table shows the accuracy of SAPSI and validates the computer program coding for transient dynamic analysis in SAPSI. The SAPSI transient analysis also was validated against the full-scale FWD field test, as will be shown in Chapter 5.

TABLE 3.1 Comparison of Transient Analysis

	Uz	Error (%)
SAPSI	4.66E-08	$\frac{\lvert \text{Maple} - \text{SAPSI} \rvert}{\text{SAPSI}} \times 100 = 1.71$
Maple	4.74E-08	$\frac{\lvert \text{Maple} - \text{SAPSI} \rvert}{\text{Maple}} \times 100 = 1.68$

3.9 SAPSI COMPUTER PROGRAM

The SAPSI computer program solves the dynamic problem of surface stationary uniform distributed circular loads on a linear visco-elastic layered system overlying a

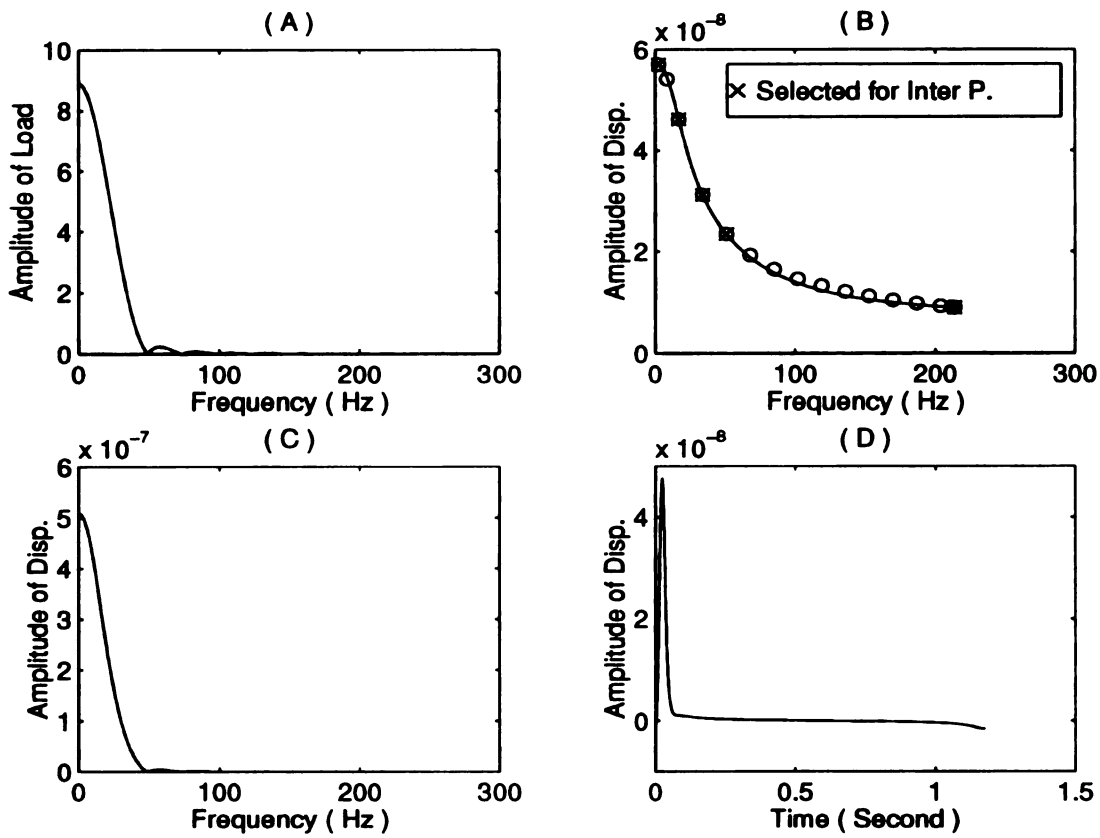

FIGURE 3.8 Validation of Interpolation Scheme by Maple

(a) Fourier Transform of the Load versus Frequency
(b) Steady-state Displacement Amplitude Due to a Unit Load versus Frequency
(c) Steady-state Displacement Amplitude versus Frequency
(d) Transient Displacement Time History

semi-infinite halfspace or a rigid bedrock. SAPSI is a FORTRAN computer program for execution on an IBM/PC AT, developed by Chen [21] at the University of California-Berkeley. The half space underlying the layered system can be simulated by vertically extending layers and a series of dashpots attached to the bottom of the extended layers. The shear modulus, damping ratio, and Poisson's ratio for each layer may be varied with the excitation frequency of the load. Multiple loads are acceptable for both the harmonic and transient cases and each loading may have a different radius and time history. A static load can be simulated by specifying a harmonic load with zero excitation frequency. The program uses a special scheme in the frequency domain to interpolate between results obtained for only a few frequencies. This provides a significant reduction in the computational effort required. The program uses a dynamic allocation technique which automatically sets the dimension of the program to accommodate the input data.

The program can be run interactively with the aid of menus shown on the screen of the monitor. The input data may be created directly from the keyboard, or read from existing files. The program is designed in such a way that the results obtained in different phases of the execution can be saved for later use. For instance, the model for the layered system, the eigensolution, the input loading, the output time histories, the coordinates of the output points, and the general printout can be saved in different files for future reference.

CHAPTER 4

DYNAMIC RESPONSE OF VISCO-ELASTIC MULTI-LAYERED SYSTEM TO MOVING ARBITRARY LOADS

4.1 INTRODUCTION

Various models have been developed to obtain the response of asphalt pavement, mostly based on layer theory or finite element method. The most commonly used models in asphalt pavement analysis are well summarized in Table 2.1 of Chapter 2. The majority of these models are for static surface loads and use linear elastic theory. The effects of inertia forces and of moving loads are usually ignored. Recent studies have shown the inertia and moving load effects to be significant.Their inclusion in pavement analysis models would, therefore, seems to be necessary in order to obtain accurate results.

The objective of a mechanistic design procedure is to use a rational approach which would be able to consider the needed complexities in modeling. An accurate prediction of the pavement response will generally require more accurate material properties and a better representation of loading conditions. Some program has been achieved in material characterization through the use of non-destructive testing (e.g. Falling Weight Deflectometer Tests) and with the development of a new generation of laboratory tests through the Strategic Highway Research Program. In recent years, there have been new attempts to develop pavement models with more realistic loading conditions; i.e. models that able to analyze moving loads with arbitrary time histories. The objective of this chapter is to develop a moving load solution for the visco-elastic multi-layered system described in Figure 1.1.

4.2 ASSUMPTIONS

Although procedures for performing dynamic analyses have become highly developed, the completely general three-dimensional dynamic analysis which would be representative of a pavement system subjected to a moving load is very complicated and requires too much computational effort to be an acceptable for routine pavement analysis. The computational effort can be reduced through simplifying assumptions regarding material properties, the type and distribution of the dynamic loads, and the geometry of the problem without a significant sacrifice in accuracy. The following sections briefly discuss these simplified assumptions and their incorporation into the development of a new solution and an associated computer program.

4.2.1 Material Properties

Although pavement materials are essentially non-linear, deflections in flexible pavement are sufficiently small under vehicle loading for the assumption of static linearity to be reasonable. Recently, Hardy and Cebon [39] showed that the instrumented pavement section used in their experiments was linear for impulse loadings over a wide frequency range.

Pavements are inherently variable in properties because of construction practices which lead to variable layer thicknesses and material properties. In addition, compaction being done in the longitudinal direction only, may cause some measure of anisotropy in the pavement layer properties. However, measurements made by Hardy and Cebon [39] indicated that the dynamic response of their test pavement was relatively isotropic over a short distance up to 2 meters.

Hence, it is assumed that each pavement layer consists of a homogeneous, isotropic, and visco-elastic material. The assumption of homogeneous and isotropic properties

simplifies the problem and enables the use of the equation of motion described in Equation (3-1). All materials are assumed to be linear visco-elastic in response to the loads. With this assumption, the laws of superposition are valid, which, in turn, provide considerable computational advantages. An additional advantage of using visco-elastic materials in the computational model is that it leads to stable algorithms and computer codes. The assumption of visco-elastic material properties for asphalt pavement was validated by several authors [97, 100].

4.2.2 Geometry

Complex geometries will inevitably lead to complicated costly computer programs. This is especially true in the case of three-dimensional analysis with moving dynamic loads. Significant simplifications can be achieved by imposing restrictions on the geometries of the pavement system and the load distribution, respectively. Many problems which are actually three-dimensional in space can be reduced with some justification to either plane or axisymmetric problems.

For pavement analysis, the single most effective restriction is to allow semi-infinite horizontally layered models. This restriction effectively reduces the problem from three to two dimensions by utilizing the axisymmetric coordinate. Each layer is infinite in the horizontal directions and has a finite depth, except for the bottom layer which may have an infinite depth. The principle of continuity on primary variables results in continuous contact between each interface of the layered system.

The axisymmetric model assumes that both the pavement geometry and loading are axisymmetric. In particular, the asphalt surface layer must be assumed to be infinitely wide and therefore the edge effect can not be considered. Non-axisymmetric multiple loads can be analyzed by superposition for linear elastic or visco-elastic materials.

4.2.3 Loads

The road response at the surface and vehicle dynamics are essentially uncoupled [16]. This is because (i) the displacement of the road surface is considerably smaller than the deflections of truck tires and suspensions and (ii) the speed of propagation of elastic waves in the road surface is generally significantly faster than the speed of the vehicles. As a result of the weak coupling between the two systems, it is reasonable to assume that the road surface is rigid when simulating the response of a vehicle to road roughness and treat the vehicle as a set of moving dynamic loads when simulating the response of the road surface.

A major challenge to the development of an efficient method for dynamic analysis of pavements is the fact that actual traffic loads move over the surface of the pavement. Tire loading is usually modeled as a circular area with uniform contact pressure. It is assumed that multiple loads that are vertical and uniformly distributed over a circular area are moving along a single direction at a constant velocity on the surface of a layered system. The loads may be constant in magnitude or may vibrate as an arbitrary function of time.

4.3 MOVING LOAD REPRESENTATION

A moving load develops a response even before reaching the point of interest due to such important factors as wave propagation, inertia and damping effects. Thus, the position of moving load with respect to a point of interest is a function of time.

Consider a uniformly distributed load over a circular area, moving at a constant velocity V on the surface of a layered system. The moving load is modeled as a series of haversine pulses with their duration equal to the time required for the wheel to pass by a point in the pavement. In order to consider the moving load effect on the response at a

fixed point x_0 in the pavement, it is necessary to include the effect of the load as it moves from one location in the pavement to the next and beyond the passage of the load by theses consecutive locations in space (either approaching or leaving x_0). Thus the response time history of the pavement at the fixed point x_0 can be obtained as the resultant of the time histories of the responses due to the load being at these consecutive positions in space. This insures continuity of loading in time and space as it moves from one location to the next.

4.3.1 Response to Moving Loads

First, the response at many points along the horizontal direction due to a stationary haversine pulse is calculated. Figure 4.1(a) illustrates the discretized pulse, which consists of a rest period of $A \cdot \Delta t$, where Δt is the time step, a haversine pulse with a duration equal to the time required for the wheel to pass by a point in the pavement, and another rest period of duration $B \cdot \delta t$. The total number of time steps should be a power of 2 in the Fast Fourier Transform algorithm. Figure 4.1(b) shows the response points in relation to the applied stationary load. The loading and all responses are in the same time domain.

From Maxwell's reciprocity theorem, these results can be converted to responses at a fixed point subjected to a single dynamic load at different locations in space. This conversion will make the responses corresponding to the different locations of the load in different time domains. In order to bring all the different responses to the same time domain (to account for a truly moving load as opposed to a quasi-moving influence line,) each response is shifted by a time period corresponding to the passage of the load from one location to the next (equal to the distance between the consecutive locations divided by the vehicle speed.) This is illustrated in Figure 4.2(a) and (b). Figure 4.3 shows the response pulses at a specific location of AC bottom as the load approaches. Note that the response

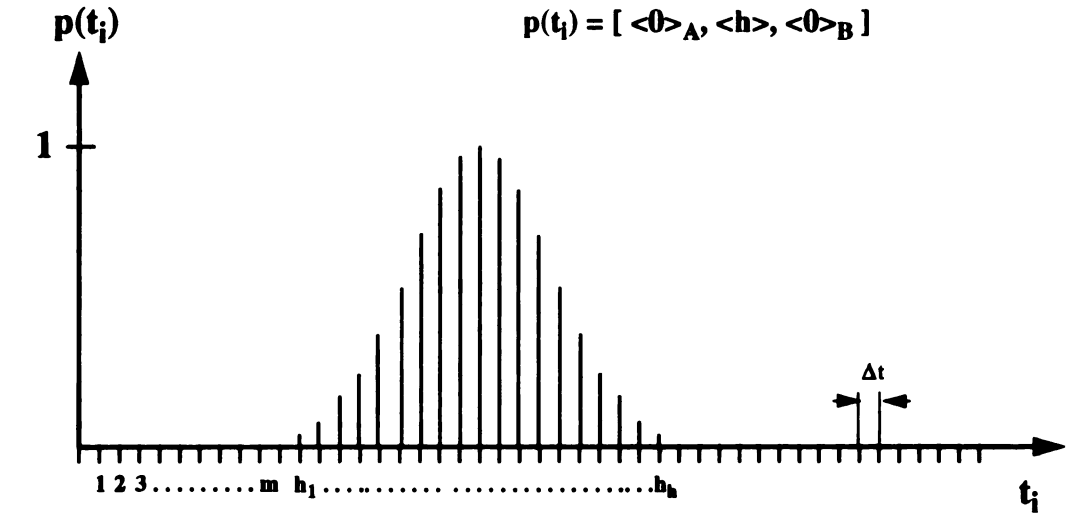

(a)

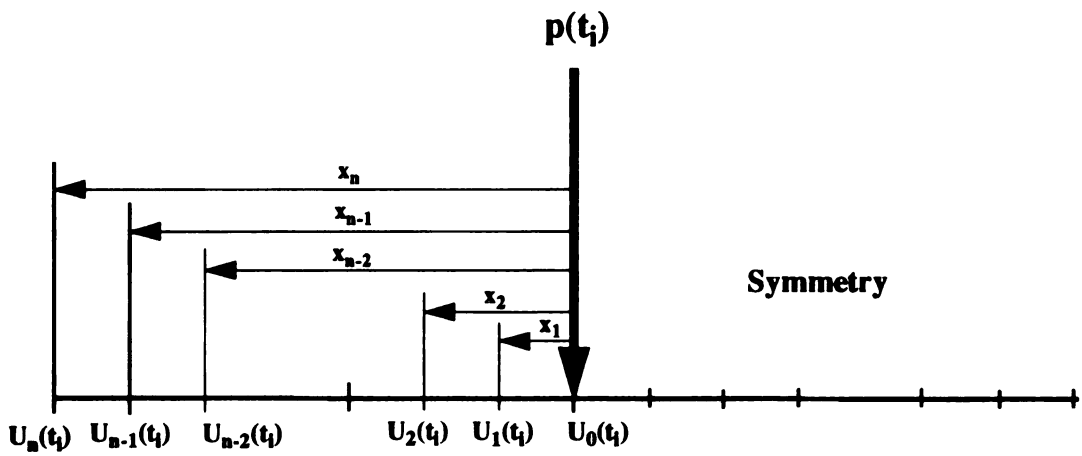

(b)

FIGURE 4.1 Interpretation of Stationary Loading Condition

(a) Discretized haversine pulse

(b) Stationary loading and responses

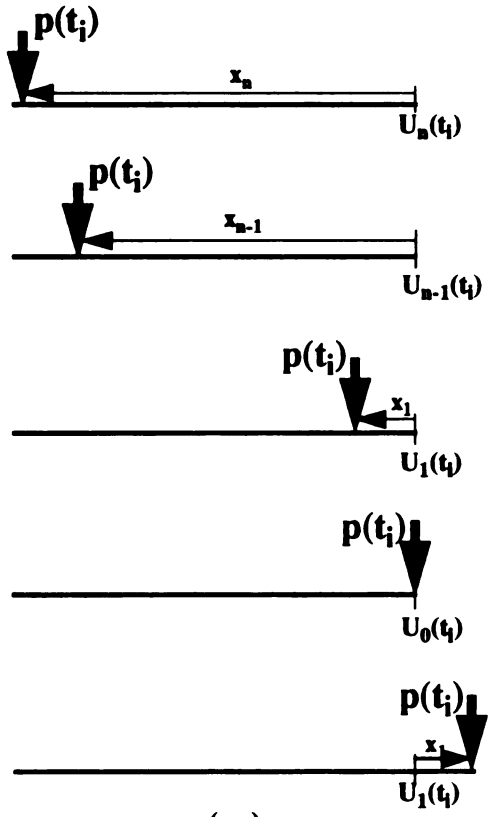

$$\frac{x_n/V}{\Delta t} = \alpha_n$$

$$p(t_i) = [\,<0>_{A-\alpha n},\ <h>,\ <0>_{B+\alpha n}\,]$$

$$U_n(t_i) = [\,<0>_{a-\alpha n},\ <H>,\ <0>_{b+\alpha n}\,]$$

$$\frac{x_{n-1}/V}{\Delta t} = \alpha_{n-1}$$

$$U_{n-1}(t_i) = [\,<0>_{a-\alpha n-1},\ <H>,\ <0>_{b+\alpha n-1}\,]$$

$$\frac{x_1/V}{\Delta t} = \alpha_1$$

$$U_1(t_i) = [\,<0>_{a-\alpha 1},\ <H>,\ <0>_{b+\alpha 1}\,]$$

$$U_0(t_i) = [\,<0>_a,\ <H>,\ <0>_b\,]$$

$$U_{-1}(t_i) = [\,<0>_{a+\alpha 1},\ <H>,\ <0>_{b-\alpha 1}\,]$$

(a) (b)

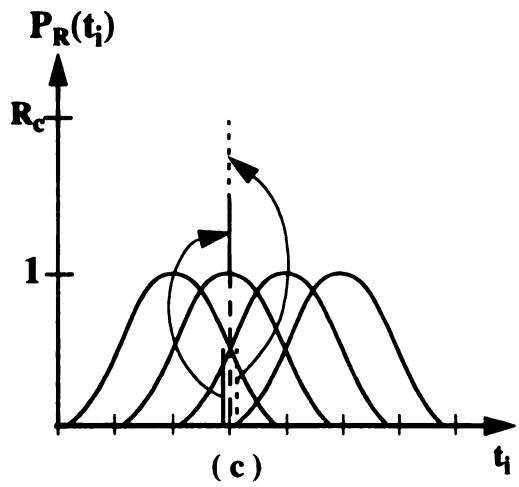

$$P_R(t_i) = [\,<0>_{A-\alpha n},\ <h_R>,\ <0>_{B-\alpha n}\,]$$

$$D_R(t_i) = [\,<0>_{a-\alpha n},\ <H_R>,\ <0>_{b-\alpha n}\,]/R_c$$

(c) (d)

FIGURE 4.2 Interpretation of Moving Load Condition

(a) Quasi-moving loads and responses

(b) Time shift in response to moving load

(c) Sequence of moving load

(d) Resultants of moving load and response

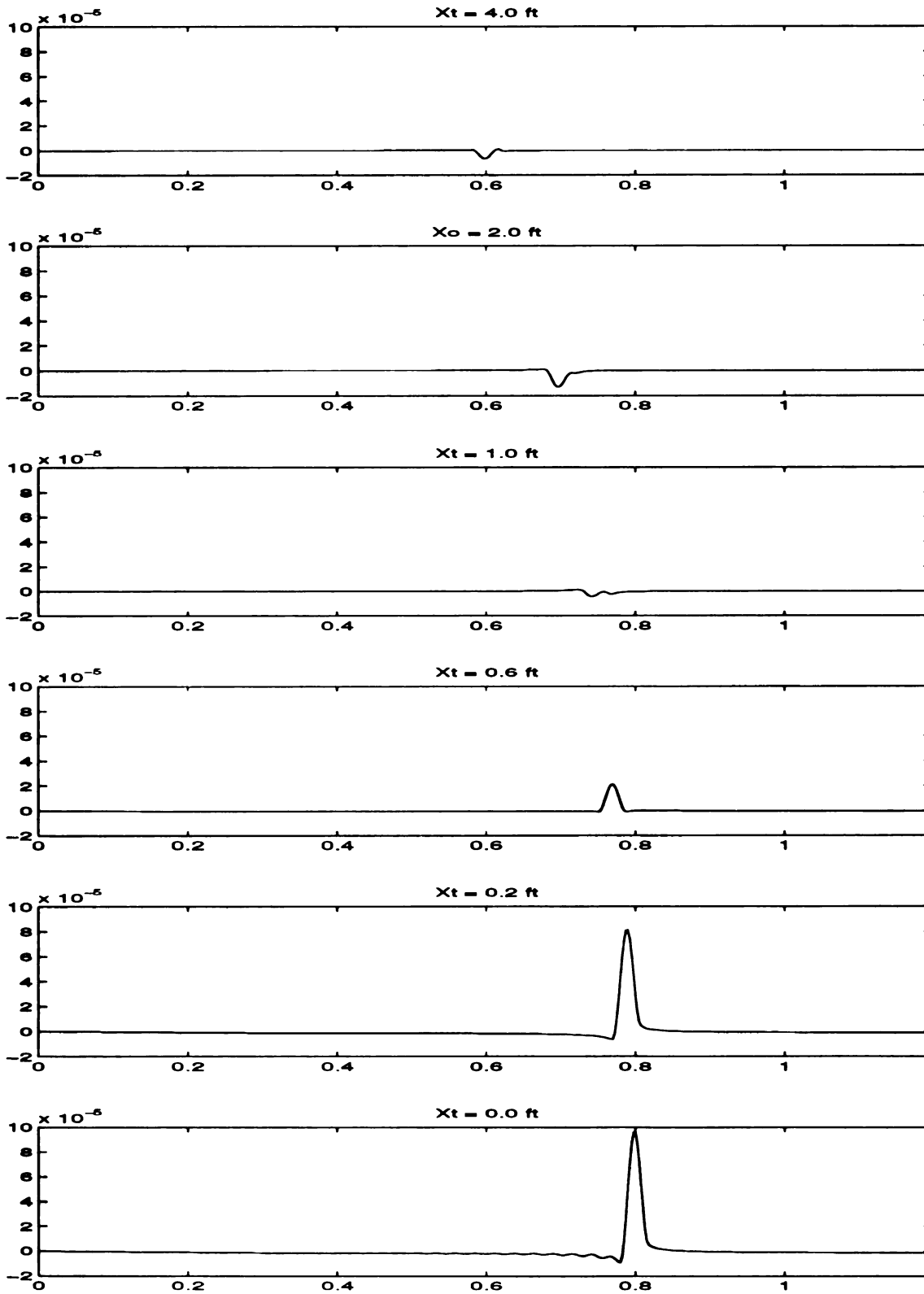

FIGURE 4.3 Response Pulses at a Specific Location of AC Bottom as the Load Approach

becomes larger gradually in compression as the load approaches, but it changes to tension abruptly when the load is near to the specific location of AC. The resultant response is obtained by adding up the response pulses corresponding to each location of the load. However, because the load pulses have a finite width they overlap with each other, as shown in Figure 4.2(c). This translates to an overloading condition. This overloading depends on the duration of the haversine pulse and on the distance between consecutive response points. The resultant response needs to be scaled back by dividing it by an overload factor equal to the sum of contributing loads at a fixed time (see Figure 4.2(d)).

To get a smoother (and more accurate) response, the sequence of response points may be made denser near the load. To account for the distance effect of the moving load the farthest response point should be chosen to be at a far enough distance from the response point in order to consider wave propagation and damping effects.

4.3.2 Response to Moving Constant Loads

Figure 4.4(a) shows the sequence of moving constant load which is discretized at an equal time interval and numbered from left to right as a general coordinate. From the discussion in the previous section, the time history of the response subjected to the moving constant load becomes the following:

$$D_R(t_i) = [U_o(t_i) + U_1(t_i) + \ldots + U_j(t_i) + \ldots + U_N(t_i)]\frac{1}{R_c} \qquad (4\text{-}1)$$

where, $U_j(t_i)$ is the stationary response time history (after time shifting) when the stationary load is applied at location j, N=2*n (n is number of response points in the stationary solution), and R_c is a load factor due to overlapping in time or space domain.

With this method, the model incorporates such important factors as wave propagation, inertia and damping effects of the medium.

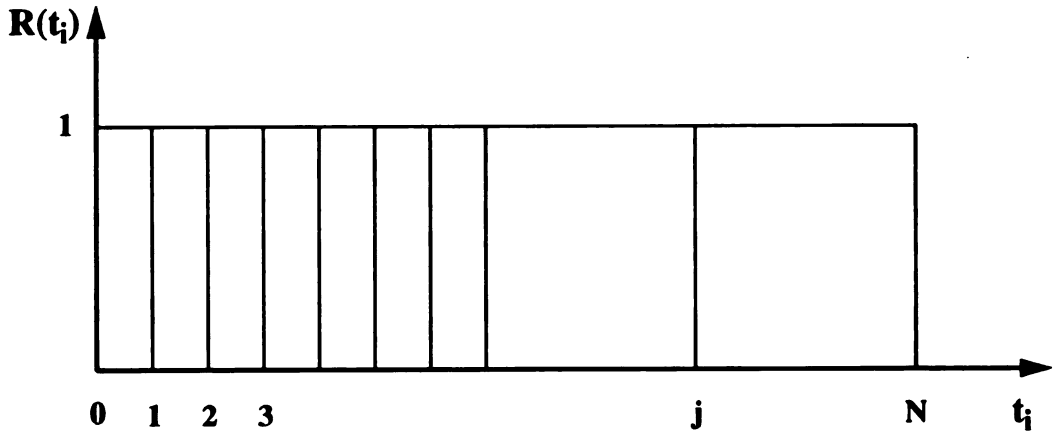

(a)

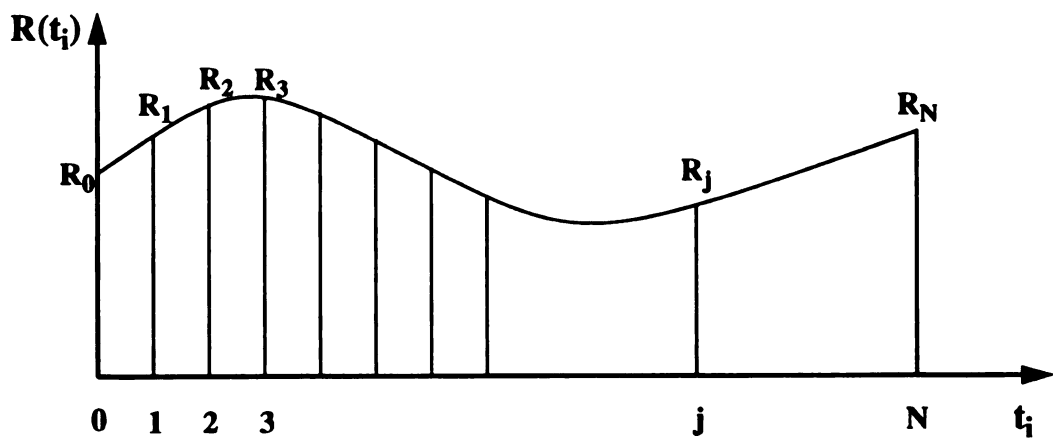

(b)

FIGURE 4.4 Discretized Moving Loads

(a) Moving Constant Load

(b) Moving Arbitrary Load

4.3.3 Response to Moving Arbitrary Loads

Figure 4.4(b) shows the time history of a moving arbitrary load. From the discussion in the previous section, the time history of the response becomes the following:

$$D_R(t_i) = [R_o U_o(t_i) + R_1 U_1(t_i) + \ldots + R_j U_N(t_i) + \ldots + R_N U_N(t_i)]\frac{1}{R_c} \qquad (4\text{-}2)$$

where, R_j is the ratio of dynamic to static load.

With this model, the effect of magnitude variation (vibration) is considered in addition to the factors such as wave propagation, inertia, and damping.

A simplified (quasi-dynamic) solution which accounts for vehicle speed but does not incorporate the effect of loading frequency can be obtained if the time history of the response due to a moving constant load is simply multiplied by the time history of arbitrary loading. Equation (4-3) describes the quasi-dynamic solution for the moving arbitrary load:

$$D_R(t_i) = [U_o(t_i) + U_1(t_i) + U_2(t_i) + \ldots + U_j(t_i) + \ldots + U_N(t_i)]\frac{R(t_i)}{R_c} \qquad (4\text{-}3)$$

This expression is some what different from Equation (4-2) in the sense that the effect of magnitude variation is not considered instantaneously. This quasi-dynamic solution was obtained for the purpose of comparison with the real dynamic solution. Note that when multiple loads are applied the multiplication of the response time history for a moving unit load by the arbitrary load time history should be prior to the superposition of the responses due to the multiple loads.

4.4 SAPSI-M COMPUTER PROGRAM

A computer program, SAPSI-M, has been written in the Fortran 77 language for the analysis of asphalt concrete pavements subjected to moving dynamic loads. The program is an extension of the stationary program SAPSI, which was developed by Chen [21] at the University of California-Berkeley. The computer program has the following characteristics:

(1) The steady-state solutions for fixed frequencies can be obtained and stored.

(2) The stationary transient solution can be obtained and stored from the steady-state solutions and using an efficient interpolation scheme.

(3) The moving dynamic solution can be obtained from the above results.

Figure 4.5 shows the flow chart of the SAPSI-M program. This section will be dedicated to the description of program layout and both steady-state and moving load solution algorithm. Uses and limitations are also discussed.

4.4.1 Program Layout

SAPSI-M has ten main subroutines. In a typical run, not all of these subroutines may be used, depending on the option chosen by the user. A number of these are "sister" subroutines which can be grouped together due to their interaction. A brief description of the function of each subroutine and its interaction with other subroutines is presented in the following:

A. AFFT

Subroutine AFFT is used only when the transient solution is required. It arranges for the performance both of the forward transformation of the input load vector from the time domain to the frequency domain using the Fast Fourier Transform algorithm and of the backward transform of the solution displacement vector from the frequency domain

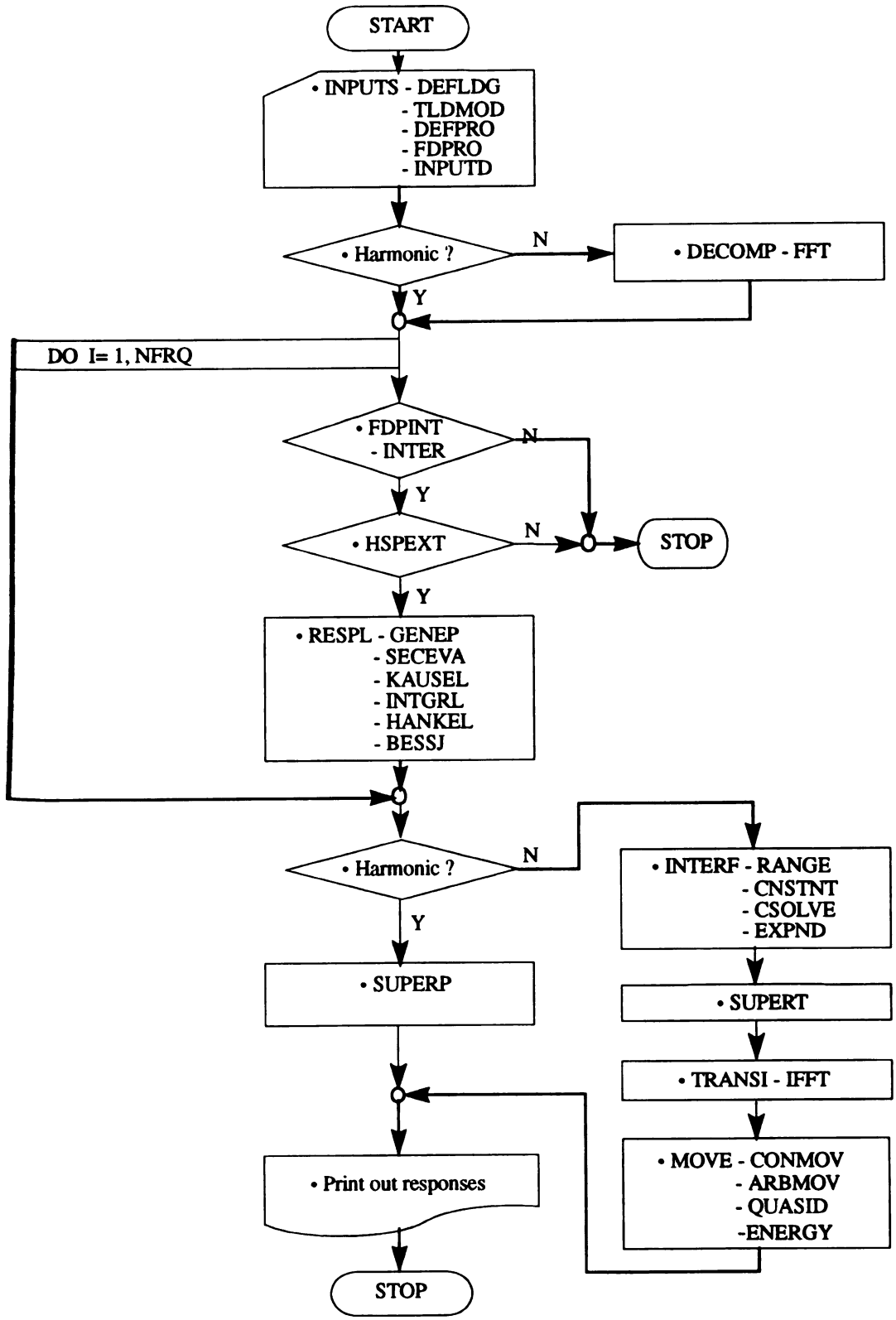

FIGURE 4.5 The Flow Chart of SAPSI-M Program

back to the time domain using the inverse FFT. This subroutine has the sister subroutines FFT, RFFT, and RFSN.

B. DECOMP

Transient dynamic analysis is used to determine the dynamic response of a structure under the action of any general time-dependent loads. Subroutine DECOMP is used only when the transient solution is required and the input load data are given in the time domain. It decomposes the dynamic loads into harmonic components to obtain the complex amplitude using Fast Fourier Transform algorithm.

C. FDPINT / HSPEXT

Subroutine FDPINT verifies that the desired frequencies are within the input data of the profile and interpolates material properties from the input material data file using of linear/linear, linear/log(freq.), log/linear(freq.) or log/log relationships within the subroutine INTER. Subroutine HSPEXT checks the input data on the sublayers and simulates the half-space using Newton's iteration method. The layered system is extended by n-additional layers having properties equal to those of the half space, according to the Variable Depth Method [20]. Refer to the section that describes the "theory" behind it.

D. INPUTS

The program SAPSI-M can be run interactively with the aid of menus to be shown on the screen of the monitor. The input data may be created directly from the keyboard or read from the existing files and they can also be modified and saved in either the old file or a new file.

Subroutine INPUTS controls the main input information of loading, configuration and profile of layers, and output informations. Thus, it has many sister subroutines. The sister subroutine CONPAR controls parameters such as frequency-dependent properties,

half space simulation, viscous dashpots on lower boundary and eigenvalue solution. For the loads information, subroutine INPUTS has sisters subroutines such as DEFLDG (define load type such as harmonic or transient), HLDMOD (read harmonic load information such as radius and location) and TLDMOD (input for transient load, and specify the desired frequencies of steady-state solutions). For the layer information, it has sister ones such as DEFPRO (define profile such as directory and status), FILMOD (read a frequency independent profile and modify it as necessary), FDPRO (read a frequency dependent profile), and INPUTD (print input data of materials). Sister subroutine OUTREQ defines response components desired and locates the points where the displacements and stresses are desired.

E. INTERF

The interpolation technique [107] interpolates the steady-state responses for specified frequencies and obtains the response for all frequencies. The technique is based on the frequency response function of a two-degree-of freedom system. Subroutine INTERF is used only when the transient solution is required. The subroutine RANGE computes the number of frequency ranges to be interpolated. The steady-state responses are recalled by subroutine READTP from a temporary file, and the subroutine CNSTNT computes interpolation constants for each frequency range with the aid of subroutine CSOLVE. Subroutine EXPND expands the amplification vector to all frequencies.

F. MAINE

Subroutine MAINE arranges the main flow of the program for computation of desired responses in either steady-state or transient analyses. It calls subroutines such as FDPINT, HSPEXT, RESPL and SUPERP in the steady-state case. In the transient case, MAIN calls DECOMP, RANGE, INTERF, SUPERT and TRANSI in addition to the subroutines that are required to compute the steady-state response.

G. MOVE

Subroutine MOVE contains the moving load solution, which computes the time history of the pavement response when subjected to moving constant or arbitrary loads. Subroutine CONMOV and ARBMOV calculate the response due to multiple constant and arbitrary moving loads, respectively, while QUASID calculates the quasi-dynamic response to moving arbitrary loads. Refer to section 4.3 for the detailed solution.

H. RESPL

This subroutine the main subroutine which computes the steady-state response. It calls a number of subroutines, including GENEP, SECEVA, KAUSEL, HANKEL, INTGRL and BESSJ. Subroutine GENEP initiates the eigenvalue problem. Subroutine SECEVA solves the eigenvalue problem using the generalized Rayleigh quotient iteration method as proposed by Wass [118]. Subroutine KAUSEL calculates displacements and stresses for the given layered system to uniformly distributed vertical circular pressure based on modified Kausel's solution. Subroutine HANKEL computes the Hankel function for Kausel's solution. Subroutine INTGRL calculates the first and second Kausel solutions. Subroutine BESSJ calculates the Bessel functions by polynomial approximation for Kausel's solution.

I. SUPERP / SUPERT

If the layered system is subjected to multiple loadings, the responses computed in the frequency domain are combined before they are transformed back to the time domain. Since the responses due to each loading are computed in local cylindrical coordinates, they have to be transformed into global cartesian coordinates prior to combination. These superpositions are done using SUPERP and SUPERT subroutines for steady-state and transient solutions, respectively. The results of SUPERP are printed in the main output file, but those of SUPERT are saved in a temporary files for future use.

J. TRANSI

Subroutine TRANSI is used only when the transient solution is required. This subroutine obtains and prints out the maximum global responses of the transient solution in the time domain from the expanded interpolation results using the inverse Fast Fourier Transform algorithm.

4.4.2 Algorithm

4.4.2.1 Steady-State Solution

The algorithm used for the steady-state solution is shown in Figure 4.6. Note that all analysis procedures are executed in the frequency domain. Basically, the following steps are undertaken:

(1) • Input the harmonic load information such as radius and locations.
- Input the profile of the layered systems.
- Input the requested output points and the desired frequencies of analysis.

(2) • Verify that the desired frequencies are within the input data of the profile.

(3) • Check input data on the sublayers to ensure that the sublayers in the simulated half-space are increasing.
- Create additional layers for half-space simulation by Newton's iteration method.

(4) • Initiate the generalized eigenvalue problem.
- Solve the eigenvalue problem by the Wass method.
- Compute Hankel and Bessel functions for the modified Kausel solution.
- Compute Green's function for a given layered system to uniformly distributed vertical circular pressures.

(5) •Transform the responses into the global coordinate system prior to combination.
- Superpose the responses and print out the global responses.

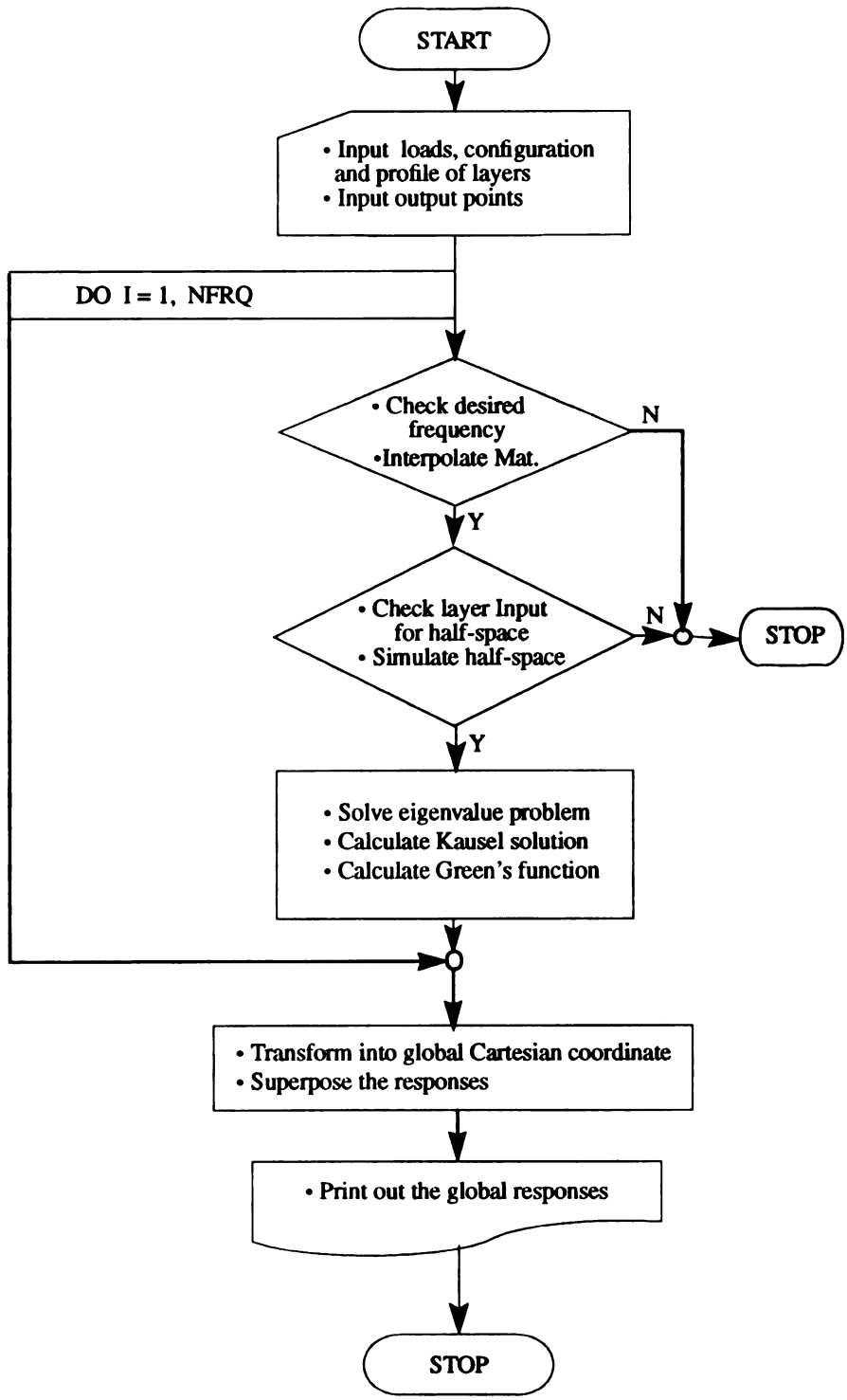

FIGURE 4.6 Algorithm for Steady-State Solution

4.4.2.2 Moving Load Solution

The algorithm used for the moving load solution is shown in Figure 4.7. Note that the basic analysis obtaining Green's function is executed in the frequency domain. The response is then converted back to the time domain to obtain the transient solution. Basically the following steps are undertaken:

(1) • Input the time load history and load information.
- Input the profile of layered systems.
- Input the requested output points and the desired frequencies.

(2) • Decompose the general dynamic load time history into complex harmonic components using the FFT algorithm.

(3) • Verify that the desired frequencies are within the input data of the profile.

(4) • Check input data on the sublayers to ensure that the sublayers in the simulated half-space are increasing
- Create additional layers for half-space simulation by Newton's iteration method.

(5) • Initiate the generalized eigenvalue problem.
- Solve the eigenvalue problem by Wass's method.
- Compute Hankel and Bessel functions for modified Kausel solution.
- Compute Green's function for a given layered system to uniformly distributed vertical circular pressure.

(6) • Calculate the interpolation function from the steady-state response at specified frequencies.
- Expand the interpolated results into all frequencies.
- Multiply the above results by the complex amplitude of the load.

(7) •Superpose the responses in the frequency domain.

(8) • Obtain the global responses in the time domain by inverse FFT.

(9) • Calculate the response time histories at a specified location subjected to moving constant or arbitrary multiple loads, as developed in this study.

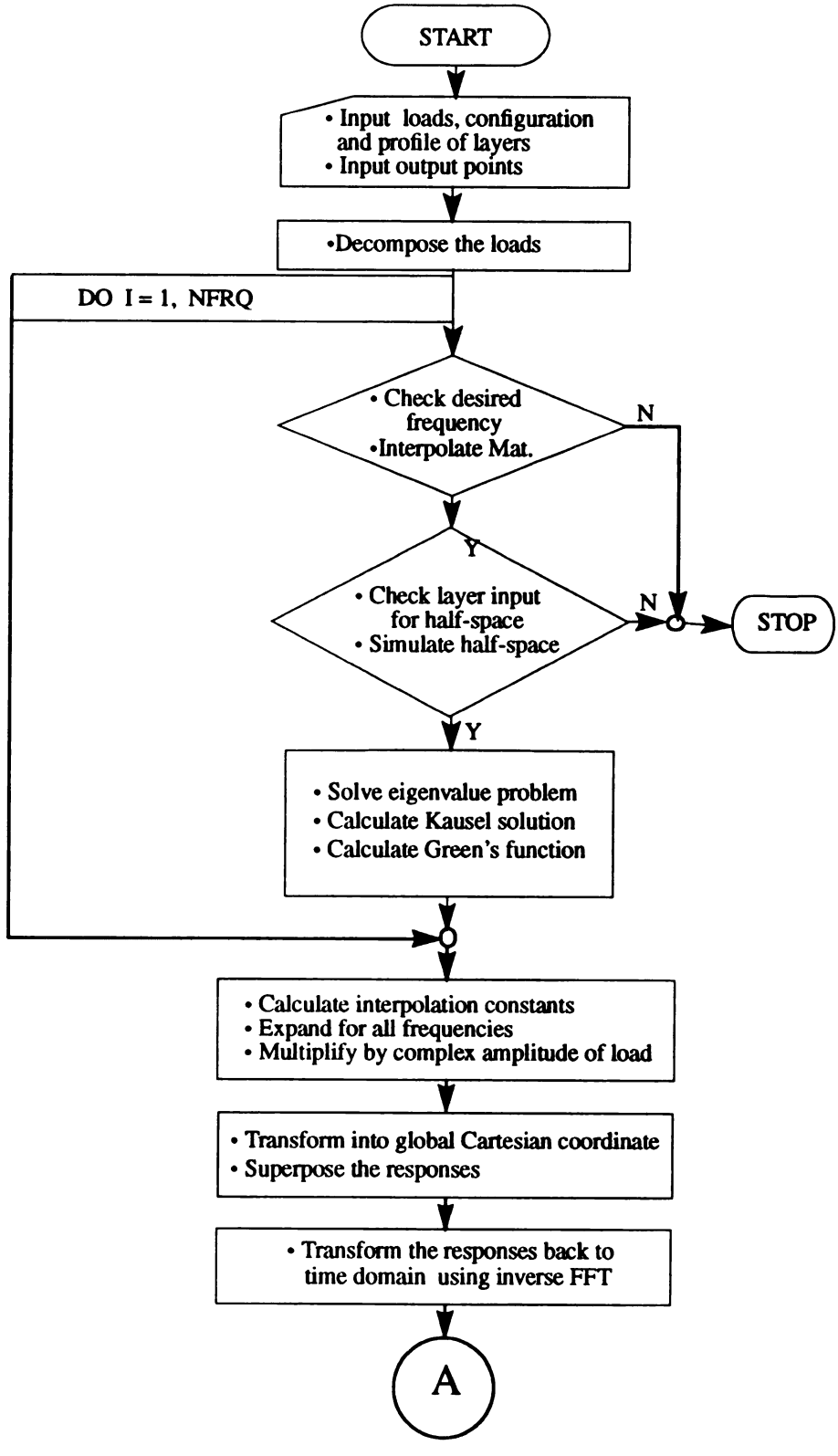

FIGURE 4.7 Algorithm for Moving Load Solution

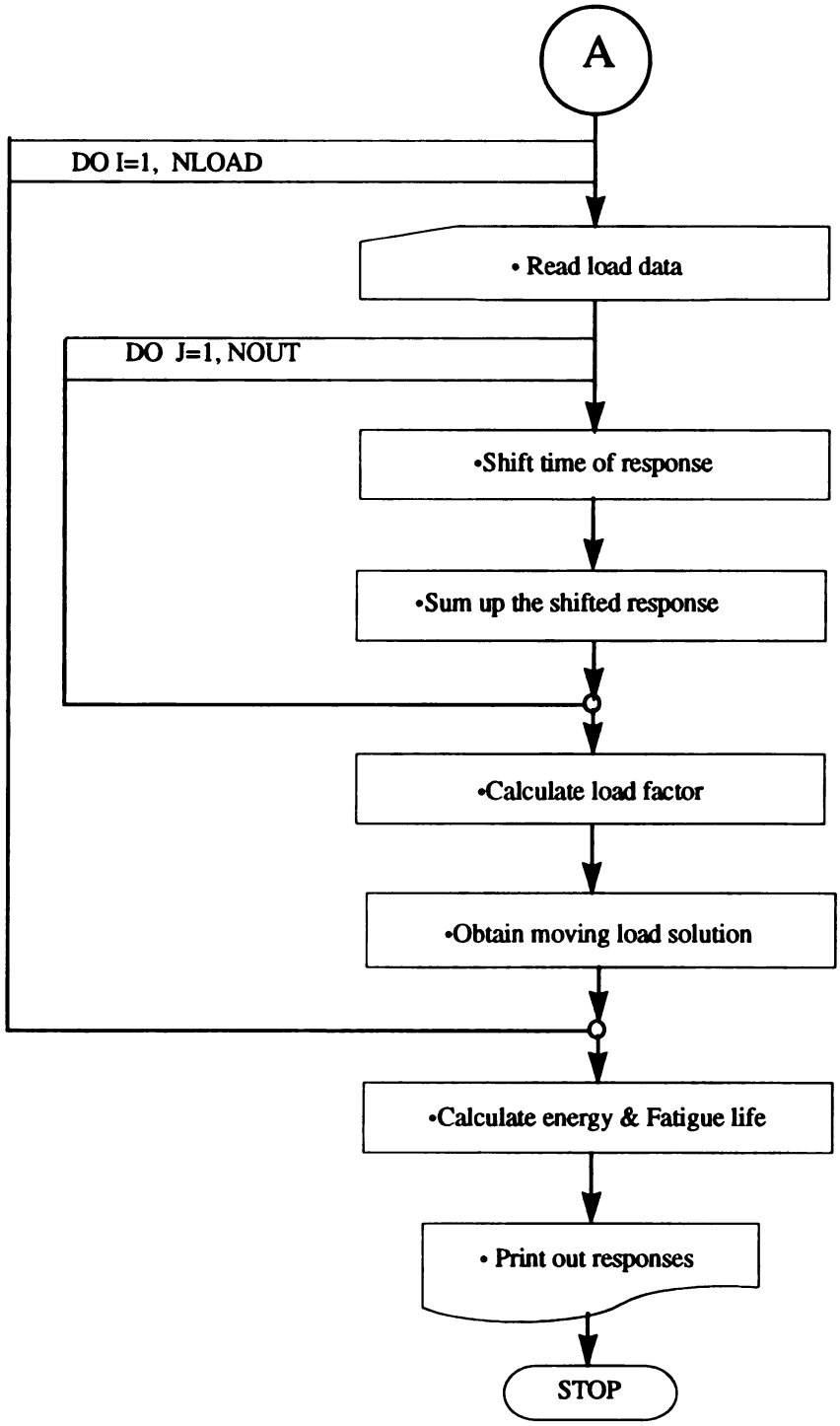

FIGURE 4.7 Algorithm for Moving Load Solution (cont'd)

4.4.3 Uses and Limitations

The proposed model contains a new solution for the dynamic analysis of asphalt concrete pavements under moving fluctuating loads. The structural model is a n-layered damped-elastic medium. The subgrade can be modeled as either a rigid base or a semi-infinite halfspace. The loads are surface pressure loads, and the analysis is under axisymmetric conditions. The moving loads are modeled as a series of pulses with a duration equal to the time required for the wheel to pass by a fixed point in the pavement.

Some limitations on the use of the model should be mentioned. This model requires a relatively large computer memory and running time to conduct the analysis. The preparation of the input data requires some effort and knowledge of dynamic analysis and pavement properties on the part of the user. It is always recommended to follow the guidelines in the manual provided in Appendix B. The capabilities and limitations of the computer program SASPI-M are listed below.

4.4.3.1 Capabilities

(1) Calculates the steady-state response at any frequency.

(2) Calculates stationary transient response.

(3) Calculates the response to multiple moving arbitrary loads.

(4) The shear modulus, damping ratio, and Poisson's ratio for each layer may be varied with the excitation frequency of the loads.

(5) Multiple loadings are acceptable for both harmonic and transient cases and each loading may have a different radius and time history.

(6) A static load can be simulated by specifying a harmonic load with zero excitation frequency.

4.4.3.2 Limitations

(1) SAPSI-M deals only with a layered system subjected to uniformly distributed circular loads.

(2) It does not calculate the response at zero frequency when using the half space simulation; instead the analysis needs to be done at near zero frequency (0.001 Hz).

(3) It does not use a cutoff frequency after which the response would be set to zero. This concept is very useful when we know that the response is essentially zero after a certain frequency (i.e contained within a certain frequency range). Had SAPSI have this option, the user would be able to use small frequency steps (for accurate interpolation in the frequency domain) with a limited number of frequencies, while keeping the time step small enough for a smooth response in the time domain.

(4) The interpolation scheme in SAPSI-M needs a minimum of five frequencies in a particular frequency range and a maximum of 64 frequencies.

(5) Often SAPSI-M would give an error message ("Real indefinite...") which halts the execution. This is due to the fact that the solution is pseudo-exact and may "blow-up" at certain frequencies. All that one needs to do is to shift the frequency at which the response is being computed by one or a few frequency steps. In the case of transient loading, this can occur at different frequencies.

5.1 I

measu

ysis w

to mov

the re

ificati

CAR

PACC

They

layer

199

(Ma

5.2

ses

5.2.

exar

CHAPTER 5

FIELD VERIFICATION

5.1 INTRODUCTION

Very few pavement response models have been validated by comparison with field measurement as discussed by Hardy and Cebon [40]. They, also, pointed out that no analysis was found in the literature of the dynamic response of a realistic layered road model to moving steady or random forces.

In this chapter, previous studies on full-scale field tests are briefly reviewed, and the results of SAPSI-M will be compared with field data. The field tests used for field verification involve a full scale asphalt concrete pavement section on a test track in the PACCAR Technical Center in Mount Vernon, Washington. The tests conducted at the PACCAR Test Track facility took place at different times during 1991, 1992 and 1993. They included Falling Weight Deflectometer (FWD) tests for both back-calculation of layer moduli and comparison of strain data (October 1991, June 1992, and February 1993), some preliminary truck tests to check the measurement and data acquisition system (May 1992), and the formal series of full-scale truck tests (September/October 1993).

5.2 PREVIOUS FULL-SCALE FIELD TEST STUDIES

This section describes existing flexible pavement test facilities and previous analyses of pavement responses due to truck loads.

5.2.1 Test Facilities

Several pavement test facilities have been built since the 1950's for the purpose of examining the correlation between theoretical predictions and measured results in real

pavements under actual loads. The various test facilities can be either linear or circular test tracks or test roads with controlled or uncontrolled loading. In most of the test facilities, the construction was controlled to allow instrumentation to be installed during the construction phase. Only a relatively small number of experiments have been conducted using instrumentation retrofitted into an existing pavement. In addition, only a few experiments applied loads from real full-scale trucks [123].

The advantage of full-scale testing include the following; (1) Excellent simulation of field conditions, (2) Possibility of examining the effect of change in the pavement structural section on pavement performance, (3) One test track allows the study of other forms of pavement distresses in addition to fatigue. The disadvantages include the following: (1) The initial investment cost and annual operation and maintenance costs are very high, (2) A parallel, supplementary laboratory testing program is still needed, since the field track tests do not directly measure fundamental mixture properties.

In order to obtain full-scale field simulation, circular and longitudinal test tracks have been designed and constructed in a number of different countries. Well-known examples include the circular tracks located at Nantes, France, and at Pullman, near the Washington State University, and the Federal Highway Administrations ALF (Accelerated Loading Facility). Other examples of full-scale tracks include those in Australia (ARRB), United Kingdom (TRRL), New Zealand (Canterbury), Denmark, and OECD Group (Organization for Economic Cooperation and Development represented by 12 countries).

5.2.2 Previous Flexible Pavement Tests

Winters [123] provides a good review of the published research on full-scale flexible pavement experiments. A summary of the major tests is contained in Table 5.1. The type of test facilities include linear track, circular test track, test road, test pit, and in ser-

TABLE 5.1 Summary of Various Instrumented Flexible Pavement Tests [123]

Reporting Agency (Reference)	Test Location	Type of Facility	Type of Strain Instrumentation	Strain Responses Measured	Pavement Structure (inches)	Type of Loading for Testing	Load Magnitude (pounds)	Source of Theoretical Computation	Year of Testing	Exposed to Normal Traffic
California Division of Highways (Zube [4])	Northern California	Linear Test Track and Test Road	SR-4 strain gauges glued to surface or placed in carrier block	Transverse at surface and bottom of AC	Six Total Sections 1: AC 3.75, BS 8.0 (CTB) 2: AC 6.75, BS 6.0 3: AC 3.75, BS 12.0 4: AC 3.0, BS 9.0 5: AC 3.0 New plus 2.0 Old, BS Variable 6: AC 2.0, BS 4.0	Duals and super single - 2 axle truck	3000 to 9000 per wheel	Boussinesq equations	1963	Yes
Dutch Road Research Centre (Nijboer [26])	Highway 1	Test Road	Strain gauge attached to a thin slab of sand asphalt	Radial at surface and bottom of AC	AC: 7.5 BS: None	Single wheel loads	2804 to 4847	Burmister 2 - layer	1967*	Yes
Shell Laboratory (Gusfeldt [29])	Hamburg, Germany	Linear Test Track	Gauge stuck to asphalt carrier block	Radial strain at various depths in AC	AC: 5.5 BS: 33.9	Linear test apparatus (single tire)	880 to 4400 per wheel	Jones' tables of stresses in 3 layer elastic system	1967*	No
Shell Research N.V. (Klomp [30])	Highway 1	Test Road	6.90 ohm electrical resistance	Horizontal at surface and various depths in AC (0-5.5 in.)	AC: 1.2 BS: 6.7 (ATB)	Single front wheel of a loaded truck	2818 to 4862 per wheel	Jones' tables of stresses in 3 layer elastic system	1967*	Yes
Shell Laboratory (Dempwolff [28])	Hamburg, Germany	Linear Test Track	Wire gauges glued into asphalt carrier blocks	Transverse and Longitudinal at various depths in the AC	AC: 8.7 Section I (Dense) Section II(Open) BS: 11.8	Linear test apparatus (single tire)	1100 to 4400 per wheel	BISTRO	1967-69 1972*	No
Nihon Univ, Japan (Miura [31])	Tomei Highway (between Tokoyo and Nagoya)	In service pavement	Electric resistance gauges molded by epoxy and polyester resin	Transverse and Longitudinal at various depths in the AC	AC: 3.9 BS: 7.1 (ATB) SB: 6.7 (CTB)	Dual wheel loads	6600 to 15,400 per wheel	Burmister (single and dual circular loading)	1972*	Yes
National Institute for Road Research, South Africa (Freeme [11])	Special Road 12/2, South Africa	In service pavement	Strain meters developed by Road Research Lab in the UK	Tensile strain at the bottom of the AC	AC: 1.0, 2.0, 3.9 (Dense and Open Grade) BS: 11.8 SB: 3.9 (LTB)	2 axle single wheel truck	2565 to 8370 per wheel	Chevron computer program	1972*	Yes

TABLE 5.1 Summary of Various Instrumented Flexible Pavement Tests (Cont'd) [123]

Reporting Agency (Reference)	Test Location	Type of Facility	Type of Strain Instrumentation	Strain Responses Measured	Pavement Structure (inches)	Type of Loading for Testing	Load Magnitude (pounds)	Source of Theoretical Computation	Year of Testing	Exposed to Normal Traffic
Koninklijke/Shell -Laboratorium (Valkering [32])	E8 Motorway, Netherlands	Trial Section	Strain gauge type not reported	Longitudinal and transverse at surface and transverse at 2.8 in depth	Section I AC: 8.3 BS: 7.1 (CTS) Section II AC: 11.0 BS: None	Wheel of a skid measurement system	450	BISAR	1972*	Yes
Royal Military College; Ontario Ministry of Transportation and Communication; Gulf Canada, Ltd.; Univ of Waterloo (Halim [33])	Royal Military College, Kingston	Test Pit	Foil type gauges bonded to top and bottom of plastic mesh; Mastic strain carriers (ARC) with two 120 ohm gauges embedded in mastic plate	Horizontal tensile strains at mesh and bottom of AC	AC: 4.5 to 9.8 (with and without plastic mesh) BS: None SG: Dry and saturated	12 in. diameter rigid circular plate	2250 to 9000	BISAR	1983*	No
Laboratoire Central des Ponts et Chaussées (LCPC) (Autret [34])	Nantes, France	Circular test track	H-gauges glued to aluminum or plexiglass backing	Horizontal strain at bottom of AC and vertical strain at top of SG	Ring B_0- Section 1 AC: 2.0 BS: 17.7	Accelerated loading device (ALD) with 4 half axles	22,500 and 29,250 per axle	ALIZE III computer program	1984	No
Organization for Economic Cooperation and Development (OECD) (Scazziga [35])	Nardò, Italy	Linear test track	H-gauges, gauges glued into carrier blocks, core gauges	Horizontal strain at a depth of 2.0 in. and at bottom of AC	AC: 5.1 BS: 6.7	2 axle truck	Front axle: 12,155 Rear axle: 25,636	Method of Equivalent Thickness (MET)	1984	No
FHWA (Bonaquist [36])	Turner-Fairbank Highway Research Facility	Linear test track	Gauge type not reported	Surface and bottom of AC	Lane 1 AC: 5.0 BS: 5.0 Lane 2 AC: 7.0 BS: 12.0	Linear ALF (one half of a dual tire single axle)	9400, 14,100 and 19,000 per half axle	ELSYM5	1988*	No
Ministry of Transport, The Netherlands (Dohmen [37])	Road and Railroad Research Laboratory	Linear test track	Dynatest strain transducer and TML embedment gauges	3 inches above bottom of AC	AC: 4.7, 7.1, and 9.4 BS: None	FWD	11,250	BISAR	1992*	No
Dutch Team, FORCE Project, OECD [38]	LCPC, Nantes, France	Circular test track	TML embedment strain gauges	Radial strain at bottom of AC	AC: 5.5 BS: 11.0	ALD (half axle)	12,938 per half axle	BISAR	1989 1991*	No

TABLE 5.1 Summary of Various Instrumented Flexible Pavement Tests (Cont'd) [123]

Reporting Agency (Reference)	Test Location	Type of Facility	Type of Strain Instrumentation	Strain Responses Measured	Pavement Structure (inches)	Type of Loading for Testing	Load Magnitude (pounds)	Source of Theoretical Computation	Year of Testing	Exposed to Normal Traffic
Ministry of Transport, The Netherlands (Dohmen [37])	LCPC, Nantes, France	Circular test track	TML embedment gauges	Bottom of AC	Section 01 AC: 4.8 BS: 11.0 Section 02 AC: 5.5 BS: 11.0	FWD	13,500 and 16,875	BISAR	1989 1992*	No
Ministry of Transport, The Netherlands (Dohmen [37])	Road and Railroad Research Laboratory	Linear test track	Gauge type not reported	Longitudinal and transverse at bottom of AC	AC: 5.9 BS: None	FWD	Not reported	3 layer system	1992*	No
Ministry of Transport, The Netherlands (Dohmen [37])	Road and Railroad Research Laboratory	Linear test track	Gauge type not reported	Longitudinal and transverse at bottom of AC	AC: 5.9 BS: None	LINTRACK Super singles and duals (half axle)	11,250 per half axle	BISAR	1992*	No
FHWA (Sebaaly [39])	Pennsylvania Transportation Institute	Linear test track	Dynatest H-gauge Kyowa gauge ARC gauge Core gauge	Bottom of the AC	Thin AC: 6.0 BS: 8.0 Thick AC: 10.0 BS: 10.0	Single drive axle tractor with a tandem axle semitrailer	3760 to 20,820 per axle	PENMOD	1989 1992*	No
Royal Institute of Technology, Sweden (Lenngren[24])	Road and Traffic Laboratory, Finland	Linear test pavement	Core gauges	Horizontal at bottom of AC	Thin Section AC: 3.1 BS/SB: 24.4 Thick Section AC: 5.9 BS/SB: 21.7	FWD	2813, 5626, and 11,250	BISAR and CLEVERCALC	1989 1991*	No
Cambridge Univ. (Hardy [40])	Transport and Road Research Lab	Test section	Metal foil gauges	Transverse at bottom of AC	AC: 7.9 BS: 11.8	Four - axle articulated vehicle	Not reported (based on dynamic load)	Convolution Theory	1992*	No

Notes:

AC = Asphalt Concrete
BS = Base Course
SB = Subbase
CTB = Cement treated base
ATB = Asphalt treated base
CTS = Cement treated sand
SG = Subgrade
LTB = Lime treated base
* = Year reported in literature

vice pavements. Loading conditions included circular plate loading, accelerated loading devices (ALD), linear test apparatus, multi-axle trucks, and falling weight deflectometer (FWD). A variety of strain gauges have been used including, wire gauges, electric resistance gauges, H-gauges, foil-type gauges, dynatest strain transducer, and core gauges. Measured responses included longitudinal and transverse strains at the top, bottom, and at various depth of the asphalt concrete layer. Theoretical predictions of pavement response were obtained from closed-form solutions such as Boussinesq equation, Burmister equation and Jone's table of stresses in 3 layer elastic system, and from numerical computer models based on layered elastic theory such as BISTRO, CHEVRON, BISAR, ELSYM5, and CLEVERCALC. Table 5.2 summarizes these ranges of experimental conditions including source of loading, load magnitude, pavement structure, gauge type, and theoretical computation [123].

The review showed several examples of acceptable agreement between measured and calculated strains in the asphalt concrete layer. Some field tests showed unacceptable agreement between measured and calculated strains without any reasonable explanation. The following observations were drawn from the review [123]:

(1) Reasonable agreement between measured and calculated strains translates to a difference of about twenty percent.

(2) The longitudinal and transverse strains are not equivalent in general; this could be due to the distribution of contact tire pressures in the case of truck tests, to misalignment between plate and gauge in the case of FWD tests, or to the anisotropy of asphalt pavement in.

(3) The effect of the thickness of the asphalt concrete layer is not significant, however the location of the strain gauge relative to the bottom of the layer is critical.

(4) The effect of lateral offset between the position of the loading and the strain gauge is very significant.

TABLE 5.2 Range of Experimental Conditions from Various Instrumented Flexible Pavement Tests [123]

Source of Load [Reference(s)]	Load Magnitude (pounds)	Pavement Structure (inches)	Gauge Type	Theoretical Comparison
Plate Loading from a Hydraulic Actuator [33]	2250 to 9000	AC: 4.5 to 9.8 BS: None	Foil gauges and mastic carriers	BISAR
FWD [24, 37]	2813 to 16,875	AC: 3.1 to 9.4 BS: 0 to 11.0	Core, TML, Dynatest	BISAR, CLEVERCALC
Single Wheel Loads (vehicular) [4, 11, 26, 30, 32, 35,]	450 to 9000 per wheel	AC: 1.0 to 11.0 BS: 0 to 33.9 CTB, ATB, CTS SB: 0 to 3.9 (LTB)	SR4, SR4 in carrier blocks, gauges attached to sand asphalt, electric resistance, UK strain meters	Boussinesq, Burmister 2-layer, Jones' Tables, Chevron, BISAR
Dual Wheel Loads (vehicular) [4, 31, 35]	5000 to 15,400 per wheel	AC: 2.0 to 10.0 BS: 4.0 to 12.0 CTB, ATB SB: 0 to 6.7	SR4, SR4 in carrier blocks, electric resistance molded by epoxy and polyester resin, H-gauges, gauges in carrier blocks, core, Kyowa, ARC	Boussinesq, Burmister, MET, BISAR, PENMOD
Single Wheel ALF [28, 29, 37]	880 to 11,250 per wheel	AC: 5.5 to 8.7 Open, Dense BS: 0 to 33.9	Gauges in carrier blocks	Jones' Tables, BISTRO, BISAR
Dual Wheel ALF [34, 36, 37, 38]	9400 to 19,000 per set of duals	AC: 2.0 to 7.0 BS: 0 to 17.7	H-gauges glued to aluminum or plexiglass backing, TML	ALIZE III, ELSYM5, BISAR

5.3 DESCRIPTION OF PACCAR FIELD TEST

A series of full-scale field tests of a flexible pavement section were conducted at the PACCAR Technical Center in Mount Vernon, Washington, about sixty miles north of Seattle, from October 1991 to September 1993. It consisted of falling weight deflectometer (FWD) and truck tests. The plane view of PACCAR test track is shown in Figure 5.1.

5.3.1 Test Section

The pavement test section is a flexible pavement with a 5.4 inch surface layer of dense graded asphalt concrete (AC, WSDOT Class B) over a 13 inch crushed stone base. The subgrade is a sandy clay. The average cross section of the PACCAR is shown in Figure 5.2. The water table was measured at a depth of 5.5 ft during installation of the instrumentation. Fifteen cores were taken from the section for installation of the instrumentation. These cores were used to evaluate thicknesses and conduct density tests. Based on the results the AC layer is relatively homogeneous and of generally uniform thickness. The instrumented section is approximately 14 ft wide and 40 ft long. It is closed to traffic except during scheduled pavement testing.

5.3.2 Instrumentation

A foil-type gauge manufactured by Micro-Measurement was used to measure the various strain responses. An Australian-made Multi-depth Deflectometer (MDD) with four linear variable differential transformers (LVDTs) was used to measure pavement layer deflections. For temperature data, a multi-sensor temperature probe manufactured by Measurement Research Corporation was used.

A total of 102 strain gauges were installed in the pavement section: Twenty (20) gauges were installed in five axial cores to measure longitudinal and transverse strains at

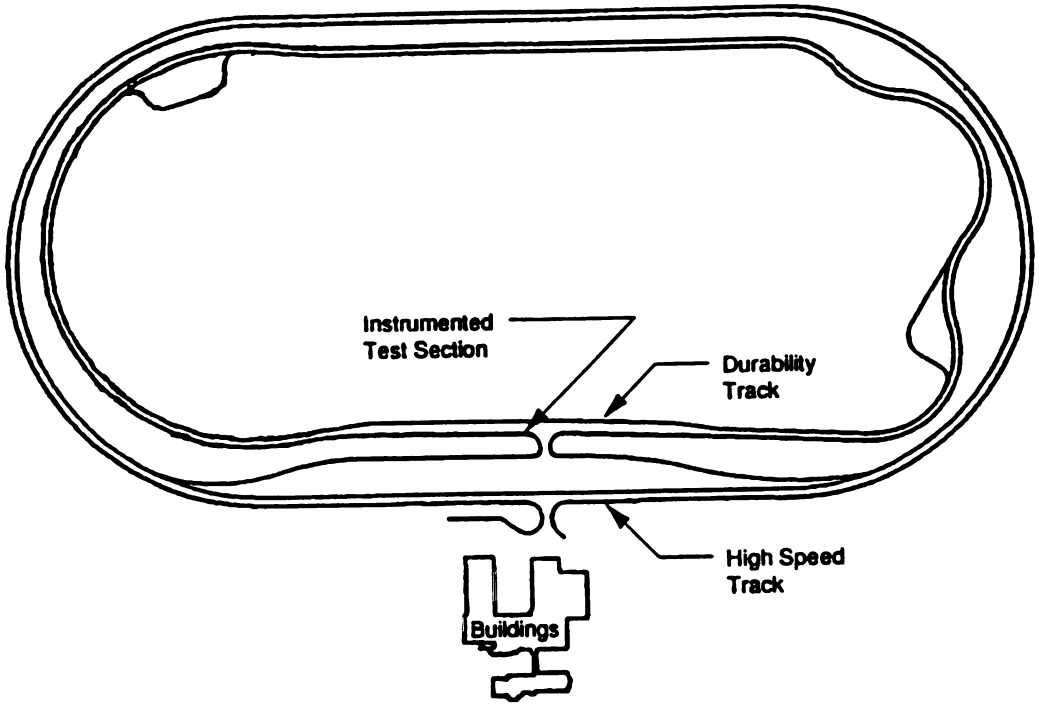

FIGURE 5.1 Plane View of PACCAR Technical Center

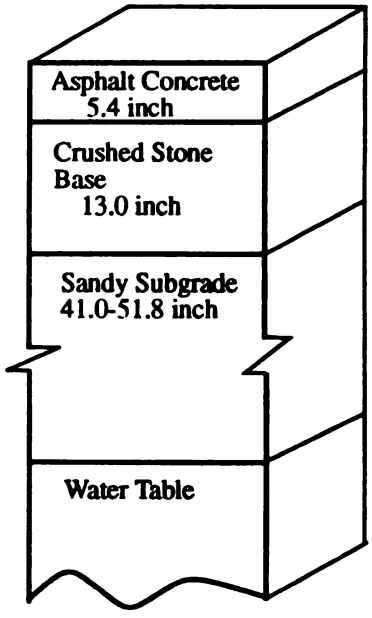

FIGURE 5.2 Cross Section of the PACCAR Test Section

the top and bottom surfaces of the AC layer; forty (40) shear strain gauges were mounted on ten cores and a long transverse slot extending from the center line to the shoulder of the pavement; and forty two (42) surface gauges (longitudinal and transverse) were placed along the wheel path at about one foot intervals.

The physical layout of these gauges is shown in Figure 5.3. The layout was designed to ensure the collection of critical pavement responses: The axial cores were chosen laterally to allow collection of strain measurements from both wheel paths and the approximate center line of the wheel base. The longitudinally oriented surface strain gauges were specifically designed to evaluate the dynamic response of a truck as it travels down the pavement section. The details of the instrumentation procedure can be found in Reference [123]. The results reported in this study concern only the axial core gauges.

Two types of epoxy were used: One type (Micro Measurement M-Bond AE-10) was used to glue the gauges to the pavement, and the other type (Sikadur 32 Hi Mod 2) was used to bond cores to the pavement or to fill the voids in the cut.

5.3.3 Test Procedure

The truck used was a Peterbilt 359 truck with a load frame and instrumented axles to calculate tire forces. The photograph and plan views of a Peterbilt 359 are shown in Figure 5.4. The front and rear axles were equipped with leaf-spring suspensions. Testing was conducted in three blocks: Mid-morning and afternoon of September 28, and mid-morning of September 29 1993. Each test block consisted of three sets of tests corresponding to three different tire pressures: 90, 58 and 31 psi. The maximum safe speed for testing on this track section was 45 mph; so for each tire pressure, three truck speeds were used: 1.7, 20 and 40 mph. The tests were conducted in triplicates and according to a random order. The total number of truck runs was seventy.

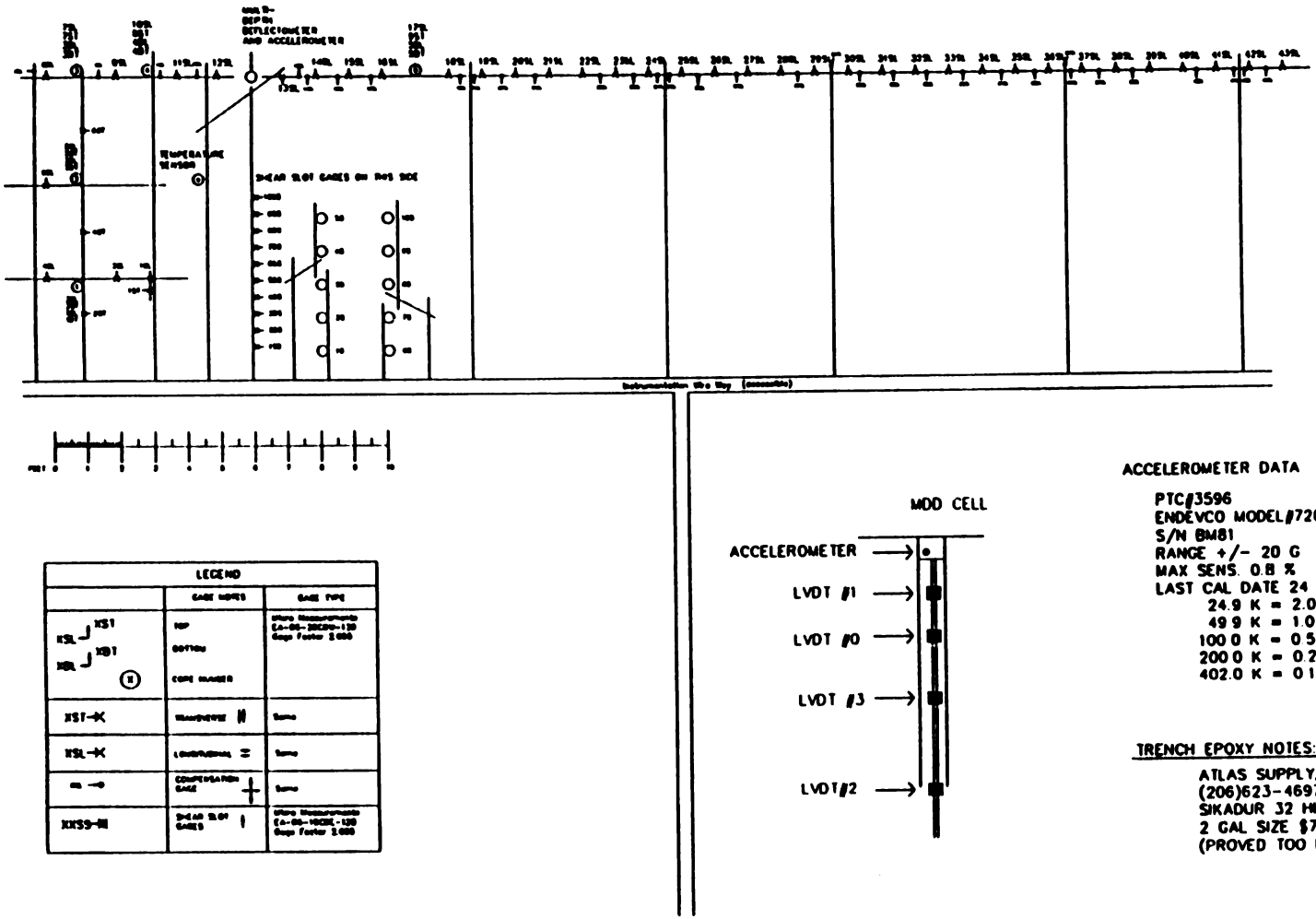

ACCELEROMETER DATA

PTC#3596
ENDEVCO MODEL#7265A-HS
S/N BM81
RANGE +/- 20 G
MAX SENS. 0.8 %
LAST CAL DATE 24 JUL 1990
24.9 K = 2.02 G
49.9 K = 1.01 G
100.0 K = 0.51 G
200.0 K = 0.25 G
402.0 K = 0.12 G

TRENCH EPOXY NOTES:

ATLAS SUPPLY, INC.
(206)623-4697
SIKADUR 32 HI MOD 2 PART EPOXY
2 GAL SIZE $70.00
(PROVED TOO FIRM)

FIGURE 5.3 Instrumentation Layout of the PACCAR Pavement Test Track

(a)

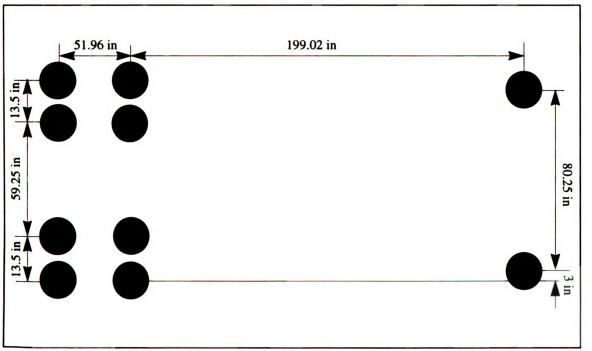

(b)

FIGURE 5.4 The Peterbilt 359 Test Truck

(a) Photograph (b) Plan View

Because some preliminary results from earlier tests showed the effect of lateral offset (between the center of the tire and the gauge) to be very significant, special care was taken in marking the pavement and reading the tire imprint. Lime dust was used to show the tire imprint. If the offset was greater than 4 inch the test was repeated.

5.3.4 Load Measurements

Measured loads were used to investigate the variability of tire loads with runs of equal truck speed and tire pressure and to study the effects of speed and pressure on tire loads. The results indicated that the variability of the load at constant truck speed and tire pressure was within 5 percent. Figure 5.5 and Figure 5.6 show the effects of truck speed and tire pressure, respectively, on the load. Both figures show insignificant variations with no particular trend. Accordingly, it was concluded that there was no need for correcting the measured response for the level of load applied. Note that this was expected because the pavement test section was newly built and its surface was fairly smooth.

5.3.5 Strain Measurements

Strain measurements were used to investigate the effects of truck speed and tire pressure on pavement response. Figure 5.7 shows typical time histories of measured strains in the AC layer.

The discussion above indicated that the variability of the load was insignificant in these tests. Other significant variables which should be accounted for in the analysis are the pavement temperature and the offset distance between the truck wheel and the strain gauge. It was noticed from the field measurements that the pavement's surface temperature did not vary much within a subset of tests with constant tire pressure; this should mean that the temperature at the bottom of the asphalt concrete layer should be very close to a constant within each subset of tests. Accordingly, no temperature correction was used in

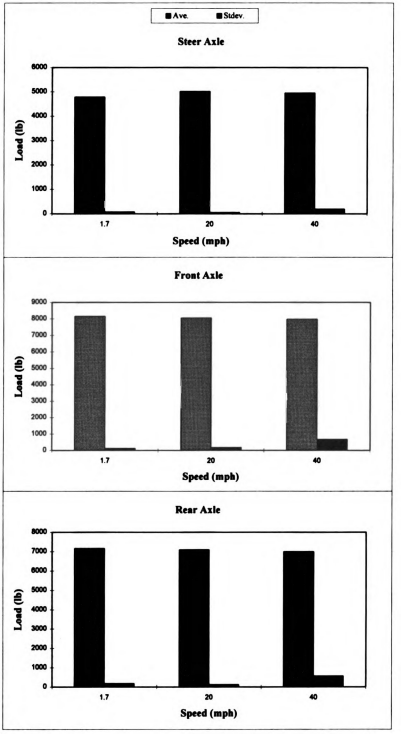

FIGURE 5.5 Effect of Truck Speed on Axle Load

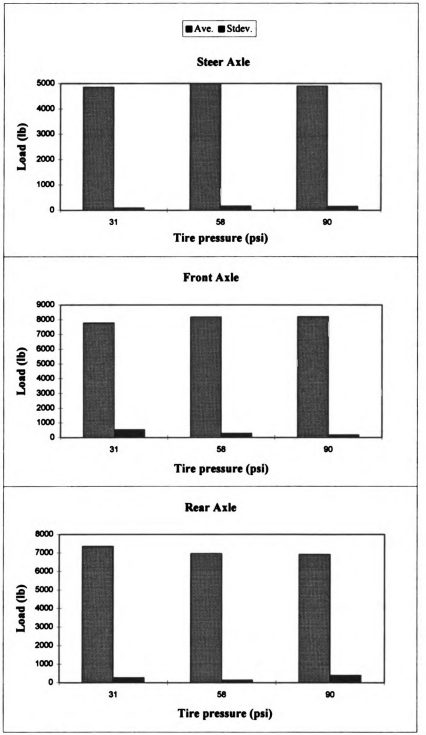

FIGURE 5.6 Effect of Pressure on Axle Load

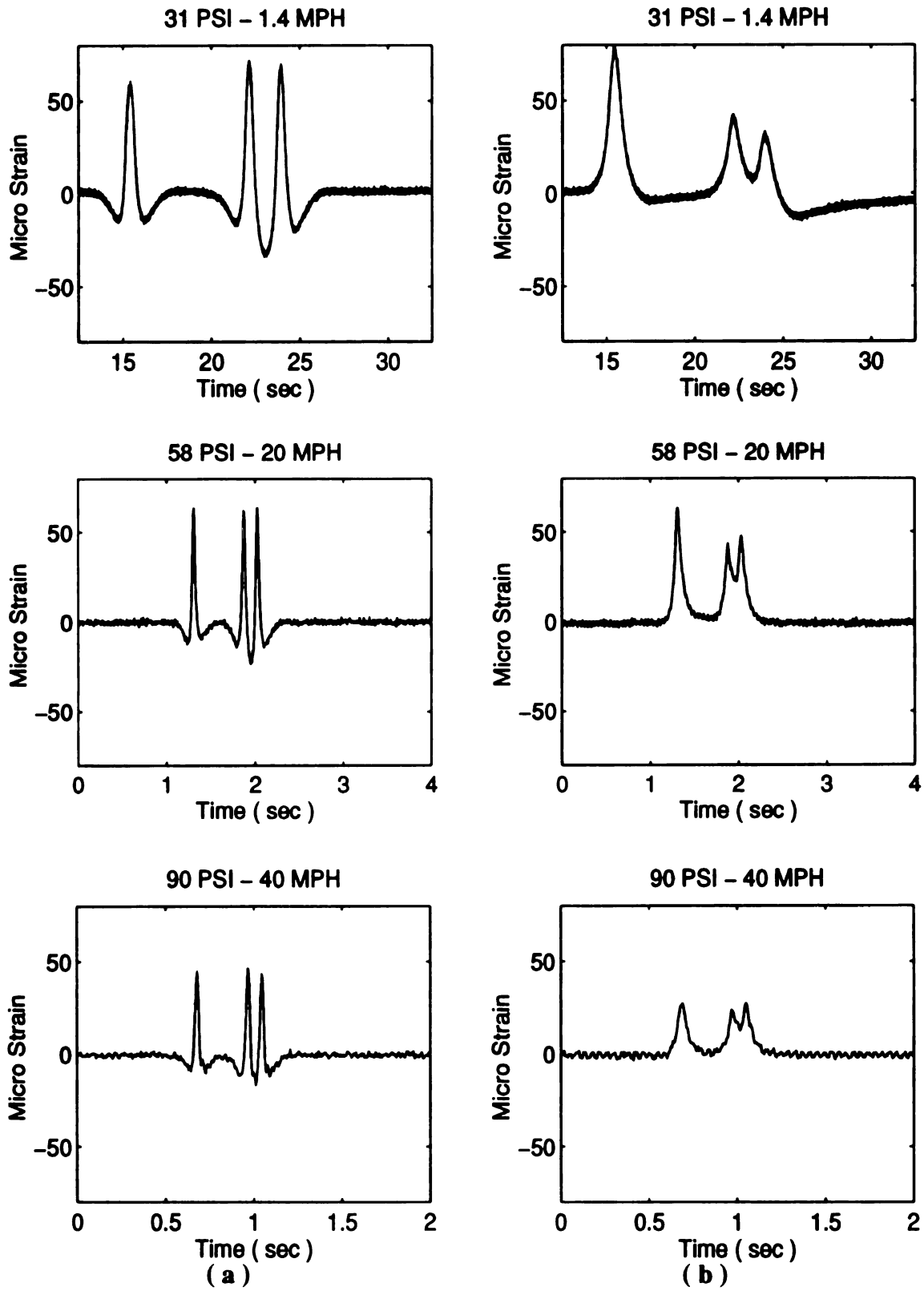

FIGURE 5.7 Typical Time Histories of Measured Strain at the Bottom of AC Layer

(a) Longitudinal strain (b) Transverse strain

analyzing the effect of truck speed for a given subset of tests with constant tire pressure. On the other hand, the effect of the offset between the applied loads and the recording strain gauge should be accounted for. This was done using the computer program SAPSI.

5.3.6 Correcting for the Effect of Lateral Offset

The computer program SAPSI was used to calculate correction factors to account for the difference in the strain response due to the lateral offset between the wheel load and the pavement strain gauge. This was done by calculating the response of the pavement at different offsets along a transverse axis underneath each axle. The SAPSI results were then normalized with respect to offset by calculating an "offset factor" as described in Equation (5-1):

$$\text{Offset factor} = \frac{\varepsilon_{x=0}}{\varepsilon_{offset}} \qquad (5\text{-}1)$$

where, $\varepsilon_{x=0}$ is response right underneath the load and ε_{offset} is response at an offset distance from the load.

Offset factor curves for both surface and bottom strains were generated for the three cores at the three different pressures and at a constant temperature of 68°F. The effect of temperature on the offset factor curves was checked by obtaining offset factors using the procedure above for different temperatures and then comparing curves. The analysis showed that the effect of temperature on the normalized offset factor curves is negligible.

5.4 MATERIAL CHARACTERIZATION OF CORES

5.4.1 Pavement Layer Characterization

The WSDOT Dynatest 8000 FWD was used to conduct deflection testing over the entire test section. Testing was done in 61 locations totaling 130 drops with more tests on the five instrumented cores. The computer program EVERCALC was used for backcalculation of layer moduli. The applied FWD loads varied from 4,874 to 17,880 pounds and sensor spacings were set at 0, 8, 12, 24, 36, and 48 in. The measured average mid-depth temperature of the AC layer during testing was 68°F. Layer thicknesses were obtained by coring. In addition, the subgrade soil was saturated at a relatively shallow depth. The shallow water table translates into the saturated subgrade soil behaving as a "stiff" layer. EVERCALC was used to back-calculate an appropriate value for the stiff layer modulus as well as to calculate the depth to the stiff layer. The approach consisted of varying the value of the stiff layer modulus from 10 ksi to 1,000 ksi and choosing the value which gave the lowest root mean square (RMS) value and the most reasonable AC modulus value (based on laboratory tests). A stiff layer modulus of 40 ksi was obtained from the convergence procedure. Because of the inability to physically measure the epoxy thicknesses, "effective" thicknesses were determined by varying the thickness of the epoxy on top and below each core until the theoretical strains (calculated by CHEVPC) matched the measured strains. Table 5.3 shows the effective layer thicknesses. The details of all of the above calculations are presented in Reference [123].

5.4.2 Back-calculation of Layer Moduli

Recently many methods for the back-calculation of layer moduli using nondestructive deflection testing have been developed. Some of the methods use the elastic layer theory while others use the finite element method. Conceptually, all methods are based on

TABLE 5.3 Effective Pavement Layer Thickness of Axial Cores (inch)

Pavement Layer	Axial Core			
	Core 1	Core 3	Core 4	Core 5
Epoxy	0.40	0.25	0.00	0.60
AC	4.90	4.90	4.90	4.90
Epoxy	0.40	1.250	0.50	0.60
Base	12.70	12.00	13.00	12.30
Subgrade (Oct'91)	42.70	46.00	46.10	43.80
Subgrade (Feb'91)	57.10	60.40	60.50	58.40
Stiff Layer	semi-infinite	semi-infinite	semi-infinite	semi-infinite

iterative routines whereby layer moduli are assumed and the pavement surface deflection is computed. If the computed values match the field measured ones, then the calculation is terminated. It should be noted that the calculated layer moduli are not unique; they depend on the assumed values of the seed moduli. Moreover, various combinations of layer modulus values may exist such that the calculated deflections match the measured ones. Nevertheless, the methods are still in the developmental stage and they can be used to estimate the material properties of each layer of an existing flexible pavement.

As mentioned above, the EVERCALC program was used to backcalculate the layer moduli. Table 5.4 and 5.5 show the backcalculated modulus values and Poisson's Ratio values for October 1991 and February 1993 tests, respectively. The average pavement temperature was 68 ^{o}F in October and 44.5^{o}F in February.

TABLE 5.4 Layer Properties for October 1991 FWD Testing

Pavement Layer	Modulus (psi)	Poisson Ratio
Epoxy	500,000	0.35
AC	562,000	0.35
Base	14,800	0.40
Subgrade	10,200	0.45
Stiff Layer	40,000	0.35

TABLE 5.5 Layer Properties for February 1993 FWD Testing

Pavement Layer	Axial Core 1		Axial Core 3, 4 & 5	
	Modulus (psi)	Poisson Ratio	Modulus (psi)	Poisson Ratio
Epoxy	500,000	0.35	500,000	0.35
AC	1,575,700	0.35	1,510,000	0.35
Base	20,300	0.40	27,500	0.40
Subgrade	10,700	0.45	13,400	0.45
Stiff Layer	50,000	0.35	50,000	0.35

5.4.3 Frequency-dependent AC Properties

Two sets of profiles were used in the analysis: One set with the properties of the asphalt concrete layer held constant with frequency and a second set where the AC properties were varied with frequency. The reason for using frequency-dependent AC properties stems from the fact that asphalt is a visco-elastic material and its properties (modulus, damping ratio and Poisson's ratio) have been shown to be strongly frequency-dependent [100]. In the frequency-independent profiles, the value for the AC modulus is the one back-calculated from FWD deflection data. In the frequency-dependent profiles, the curves for the AC properties were developed using a similar procedure to the one reported by Siddhartan et al. [97]. In this procedure, the curves reported by Sousa [100] are used to describe the variation with frequency of the dynamic Young and shear moduli ($|E^*|$ and $|G^*|$) as well as the damping ratio of the AC layer (see Figure 5.8(a) and (c)). The intercept for $|E^*|$ is obtained by iteration until the peak transient strain due to a unit FWD pulse is equal to the static strain which corresponds to the back calculated AC modulus:

$$\varepsilon = \max \sum_{s=0}^{N/2} \frac{P_s}{|E^*_s|} = \frac{1}{E_{FWD}} \qquad (5\text{-}2)$$

where, P_s is Fourier transform of the load and s is frequency number.

Convergence was reached for $|E_0^*| = 273{,}500$ psi. The initial Poisson's ratio was obtained from the measured initial values of $|E^*|$ and $|G^*|$, as reported by Sousa, using elasticity. The computed value was 0.537 which is close but exceeds the maximum allowable value in elasticity of 0.5. Therefore a value of 0.499 was assumed. The initial shear modulus, $|G_0^*|$, was then computed from elasticity. The variation with frequency of Poisson's ratio was made to fit the observed trends in $|E^*|$ and $|G^*|$. Figure 5.8 (b) and (d) shows the final curves used for the moduli and Poisson's ratio respectively. To check the

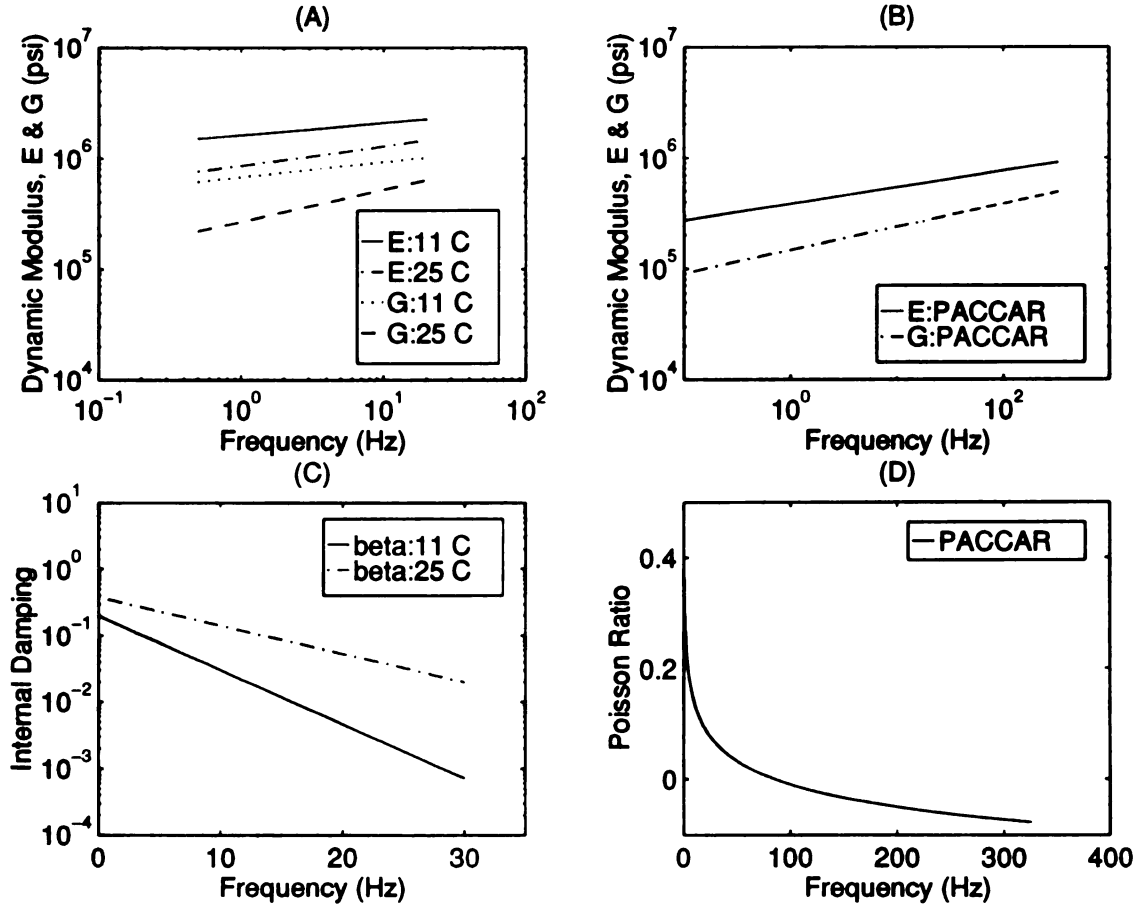

FIGURE 5.8 Asphalt Concrete Properties Versus Frequency

(a) Laboratory-measured Dynamic Moduli [100]

(b) Iterated Dynamic Moduli Used In The Analysis

(c) Laboratory Measured Material Damping [100]

(d) Poisson Ratio Used In The Analysis

validity of the procedure the profile was subjected to the FWD pulse, and the tensile strain at the bottom of the AC layer was compared with the measured value. The agreement was excellent: 133 micro-strains versus 130 measured.

5.5 VERIFICATION OF MOVING CONSTANT LOAD SOLUTION

5.5.1 Modeling of the Moving Wheel Load

Consider a uniformly distributed load over a circular area, moving at a constant velocity on the surface of a layered pavement system. In order to consider the moving load effect on the response at a fixed point in the pavement, it is necessary to include the effect of the load as it moves from one location to the next in the pavement and before and after the load passage by theses consecutive locations in space. The moving load is modeled as a series of haversine pulses with their duration equal to the time required for the wheel to pass by a point in the pavement. Thus the response time history of the pavement at the fixed point can be obtained as the resultant of the time histories of the responses due to the load being at these consecutive positions in space. This insures continuity of loading in time and space as it moves from one location to the next.

5.5.2 Modeling of Pavement Cores

The same profiles for October 1991 were used in the analysis of September 1993 truck tests because the weather conditions were nearly identical. Theoretical strains were calculated for Axial Cores 1, 3 and 4 using the back-calculated frequency-independent profiles as well as profiles with frequency-dependent AC layer properties, as described in the previous section. The numerical discretization of the different pavement layers into sublayers was done according to the accuracy guidelines provided in previous research [19]. Figure 5.9 shows the modeling of the different cores. The temperature at the bottom

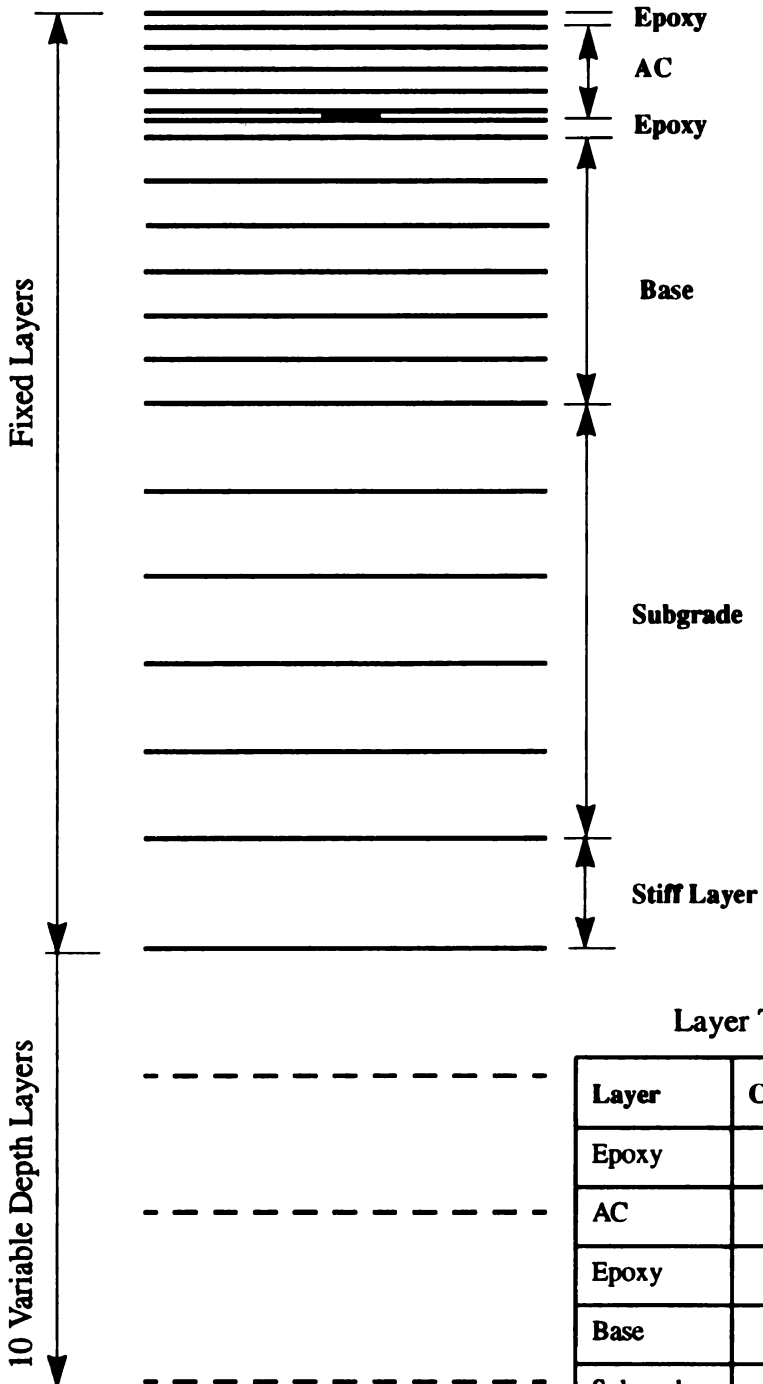

Layer Thickness (inch)

Layer	Core 1	Core 3	Core 4
Epoxy	0.40	0.25	0.00
AC	4.90	4.90	4.90
Epoxy	1.25	1.25	0.50
Base	12.70	12.00	13.00
Subgrade	42.70	46.00	46.10

▬ : **Location of calculated strain**

FIGURE 5.9 SAPSI-M Model Used in the Analysis

of asphalt concrete layer was assumed to fluctuate less than the surface temperature because of the thickness of asphalt concrete. The temperature was assumed to be uniform through the asphalt concrete and to be 68°F. Theoretical strains and deflections were calculated at the bottom of the asphalt concrete, not at the bottom of epoxy, because the strain gauges were glued to the asphalt concrete with epoxy which was then used to fill the voids in the core.

5.5.3 Results of SAPSI-M Analysis

SAPSI-M was used to predict the horizontal strains in the asphalt concrete layer at the three different cores, and the theoretical predictions were compared with experimental results. Most of the analysis shown in this study considers only a single wheel for the purpose of simplicity. A few runs were done with a half-truck in order to compare strain pulses from single and tandem axles.

5.5.3.1 Typical Response Curves of Moving Constant Loads

Typical response curves for longitudinal and transverse strains are shown in Figure 5.10 and Figure 5.11 respectively. Note that the steer and drive axles have different offsets from the measuring point (three inch) difference between the center of steer's tire and that of the outside dual tire. For this reason the peak strain magnitudes from the steer axle and the drive (dual tires) axle are very similar. If the strains (transverse direction, in particular) were measured right underneath the tire the strains due to the single tire of the steer axle would have been significantly higher than those due to the dual tires of the drive axle [36].

Figure 5.10 shows excellent agreement in magnitude and shape between the field measurements and the strains calculated using SAPSI-M. Of particular interest is the response curve for longitudinal strain at the bottom of the asphalt concrete layer. The

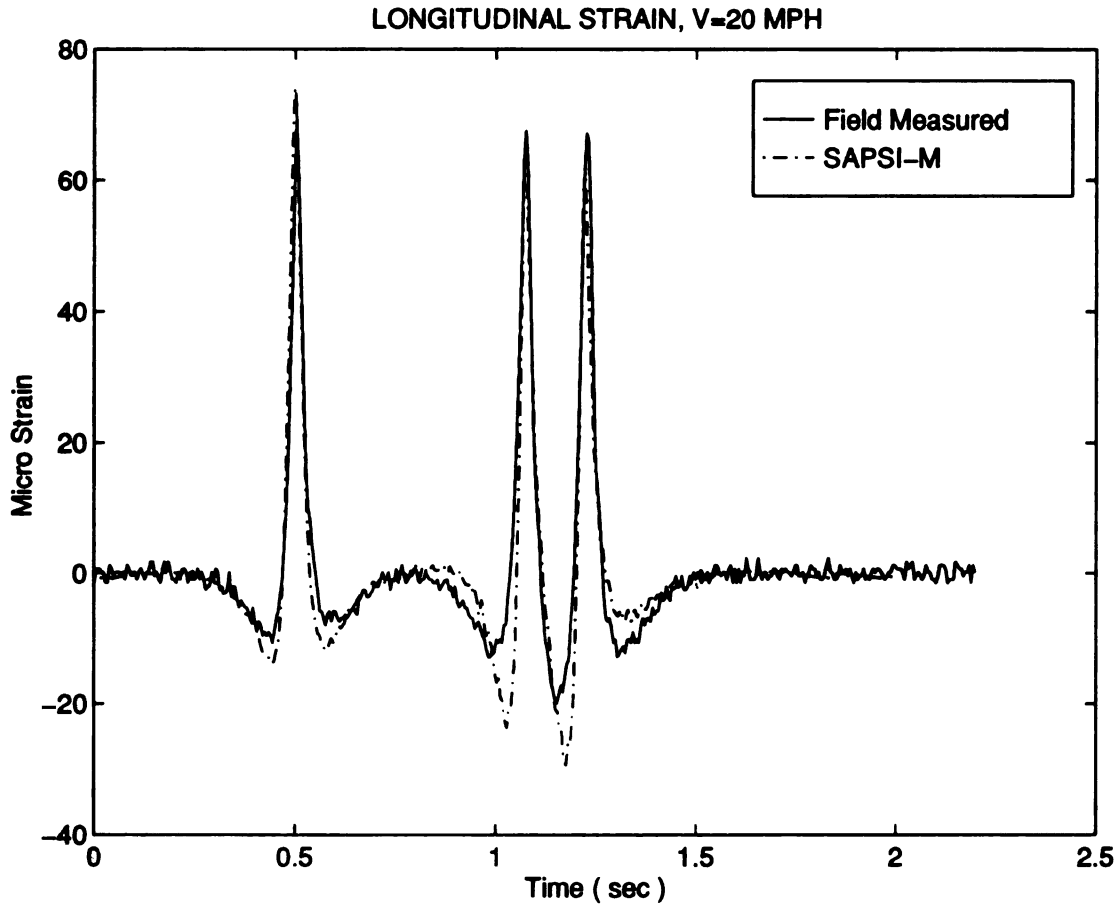

FIGURE 5.10 Typical Response of Longitudinal Strain for Moving Constant Loads

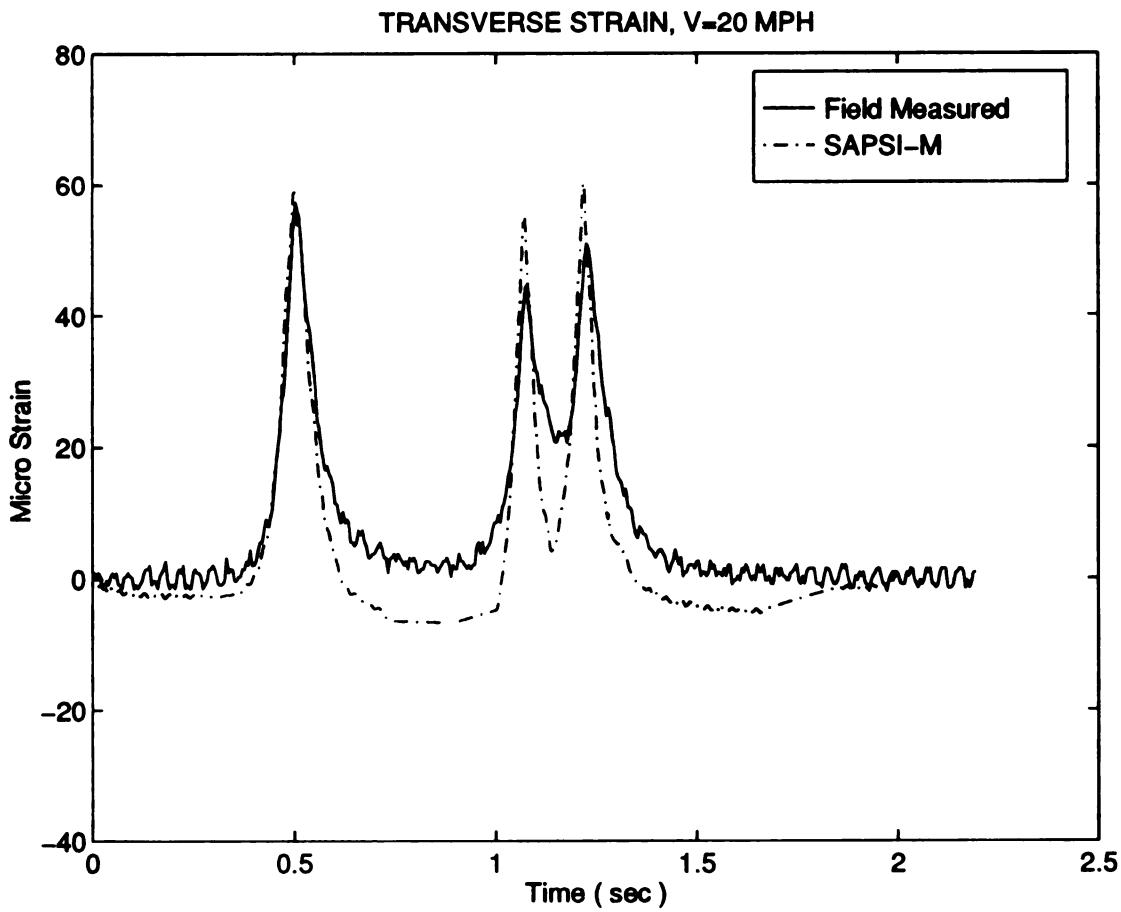

FIGURE 5.11 Typical Response of Transverse Strain for Moving Constant Loads

curve shows a strain reversal from compression to tension as the load passes over the measuring point, and it is asymmetric.

The response curves for the transverse strain, on the other hand, do not show compressive strains as the load approaches and leaves the measuring point. Figure 5.11 shows good agreement between measured and calculated values, although not as good as for longitudinal strains. This could be due to the fact that the model in SAPSI-M is axisymmetric, whereas the pavement is constructed in lanes less than 12 ft wide. The horizontal bending strains in the "short" (transverse) direction should be less than those in the "long" (longitudinal) direction due to smaller constraint. Another factor could be the uncertainty in the measured dynamic loads at the peak strain points as the truck moves, i.e. matching the load time history to the position of the load relative to the pavement.

5.5.3.2 The Effect of Frequency-Dependent AC Properties

SAPSI-M results using both frequency-dependent and frequency-independent AC layer properties were compared with field data. Figure 5.12 compares measured longitudinal strains and predicted values using both frequency-dependent and frequency-independent AC layer properties in Core 1, with the truck moving at increasing speeds. The field data and the calculated values show a consistent decrease as the truck speed increases. Increasing the speed from creep to 40 mph causes the strain to decrease by about only 10% for the frequency-independent profile, while it is 28% for the frequency-dependent profile, and 32% for the actual tests. Clearly, the profile with frequency-dependent AC properties gives much closer results to the field data than does the profile with frequency-independent properties. This is an indirect field verification of the laboratory test results obtained by Sousa [100] and others indicating that the asphalt concrete properties are strongly dependent on the frequency of loading.

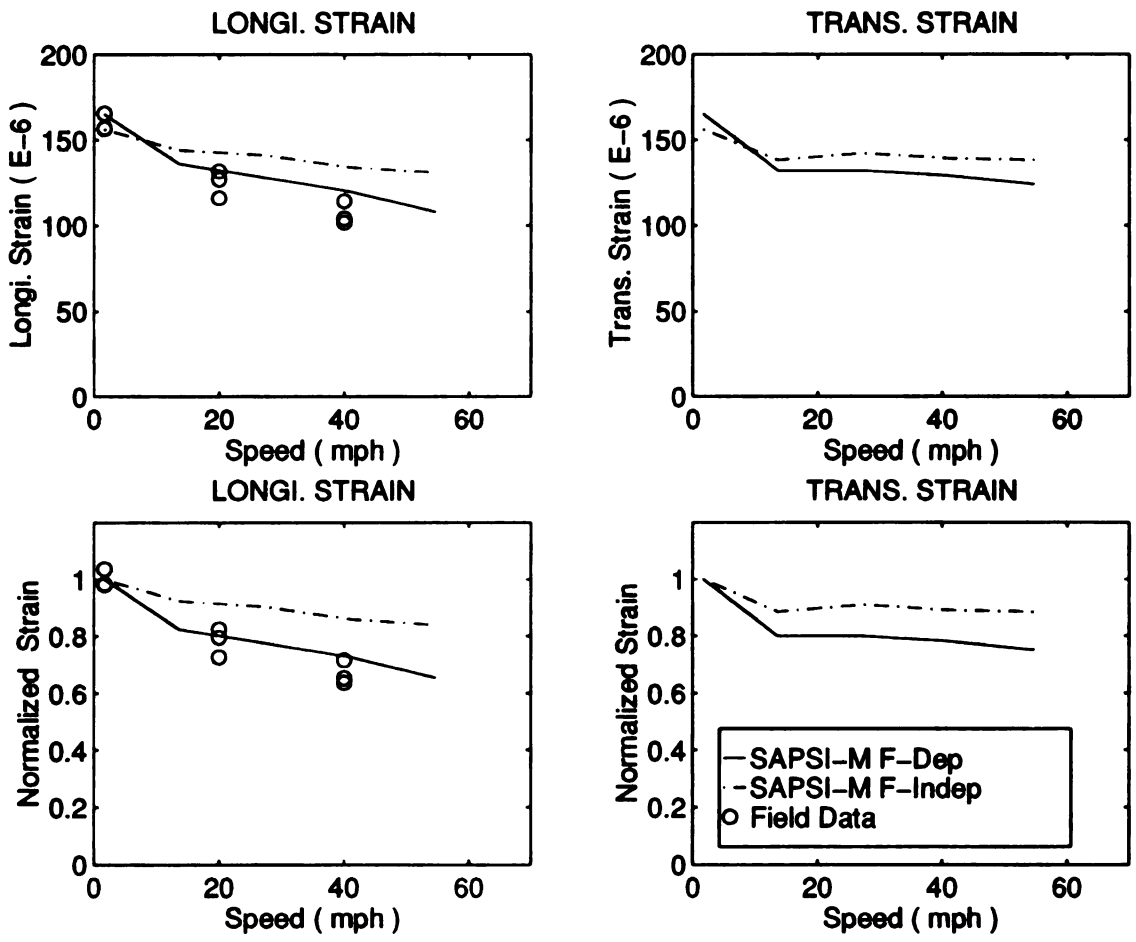

FIGURE 5.12 Comparison of Calculated and Measured Strains at Different Speeds -Core 1

5.5.3.3 Effect of Truck Speed

The effect of truck speed on longitudinal and transverse strain at the bottom of the AC layer is shown in Figure 5.13 and Figure 5.14 for Cores 3 and 4 respectively. Both measured and calculated strains (using the frequency-dependent profile) show a consistent decrease as the truck speed increases. For Core 3, increasing the speed from creep to 40 mph causes the predicted longitudinal strain to decrease by about 27% as compared to 30% in the actual tests. Core 4 results show a predicted decrease in strain of 24% versus an average of 32% in the field. The agreement in the speed effect is excellent. However, the absolute values of the measured and predicted response are significantly different for Core 4. Considering that both Cores 1 and 4 have the same properties and very similar thicknesses of the AC and epoxy layers, and the fact that Figure 5.12 and Figure 5.14 show the calculated strains for Cores 1 and 4 to be very close to each other and that measured strains from FWD tests also showed the responses of Cores 1 and 4 to be very similar in magnitude [18], calculated strains are thought to be more reasonable than the field data in the case of Core 4. This discrepancy could be due to calibration after two years have passed since the installation of strain gauges.

In the case of transverse strains, increasing the speed from creep to 40 mph causes a decrease of 20% for both calculated and measured values in Core 3 (Figure 5.13), whereas Core 4 shows a decrease of 22% in calculated strains versus 40% in the field. This means that measurements of transverse strains show larger variability than those of longitudinal strains.

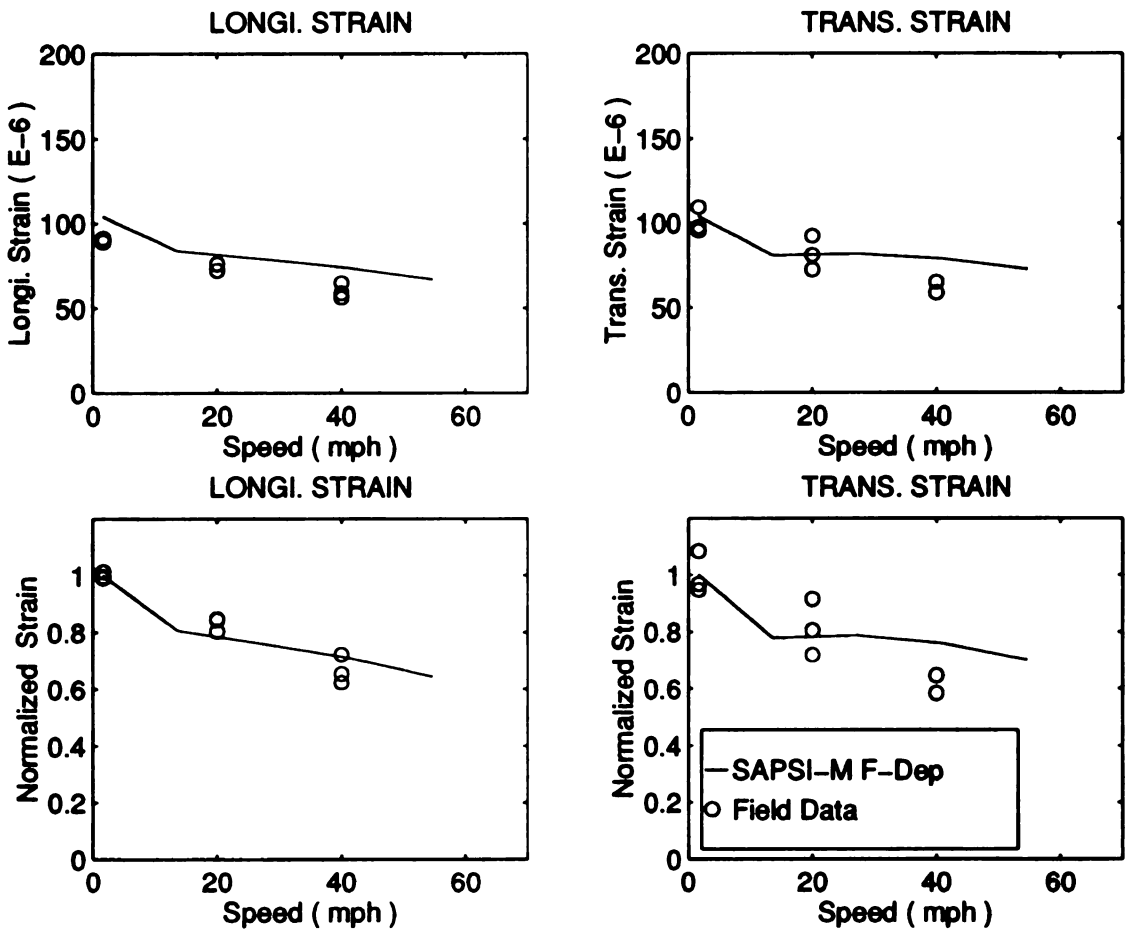

FIGURE 5.13 Comparison of Calculated and Measured Strains at Different Speeds -Core 3

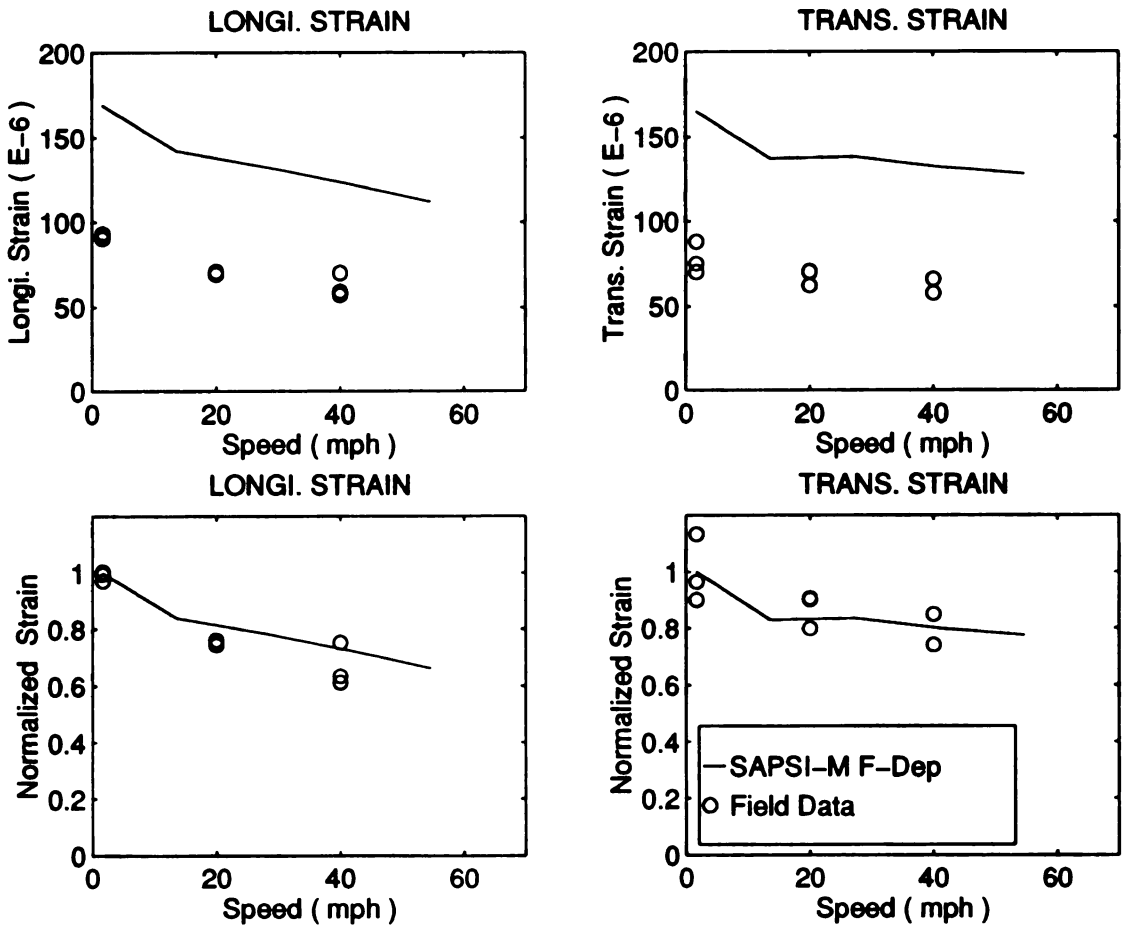

FIGURE 5.14 Comparison of Calculated and Measured Strains at Different Speeds -Core 4

5.6 VERIFICATION OF MOVING ARBITRARY LOAD SOLUTION

5.6.1 Moving Arbitrary Load Time History

Ramp test were conducted to investigate the theory of "spatial repeatability". This concept states that for any given truck speed, the wheel load time histories generated by a particular heavy vehicle are repeated closely on successive passes over a given stretch of road. Since all heavy commercial vehicles have approximately the same natural frequencies and are driven at approximately the same speed on highways, then for a given pavement the dynamic wheel load peaks would always occur within a relatively narrow band of road sections [36]. Accordingly, the issue of spatial repeatability is central to truck-pavement interaction because some portions of the road may incur much larger damage than other portions. The excitation source was a test ramp designed to excite the rigid body sprung mass modes of the test vehicles and not the unsprung mass modes (i.e. axle hop). This was done to help simplify and analyze the pavement strain response data. The ramp design consisted of a 4 ft by 2 inch ramp-up, a 7 ft flat section, and a 4 ft by 2 inch ramp-down.

The load measurement from the ramp tests was taken to simulate the moving arbitrary load. Figure 5.15(a) shows the measured time histories of the vibrating component of the loads for left front steer, left front drive and left real drive axles. They show a large variation in magnitude due to the ramp which was installed just ahead of the instrumented track. Because these loads are moving, it is necessary to shift the time history such that they match the locations of the wheels relative to the pavement. Figure 5.15(b) shows the load history in space, which was obtained from Figure 5.15(a) by adding the static loads and converting the load history in time to the history in space. Note that these load histories in space are used in the SAPSI-M analysis.

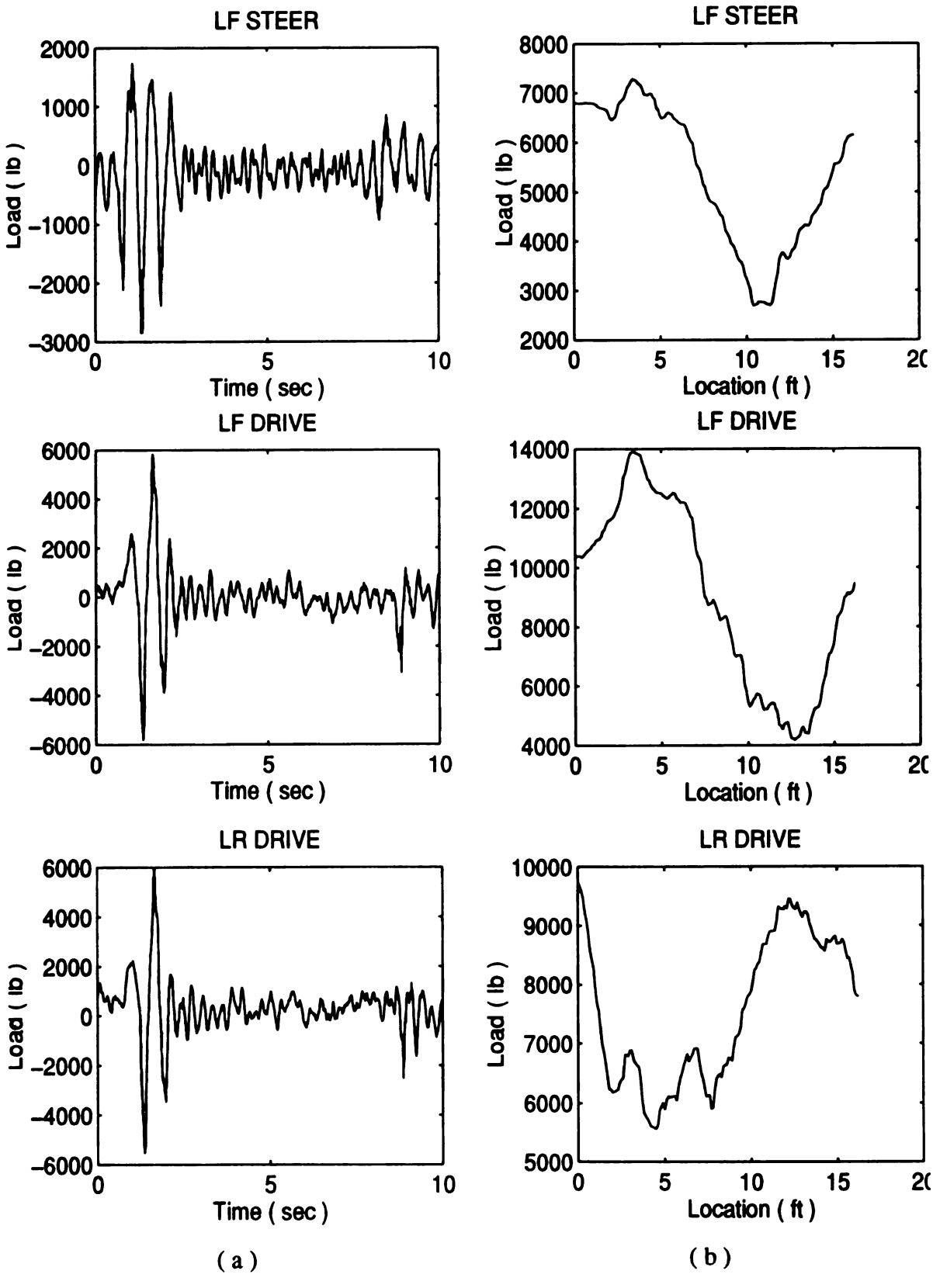

FIGURE 5.15 Measured Wheel Loads (a) in Time (b) in Space Domain

5.6.2 Typical Response Curves of Moving Arbitrary Loads

The measured time history of surface longitudinal strain due to one truck passage was compared to the predicted response using the solution for moving arbitrary loads. Typical response curves for longitudinal strain using moving arbitrary dynamic loads is shown in Figure 5.16. The figure shows excellent agreement in magnitude and shape between the field test and calculated from SAPSI-M computer program. This response curve, also, shows a strain reversal when the load passed over the measuring point.

Figure 5.17 shows a typical response curves for longitudinal strain using moving arbitrary quasi-dynamic loads (non-vibrating moving loads). Although the agreement in magnitude and shape between the field response curve and the calculated curve is less than Figure 5.16, it is still very good.

Agreement between SAPSI-M's predictions and field measurements of longitudinal strain was excellent in the moving arbitrary dynamic analysis and very good in the quasi-dynamic analysis in both the shape and magnitude of the response. These results show that although the amplitude of load vibrations is high, neglecting the effect of frequency, while maintaining correct allowance for truck speed and the magnitude of the dynamic wheel loads, does not change the response in any significant way. Therefore, a simplified solution where the moving loads are assumed to be non-vibrating seems to be sufficient for accurately predicting the pavement response. A similar conclusion was reached by Hardy and Cebon using a simplified beam on Winkler foundation model [40].

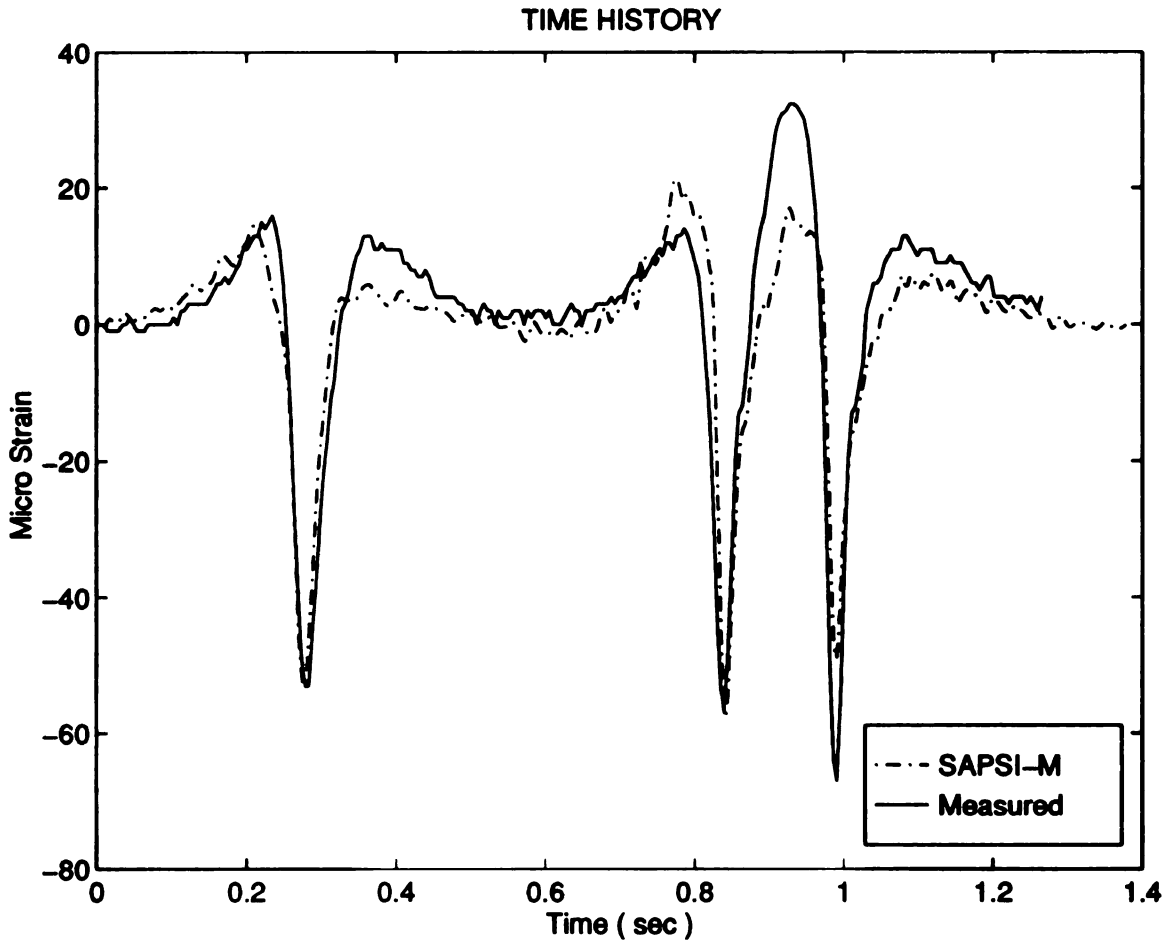

FIGURE 5.16 Comparison of Measured and Predicted Response Curves of Moving Arbitrary Dynamic Solution

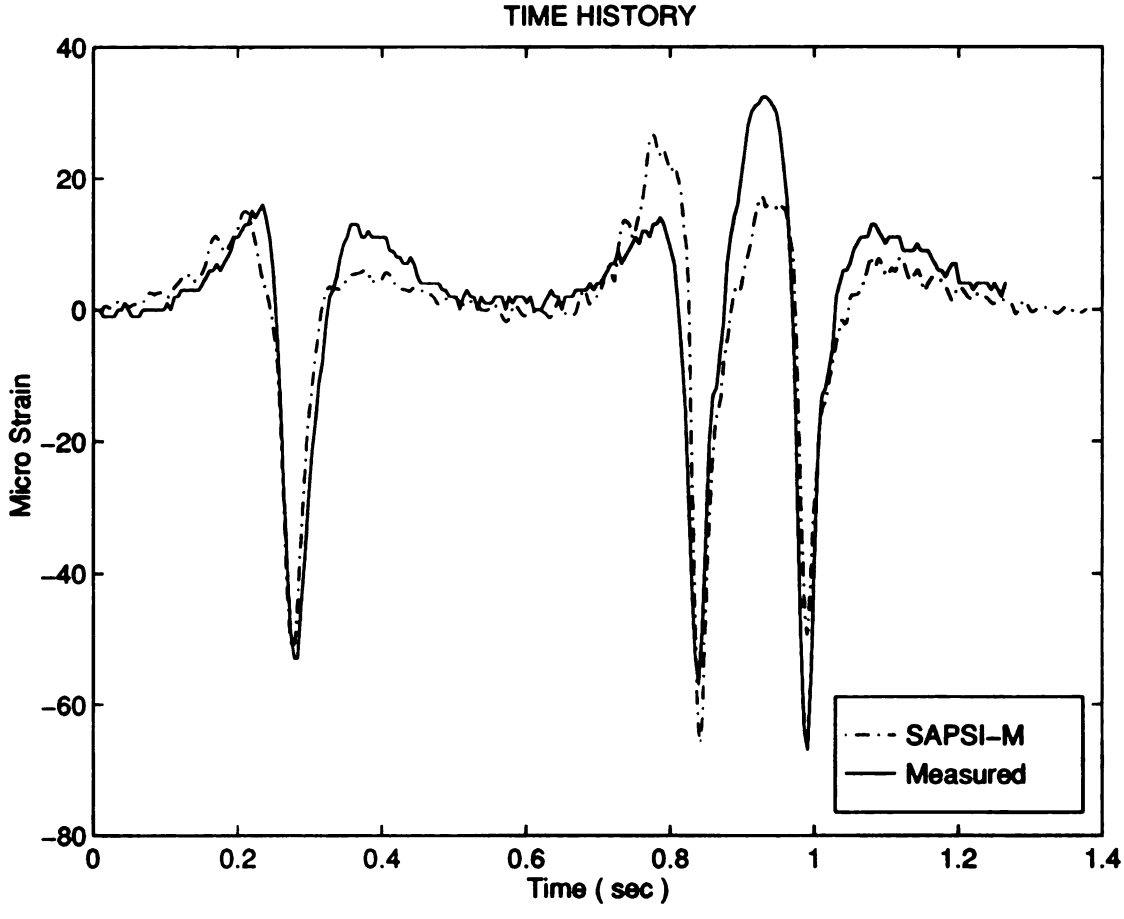

FIGURE 5.17 Comparison of Measured and Predicted Curves of Moving Arbitrary Quasi-Dynamic Solution

5.7 VERIFICATION OF SAPSI TRANSIENT ANALYSIS USING FWD TESTS

The response of AC pavement to Falling Weight Deflectometer (FWD) tests was examined by Hoffman and Thompson [47] as part of an extensive investigation on a number of nondestructive testing devices. They concluded that the FWD deflection pulse width is of the order of 30 millisecond. Thus, the analysis of FWD pulse tests consists a good transient analysis of pavement.

The asphalt concrete test section was tested using WSDOT's Kuab 8000 Falling Weight Deflectometer (FWD). The FWD tests were conducted in October 1991, June 1992 and February 1993. This section describe the validation of SAPSI transient analysis against the full-scale FWD test and static predictions.

5.7.1 Characteristics of FWD Field Data

5.7.1.1 Linearity of FWD Field Data

To investigate the linearity of FWD field data, the measured longitudinal strain values from all three FWD test series were plotted against the applied FWD load for all cores. Figure 5.18 indicates that the FWD measured strain data does not exhibit any significant non-linearity for the range of applied loads for all three seasons and for all four cores. The figure also shows that the stiffness (which is obtained from the slope of the curve) is highest in February 1993 and has about the same value in October 1991 and June 1992. This is expected and is due to the pavement temperature: The average mid-depth temperature at the test site was measured to be about 44.5 ^{0}F in February 1993 versus 68^{0}F in October 1991 and 71 ^{0}F in June 1992.

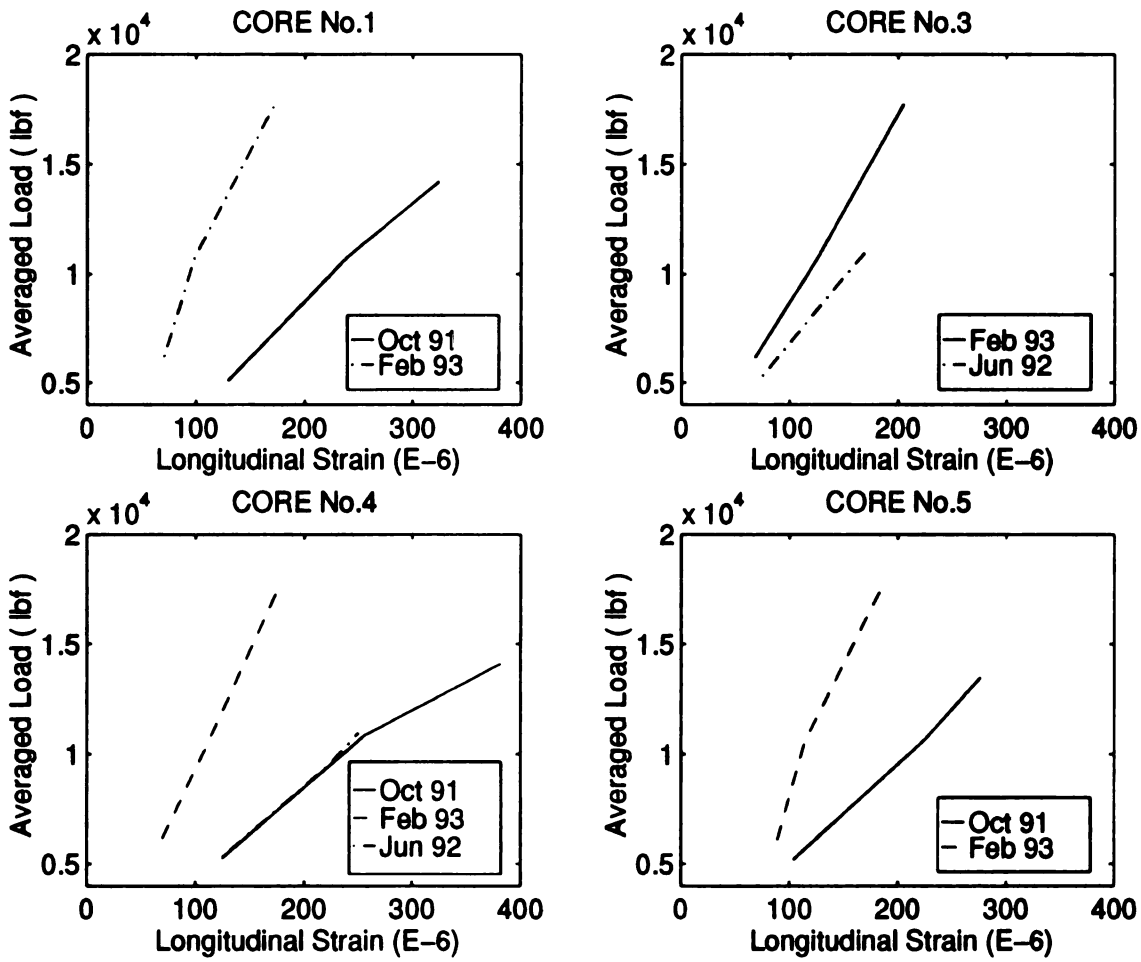

FIGURE 5.18 Linearity of Strain Measurement in FWD Tests

5.7.1.2 Isotropy of FWD Field Data

To investigate the isotropy in strain measurement, the ratio of transverse to longitudinal strains was plotted as a function of the applied load for all cores and seasons (Figure 5.19). The flatness of the curves indicates that the transverse strain data also shows a linear behavior. Ideally, the ratio should be equal to one if the material is perfectly isotropic and the boundary conditions are perfectly symmetric. Figure 5.19 shows that the transverse to longitudinal strain ratio varies from about 0.65 to 1.6 considering all tests. Within the same core, i.e. for the same strain gauges, the ratio can vary by as much as 50% in either direction from one test to another, indicating that the error is probably due to measurement and not to any fundamental physical behavior. This could also be an indication to the fact that measurement should be done as soon as possible after installing strain gauge in the field.

5.7.2 Static and Dynamic Predictions of Strains

The SAPSI transient solution was predicted and compared with FWD field test, together with static prediction using CHEVRON computer program. The computer program CHEVRON was used to calculate the horizontal strains at the bottom of the AC layer using the backcalculated moduli. The program is very well known; it uses static analysis and the linear-elastic layered theory. In the dynamic analysis, the SAPSI computer program was used.

The FWD load is modeled as a haversine pulse with a duration of 30 milli seconds. Figure 5.20 shows the closeness of the match between the recorded pulse from FWD testing provided by WSDOT and the simulated pulse. Using effective layer thicknesses for Axial Cores 1, 3, 4 and 5, and back-calculated layer properties, theoretical transient strains were calculated by SAPSI. Figure 5.9 shows the SAPSI model used in the analysis. The

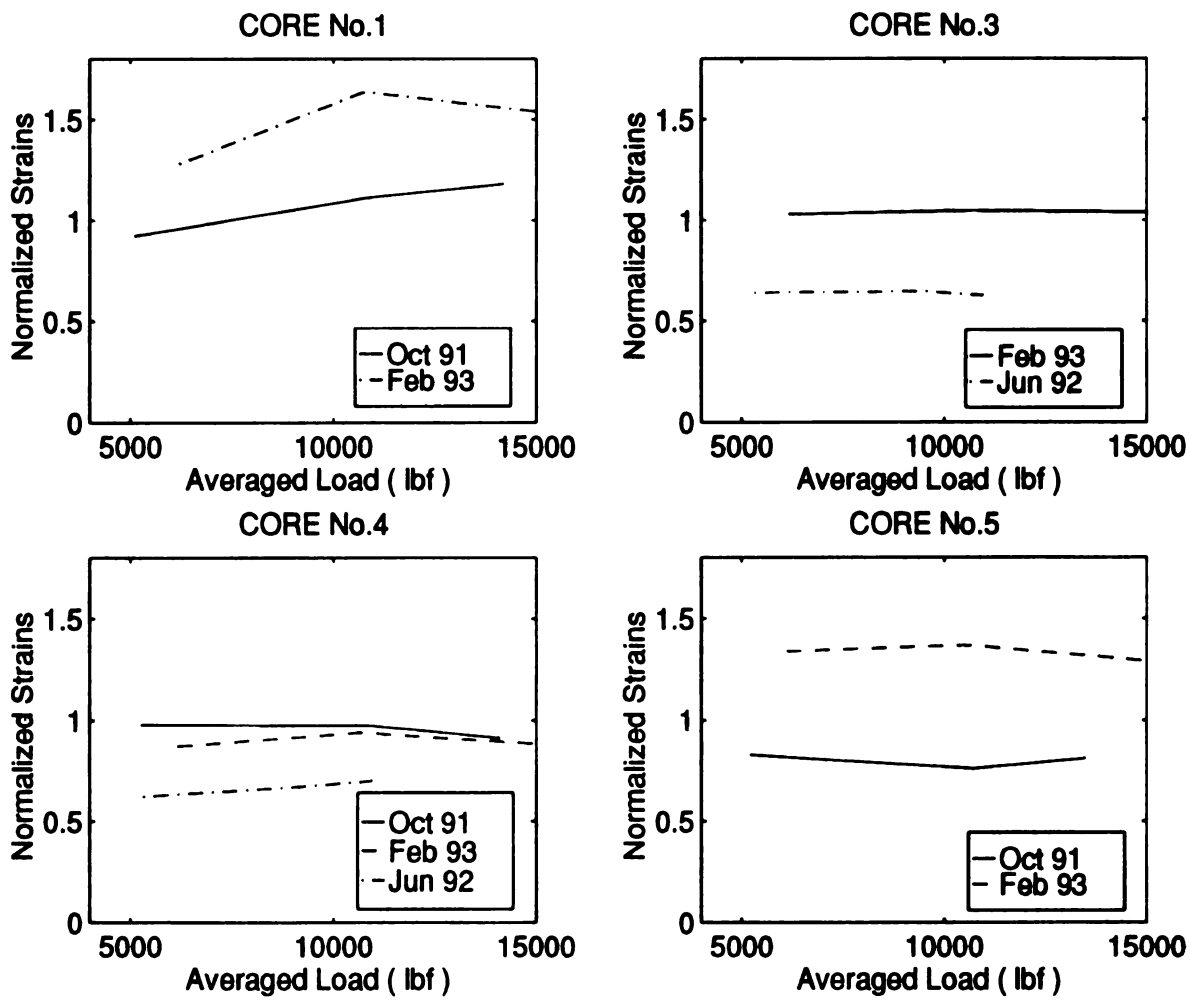

FIGURE 5.19 Ratio of Transverse to Longitudinal Strains in FWD Tests

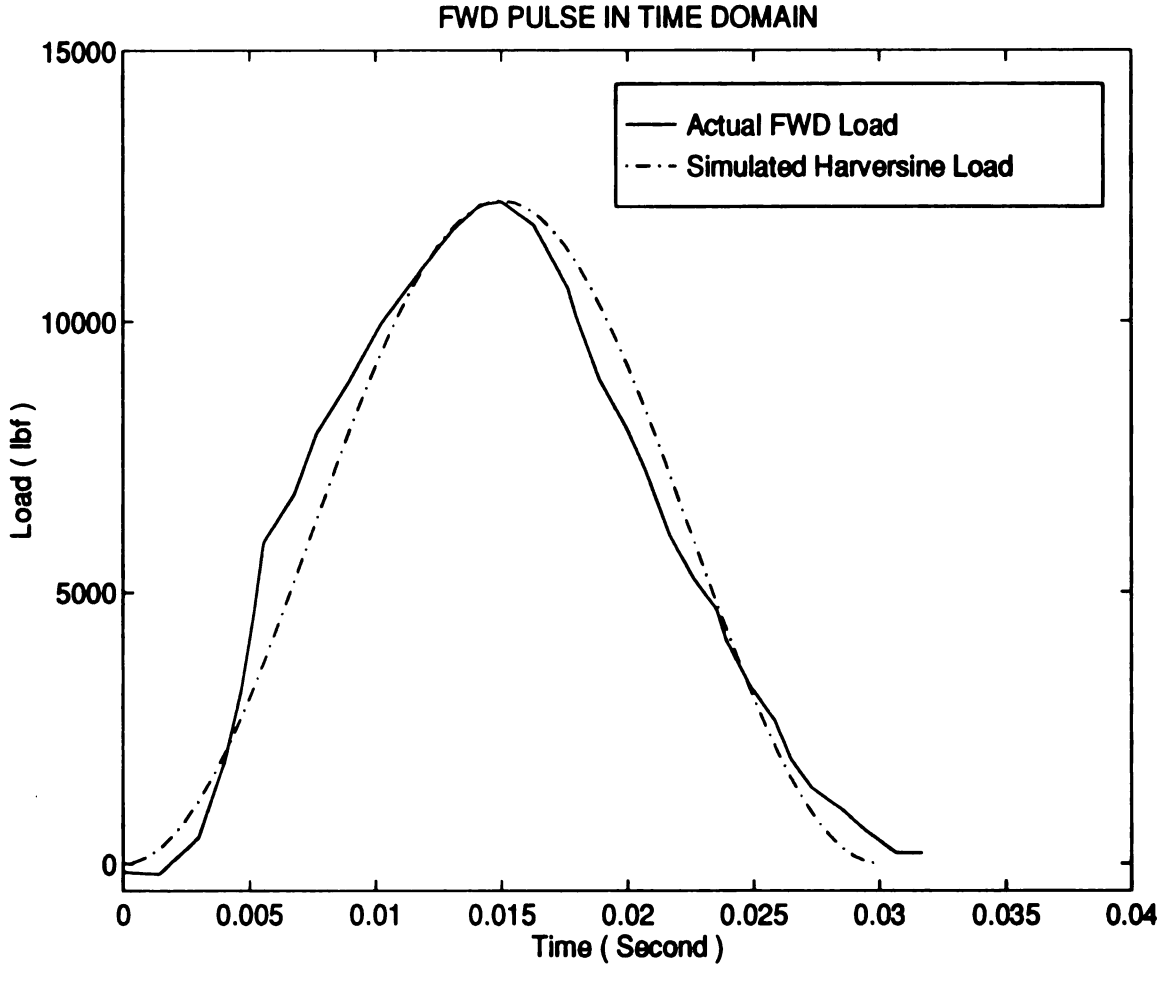

FIGURE 5.20 Actual and Simulated FWD Load Pulses

results for all three test series are shown in Table 5.6 through Table 5.8. Figure 5.21 through Figure 5.23 show comparisons of measured strains with calculated static strains from CHEVRON and dynamic strains from SAPSI.

5.7.2.1 October 1991 FWD Tests

SAPSI predictions were obtained using profiles with both frequency-independent and frequency-dependent AC layer properties. The results for all cores are shown in Table 5.6 which also includes CHEVRON (static) predictions for comparison purposes. Figure 5.21 shows a graphical comparison between predicted and measured strains. Very good agreement exists between measured and predicted (both static and dynamic) strains: Ninety percent of measured strains are within ±10 10 percent of their calculated values. Static and dynamic predictions using both frequency-dependent and frequency-independent AC layer properties are within 10%. SAPSI's predictions using frequency-dependent AC properties gave the best fit to field data. CHEVRON's static predictions gave a somewhat better fit to field measurements than SAPSI's calculations using frequency-independent AC properties. Nonetheless, very good agreement with field measurement was obtained in all cases.

5.7.2.2 June 1992 FWD Tests

The same profiles as in October 1991 FWD tests were used because conditions were nearly identical for both tests. The dynamic load consisted of the same haversine pulse with a duration of 30 milliseconds. The results are shown in Table 5.7. In the case of longitudinal strains, agreement with measured values is very good for both static and dynamic analyses. All measured longitudinal strains are within ±10 percent of their calculated values. Figure 5.22 shows a graphical comparison between predicted and measured longitudinal strains. The measured transverse strains are about seventy percent of

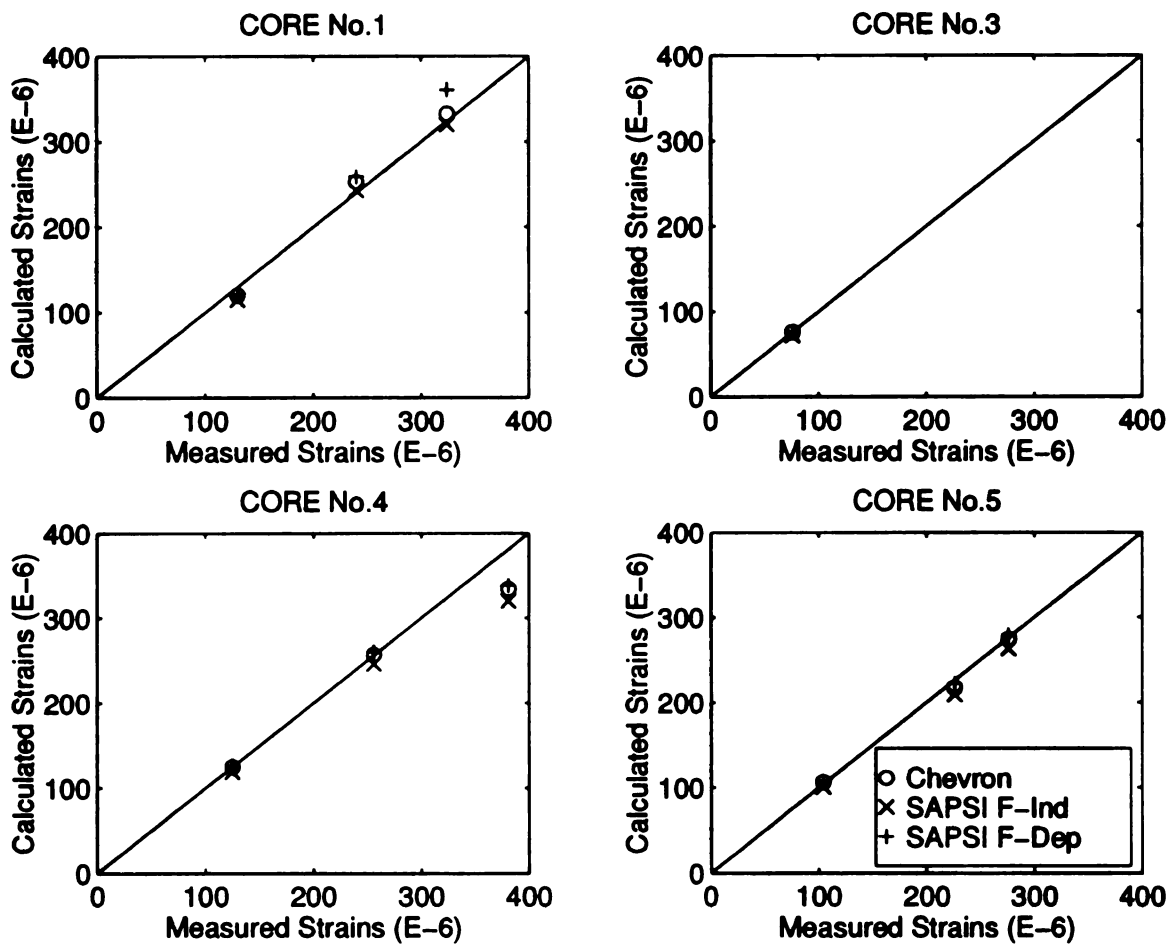

FIGURE 5.21 Comparison of Measured to Calculated Strains - Oct. 1991 FWD Tests

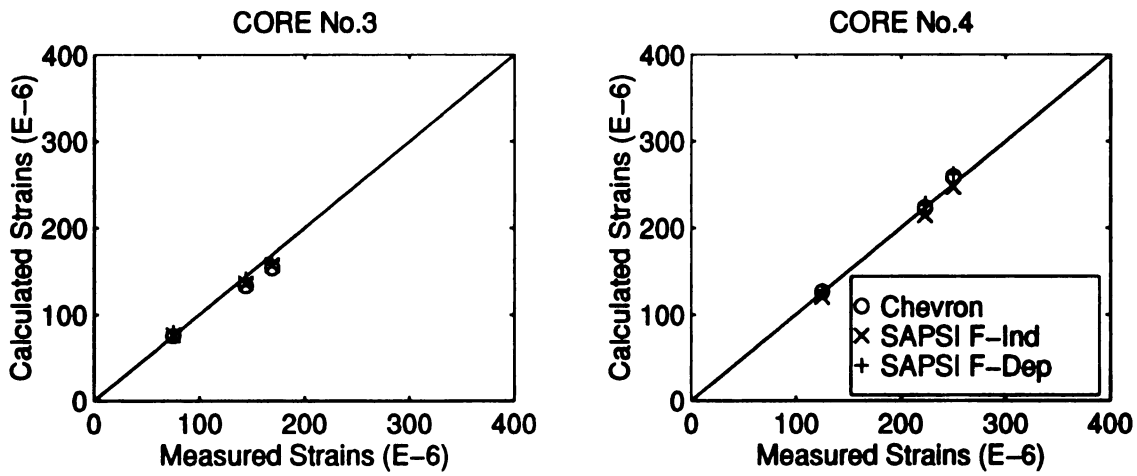

FIGURE 5.22 Comparison of Measured to Calculated Strains - June 1992 FWD Tests

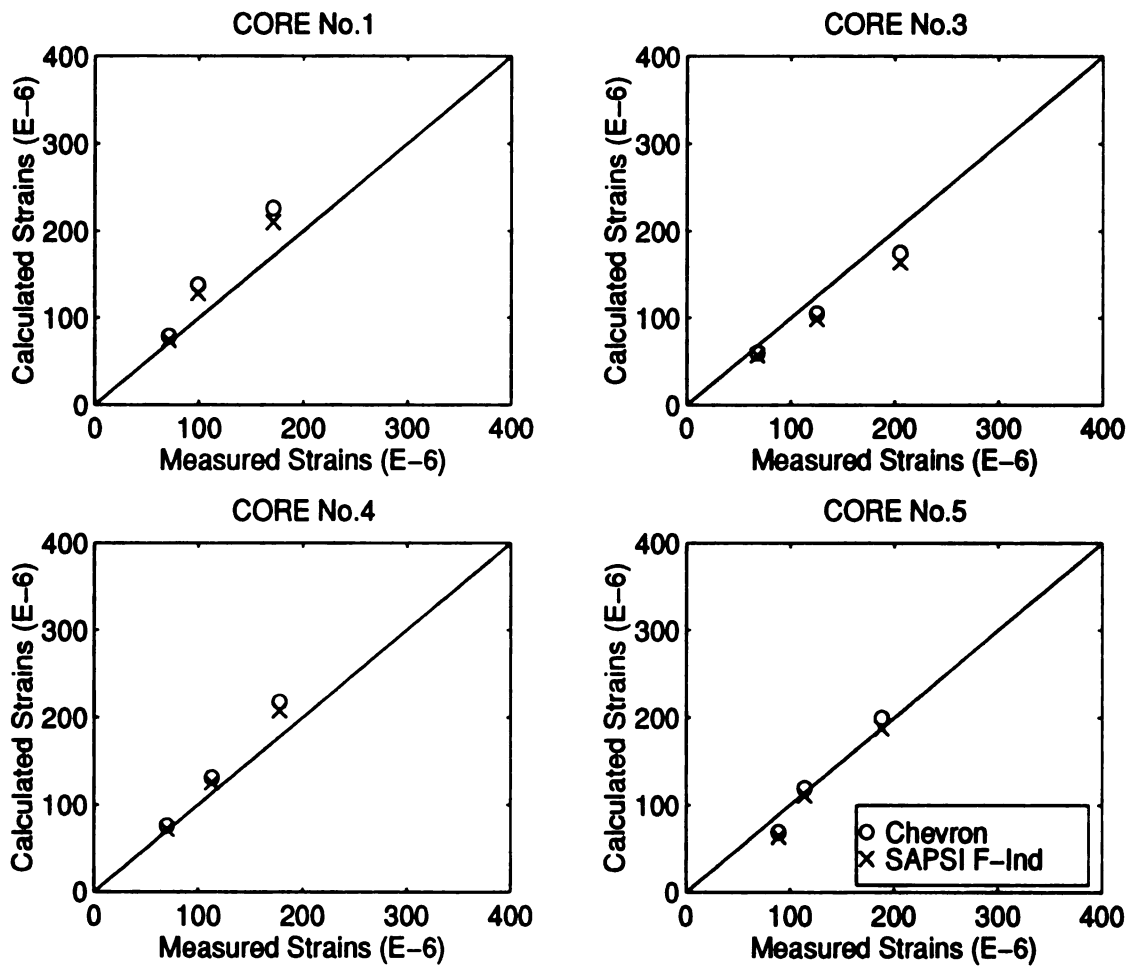

FIGURE 5.23 Comparison of Measured to Calculated Strains - Feb. 1993 FWD Tests

TABLE 5.6 Comparison of Measured and Calculated Strains - October 1991 FWD Testing

Axial Core	Averaged Load (lbf)		Microstrain				Ratio (meas/calc)		
			Measured	CHEVRON	SAPSI		CHEVRON	SAPSI	
					F-Indepen	F-Depen		F-Indepen	F-Depen
1	5,109	L	130	120	115	122	1.08	1.15	1.06
		T	120				1.00	1.04	0.98
1	10,785	L	240	253	243	259	0.95	0.99	0.93
		T	267				1.06	1.10	1.03
1	14,196	L	324	333	320	361	0.97	1.01	0.90
		T	383				1.15	1.20	1.06
3	5,110	L	76	76	72	76	1.00	1.04	1.00
		T							
4	5,268	L	125	125	119	126	1.00	1.05	1.00
		T	122				0.98	1.03	0.97
4	10,849	L	256	257	246	260	1.00	1.04	0.98
		T	249				0.97	1.01	0.96
4	14,099	L	381	334	320	338	1.14	1.20	1.13
		T	348				1.04	1.09	1.03
5	5,204	L	104	106	101	107	0.98	1.03	0.97
		T	86				0.81	0.85	0.80
5	10,718	L	226	217	209	215	1.04	1.09	1.05
		T	172				0.79	0.82	0.80
5	13,479	L	276	274	263	279	1.01	1.05	0.99
		T	224				0.82	0.85	0.86

TABLE 5.7 Comparison of Measured and Calculated Strains - June 1992 FWD Testing

Axial Core	Averaged Load (lbf)		Microstrain				Ratio (meas/calc)		
			Measured	CHEVRON	SAPSI		CHEVRON	SAPSI	
					F-Indepen	F-Depen		F-Indepen	F-Depen
3	5,313	L	75	75	76	79	1.00	0.99	0.96
		T	48				0.64	0.63	0.61
3	9,493	L	144	133	136	141	1.08	1.06	1.02
		T	94				0.71	0.69	0.67
3	10,946	L	169	154	157	162	1.10	1.08	1.04
		T	106				0.69	0.68	0.65
4	5,313	L	125	126	120	127	0.99	1.04	0.98
		T	78				0.62	0.65	0.61
4	9,493	L	223	223	214	227	1.00	1.04	0.98
		T	151				0.68	0.71	0.67
4	10,946	L	250	259	247	262	0.96	1.01	0.95
		T	175				0.68	0.71	0.67

TABLE 5.8 Comparison of Measured and Calculated Strains - February 1993 FWD Testing

Axial Core	Averaged Load (lbf)		Microstrain			Ratio (meas/calc)	
			Measured	CHEVRON	SAPSI F-Indepen	CHEVRON	SAPSI F-Indepen
1	6,205	L[1]	71	79	74	0.90	0.96
		T[2]	91			1.15	1.23
1	10,753	L	99	138	128	0.72	0.77
		T	162			1.17	1.26
1	17,614	L	171	226	210	0.76	0.81
		T	253			1.12	1.20
3	6,160	L	68	60	57	1.13	1.19
		T	70			1.17	1.23
3	10,660	L	125	105	99	1.19	1.26
		T	131			1.25	1.32
3	17,730	L	205	175	164	1.17	1.25
		T	212			1.21	1.29
4	6,160	L	70	76	72	0.92	0.97
		T	61			0.80	0.85
4	10,660	L	113	131	125	0.86	0.90
		T	106			0.81	0.85
4	17,730	L	178	218	208	0.82	0.86
		T	151			0.69	0.73
5	6,114	L	89	69	64	1.29	1.39
		T	119			1.72	1.86
5	10,563	L	114	119	111	0.96	1.03
		T	156			1.31	1.40
5	17,853	L	188	200	188	0.94	1.00
		T	233			1.17	1.24

L[1]: Longitudinal Strain

T[2]: Transverse Strain

the longitudinal strains, and since SAPSI's solution is axisymmetric the predicted values for transverse strains are about 30 percent higher than the measured values. This ratio between transverse and longitudinal strains is different from the ratio reported in October 1991 which was closer to one.

5.7.2.3 February 1993 FWD Tests

The same effective layer thicknesses as in the October 1991 profiles were used in the February 1993 calculations with the exception of the depths to stiff layer. The new back calculated depths are shown in Table 5.3. Table 5.5 shows the back calculated layer moduli for Axial Cores 1, 3, 4, and 5 as well as the assumed values of Poisson's ratio. The same haversine pulse with a 30 millisecond duration was applied. The results are shown in Table 5.8. Figure 5.23 shows a graphical comparison between predicted and measured longitudinal strains. Agreement with measured values is not as good as in the October 1991 tests for both static and dynamic analysis. About 70 percent of the measured strains are with in ±20 percent of their calculated values. This could be due to measurement errors. As time passes after the initial installation of strain gauges and the refitting of the cores into the pavement section, exposure to moisture and temperature fluctuations in the pavement causes the sensitivity and reliability of the strain gauges to decrease. Also, the fact that the pavement is significantly cooler in February could have an effect on the measured response because strain gauges, and any instrumentation in general, are very sensitive to hot and cold weather especially for dynamic measurements. Another indication of questionable measurement is the difference between longitudinal and transverse strains which was greater in February 1993 than in October 1991 tests.

Considering all the possible sources of error in measurement such as temperature and moisture conditions, linearity of measurement and performance of the bonded pavement cores, as well as the errors that accompany any numerical modeling, these results

constitute a very good field verification for both CHEVRON's closed-form solution and SAPSI's transient solution. The results also imply that static analysis of pavements using statically back-calculated layer moduli seems to be sufficient for accurately predicting the pavement's field response under stationary dynamic FWD pulse loads.

5.8 SUMMARY

A new method and associated computer program, SAPSI-M, for the analysis of asphalt concrete pavements under moving transient loads have been developed. The program was verified with field data from full-scale pavement tests on an instrumented asphalt concrete section on a test track in the PACCAR Technical Center in Mount Vernon, Washington. The analysis has led to the following conclusions:

(1) Agreement between SAPSI-M's predictions and field measurements was excellent for longitudinal strains and good for transverse strains, in both shape and magnitude.

(2) The effect of truck speed on the response of asphalt concrete pavements is significant. The test results showed that increasing truck speed form creep speed to 40 mph reduced the peak longitudinal strain by about 35 percent. Transverse strain showed more variability with the effect of speed ranging from 20 to 40 percent.

(3) The analytically-predicted horizontal strains in the asphalt concrete layer using frequency-dependent properties for the asphalt concrete layer were closer to the field measured values than those using frequency-independent AC properties. This is an indirect field verification of the strong dependency of asphalt concrete properties on the frequency of loading and an indication that the speed effect on horizontal strain is in part due to the frequency-dependent visco-elastic properties of asphalt concrete.

(4) A simplified solution where the moving loads are assumed to be non-vibrating seems to be sufficient in accurately predicting the response.

A series of Falling Weight Deflectometer (FWD) tests was also conducted. The comparison of the measured strain from FWD tests with static and dynamic theoretical predictions were made using CHEVRON and SAPSI computer programs, respectively. The following conclusions can be made:

(1) Ninety percent of the measured strains in October 1991 FWD tests and all measured strains in June 1992 FWD tests were within ±10 percent of their calculated values, using both static and dynamic analyses. Seventy percent of the measured strains in February 1993 were within ±20 percent. These results constitute a very good field verification of the stationary transient solution in the SAPSI computer program.

(2) Static analysis using statically back-calculated layer moduli seems to be sufficient in analyzing FWD field tests, despite the fact that static back-calculation using FWD (dynamic) deflections will lead to "stiffened" elastic properties.

CHAPTER 6

APPLICATION OF SAPSI-M PROGRAM TO PREDICTING FATIGUE DAMAGE

6.1 INTRODUCTION

Distress in pavements is a form of failure with respect to certain criteria. It is a phenomenon that causes considerable maintenance or loss of serviceability in a structure system. Most commonly, the forms of distress in flexible pavements are fatigue cracking, permanent deformation or rutting and thermal cracking. This study is mainly concerned with fatigue distress. Prediction of fatigue distress for an asphalt concrete pavement is possible through the use of dissipated energy concepts.

An energy-based fatigue method incorporates visco-elastic properties of materials and establishes relationships between the repetitive stresses and strains and the pavement's performance or fatigue life via the dissipated energy. Dissipated energy is defined as the area within a stress-strain loop and represents the energy lost (being dissipated) over one cycle or summed over a number of cycles to obtain the cumulative dissipated energy in the pavement as a result of a traffic passage.

With the SAPSI-M computer program, it is possible to solve for the primary response (stresses, strains, displacements) of asphalt pavement layered systems with visco-elastic material properties. Using the program, the stress and strain time histories and the corresponding energy dissipated at any point within the asphalt concrete layer due to the passage of a moving load may be determined. This dissipated energy will be linked to the fatigue distress by a relationship between the fatigue life and the energy dissipated.

The objective of this study is to present an approach based on energy dissipation and visco-elastic properties of an asphalt pavement for predicting the fatigue life of asphalt concrete pavements.

6.2 REVIEW OF FATIGUE LAWS IN FLEXIBLE PAVEMENTS

Modern design of pavements should incorporate a mechanistic analysis to predict distresses in pavements so that damage and life of pavements would be assessed in a rational way. It is important to know the fatigue characteristics of asphaltic materials over a wide range of mixture and environmental conditions in order to be able to incorporate sound fatigue criteria in the design method. Many research studies have been done on the fatigue characteristics of asphalt concrete. This section will describe some of these previous studies.

6.2.1 Prediction of Fatigue Life

Fatigue cracking is considered to be a tensile phenomenon. It is the repetitive application of tensile strain or stress, at levels considerably below that required to induce immediate fracture, which is responsible for the initiation and propagation of fatigue cracks. Fatigue cracking is usually related to the magnitude of tensile strain at the bottom of the asphalt pavement layer. Sometime, however, fatigue cracking may be initiated at a different location, even at the pavement surface. Estimating the potential for such cracking has been a challenge facing the pavement researchers [76].

Fatigue in pavements has been studied through field observations and accelerated performance tests in the laboratory. Published results from field surveys along with theoretical and empirical models are used to predict fatigue in pavements by use of material properties and other engineering parameters.

Material properties influence the occurrence of significant distresses. It is very important to characterize asphalt pavement materials in terms of fundamental properties, since design systems are becoming more and more based on elastic and visco-elastic theories. Mathematical models of pavements predict the response of pavement systems based on linear elasticity or visco-elasticity under repeated loading. The prediction of fatigue life of pavement systems can be obtained from the relationship(s) between material properties and distress at different stress or strain levels.

Tensile strain is the major pavement response related to fatigue damage or cracking. Most of the research conducted in this area has so far singled out peak tensile strain as the cause or determinant of fatigue damage. There is a tendency, however, to use the dissipated energy concept that relates the number of cycles to failure to the amount of energy dissipation during repetitive loading. In a later section, comparison between the fatigue life predicted using conventional fatigue models based on peak tensile strain and that predicted from energy dissipation will be made.

6.2.2 Accelerated Performance Tests

The study of in-service pavements to formulate fatigue model, is often difficult and time consuming. Many procedures and test methods have been published for defining the fatigue characteristics of asphalt mixtures from an available information obtained from both laboratory and field tests. These procedures involve a variety of test techniques, equipment and test conditions. Different laboratory tests, however, can provide widely different results, which can influence the predicted structural performance of the pavement. The differences in fatigue test results should be evaluated and explained in order to compare different test results and relate them to actual conditions, before applying them to design.

Tests which have been used for studying fatigue in asphalt concrete mixtures include the simple flexure test (center and third point bending), two point trapezoidal test, rotating cantilever test, direct axial load test, tri-axial test, wheel-tracking test, fracture mechanics test and repeated load indirect tensile test. Criteria used to evaluate each method for its potential use as a laboratory standard include: (i) The ability to simulate field conditions, (ii) the applicability of test results with performance of in-service pavements. Factors affecting fatigue response include specimen fabrication, mode of loading, mixture variables, and loading and environmental conditions.

For most of the laboratory test types, two basic modes of loading can be used, controlled-strain which is applicable to, or representative of, thin flexible pavements, and controlled-stress for materials in thicker pavements. As the number of load applications increases, the stress remains constant and the strain increases as a specimen is damaged in a controlled-stress test, whereas strain stays constant while the stress decreases in a controlled-strain test. In controlled-stress tests, stiffer mixtures exhibit longer fatigue lives while in controlled-strain tests, the more flexible mixtures have longer fatigue lives. For the same mixture type, controlled-stress loading results in a shorter life than controlled-strain loading [76].

6.2.3 Factors Affecting Fatigue Life

Many factors have been found to affect the fatigue behavior of asphalt mixtures. These factors may be categorized into loading, mixture and specimen, and environmental variables [29].

The factors related to load include magnitude, mode, frequency, duration and rest period. It should be noted that rest period, load duration and frequency are dependent on each other such that the load duration added to the rest period determine the frequency of

loading. Hence the separate effects of these variables on fatigue life might be difficult to ascertain in a conclusive manner.

Epps et al. [32] and Kennedy et al. [58] have discussed the effect of mode of loading and have concluded that longer fatigue life is obtained with materials tested under controlled-strain mode. Monismith has explained this result in terms of energy dissipation, where it was found that it is larger for controlled-stress tests, resulting in reduced fatigue life.

Though van Dijk [116] claimed that there was no apparent effect produced by frequency of loading on fatigue life, Deacon and Monismith [29] reported that increasing the frequency of load application in the range of 30 to 100 cycles per minute significantly decreased fatigue life by about 20 percent. In another study, Pell and Taylor [80] found a significant effect of frequency, with higher frequencies producing a longer fatigue life. Hence it can be argued that the effect of frequency of loading on fatigue life is not well established and further investigations are needed to verify previous claims.

Fatigue life is significantly affected by duration of load. Laboratory test results have indicated that reduced duration of applied stresses lead to an increased fatigue life [58]. Craus et al. [28] reported that a loading time in the range of 0.04 to 0.1 second is appropriate for fatigue testing, in a study aimed at investigating the relationship between loading time and thickness of asphalt layer for various vehicle speeds.

Mixture variables include asphalt content, asphalt type, aggregate type and gradation and air void content. Increasing the asphalt content increases fatigue life; however, there is an optimum asphalt content for a mix which maximizes fatigue life without compromising stability and consistency.

Porter and Kennedy [82] indicated that though the effects of aggregate type and gradation are not fully understood, tests have shown that mixtures containing aggregates with increased roughness and angularity and finer gradation have longer fatigue lives. Aggregate gradation and type also have a complex effect on air void content, which is a function of mixture composition and compaction. There is evidence that increased air void content results in a decreased fatigue life.

Craus et al. [28] reported the fabrication of specimens to be an important factor when studying fatigue characteristics of asphalt mixtures from laboratory specimens. The primary objective of specimen compaction is to produce realistic test specimens which reasonably duplicate corresponding asphalt paving in all major respects including composition, density and engineering properties.

Environmental factors influence the fatigue resistance of asphaltic pavements. There are immediate effects and long-term changes produced by temperature and moisture variations, in fatigue characteristics of asphalt mixtures. Temperature is the more important variable as most studies indicating that fatigue life increase with decreasing temperature.

6.2.4 Existing Fatigue Models

The fatigue properties of materials are expressed as a relation between an arbitrarily chosen criterion of fatigue life and the corresponding stress or strain. Usually, the fatigue characteristics of a bituminous material are expressed as a relation between the initial strain at the beginning of the experiment and the number of load repetitions to failure. The number of load applications to failure, N, is defined in a number of ways, depending upon the nature of test such as controlled-stress or controlled-strain. Fatigue life may be defined as the number of load applications up to the point when the stiffness value of a

material is reduced to half the initial value in the case of controlled-strain, while it may be defined as the number of applications at which a full crack develops in the case of controlled-stress beam tests or permanent deformations reaches 0.25 inches at indirect tensile tests.

Laboratory results are usually presented as plots of strain versus number of load repetitions to fatigue failure. Strain is the repeated constant strain in controlled-strain tests while it is usually taken to be the initial strain in controlled-stress tests. Pell [79] theorized that much of the variation caused by the state of stress, temperature and mixture properties can be explained and accounted for by considering strains rather than stresses from tests when establishing fatigue life relationships. Strain-fatigue life relationships have been shown to be fairly independent of the variables mentioned.

Early fatigue studies have found that fatigue life is often better correlated with tensile strains than with tensile stress. Statistical analysis is used to fit lines through scatter test data points, and the slope and relative level of the plots characterize the fatigue behavior of materials. A linear relationship is assumed to exist between the logarithm of applied tensile strains and the logarithm of fatigue life which is expressed as follows [58]:

$$N_f = k\left(\frac{1}{\varepsilon_t}\right)^n \qquad (6\text{-}1)$$

where, N_f is the fatigue life, ε_t is the applied tensile strain, and k and n are material constants determined from laboratory testing. The coefficients k and n completely describe the relationship between fatigue life and strain and can be used to describe the fatigue properties of asphalt mixtures. The value of n normally varies between 4 and 6. Values of 3 and 7 may occasionally be found under extreme measuring conditions of temperature and frequency. In order for Equation (6-1) to be used in the analysis and design

of pavement structures, ε_t is assumed to be the maximum principal tensile strain, a quantity identical to the maximum applied strain in uni-axial laboratory tests and determined from the complex, multi-dimensional stress state imposed by traffic on pavements.

In an attempt to account for differences observed in the fatigue life-strain relationship due to added factors such as loading frequency and temperature variation, a mixture stiffness term may be added to the previous equation as follows [73]:

$$N_f = a\left(\frac{1}{\varepsilon_t}\right)^b (S_{mix})^c \qquad (6\text{-}2)$$

where, S_{mix} is the stiffness modulus of the asphalt mixture and c is a third calibration material constant obtained from laboratory.

The mode of loading, air-void content have also been found to be important to the fatigue behavior of asphalt mixture. Monismith et al. [76] proposed a model which includes these factors as well as the initial strain and the mix stiffness, as follows:

$$N_f = a e^{bMF} e^{cV_o} \varepsilon_o^d S_o^e \qquad (6\text{-}3)$$

where, MF is the mode factor assuming values of 1 and -1 for controlled-strain and controlled-stress, respectively, V_o is the initial air-void content in percent, ε_o is the initial strain, S_o is the initial mix stiffness in psi, and a, b, c, d, e are regression constants.

Baladi [7] proposed a fatigue model considering that temperature, air void, viscosity and aggregate angularity are also important to the fatigue behavior, as follows:

$$\ln(N_f) = a - b(TT) - c\ln(CL) - d(AV) - e(KV) + f(ANG) \qquad (6\text{-}4)$$

where, TT is the test temperature, CL is the cyclic load, AV is the percent air void, KV is the kinematic viscosity at 275^{0}F, ANG is aggregate angularity, and a, b, c, d, e are regression constants.

In practice, fatigue models incorporate several of the important variables mentioned earlier as affecting fatigue characteristics and these equations derived from experimental results and regression analyses are expressed in terms of the relevant independent variables. Figure 6.1 shows the comparison of fatigue models from different test methods [37]. It is necessary to compare values estimated or predicted by the regression equations with measured values from an independent set of data which was not used to derive the equations in order to provide some validation of the equations.

A major difficulty with fatigue testing is developing a relationship between the results of the laboratory tests and field performance. To account for differences between laboratory and field response, shift factors are necessary to translate laboratory fatigue characteristics to those considered to be representative of in-situ performance. Unfortunately, there is no unique relationship. The shift factor appears to be dependent on the asphalt characteristics, test types, test conditions, and the field conditions to which the laboratory test results are being compared.

6.3 REVIEW OF ENERGY-BASED FATIGUE DAMAGE MODELS

6.3.1 Road Damage Prediction

Road damage refers to degradation of the structural integrity or surface profile of a road by traffic passage. Current mechanistic pavement design practice in many countries is to optimize resistance to fatigue and rutting. Analytical models are used to determine the

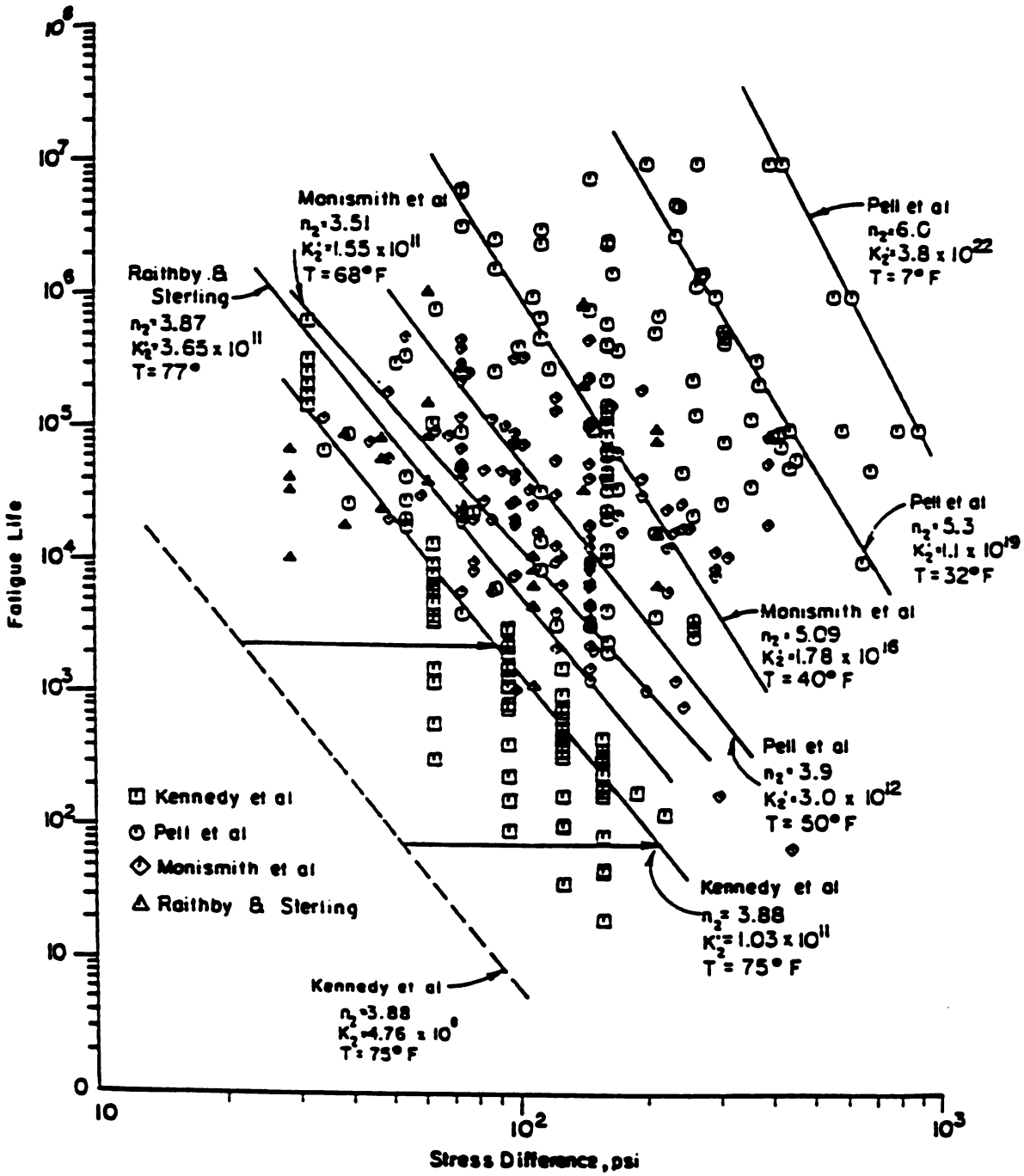

FIGURE 6.1 Comparison of Fatigue Models at Various Test Methods [37]

primary responses of a layered pavement structure due to a static, standard wheel load. The fourth power law is frequently used to convert the estimated traffic during the service life into an equivalent number of standard wheel loads. The fourth power law stemmed from the AASHTO road test [1, 45, 46] which showed that the decrease in pavement serviceability caused by a heavy vehicle axle could be related to the fourth power of its static load. Experimental fatigue and pavement deformation characteristics of the road material are then combined with the calculated primary response to evaluate suitable pavement layer thicknesses and material property specifications.

For in-service pavements, strains induced in the structure vary widely as a result of variations in the types of axles, their loaded weight, tire pressure, lateral placement, etc. Miner's hypothesis [71] seems to be a good means for accumulating the damaging effects of mixed loading. This linear summation of cycle ratios is given by:

$$\frac{n_1}{N_{1f}} + \frac{n_2}{N_{2f}} + \ldots + \frac{n_i}{N_{if}} + \ldots + \frac{n_m}{N_{mf}} \leq 1 \qquad (6\text{-}5)$$

where i is the ith level of applied strain at a critical point within the pavement structure, n_i is the actual number of load application at strain i, and N_{if} is the number of expected fatigue failure under the application of strain. Failure is expected to occur when the linear summation of cycle ratios reaches one.

For the analysis of fatigue damage, the most commonly used primary responses are the horizontal tensile stress or strain at the bottom of the asphalt layer, since analytical models generally predict the maximum tensile strain occurring at this location under the wheel load.

An alternative to using these horizontal tensile stress or strain is that of considering the constancy of dissipated energy. The number of cycles to failure is related to the amount

of energy dissipated during repetitive loading. The fact that the total energy dissipated by a material which fails under repetitive loading could turn out to be constant irrespective of test conditions is an important consideration for identification of materials and prediction of performance, which could be incorporated in design.

Several investigators have concluded that a unique relationship between the number of load applications to failure and the corresponding total dissipated energy per unit volume exists for a particular asphalt concrete mixture.

This study involves using the entire response time history of stress and strain at a point in the pavement to predict fatigue damage, rather than using just the peak tensile strain. This is relevant because field measurements have shown that a moving load will generate a flexural strain influence line with one tension peak and two compression zone (beyond and after the peak) at the bottom of the asphalt concrete layer.

6.3.2 Energy Concepts for Fatigue Damage

The use of energy methods to describe and study fatigue response of asphaltic materials has gained ground in recent years. One such method has been the concept of energy dissipation. Fatigue of visco-elastic materials like asphalt concrete subjected to repeated dynamic loading has been associated with the energy loss such that the fatigue life can be related to the total energy dissipated during the period before failure.

Dissipated energy is defined as the area within a stress-strain hysteresis loop and represents the energy lost at a fixed point in the pavement as a result of traffic passage. Figure 6.2(a) and (b) show a typical stress-strain hysteresis loops obtained in controlled-strain and controlled-stress tests, respectively [102]. The energy can be considered as being dissipated over one cycle or summed over a number of cycles to obtain the cumulative dissipated energy. Fatigue tests of asphalt concrete mixtures under laboratory condi-

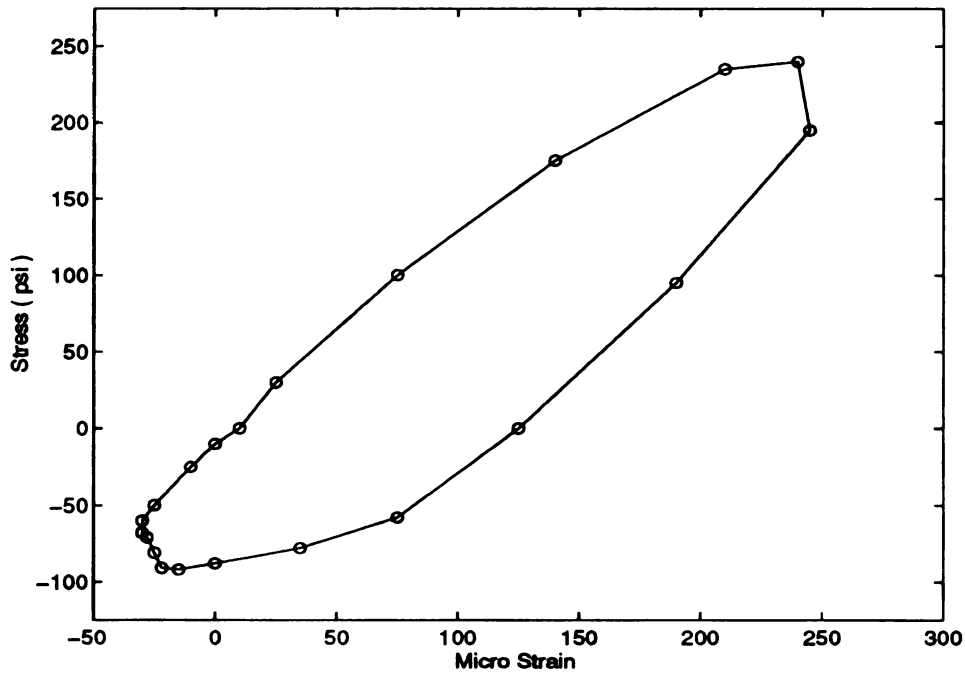

(a)

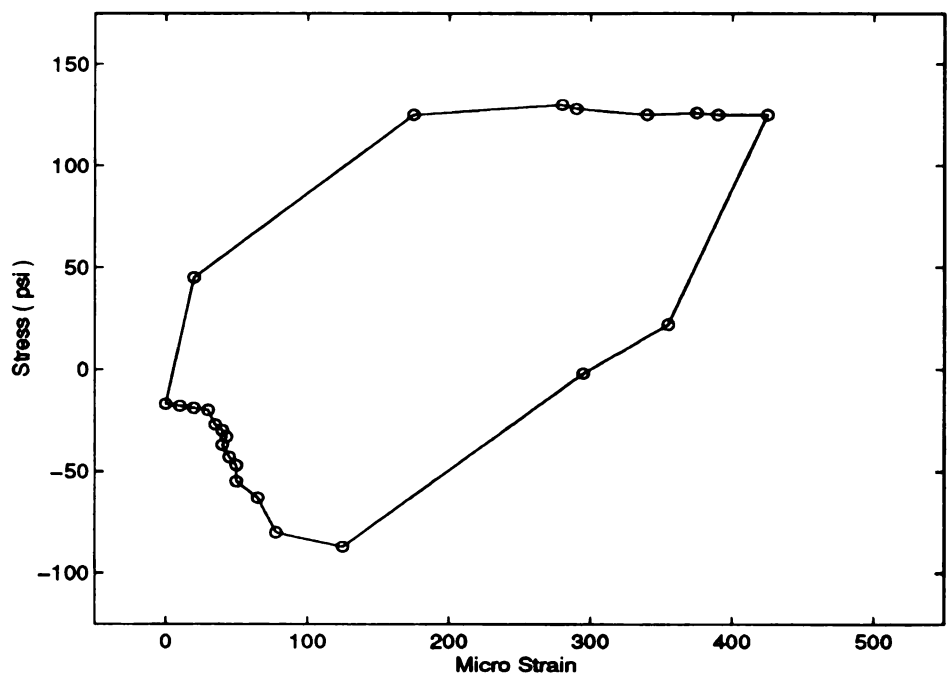

(b)

FIGURE 6.2 Typical Stress-Strain Hysteresis Loop [102]

(a) Strain Control Test

(b) Stress Control Test

tions have demonstrated that there is a unique relationship between the fatigue life of the mixture and the cumulative energy dissipated by the mixture during the fatigue test.

Figure 6.3(a) shows the variation of dissipated energy per cycle with the number of load repetitions [102]. The dissipated energy per cycle decreases with increasing load repetitions in the controlled-strain fatigue tests; whereas, for the controlled-stress tests, the dissipated energy per cycle increases as the number of load repetitions increases. Figure 6.3(b) shows the increase of the total energy dissipated during fatigue tests as a function of the number of load repetitions [114]. It shows how the cumulative dissipated energy changes at the controlled-strain and stress test modes. It is seen that the total energy dissipated in practically the same in both cases.

6.3.3 Previous Studies

Early researchers noticed that a unique relationship might possibly exist between the number of cycles to failure and the cumulative energy dissipated to failure. If so, laboratory testing could be abbreviated, and compound loading could be handled more directly. This means that loading mode, temperature, and frequency of loading dot not have a significant influence on the total energy dissipated prior to failure. Accordingly, it is argued that this approach permits prediction of the fatigue life of a mixture over a wide range of conditions based on a few simple fatigue tests. Because of these advantages, considerable effort has been made to investigate possible relationships between cycles to failure and cumulative dissipated energy. In this method the number of cycles to failure is related to the amount of energy dissipated during repetitive loading.

Van Dijk[115] is one of the first researchers who employed energy methods to fatigue tests. From tests conducted with different modes of loading, he concluded that the total energy dissipation due to repeated loading at failure for a certain type of asphaltic

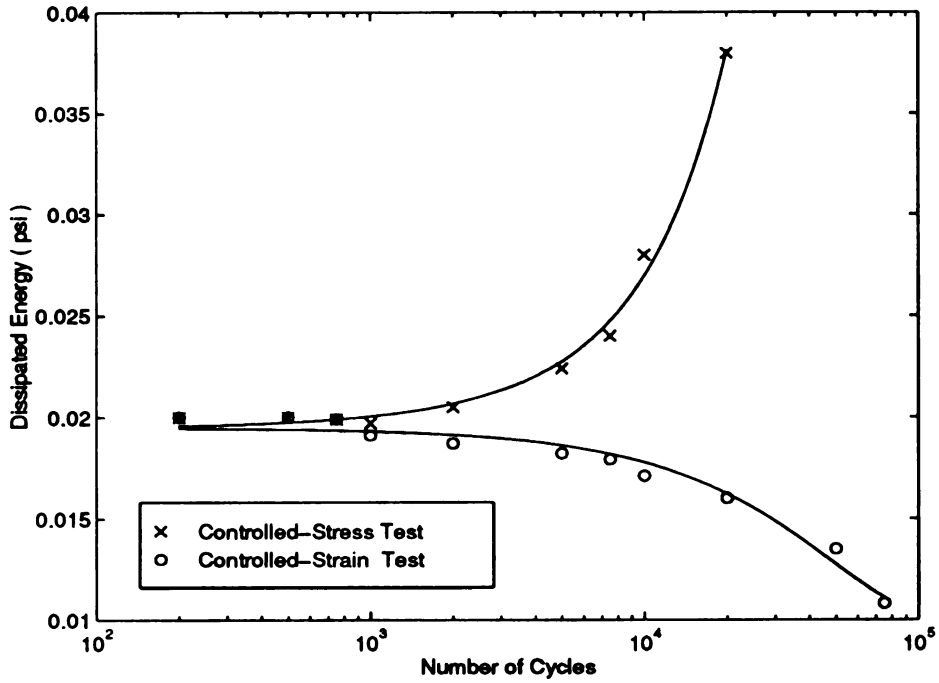

(a)

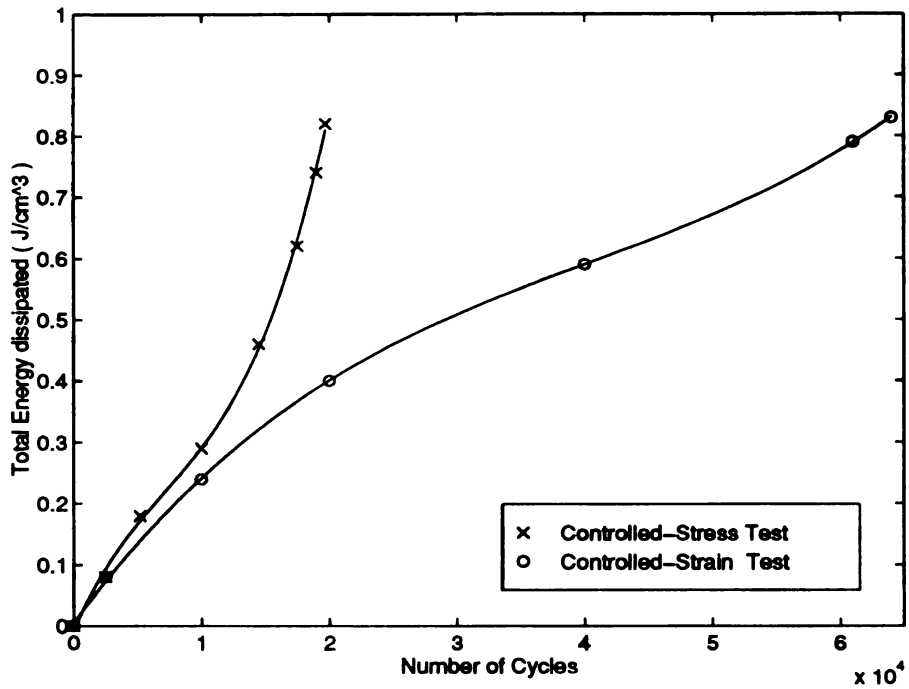

(b)

FIGURE 6.3 Typical Curve of Dissipated Energy versus Number of Cycles

(a) Dissipated energy per cycles [102] (b) Total dissipated energy [114]

material remains constant irrespective of the test mode used. Nevertheless, he indicated that the controlled-stress mode of loading dissipates energy much faster than the controlled-strain mode. Later, Van Dijk [116] also reported that the cumulative dissipated energy versus the number of cycles relationship is not independent of the mix formulation but is independent of test methods (two and three point bending), temperature (50 ^{o}F to 104 ^{o}F), mode of loading (controlled-stress, controlled-strain), and frequency (10 to 50 Hz). Chomton and Valayer [22] also concluded that cumulative energy is the sole independent factor that predicts fatigue life, and that energy seems to be independent of the mixtures.

Monismith et al. [76] reported that the uniqueness of this relationship for different types and conditions of testing could not be sustained. In fact, detailed investigation revealed that these relationships are different for different mixes and are affected by both test temperature and mode of testing. Despite this disappointment, dissipated energy remains a useful concepts in fatigue investigation, because the energy dissipated during the initial loading cycle which captures not only the effect of the imposed strain level but also of the dynamic mix properties, is a good predictor of cycles to failure and is thus a key component of surrogate models. Furthermore, dissipated energy is highly correlated with stiffness decrements during fatigue testing and helps to explain the effects of mode of loading on mix behavior.

Tangella et al. [108] summarized well the advantages and disadvantages of the dissipated energy methods. The following are considered to be advantages of this approach:

(1) According to Van Dijk [116], the major advantage of this method is that loading, temperature, frequency of loading, and occurrence of rest period do not have a significant influence on the total dissipated energy. The number of cycles to failure is mainly related to the amount of energy dissipated during the test. If validated, this could lead to dramatic reduction in laboratory testing, and

avoidance of the mode of loading issue in laboratory work would be a great advantage.

(2) This method is based on a physical phenomenon which explains the fatigue behavior of visco-elastic materials through the accumulation of the distortional energy resulting from load repetitions.

(3) For both stress and strain controlled flexural tests, there exists a unique relation between the total dissipated energy per unit volume and the number of load applications to fatigue failure.

(4) Prediction of fatigue life is possible as a first approximation if initial stiffness and phase angle are known.

(5) Structural design of an asphalt concrete layer to consider fatigue effect is possible as a first approximation.

The disadvantages of this method include:

(1) Accurate prediction of fatigue behavior is not possible without conducting detailed fatigue tests.

(2) The procedure proposed in this method can not be considered as a design technique: rather, it serves to indicate the general magnitude of the fatigue life of a given asphalt mixture.

6.3.4 Dissipated Energy versus Fatigue Life

Several investigators have proposed dissipated energy as a controlling parameter for the fatigue of asphalt mixes.

Van Dijk [115] suggested that the initial dissipated energy per unit volume per cycle for a sinusoidal loading can be obtained as follows:

$$w_o = \pi \sigma_o \varepsilon_o \sin \phi_o \qquad (6\text{-}6)$$

where, σ_o, ε_o are initial stress and strain amplitudes respectively, and ϕ_o is a phase angle between stress and strain wave signals.

Since the phase angle keeps changing during fatigue test, the fatigue life may be divided into intervals in which the phase angle is relatively constant and total dissipated energy is found by summing the dissipated energy of each interval i, as follows:

$$W_{fatigue} = \sum_{i=1}^{n} w_i \qquad (6\text{-}7)$$

The result of these energy calculations for different asphalt mixes may be expressed as a function of the number of strain repetitions to fatigue. An independent energy relationship for each mix has been found between the number of load applications to fatigue, N_f, and the total dissipated energy per unit volume, $W_{fatigue}$, expressed by:

$$W_{fatigue} = AN_f^{\,z} \qquad (6\text{-}8)$$

where, A and z are material parameters. For an asphalt concrete Van Dijk found that z was equal to 0.63 and A was equal to 6.76×10^4 J/m^3 [115].

Sousa et al. [102] proposed a fatigue model based on the dissipated energy from the flexural beam test that consisted of a 1/2 factorial experimental design for mixtures composed of two aggregates, two asphalts, with two asphalt contents, at two compaction levels, using two temperatures and two loading modes: Controlled-stress and controlled-strain. They defined energy dissipation as an exponential function of the number of load repetitions:

$$W_f = Ae^{BN_f} \qquad (6\text{-}9)$$

where W_f is the total dissipated energy up to failure, e is base of natural logarithms, A is a material parameter corresponding to the energy dissipated in the first cycle, B is a material parameter representing how fast the energy dissipated per cycle changes, and N_f the is number of cycles to failure. For controlled-stress tests, B is positive whereas it is nega-

tive for controlled-strain tests. The ratio of energy dissipated, R_f, was introduced for convenience, as follows:

$$R_f = W_N/A = e^{BN_f} \tag{6-10}$$

where R_f is the ratio of the energy dissipated at failure to the energy dissipated in the first cycle. Sousa et al. [102] used a least square technique to determine the value of R_f for controlled-stress and controlled-strain tests. They obtained R_f as 2.1 for controlled-stress tests and 0.5 for controlled-strain tests. These results indicate that, for controlled-stress tests, failure occurs when the area of the loop doubles from the initial value, whereas for controlled-strain tests the failure occurs when the area of the stress-strain loop reaches 50% reduction from the initial value. Combining the above results into the equations (6-9) and (6-10) produces, the following relationship of fatigue life and the dissipated energy in cycle one:

$$N_f = \ln(2.1)/(0.0071 \times A^{1.43}) \qquad \text{for controlled-stress test} \tag{6-11}$$

$$N_f = \ln(0.5)/(-0.00247 \times A^{1.33}) \qquad \text{for controlled-strain test} \tag{6-12}$$

Monismith et al. [76] evaluated the fatigue performance of a thin asphalt pavement section (3.5inch asphalt concrete layer over 12 inch in base) at FHWA's Accelerated Loading Facility. All tests were performed under a controlled-strain mode of loading at a frequency of 10 Hz under sinusoidal loading with no rest periods at the temperature of 68 ^{o}F. Fatigue tests were summarized in the form of relationships between fatigue life and initial strain, and initial dissipated energy per cycle. The following equations were developed using linear regression analysis:

$$N_f = 8.959 \times 10^{-8} (\varepsilon_o)^{-3.574} \qquad R^2=0.987 \tag{6-13}$$

$$N_f = 425.81(w_o)^{-1.846} \qquad R^2=0.987 \qquad (6\text{-}14)$$

where, N_f the is fatigue life, ε_o the is initial peak-to-peak tensile strain, and w_o is the initial dissipated energy per cycle in psi.

6.4 PREDICTION OF PAVEMENT FATIGUE DAMAGE USING SAPSI-M PROGRAM

The prediction of field performance using the concept of energy dissipation requires the use of a computer program to solve the boundary value problems representative of pavement systems with visco-elastic material properties. The problem is reduced to determining the energy dissipated at any given point in the asphalt concrete layer with the passage of a moving wheel load. A crack will initiate from the point where the most energy is being dissipated.

With the SAPSI-M computer program, it is possible to solve the problems for layered asphalt concrete pavement systems with visco-elastic material properties. Using the program, the stress and strain time histories and the corresponding energy dissipated at any point within the asphalt concrete layer due to the passage of a moving load may be determined. This dissipated energy will be linked to the fatigue distress by a relationship between the fatigue life and the energy dissipated.

The objective of this part of the study is to investigate the possibility of using an approach based on energy dissipation to predict fatigue damage of an asphalt concrete pavement using the computer program SAPSI-M.

6.4.1 Calculation of Dissipated Energy in SAPSI-M

As discussed previously, the dissipated energy is defined as the area within a stress-strain hysteresis loop for a specific location in the pavement corresponding to an application of moving loads. Using the SAPSI-M program, the dissipated energy at any point in the pavement structure may be calculated by obtaining the stress-time and strain-time histories and calculating the area within the corresponding hysteresis loop. This procedures, however, would require two SAPSI-M runs to calculate the dissipated energy per cycle.

Given the stress time history from a single run of SAPSI-M program, the strain time history can be predicted immediately using the appropriate stress-strain relationship. This will simplify the procedure and will save computer run time. In the following, the calculation of energy dissipation per cycle in the frequency domain will be shown using the stress time history only at a point due to the passage of the load.

6.4.1.1 Derivation of Energy Dissipation in 1-D

The dissipated energy in any direction can be expressed analytically as the work integral:

$$W = \int_0^T \sigma(t) \cdot \frac{\partial \varepsilon}{\partial t} dt \qquad (6\text{-}15)$$

Using complex representation, the stress time history can be written in a Fourier series, as follows:

$$\sigma(t) = \mathrm{Re}\sum_{s=0}^{N/2} \Omega_s \cdot e^{i\omega_s t}$$

$$= \mathrm{Re}\left(\sum_{s=0}^{N/2} \Omega_s(\cos(\omega_s t) + i\sin(\omega_s t))\right) \qquad (6\text{-}16)$$

$$\Omega_s = \mathrm{Re}\Omega_s + i\mathrm{Im}\Omega_s$$

$$\dot{\varepsilon}(t) = \mathrm{Re}\sum_{s=0}^{N/2} i\omega_s \frac{\Omega_s}{E_s} \cdot e^{i\omega_s t} \qquad (6\text{-}17)$$

Then the Equation (6-15) becomes:

$$W = \int_0^T \left(\mathrm{Re}\sum_{s=0}^{N/2} \Omega_s \cdot e^{i\omega_s t}\right)\left(\mathrm{Re}\sum_{s=0}^{N/2} i\omega_s \frac{\Omega_s}{E_s} \cdot e^{i\omega_s t}\right) dt \qquad (6\text{-}18)$$

where:

$$\begin{aligned} \Omega_s &= \mathrm{Re}\Omega_s + i\mathrm{Im}\Omega_s \\ E_s &= |E_s| e^{i\delta_s} \\ E^* &= E e^{i\delta} \\ &\approx E e^{2i\beta} \qquad \text{for} \qquad \beta \ll 1 \end{aligned} \qquad (6\text{-}19)$$

and

$$\begin{aligned} \tan\delta &= \frac{2\beta\sqrt{(1-\beta^2)}}{1-2\beta^2} \\ \delta &= 2\beta \qquad \text{for} \qquad \beta \ll 1 \end{aligned} \qquad (6\text{-}20)$$

with

E^* = Complex Modulus of Elasticity
μ = Poissons ratio
δ = Loss angle
β = Damping ratio

Then

$$\mathrm{Re}\sum_{s=0}^{N/2}\Omega_s\cdot e^{i\omega_s t} = \sum_{s=0}^{N/2}[\mathrm{Re}\Omega_s\cdot\cos\omega_s t-\mathrm{Im}\Omega_s\cdot\sin\omega_s t] \tag{6-21}$$

$$\begin{aligned}\mathrm{Re}\sum_{s=0}^{N/2} i\omega_s\frac{\Omega_s}{E_s}\cdot e^{i\omega_s t} &= \mathrm{Re}\sum_{s=0}^{N/2}\frac{i\omega_s}{|E_s|}\cdot[(\mathrm{Re}\Omega_s\cdot\cos\omega_s t-\mathrm{Im}\Omega_s\cdot\sin\omega_s t)\\ &\quad+i(\mathrm{Im}\Omega_s\cdot\cos\omega_s t+\mathrm{Re}\Omega_s\cdot\sin\omega_s t)][\cos\delta-i\sin\delta]\\ &= \sum_{s=0}^{N/2}\frac{\omega_s}{|E_s|}\cdot[(\mathrm{Re}\Omega_s\cdot\sin\delta-\mathrm{Im}\Omega_s\cdot\cos\delta)\cos\omega_s t\\ &\quad-(\mathrm{Im}\Omega_s\cdot\sin\delta+\mathrm{Re}\Omega_s\cdot\cos\delta)\sin\omega_s t]\end{aligned} \tag{6-22}$$

Substituting the above results into Equation (6-18) and taking advantage of the orthogonality relations of the sine and cosine functions, the expression for the energy dissipation in the 1-dimension is expressed as following:

$$\begin{aligned}W &= \sum_{s=0}^{N/2}\frac{\pi s}{|E_s|}\cdot|\Omega_s|^2\cdot\sin\delta_s\\ &= \sum_{s=0}^{N/2}\frac{\pi s}{2|E_s|}\cdot\Omega_s\overline{\Omega}_s\cdot\sin\delta_s\end{aligned} \tag{6-23}$$

6.4.1.2 Derivation of Energy Dissipation in 3-D

The dissipated energy in three-dimensions can be expressed analytically in matrix form as follows:

$$W = \int_0^T[\sigma(t)]^T\cdot[C]\cdot[\dot{\sigma}(t)]dt \tag{6-24}$$

where:

$$\{\sigma(t)\}^T = \{\sigma_x\ \ \sigma_y\ \ \sigma_z\ \ \sigma_{xy}\ \ \sigma_{xz}\ \ \sigma_{yz}\}^T$$

$$[C] = \frac{1}{E^*}\begin{bmatrix} 1 & -\mu & -\mu & 0 & 0 & 0 \\ & 1 & -\mu & 0 & 0 & 0 \\ & & 1 & 0 & 0 & 0 \\ & & & (1+\mu) & 0 & 0 \\ & & & & (1+\mu) & 0 \\ & & & & & (1+\mu) \end{bmatrix}$$

The stress-strain relationship is defined in the usual manner.

$$\varepsilon_{ij} = \frac{1}{E^*}(-\delta_{ij}\mu\sigma_{kk} + (i+\mu)\sigma_{ij}) \tag{6-25}$$

If only tensile stress/strain is considered in x-direction, the dissipated energy will be simplified as follows:

$$W_x = \int_0^T \frac{1}{E^*}\{\sigma_x\dot{\sigma}_x - \mu(\sigma_x\dot{\sigma}_y + \sigma_x\dot{\sigma}_z)\}dt \tag{6-26}$$

Substitute Equation (6-16) and (6-17) into the above equation gives the following:

$$W_x = \mathrm{Re}\int_0^T \frac{1}{E^*}\sigma_x\dot{\sigma}_x dt - \mathrm{Re}\int_0^T \frac{\mu}{E^*}\sigma_x\dot{\sigma}_y dt - \mathrm{Re}\int_0^T \frac{\mu}{E^*}\sigma_x\dot{\sigma}_z dt \tag{6-27}$$

From the derivation of the one-dimensional problem and after taking advantage of the orthogonality relations of the sine and cosine functions, the expression for the energy dissipated in the x-direction is expressed as follows:

$$\begin{aligned} W_x = & \sum_{s=0}^{N/2} \frac{\pi s}{E_s}(\sin\delta_s(\mathrm{Re}^2\Omega_{xs} + \mathrm{Im}^2\Omega_{xs})) \\ & - \sum_{s=0}^{N/2} \frac{\pi s}{E_s}(\mu\sin\delta_s(\mathrm{Re}\Omega_{xs}(\mathrm{Re}\Omega_{ys} + \mathrm{Re}\Omega_{zs}) + \mathrm{Im}\Omega_{xs}(\mathrm{Im}\Omega_{ys} + \mathrm{Im}\Omega_{zs}))) \\ & + \sum_{s=0}^{N/2} \frac{\pi s}{E_s}(\mu\cos\delta_s(\mathrm{Re}\Omega_{xs}(\mathrm{Im}\Omega_{ys} + \mathrm{Im}\Omega_{zs}) - \mathrm{Im}\Omega_{xs}(\mathrm{Re}\Omega_{ys} + \mathrm{Re}\Omega_{zs}))) \end{aligned} \tag{6-28}$$

The expression in the y and z directions may be obtained by substitution, as follows:

$$W_y = \sum_{s=0}^{N/2} \frac{\pi s}{E_s}(\sin\delta_s(Re^2\Omega_{ys} + Im^2\Omega_{ys}))$$
$$- \sum_{s=0}^{N/2} \frac{\pi s}{E_s}(\mu \sin\delta_s(Re\Omega_{ys}(Re\Omega_{ys} + Re\Omega_{zs}) + Im\Omega_{ys}(Im\Omega_{ys} + Im\Omega_{zs}))) \quad (6\text{-}29)$$
$$+ \sum_{s=0}^{N/2} \frac{\pi s}{E_s}(\mu \cos\delta_s(Re\Omega_{ys}(Im\Omega_{ys} + Im\Omega_{zs}) - Im\Omega_{ys}(Re\Omega_{ys} + Re\Omega_{zs})))$$

$$W_z = \sum_{s=0}^{N/2} \frac{\pi s}{E_s}(\sin\delta_s(Re^2\Omega_{zs} + Im^2\Omega_{zs}))$$
$$- \sum_{s=0}^{N/2} \frac{\pi s}{E_s}(\mu \sin\delta_s(Re\Omega_{zs}(Re\Omega_{ys} + Re\Omega_{zs}) + Im\Omega_{zs}(Im\Omega_{ys} + Im\Omega_{zs}))) \quad (6\text{-}30)$$
$$+ \sum_{s=0}^{N/2} \frac{\pi s}{E_s}(\mu \cos\delta_s(Re\Omega_{zs}(Im\Omega_{ys} + Im\Omega_{zs}) - Im\Omega_{zs}(Re\Omega_{ys} + Re\Omega_{zs})))$$

The energy dissipation due to shear is expressed by:

$$W_{ij} = \sum_{s=0}^{N/2} \frac{\pi s(1+\mu)}{E_s} \sin\delta_s(Re^2\Omega_{ij} + Im^2\Omega_{ij}) \quad (6\text{-}31)$$

From the above derivations, it is possible to calculate the energy dissipation per cycle in the frequency domain from a single SAPSI-M run with the stress time history as output. For fatigue analysis, only the contributions from the tensile stresses/strains in the x and y directions are of significance.

6.4.2 Strain, Dissipation Energy and Fatigue Life

Monismith et al. [76] developed fatigue models based on both peak tensile strain and initial dissipated energy from FHWA-ALF pavement fatigue test. The test was performed on a thin asphalt pavement section (3.5inch asphalt concrete layer over a 12 inch base) and included single and dual tire loadings consisting a full scale field test subjected to an uni-directional moving load in the speed of 10.5 MPH. Beam specimens (2.5 inch x

2.0 inch x 15.0 inch) were made from the sawed asphalt concrete slab sections which were delivered to the University of California-Berkeley. Controlled-strain fatigue tests were performed on these specimens at four strain levels at a frequency of 10 Hz under sinusoidal loading with no rest periods, and at 68^{0}F. The fatigue test results were summarized in the form of equations (6-13) and (6-14).

Monismith et al. [76] also simulated the in situ mix performance using an elastic analysis of the response of the given pavement section under single and dual tires with 12,000 lbs wheel load (24 kips axle load) and 140 psi tire pressure. The thickness were 3.5 inch and 12 inch for asphalt concrete and base, respectively. The stiffness values were 700,000 psi and 15,000 psi for asphalt concrete and base layers, respectively. The maximum tensile strain at the bottom of AC layer were determined from the elastic analysis, and the fatigue life was determined using Equation (6-13) as shown in Table 6.1. They compared the estimated fatigue life to the in situ FHWA-ALF fatigue test results. Figure 6.4 shows the in situ FHWA-ALF fatigue test results [76].

As mentioned before, Monismith et al. simulated the test section using an elastic analysis and estimated the fatigue life only from peak tensile strain. However, in this study, the peak tensile strain and initial dissipated energy per cycle are determined for the same test section using the SAPSI-M program in order to calculate the fatigue life. The same layer properties are utilized: however, some properties, which are necessary for visco-elastic analysis, are assumed based on the PACCAR field test. The moving load is simulated at 10.5 MPH. Results are compared to the in-situ FHWA-ALF field fatigue tests. These results are summarized in Table 6.2.

The initial dissipated energy per cycle is largest under the single tire configuration with subgrade stiffness of 5,000 psi, and it is smallest under the dual tire with subgrade

TABLE 6.1 Estimated Fatigue Life of FHWA-ALF Section using Elastic Analysis [76]

Tire Configuration	Subgrade Stiffness (psi)	Tensile Strain at AC Bottom	Fatigue Life from Peak Strain	Fatigue Life from In-situ Test
Single	5,000	$551*10^{-6}$	40,000	52,000
	10,000	$526*10^{-6}$	47,000	
Dual	5,000	$467*10^{-6}$	72,000	109,000
	10,000	$443*10^{-6}$	87,000	

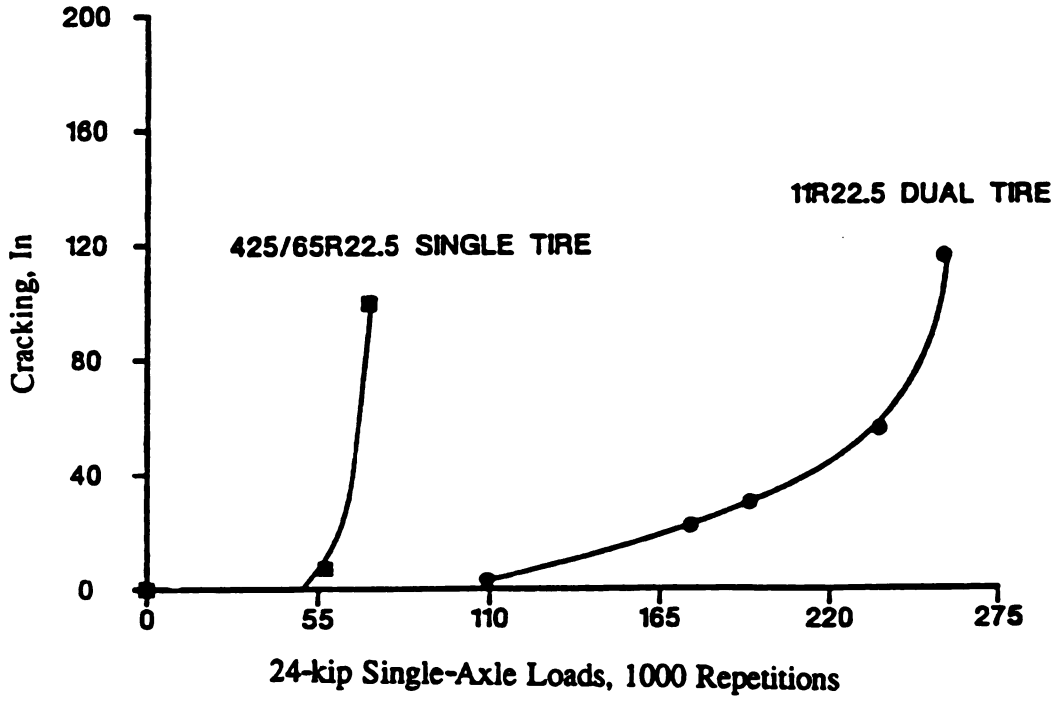

FIGURE 6.4 In Situ FHWA-ALF Fatigue Test for Surface Cracking [76]

stiffness of 10,000 psi. This results in the shortest and longest fatigue life, respectively. The estimated fatigue lives from peak tensile strains compare well to the ones using linear elastic analysis, with both showing a consistent. The fatigue lives from the initial dissipated energy are underestimated at high dissipated energy level and overestimated at lower energy level relative to those from peak strain. However, these fatigue lives compare well with the field fatigue test results as shown in Table 6.2.

TABLE 6.2 Fatigue Life based on Dissipated Energy from Moving Load Solution

Tire Configuration	Subgrade Stiffness (psi)	Initial Dissipated Energy Wx (psi)	Peak Tensile Strain $\varepsilon_x(*10^{-6})$	Fatigue Life		
				Dissipateed Energy Wx	Peak Strain ε_x	Field
Single	5,000	0.0903	545	36,000	41,500	52,000
	10,000	0.0815	511	43,500	51,900	
Dual	5,000	0.0517	471	101,000	69,900	109,000
	10,000	0.0462	439	124,000	89,400	

The findings from this validation effort may be summarized as follows:

(1) The estimated fatigue life based on the peak tensile strain model from the moving load solution compares well with the estimated fatigue life from linear elastic analysis and that of the in-situ pavement. This constitutes another field validation of SAPSI-M's moving load solution.

(2) The estimated fatigue life based on energy dissipation for the dual-tire configuration is approximately triple compared to that of the single-tire configuration. The actual pavement fatigue life to surface crack initiation is approximately double that for the dual-tire configuration compared to the single-tire configuration.

(3) The fatigue model based on energy dissipation of Equation (6-14) seems to underestimate fatigue life at higher dissipated energy levels and overestimate fatigue life at lower dissipated energy levels.

(4) The above findings constitute the possibility of using an approach based on energy dissipation to predict fatigue damage of an asphalt concrete pavement by computer program SAPSI-M.

6.4.3 The Effect of Speed on Energy Dissipation

The same profile as in the previous section with a subgrade stiffness of 5,000 psi was used to study the speed effect by means of initial dissipated energy per cycle and fatigue life. Three additional speeds (4 MPH, 30 MPH and 60 MPH) were used in the SAPSI-M simulation, in addition to the previous result of 10.5 MPH. The results are shown in Table 6.3.

The table shows that peak tensile strains decrease by 23 percent, which leads to increasing the fatigue life by 2.37 times, while, the initial dissipated energy decreases by 52 percent, resulting in increasing the fatigue life by 4.93 times, as speed increases from 4 to 60 MPH. This suggests that the speed effect is more significant relative to energy dissipation than to peak tensile strain, and that it affects fatigue life significantly. It should be noted, however, that speed will generally increase the truck axle vibrations which would lead to higher loads, and consequently lower fatigue lives. Therefore the speed effects on load magnitude and pavement response offset each other to a certain extent.

TABLE 6.3 Observation of Speed Effect by Energy Dissipation

Speed (mph)	Initial Dissipated Energy Wx (psi)	Peak Tensile Strain (ε_x)	Fatigue Life	
			Dissipateed Energy Wx	Peak Strain ε_x
4.0	0.1350	$586*10^{-6}$	17,300	32,000
10.5	0.0903	$545*10^{-6}$	36,000	41,500
30.0	0.0688	$503*10^{-6}$	59,600	55,100
60.0	0.0566	$460*10^{-6}$	85,300	75,800

6.4.4 Load Equivalency Factors from Energy Dissipation

The load equivalency factor represents the ratio of the number of repetitions of any axle load and axle configuration necessary to cause the same damage (example: reduction in PSI, and damage in general) as one application of an 18 kips single axle load. Since PSI (Present Service Index) is obtained from measurement of roughness and distress, e.g., cracking, patching and rut depth at a particular time during the service life of the pavement, the load equivalency factor may be obtained using energy dissipation.

The same profile as in the previous section (3.5 inch AC thickness with 5,000 psi subgrade stiffness) was used to simulate the in-situ pavement system. A single tire configuration (24 kips axle load) was used with the load moving at 10.5 MPH, in order to compare with the available data. An 18 kips single axle load (9 kips wheel load) with 140 psi was also used to calculate the load equivalency factor.

Figure 6.5 shows the types of axle configurations used to investigate the effects of axle number (single, tandem and tridem) and space between axles. Figure 6.6 shows the stress-strain hysteresis loops together with the strain- and stress-time histories of axle type-1. Due to the compressive strain/stress that the pavement experiences before and after the moving load passes by a fixed point in the pavement, the stress-strain hysteresis loops start and finish in the negative quadrant. The four hysteresis loops are overlapped almost exactly because the four axles are far enough apart not to interface with each other. This axle type causes exactly the same damage as four applications of a single axle load (24 kips) based on the observations of strain and.

Figure 6.7 shows the stress-strain hysteresis loops for axle-3. The axle-2 type configuration is not shown because it consists of two hysteresis loops; one inside, and one outside (instead of two in Figure 6.7). The strain and stress time histories show the larger

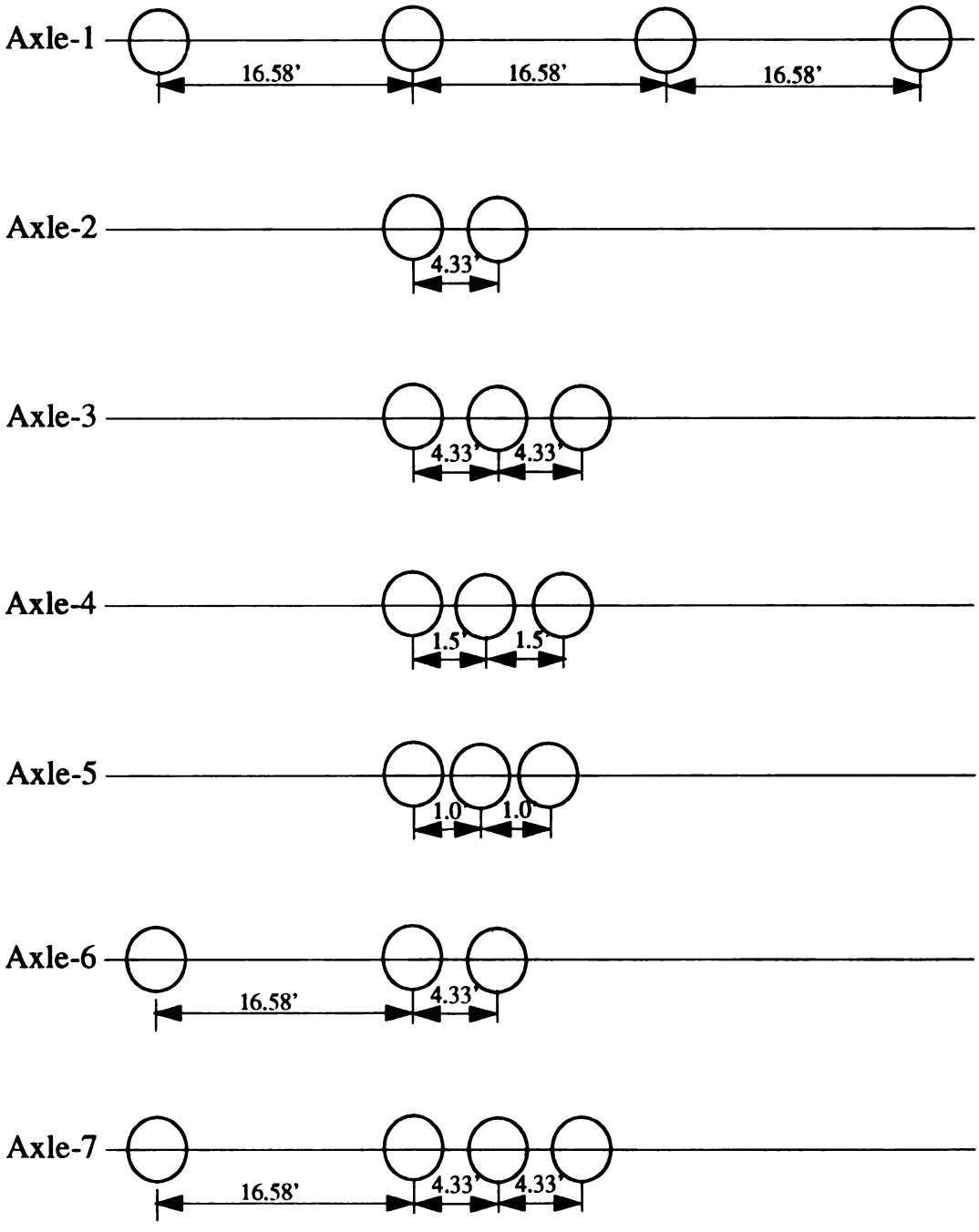

FIGURE 6.5 Types of Axle Configuration for Load Equivalency Factor

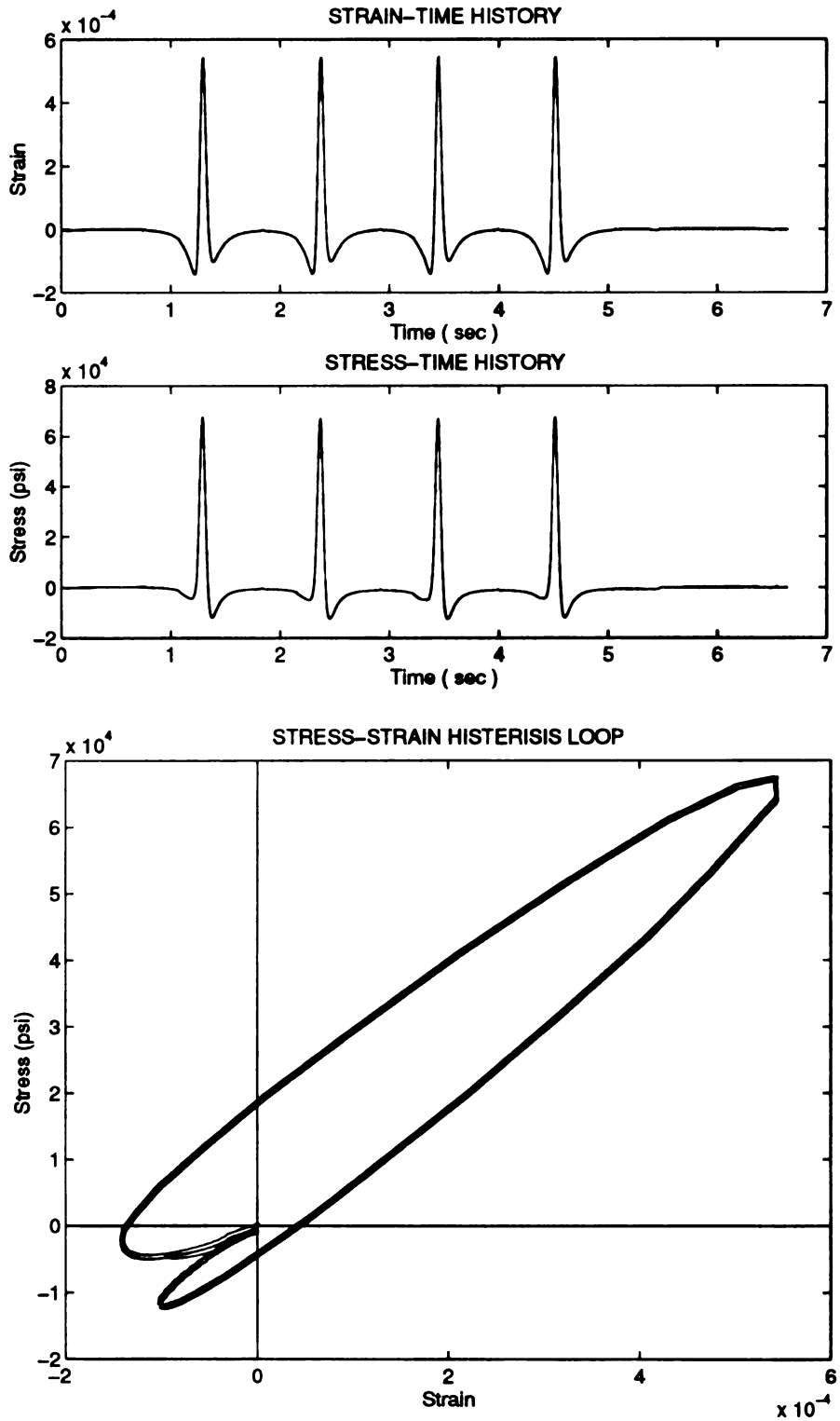

FIGURE 6.6 Stress-Strain Hysteresis Loop -Axle Type-1

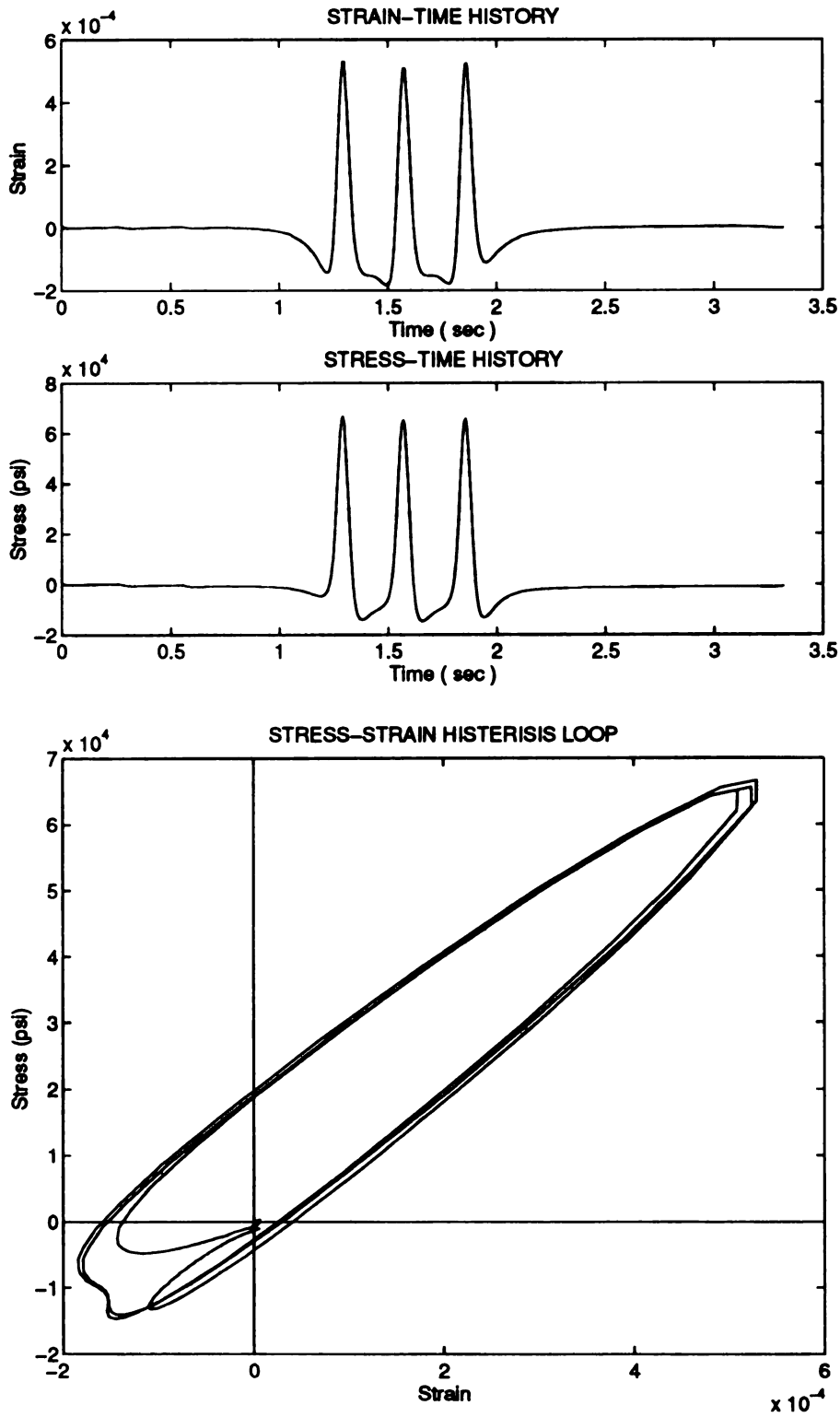

FIGURE 6.7 Stress-Strain Hysteresis Loop -Axle Type-3

strain/stress reversal after the first and the second load applications due to the interface between axles. The hysteresis loop for the axle-3 type consists of some additional areas in the negative direction compared to the axle-1 type due to larger negative stress/strain after the first and second load applications. Due to these additional area, the dissipated energy becomes larger and thus results in a shorter fatigue life.

Figure 6.8 shows the stress-strain hysteresis loop together with the strain and stress time histories due to the axle-4 configuration. Because of the shorter distance between the axles, there are no stress/strain reversals between load applications; the stress/strain remains tensile between the load applications. This result in a smaller energy dissipation and thus longer fatigue life. This type of stress strain time history can be exhibited in thicker, stiffer asphalt concrete pavements. It may be noted that the strain time history of tandem axle configuration is strongly dependent on the space between the axles by comparing the Figure 6.7 and Figure 6.8.

Figure 6.9 shows the stress-strain hysteresis loop corresponding to axle-7 configuration, which consists of two outside loops and two inside loops. The axle-6 configuration consists of 3 hysteresis loops: Two inside loops, and one outside loop instead of two loops. These axle configurations consist of one single axle with a tandem (axle-2) or a tridem (axle-3), respectively.

A substantial presence of compressive strains at the bottom of asphalt concrete layer is clear from the Figure 6.6 to Figure 6.9. This behavior is important, especially when laboratory tests are needed to estimate the fatigue strength or life of AC. The most current laboratory procedures use a pulse load that creates only tension in the specimen. For realistic fatigue life estimation, the whole strain history (combination of tension and compressive) may be important, instead of the current laboratory that include tensile strain only.

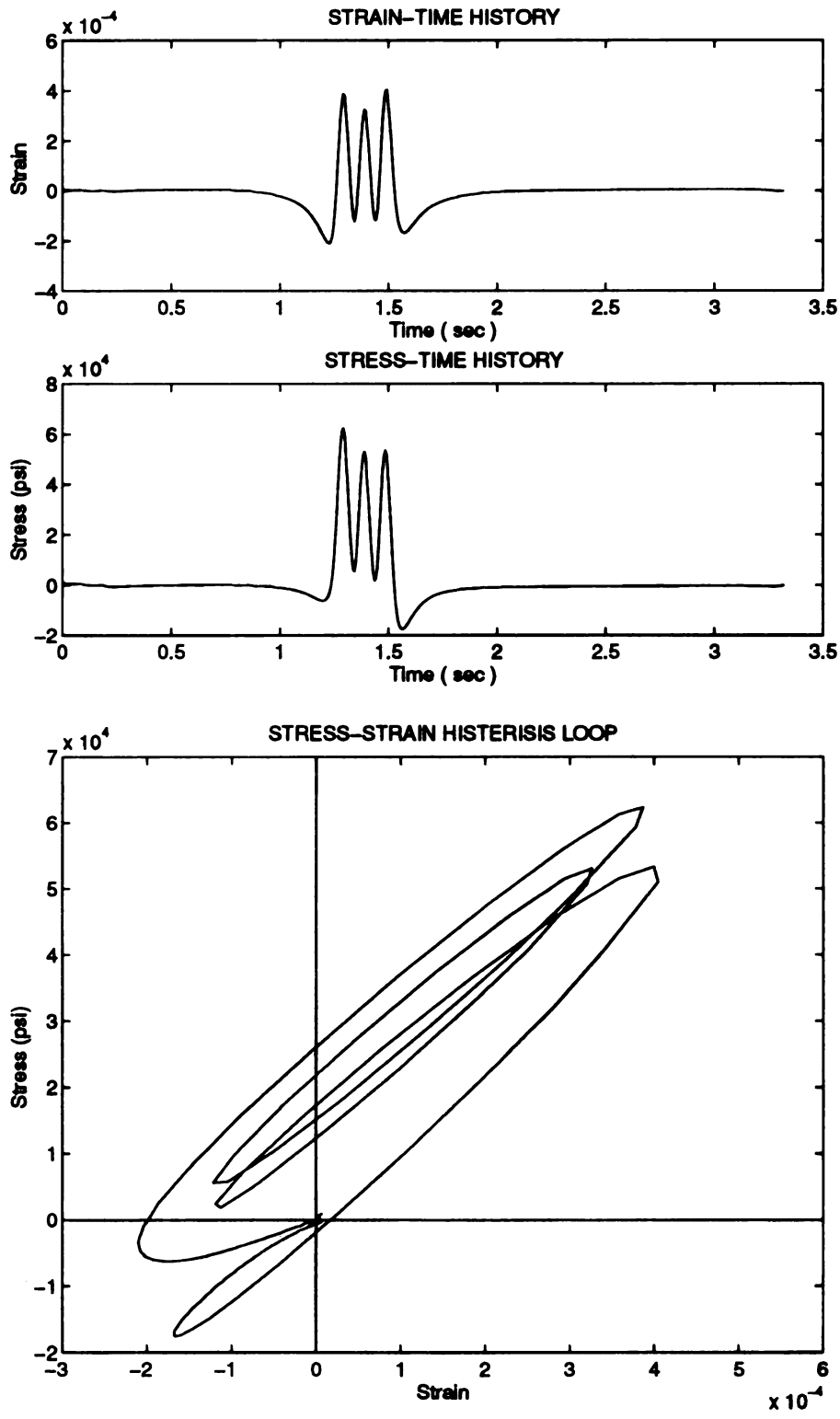

FIGURE 6.8 Stress-Strain Hysteresis Loop -Axle Type-4

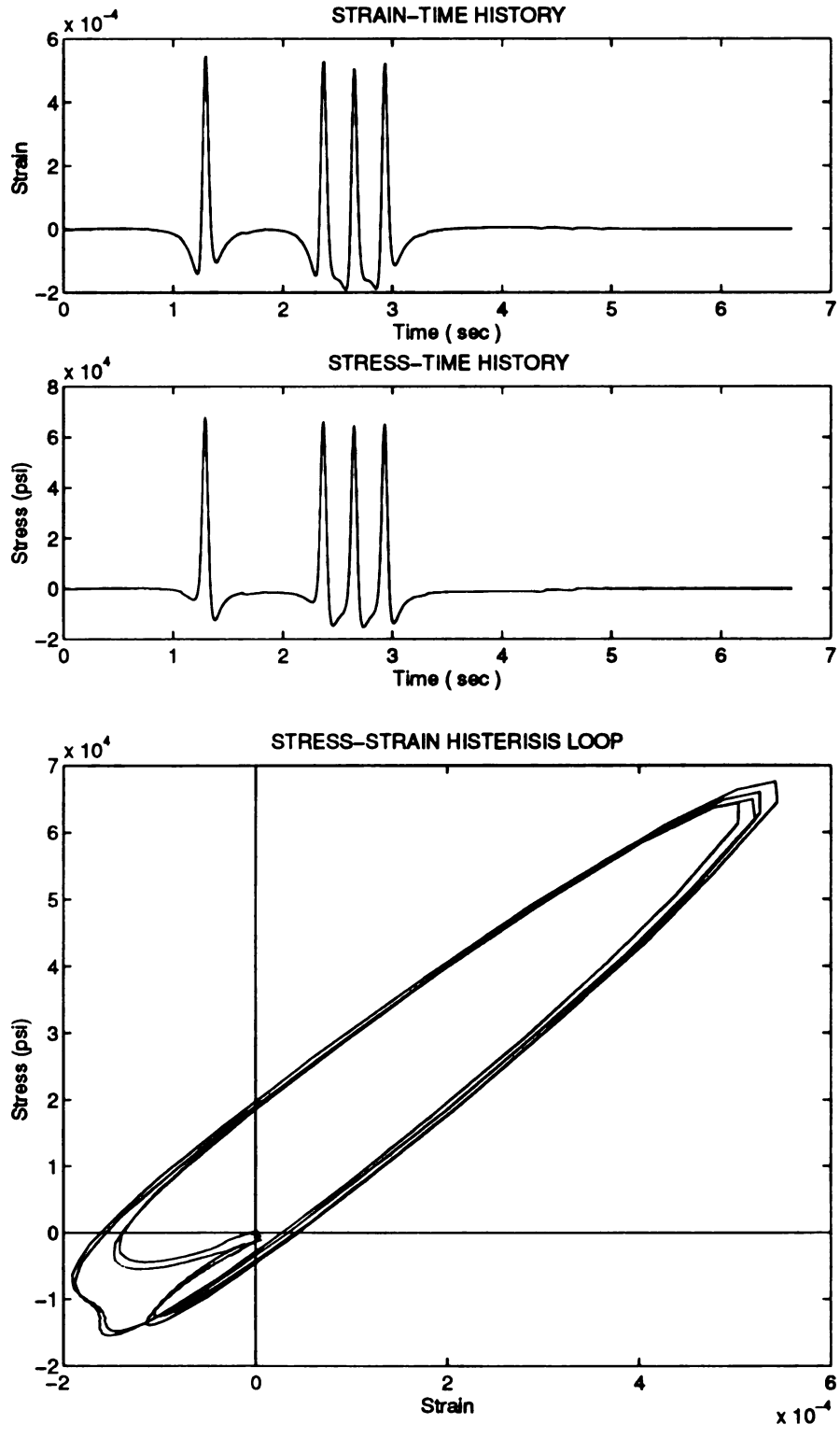

FIGURE 6.9 Stress-Strain Hysteresis Loop -Axle Type-7

TABLE 6.4 Load Equivalency Factor by Dissipated Energy

Type of Axle	No of Axles	Mean Dissipated Energy per Axle Wx (psi	Peak Tensile Strain ε_x (*10^{-6})	Mean Fatigue Life per Axle		Load Equivalency Factor	
				Energy Wx	Strain ε_x	Wx/W_{18kips}	$\varepsilon_x/\varepsilon_{18kips}$
Axle-1	4	0.0889	545	37,100	41,300	1.443	1.167
Axle-2	2	0.0911	528	35,500	46,200	1.479	1.131
Axle-3	3	0.0916	529	35,100	46,000	1.487	1.133
Axle-4	2	0.0439	405	137,000	120,000	0.713	0.867
Axle-5	3	0.0433	400	140,000	125,000	0.703	0.856
Axle-6	3	0.0894	544	36,800	41,700	1.451	1.165
Axle-7	4	0.0898	544	36,400	41,700	1.458	1.165
18 kips Single	1	0.0616	467	73,000	71,800	1.000	1.000

Table 6.4 summarizes the results by expressing them as mean initial dissipated energy, peak tensile strain, fatigue life and load equivalency factor for each axle type. The initial dissipated energy and peak tensile strain are a function of axle type and configuration. The load equivalency factor is also dependent on the axle type and configuration. The LEF (Load Equivalency Factor) based on dissipated energy is more sensitive than that from peak strain. Thus, it is believed that the LEF's which are based on energy dissipated are more appropriate than those for peak strain.

6.5 SUMMARY

An approach based on energy dissipation and visco-elastic properties of an asphalt pavement for predicting the fatigue life of asphalt concrete pavements has been presented. Using the SAPSI-M computer program, the stress and strain-time histories and the corresponding energy dissipated at any point within the asphalt concrete layer due to the passage of a moving load was determined. This dissipated energy was linked to the fatigue distress by a relationship between the fatigue life and the energy dissipated. The analysis has led to the following conclusions:

(1) The estimated fatigue life based on the peak tensile strain model from the moving load solution compares well with the estimated fatigue life from linear elastic analysis and that of the in-situ pavement. This constitutes another field validation of SAPSI-M's moving load solution.

(2) The estimated fatigue life based on energy dissipation for the dual-tire configuration is approximately triple compared to that of the single-tire configuration. The actual pavement fatigue life to surface crack initiation is approximately double that for the dual-tire configuration compared to the single-tire configuration.

(3) The fatigue model based on energy dissipation of Equation (6-14) seems to underestimate fatigue life at higher dissipated energy levels and overestimate fatigue life at lower dissipated energy levels.

(4) The above findings constitute the possibility of using an approach based on energy dissipation to predict fatigue damage of an asphalt concrete pavement using the computer program SAPSI-M.

(5) The speed effect on dissipated energy is higher than that on peak tensile strain, and may be even more significant in pavement systems based on laboratory fatigue models. However the effect of in-situ speed on the load vibration will be an offset factor.

(6) The initial dissipated energy and peak tensile strain are functions of axle type and configuration. The load equivalency factor is also dependent on the axle type and configuration. It appears that the load equivalency factor using the energy dissipation method are more sensitive than those using the peak tensile strain approach.

CHAPTER 7
CONCLUSION

7.1 SUMMARY AND CONCLUSION

A new method of analysis to study the dynamic response of horizontally n-layered damped-elastic systems to surface moving arbitrary loads under axisymmetric conditions has been developed. An associated new computer program called SAPSI-M has been written in the FORTRAN 77 language to incorporate the proposed method. The method and program builds on an existing model for stationary loads, SAPSI, which was developed at the University of California-Berkeley.

The proposed method uses the complex response method of transient analysis with a continuum solution in the horizontal direction and a finite element solution in the vertical direction, incorporating such important factors as wave propagation, inertia, and damping effects of the medium as well as frequency-dependent asphalt concrete properties. The method and the associated computer program SAPSI-M have the following characteristics, capabilities and limitations:

1. The structural model is a n-layered damped-elastic medium. Each layer is infinite in the horizontal directions and has a finite depth, except for the bottom layer. The subgrade can be modeled as either a rigid base or a semi-infinite halfspace. With these axisymmetric assumptions, a three dimensional problem can be reduced to a two-dimensional one, except that the edge effect can not be considered.

2. It is assumed that multiple loads that are vertical and uniformly distributed over a circular area are moving along a single direction at a constant velocity on the surface of a layered system. The loads may be constant in magnitude or may vibrate as an arbitrary function of time. The moving loads are modeled as a series of pulses with a

duration equal to the time required for the wheel to pass by a fixed point in the pavement. The proposed method can handle any load configuration, thus making it possible to model multiple wheel configurations of truck axles as well as airplane landing gears.

3. All materials are assumed to be linear visco-elastic in response to the loads. It is assumed that each pavement layer consists of a homogeneous, isotropic, and visco-elastic material. The asphalt material properties can be frequency dependent or independent. The shear modulus, damping ratio, and Poisson's ratio for each layer may be varied with the excitation frequency of the loads.

The accuracy of the proposed method and of the corresponding program has been validated with available field data. The moving load solution of the developed program, SAPSI-M, has been validated with the PACCAR full-scale field truck tests. The transient analysis in the SAPSI program has been validated with Falling Weight Deflectometer (FWD) tests. The analysis has led to the following conclusions:

1. Agreement between SAPSI-M's predictions and field measurements was excellent in the moving constant dynamic analysis for longitudinal strains and good for transverse strains, in both shape and magnitude.

2. Considering all the possible sources of error in measurement such as temperature and moisture conditions, linearity of measurement and performance of the bonded pavement cores, as well as the errors that accompany any numerical modeling, this constitute a very good validation of the moving load solutions in SAPSI-M.

3. The effect of truck speed on the response of asphalt concrete pavements is significant. The test results showed that increasing truck speed form creep speed to 40 mph reduced the peak longitudinal strain by about 35 percent. Transverse strains showed more variability with the effect of speed ranging from 20 to 40 percent.

4. The analytically-predicted horizontal strains in the asphalt concrete layer using frequency-dependent properties for the asphalt concrete layer were closer to the field measured values than those using frequency-independent AC properties. This is an indirect field verification of the strong dependency of asphalt concrete properties on the frequency of loading. The results also show that the frequency dependent properties of the asphalt concrete are a major contributor to the speed effect.

5. Agreement between SAPSI-M's predictions and field measurements of longitudinal strain was excellent in the moving arbitrary dynamic analysis and very good in the quasi-dynamic analysis in both the shape and magnitude of the response. These results show that although the amplitude of load vibrations is high, neglecting the effect of frequency, while maintaining correct allowance for truck speed and the magnitude of the dynamic wheel loads, does not change the response in any significant way. Therefore, a simplified solution where the moving loads are assumed to be non-vibrating seems to be sufficient for accurately predicting the pavement response. A similar conclusion was reached by Hardy and Cebon using a simplified beam on Winkler foundation model [40].

The comparison of Falling Weight Deflectometer (FWD) test results with static and dynamic theoretical predictions was made using CHEVRON and SAPSI computer programs, respectively. The following conclusions can be made from these results:

1. Ninety percent of the measured strains in October 1991 FWD tests and all measured strains in June 1992 FWD tests were within ±10 percent of their calculated values, using both static and dynamic analyses. Seventy percent of the measured strains in February 1993 were within ±20 percent.

2. Considering all the possible sources of error in measurement, the above results constitute a good validation of SAPSI's transient analysis.

3. Static analysis using statically back-calculated layer moduli seems to be sufficient in analyzing FWD field tests, despite the fact that static back-calculation using FWD (dynamic) deflections will lead to "stiffened" elastic properties.

An approach based on energy dissipation and visco-elastic properties of asphalt concrete for predicting the fatigue life of asphalt concrete pavements has been presented. Using the SAPSI-M computer program, the stress and strain time histories and the corresponding energy dissipated at any point within the asphalt concrete layer due to the passage of a moving load were determined. This dissipated energy was linked to the fatigue distress by a relationship between the fatigue life and the energy dissipated. The analysis has led to the following conclusions:

1. The estimated fatigue life based on the peak tensile strain model from the moving load solution compares well with the estimated fatigue life from linear elastic analysis and that of the in-situ pavement. This constitutes another field validation of SAPSI-M's moving load solution.

2. The estimated fatigue life based on energy dissipation for the dual-tire configuration is approximately triple compared to that of the single-tire configuration. The actual pavement fatigue life to surface crack initiation is approximately double that for the dual-tire configuration compared to the single-tire configuration.

3. The fatigue model based on energy dissipation of Equation (6-14) seems to underestimate fatigue life at higher dissipated energy levels and overestimate fatigue life at lower dissipated energy levels.

4. The above findings constitute the possibility of using an approach based on energy dissipation to predict fatigue damage of an asphalt concrete pavement using the computer program SAPSI-M.

5. The speed effect on dissipated energy is higher than that on peak tensile strain, and may be even more significant in pavement systems based on laboratory fatigue models. However increased speed and pavement roughness will cause higher dynamic loads, thus potentially offsetting the speed effect.

6. The initial dissipated energy and peak tensile strain are functions of axle type and axle configuration. The load equivalency factor is also dependent on the axle type and axle configuration. It appears that load equivalency factors using the energy dissipation method are more sensitive than those using the peak tensile strain approach.

7.2 RECOMMENDATIONS FOR FUTURE RESEARCH

Based on the results and findings of this study, the following general recommendations are suggested for future research on the analysis of asphalt concrete pavement response:

1. Further research into the effect of moving loads, pavement roughness, axle configurations and suspension types on pavement damage should be undertaken.

2. Further research in using the energy approach to assess load equivalency and pavement damage is called for.

3. There is a need for assessing the SAPSI-M model in terms of its degree of efficiency and accuracy in the future.

BIBLIOGRAPHY

LIST OF REFERENCES

[1] AASHTO, *Final Report on Road Test One -MD*, HRB Special Report 4, 1952.

[2] Abbo, E., *The Influence of Heavy Vehicle Dynamics on Rigid Pavement Response*, M.Sc. Thesis, Massachusetts Institute of Technology, 1987.

[3] Achenback J. D., Keshava, S. P., Hermann G., "Moving Load on a Plate Resting on an Elastic Halfspace," Trans. ASME J. Applied Mechanics, December 1967, pp. 910-914.

[4] Aedimila, A.S., Kennedy, T.W., *Fatigue and Resilient Characteristics of Asphalt Mixtures by Repeated Load Indirect Tensile Test*, Research Report 183-5, University of Texas, Austin, Aug. 1975

[5] Aglan, H.A., Figueroa, J.L., "Damage Evolution Approach to Fatigue Cracking in Pavements," Journal of Engineering Mechanics, Vol. 119, No. 6, 1993

[6] Ahlborn, G., *ELSYM5, Computer Program for Determining Stresses and Deformations in Five Layer Elastic System*, University of California, Berkeley, 1972.

[7] Baladi, Gilbert, "Fatigue Life and Permanent Deformation Characteristics of Asphalt Concrete Mixes," Transportation Research Record, No.1227, pp75-87.

[8] Barenberg, E. J., "Role of Instrumented Pavements in Establishing Load Equivalencies," FHWA Load Equivalence Workshop, Washington D.C., September 1988, 27p.

[9] Battiato, G., Verga, C., Ronca, G., "Visco-elastic deformation in a two layered paving system predicted from laboratory creep results," Transp. Res. Rec., 640 TRB, 1977, pp34-38.

[10] Bonaquist, R., Surdahl, R. and Mogawer, W., "Effect of Tire Pressure on Flexible Pavement Response and Performance," Transportation Research Record 1227, pp97-106.

[11] Boquenet, D., Le Houedec, D., "Comportement d'une chaussée reposant sur un matelas antivibratile et soumise à des charges roulantes vibratoires se déplaçant à

vitesse constante," Annales de l'Institut Technique du Bâtiment et des Travaux Publics, Paris, série, Essais et Mesures, Mar. 1979, pp.33-56.

[12] Burmister, D. M., "The Theory of Stresses and Displacements in Layered Systems," Journal of Applied Physics, Vol.16, Nos.2,3, and 5, 1945.

[13] Burmister, D.M., "Application of Layered System Concepts and Principles to Interpretations and Evaluations of Asphalt Pavement Performances and to Design and constructions," Proceeding of the International Conference on structural Design of Pavement, University of Michigan, 1962, pp441-453.

[14] Cebon, D., *An Investigation of the Dynamic Interaction Between Wheeled Vehicles and Road Surfaces*, Ph.D. dissertation, University of Cambridge, 1985.

[15] Cebon, D., "Road Damaging Effects of Dynamic Axle Loads," Proc. Int. Symp. on Heavy Vehicle Weights and Dimensions, Kelowna, British Columbia, 1986.

[16] Cebon, D., "Vehicle-Generated Road Damage: A Review," Vehicle System Dynamics, 18(1-3), 1989, pp. 107-150.

[17] Chatti, K., *Dynamic Analysis of Jointed Concrete Pavements Subjected to Moving Transient Loads*, Ph.D. Dissertation, the University of California-Berkeley, 1992.

[18] Chatti, K. Yun, Kyong K. and Mahoney, J.P., "Comparison of Static and Dynamic Predictions of Pavement Strains from FWD Tests," Submitted for presentation at the 76th Annual TRB Meeting, National Research Council, Washington, D. C., 1996.

[19] Chatti, K., Yun, K. K., Kim H. B., and Utamsingh, R., *PACCAR Full-Scale Pavement Tests*, Final Report to the University of Califonia -Berkeley and the Califonia Department of Transportation, Michigan State University, April 1995.

[20] Chen, J-C., *Analysis of Local Variation in free Field Seismic Ground Motions*, Ph.D. Dissertation, University of California-Berkeley, 1980.

[21] Chen, S.S., *The Response of Multi-layered Systems to Dynamic Surface Loads*, Ph.D. Dissertation, University of California-Berkeley, 1987.

[22] Chomton, G. and Valayer, P.J., "Applied rheology of Asphalt Mixes, Practical Applications," Proceedings, Third International Conference on the Structural Design of Asphalt Pavements, London, Vol I, September, 1972.

[23] Chou, Y. T., *Structural analysis computer programs for rigid multi-component pavements with discontinuities- WESLIQUID and WESLAYER*, Tech. Reports 1,2, and 3, U.S. Army Engineer Waterways Station, Vicksburg, Miss., May 1981.

[24] Clough, R. W. and Penzien, J., *Dynamics of Structures*, McGraw Hill, 1975.

[25] Cole, J and Huth, J., " Stress Produced in a Half Plane by Moving Loads," J. of Applied Mechanics, 433, December 1958.

[26] Cook, R. D., *Concepts and Applications of Finite Element Analysis*, 2nd ed. Wiley, 1991.

[27] Cooley, J. W. and Tuckey, J. W., "An Algorithm for the Machine Calculation of Complex Fourier Series," Mathematics of Computations, Vol. 19, 297-301, 1965.

[28] Craus, J., Deacon, J.A., Monismith, C.L., Tangella, R., *Summary Report on Fatigue Response of Asphalt Mixtures*, SHRP Project A-003-A, University of California, Berkeley, 1990

[29] Deacon, J.A., Monismith, C.L., "*Laboratory Flexural Fatigue Testing of Asphalt Concrete with Emphasis on Compound Loading Tests*", Highway Research Record No.158, 1967

[30] DeJong, D. L., Peutz, M. G. F. and Korswagen, A. R., *Computer Program BISAR. Layered Systems under Normal and Tangential Loads*, Koninklijke Shell-Laboratorium, Amsterdam, External Report AMSR.0006.73, 1973.

[31] Duncan, J., Monismith, C. L. and Wilson, E. L., "Finite Element Analysis of Pavements," HRR, Vol. 228, HRB 1968.

[32] Epps, J.A., Monismith, C.L., "Fatigue of Asphalt Concrete Mixtures-Summary of Existing Information", ASTM STP508, 1972

[33] Finn, F., et al., *Development of Pavement Structural Subsystems*, NCHRP Report 291, Transportation Research Board, 1986.

[34] Fryba, L., *Vibration of Solids and Structures under Moving Loads*, Noordhoff International Publishing, Groningen, Netherlands, 1972.

[35] Gillespie, T.D. and MacAdam, C.C., *Constant Velocity Yaw/Roll Program, User's Manual*, University of Michigan Transportation Research Institute, UMTRI-82-39 (1982) 119p.

[36] Gillespie, T.D., et al, *Effects of Heavy-Vehicle Characteristics on Pavement Response and Performance*, NCHRP Report 353, 1993.

[37] Gonzalez, G., Kennedy, T.W., Anagnos, J.N., *Evaluation of the Resilient Elastic Characteristics of Asphalt Mixtures Using Indirect Tensile Test*, Research Report No. 183-6, University of Texas, Austin

[38] Hanazato, T., Ugai, K., Mori, M., Sakaguchi, R., "Three-Dimensional Analysis of Traffic-Induced Ground Vibrations", ASCE Journal of Geotechnical Engineering, Vol. 117, No.8, August, 1991.

[39] Hardy, S.A., and Cebon, D., "The response of a flexible pavement to moving dynamic loads," Proc. Inst. Acoustics, Vol.10, PArt 2, 1988.

[40] Hardy, S.A., and Cebon, D., "Response of Continuous Pavements to Moving Dynamic Loads," ASCE Journal of Engineering Mechanics, Vol. 119, No.9, August, 1993, pp. 1762-1780.

[41] Harichandran, R.S., Yeh,M.S. and Baladi,G.Y., "MICH-PAVE, A Nonlinear Finite Element Program for Analysis of Flexible Pavements," In Transportation Research Record 1286, TRB National Research Council, Washington, D.C., 1990, pp. 123-131.

[42] Harr, M. E., "Influence of Vehicle Speed on Pavement Deflections," Proc. Highway Research Board, No. 41, 1962, pp. 77-82.

[43] Harr, M.E., *Foundation of Theoretical Soil Mechanics*, McGraw Hill, NewYork, 1966.

[44] Hedrick, J. K., Markow, M. J. and Brademeyer, B., *The Simulation of Vehicle Dynamic Effects on Road Pavements*, Final Report to USDOT - Office of University Research - under Contract DTRS5684-C-0001, December 1988.

[45] Highway Research Board, *The AASHO Road Test*, HRB Special Report 61, 1962.

[46] Highway Research Board, R*oad Test One-MD*, HRB Special Report 4, 1952.

[47] Hoffman, M.S. and Thompson, M.R.,"Comparative Study of Selected Nondestructive Testing Devices," Transportation Research Record 852, 1982.

[48] Holder, B. W., Michalopoulos, C. D., "Response of a Beam on an Inertial Foundation to a Traveling Load," AIAA Journal, Vol.15, No.8, August 1977, pp. 1111-1115.

[49] Huang, Y. H., *Pavement Analysis and design*, Prentice Hall, New Jersey, 1993.

[50] Huang, Y. H., "Finite element analysis of slabs on elastic solids," J. Trans. Engineering., ASCE, Vol. 100, No. 2, 1974, pp. 403-416.

[51] Huang T. C., Shah V. N., "Elastic System Moving on an Elastically Supported Beam," J. Vibration, Acoustics, Stress and Reliability in Design, (ASME Trans.) Vol.106, April 1984, pp. 292-297.

[52] Hwang, D. and Witczak, M. W., *Program DAMA(CHEVRON), User's Manual*, Department of Civil Engineering, University of Maryland, 1979.

[53] Ishihara, K. and Kimura, T., "The Theory of Visco-elastic Two-layered Systems and Conception of its Application to the Pavement Design," Proc. 2nd Int. Structural Design of Asphalt Pavements, University of Michigan, Ann Arbor, 1967, pp245-254.

[54] Kausel, E., *An Explicit Solution for The Green Functions for Dynamic Loads in Layered Media*, Report No. R81-13, Order No. 689, Dept. of Civil Engineering, MIT, Cambridge, Mas., February 1981.

[55] Kausel, E. and Roesset, J.M., "Stiffness Matrices for Layered Soils," Bulletin of the Seismological Society of America, Vol. 71, No.6, pp 1743-1761, December, 1981.

[56] Kausel, E. and Peek R., "Dynamic loads in the Inertia of Layered Stratum, An Explicit Solution." Bulletin of the Seismological Society of America, Vol. 72, No.5, October 1982, pp 1459-1481.

[57] Kenis, W. J., *Predictive Design Procedures, VESYS User's Manual, An Interim Design Method for Flexible Pavements Using the VESYS Structural Subsystem*, FHWA, Final Report FHWA-RD-77-154, Washington, D. C., January 1978.

[58] Kennedy, T.W., Anagnos, J.N., *Procedures for the Static and Repeated Load Indirect Tensile Test*, Research Report No. 183-14, University of Texas, Austin, Aug. 1983

[59] Kukreti, A. R., Taheri, M. R., Ledesma, R. H., "Dynamic Analysis of Rigid Airport Pavements with Discontinuities," J. Transp. Engr., ASCE, Vol. 118, No. 3, 1992, pp. 341-360.

[60] Le Houedec D., "Response of a Roadway Lying on an Elastic Foundation to Random Traffic Loads," J. Applied Mechanics, (ASME Trans.) Vol.47, March 1980, pp. 145-149.

[61] Love, A.E.H.,*A Treatise on the Mathematical Theory of Elasticity*, Dover Publications, Inc., New York, 1944.

[62] Lysmer, J., Tabatabaie, M. B., Tajirian, R., Vahdani S., Ostadan, F., *SASSI - A System for Analysis of Soil-Structure Interaction*, Report No. 81-02, UCB/GT, University of California-Berkeley, April 1981.

[63] Lysmer, J. and Kuhlemeyer,R.L., "Finite Dynamic Model for Infinite Media," J. of ASCE, Vol. 95, EM4, August 1969, pp 859-877.

[64] Lysmer, J., Udaka, T., Tsai, C. F., and Seed, H. B., *FLUSH - A ComPuter Program for Approximate 3-D Analysis of Soil-Structure Interaction Problems*, Earthquake Engineering Research Center, Report No. EERC 75-30, University of California-Berkeley, November 1975.

[65] Lysmer, J. and Richart, F. E. Jr., "Dynamic Response of Footings to Vertical Loading," ASCE Journal of Soil Mechanics and Foundation Division, Jan. 1966.

[66] Lysmer, J. and Wass, G., "Shear waves in Plane Infinite Structures," J. of ASCE, Vol. 18, EM1, February 1972, pp 85-105.

[67] Mahoney, J. P., "The Relationship Between Axle Configurations," Wheel Loads and Pavement Structures," SAE Conference on Vehicle/Pavement Interaction, SP765, SAE Trans. 881844, Indianapolis, SAE, 1988.

[68] Mahoney, J. P., Winters, B.C., Chatti, K., and Moran, T., *Vehicle/Pavement Interaction at the PACCAR Test Site*, Final Report submitted to Washington State Department of Transportation, June 1995.

[69] Michelow, J., *Analysis of Stress and Displacements in an N-Layered Elastic System under a load uniformly Distributed on a Circular Area*, California, Research Corporation, Richmond, CA, 1963.

[70] Milovic, D.M., " Constraintes et deplacements dans une fondation circulaire," Le Genie Civil, T.147, No.5, 1970, pp281-285.

[71] Miner, M. A., "Cumulative Damage in Fatigue," ASME Transactions, Vol. 67, 1945.

[72] Moavenzadeh, F. and Ellitott, J.F., *Moving Load on A Visco-elastic Layered System*, Research Report R68-37, Prepared for the U.S. Department of Transportation, Massachusetts Institute of Technology, Cambridge, Massachusetts, June 1968.

[73] Monismith, C. L., Epps, J.A., and Finn, F.N., "Improved Asphalt Mix Design," Proceedings, the Association of Asphalt Paving Technologist, Vol. 54, 1985, pp 347-392.

[74] Monismith, C. L., Sousa, J. and Lysmer, J., "Modem Pavement Design Technology Including Dynamic Load Conditions," SAE Conference on Vehicle/Pavement Interaction, SP765, SAE Trans. 881845, Indianapolis, 1988.

[75] Monismith, C. L., Lysmer, J., Sousa, J. and Hedrick, J. K., "Truck Pavement Interactions - Requisite Research," SAE Conference on Vehicle/Pavement Interaction. SP765. SAE Trans. 881845, Indianapolis, 1988.

[76] Monismith, C.L., et al., *Fatigue Response of Asphalt-Aggregate Mixes*, Strategic Highway Research Program, National Research Council, Washington, DC, 1994.

[77] Nair, K., Smith, W.S. and Chang, C.Y., "Application of a linear Visco-elastic Characterization for asphalt Concrete," Third International Conference on the Structural Design of Asphalt Pavements, Vol I, London, 1972.

[78] Nasim, M. A. et al., "The Behavior of Rigid Pavement under Moving Dynamic Loads," Transportation Research Board 1307, 1990, pp129-135.

[79] Pell, P.S., "Characterization of Fatigue Behavior", SR 140, Highway Research Board, 1973

[80] Pell, P.S., Taylor, I.F., "Asphaltic Road Materials in Fatigue", Proceedings Proceeding of the Association of Asphalt Paving Technologist, vol.38, 1969

[81] Pister,K.S. and Westmann, R.A., "Analysis of visco-elastic Pavement Subjected to Moving Loads", Proceeding of the International Conference on structural Design of Pavement, University of Michigan, 1962, pp522-529.

[82] Porter, B.W. and Kennedy, T.W., *Comparison of Fatigue Test Methods for Asphalt Materials*, Research Report No. 183-4, University of Texas, Austin, April 1975

[83] Raad, L. and Figueroa, J.L., "Load Response of Transportation Support System," ASCE, Journal of Transportation Engineering, Vol.106, 1980, pp111-128.

[84] Raithby, K.D., Sterling, A.B., "The Effect of Rest Periods on Fatigue Performance of Hot Rolled Asphalt", Proceeding of the Association of Asphalt Paving Technologist , Vol.39, 1970

[85] Rauhut, J. B., Roberts, F. L., Kennedy, T. W., "Response and Distress Models for Pavement Studies," Transportation Research Record 715 TRB, 1979, pp 7-14.

[86] Richart, F. E. Jr., Hall, J. R., Woods, R. D., *Vibrations of Soils and Foundations*, Prentice-Hall, 1970.

[87] Roberts, F. L., "Flexible Pavement Strains Caused by Auto Tyres," ASCE J. Transportation Engineering, Vol.113, No.5, Sept. 1987.

[88] *SASSI Theoretical Manual*, Bechtel Power Corporation, 1988.

[89] *SASSI User Manual*, Bechtel Power Corporation, 1988.

[90] *SASSI Verification Manual*, Bechtel Power Corporation, 1990.

[91] Sebaaly, B. E., *Dynamic Models for pavement Analysis*, Ph.D. Dissertation, Dept. of Civil Engineering, Arizona State University, 1987.

[92] Sebaaly, P. E., Mamlouk, M. S., "Pavement Response to Dynamic Loads," FHWA Load Equivalence Workshop, Washington D.C., September 1988, 29p.

[93] Sebaaly, P., Tabatabaee, N,, "Effect of Tire Parameters on Pavement Damage and Load-Equivalency Factors," ASCE, J. of Transportation Engineering, Vol. 118, No.6, Nov/Dec, 1992. pp805-819.

[94] Sebaaly, P., and Tabatabaee, N., "Influence of Vehicle Speed on Dynamic Loads and Pavement Response," Transportation Research Board 1410, pp107-114.

[95] Sebaaly, P., Tabatabaee, N. and Scullion, T., *Instrumentation for Flexible Pavements*, Report FHWA-RD-89-084. McLean, Virginia, Federal Highway Administration, 1989.

[96] Shah, V. N., Cook, R. D. and Huang, T. C., "Loads Moving on a Beam Supported by a Layered Elastic Foundation," J. Mechanical Design, (ASME Trans.) Vol.102, April 1980, pp.295-302.

[97] Siddharthan, R., Sebaaly, P., and Zafir. Z., "Pavement Strains Induced by Spent Fuel Transportation Trucks," Preprint Paper No. 940125, TRB, National Research Council, Washington, D.C., 1994.

[98] Small, J.C. and Brooker, J. R., *Finite Layer Analysis of Layered Elastic Material using a Flexibility Approach*, Report No. R418, School of Civil and Mining Engineering, The University of Sydney.

[99] Sneedon, I.N., *The Use of Integral Transforms*, McGraw Hill Company, Inc., New York, 1972.

[100] Sousa, J. M. B., *Dynamic Properties of Pavement Materials*, Ph.D. Dissertation, University of California-Berkeley, 1986.

[101] Sousa, J. B., Lysmer, J., Chen, S. S., and Monismith, C. L., "Effects of Dynamic Loads on Performance of Asphalt Concrete Pavements," Trans. Res. Record 1207, 1988, pp. 145-168.

[102] Sousa, J.B., Rowe G., Tayebali, A.A., "Dissipated Energy and Fatigue of Asphalt Aggregate Mixtures", Paper prepared for the Annual Meeting of Association of Asphalt Paving Technologists, University of California, Berkeley, Feb. 1992.

[103] Soussou, T.E., Moavenzadeh, F., and Findakly, H.K., "Synthesis of Rational Design of Flexible PAvements," Civil Enginering Dept., Report, Massachusetts Institute of Technology, January 1973.

[104] Sung, T.Y., "Vibrations in Semi-Infinite Solids Due to Periodic Loading", Symposium on Dynamic Testing of Soils, ASTM Special Technical Publication No. 156, 1953.

[105] Tabatabaie, A. M., "Dynamic Analysis of Pavement Systems-Model Evaluations", paper presented at the 70th Annual TRB Meeting, Washington, D. C., 1991.

[106] Tabatabaie, M. R., *The Flexible Volume Method for Dynamic Soil-Structure Interaction Analysis,* Ph.D. dissertation, University of California-Berkeley, 1982.

[107] Tajirian, Fredrick F., *Impedance Matrices and Interpolation Techniques for 3-D Interaction Analysis by the Flexible Volume Method*, Ph.D. dissertation, University of California-Berkeley, 1981.

[108] Tangella, S.R., Craus, J., Deacon, J.A., and Monismith, C.L., *Summary Report on Fatigue Response of asphalt Mixtures*, Report for Strategic Highway Research Program, TM-UCB-A003A-89-3. University of California, Berkeley, Feb. 1990.

[109] Tayabji, S. D., Colley, B. E., *Analysis of Jointed Concrete Pavements*, Interim Report to FHWA, Report No. FHWA/RD-86/041, February 1986.

[110] Thompson, M.R., *ILLI-PAVE, User's Manual,* Transportation FAcilities Group, Dept. of Civil Engineering, University of Illinois, November, 1986.

[111] Timoshenko, S. and Goodier, J.N., *Theory of Elasticity*, 2nd Ed. McGraw-Hill Book Company, New York, 1951.

[112] Ueshia, K. and Meyerhof, G.G., Surface Displacement of An Elastic Layer under Uniformly Distributed Loads, Highway Research Record No. 228, 1968, pp1-10.

[113] Ullidtz, P., *Pavement Analysis,* Developments in Civil Engineering Series No.19, Elsevier, 1987.

[114] Van Dijk, W. Moreaud, H., Quedeville, A., and Uge, P., "The Fatigue of Bitumen and Bituminous Mixes," Proce. 3rd International Conference on the Structural Design of Asphalt Pavement, London, England, Vol.1, Sep 11-15, 1972, pp354-366.

[115] Van Dijk, W. "Practical Fatigue Characterization of Bitumunous Mixes," Proceedings, Association of Asphalt Paving Technologists, Vol. 44, Phoenix, AZ, February, 1975, pp38-75.

[116] Van Dijk, W. and Visser, W., "The Energy Approach to Fatigue for Pavement Design," Proceedings of Association of Asphalt Paving Technologists, Vol. 46, San Antonio, TX, February, 1977, pp40.

[117] Warren, H., and W. L. Dieckmann., *Numerical Computation of Stresses and Strains in a Multiple-Layer Asphalt Pavement System*, Internal Report, CHEVRON Research Corporation, Richmond, CA, 1963.

[118] Waas, Gunter., *Linear Two-dimensional Analysis of Soil Dynamic Problems in Semi-infinite Layer Media*, Ph.D. Dissertation, University of Califonia, berkeley, 1972.

[119] Waas, G., *Earth Vibration Effects and Abatement for Military Facilities, Report 3, Analysis Method for Footing Vibrations Through Layered Media*, Technical Report S-71-14, Report 3, Prepared for U. S. Army Engineer Waterways Experiment Station, CE, under Contract No. DACA39-70-C-0023, Sept. 1972.

[120] Westergaard H.M., "Stresses in concrete pavements computed by theoretical analysis," Public Roads, Vol.7, No.2, April 1926.

[121] Westmann, R. A., "Visco-elastic Layered System Subjected to Moving Loads," Proc. ASCE, J. of Engineering Mechanics Div., EM3, June 1967, pp201-218.

[122] Winkler, E., *Study of Elasticity and Strength*, H. Dominikus, Prague, 1867.

[123] Winters, B. C., *The PACCAR Pavement Test Section - Instrumentation and Validation*, M.S. Thesis, University of Washington-Seattle, 1993.

[124] Yodar, E.J. and Witczak, M.W., *Practical of Pavement Design*, John Wiley and Sons, Inc., 2nd Edition, New York, 1975.

[125] Yoshida, D. M. and Weaver, W., "Finite-Element Analysis of Beams and Plates with Moving Loads," Inl. Assoc. Bridge Struc. Engr. Vol. 31 (l), pp. 179-195, 1971.

[126] Zafir, Z., *Response of Layered Media to Moving Loads*, Ph. D. Dissertation, University of Nevada, Reno, 1993.

[127] Zafir, Z., Siddharthan, R. and Sebaaly, E., "Dynamic Pavement-strain Histories from Moving Traffic Load," ASCE, Journal of Transportation Engineering, Vol. 120, No. 5, September, 1994. pp821-842.

[128] Zienkiewiz, O.C and Chung, Y.K., *The Finite element Method in Structural and Continuum Mechanics*, McGraw-Hill, New York, 1967.

APPENDICES

APPENDIX A

PARAMETRIC STUDY

A.1 INTRODUCTION

A.1.1 DESCRIPTION OF SAPSI-M COMPUTER PROGRAM

SAPSI-M is a FORTRAN computer program to calculate the response of a visco-elastic layered system subjected to moving arbitrary loads at surface. The half space underlying the layered system may be simulated by vertically extending layers and a series of dashpots attached to the bottom of the extended layers. The shear modulus, damping ratio, and Poisson's ratio for each layer may be varied with the excitation frequency of the load. Multiple loads are acceptable for the harmonic, transient and moving load cases and each loading may have a different radius and time histories. A static load can be simulated by specifying a harmonic load with zero excitation frequency. The program uses a special scheme in the frequency domain to interpolate between results obtained for only a few frequencies. This provides a significant reduction in the computational effort required. The program uses a dynamic allocation technique which automatically sets the dimension of the program to accommodate the input data.

The program can be run interactively with the aid of menus shown on the screen of the monitor. The input data may be created directly from the keyboard, or read from existing files. The program is designed in such a way that the results obtained in different phases of the execution can be saved for later use. For instance, the model for the layered system, the eigen solution, the input loading, the output time histories, the coordinates of the output points, and the general printout can be saved in different files for future reference.

The user's guide for informations on input and output operations in the program is provided in Appendix B.

A.1.2 THE USE OF SAPSI-M FOR PAVEMENT ANALYSIS

The SAPSI-M computer program is used to predict the primary response (stress, strain, displacement) of a pavement system subjected to truck moving loads. Current

design methods treat the pavement as a quasi-static system choosing material characteristics which are related to the speed of the vehicle and the expected temperature conditions. However, the actual dynamic effects due to moving loads are specifically considered.

The passage of a truck over a fixed point in the pavement can be modeled in a number of ways. The truck load can be treated as:

1-a vertically vibrating force which moves in the horizontal direction;

2-a vertically vibrating force which is stationary in space;

3-a constant force which moves in the horizontal direction;

4-a static force.

At present the SAPSI-M computer program can treat the load all the cases. Sometime, the movement of the load in the horizontal direction may be approximated by using the concept of an influence line. This concept is useful in determining the general shape of the response of a fixed point in the pavement as a truck passes by it. An influence line gives the variation in the static response at one (fixed) point due to a unit load traversing the pavement. It has been shown that this simplified method can produce essentially the same results as does the much more complicated dynamic analysis.

A.2 NUMERICAL CRITERIA ON ACCURACY

A.2.1 COMPARISON WITH AN "EXACT" SOLUTION

The validation of the SAPSI computer program was done by comparing its predictions with those from an exact solution by Sung. A homogenous half space which has a shear modulus, $G = 1.49 \times 10^6$ psf, a shear wave velocity, $V_s = 619.5$ fps, a Poisson's ratio, $\mu = 0.25$ and a mass density, $\rho = 3.8824$ lb.sec^2/ft^4, was considered. The half space was subjected to a surface disk load with a uniform pressure, q = 1000 psf.

Two cases corresponding to different loading radii were studied. The half space was simulated by frequency-dependent layers and dashpots attached to the bottom of the layered system. For the case in which the loading radius, r_0, was 0.5 ft, the frequency was varied from 0.01 to 200 Hz and for the case in which r_0 was 1.0 ft, the frequency was varied from 0.01 Hz to 100 Hz in the exact solution. Since the program SAPSI-M uses the same routines to perform both static and dynamic analyses, only dynamic loads were con-

sidered in the verification example. The vertical surface displacements at the center of the loaded area were computed and compared with those obtained by Sung.

A.2.2 ANALYSIS

Using the above layer properties, a one-layer profile was designed with the only layer being the response layer, since the response was sought at the surface. For each frequency, and using 10 layers for half space simulation the response thickness was reduced in each run until it converged to the exact solution. The variation in response thickness for each frequency is in Figure A-1. The figure shows that the curve for the static case is not smooth. The reason for this is that the sublayer thicknesses of the simulated half space (generated by the geometric series described above) do not match the attenuation curve for the Rayleigh wave motion. Therefore the number of layers in the half space was varied as 10, 15, 20 and 25. As seen from Figure A-1, the 20-layer half space gives the best results. Thus we can conclude that for static analysis, more than 10 layers are needed to accurately simulate a halfspace.

For higher frequencies (> 50 Hz, in this case), increasing the number of layers to simulate the half space from 10 to 15, 20 and 25 did not make any difference, as shown in Figure A-2. The analysis shows that for the percent error to be less than about 10%, the response thickness should be less than about 0.2 ft for the static case and about $0.001\lambda_s f_{max}$ for the dynamic case. Table A-1 contains the wavelength, for each frequency, $\lambda = V_s/f$.

A.3 DETERMINATION OF LAYERED PROFILES FOR USE IN THE ANALYSIS

The objective of this part of the study was to determine layer thickness requirements for the accuracy of SAPSI-M and to design the optimum profiles for Cores 1,3,4 and 5. Table 5.3 in Chapter 5 gives the effective layer thicknesses used for Axial Cores 1,3,4 and 5; and Table 5.4 gives the material properties for each layer in the flexible pavement. The load applied on the flexible pavement was taken as 10,000 lbs and the area of

Table A-1 Wave Length at Different Frequencies

Frequency (Hz)	0.01	50	100	200
Wave Length (ft)	61,950	12.4	6.2	3.1

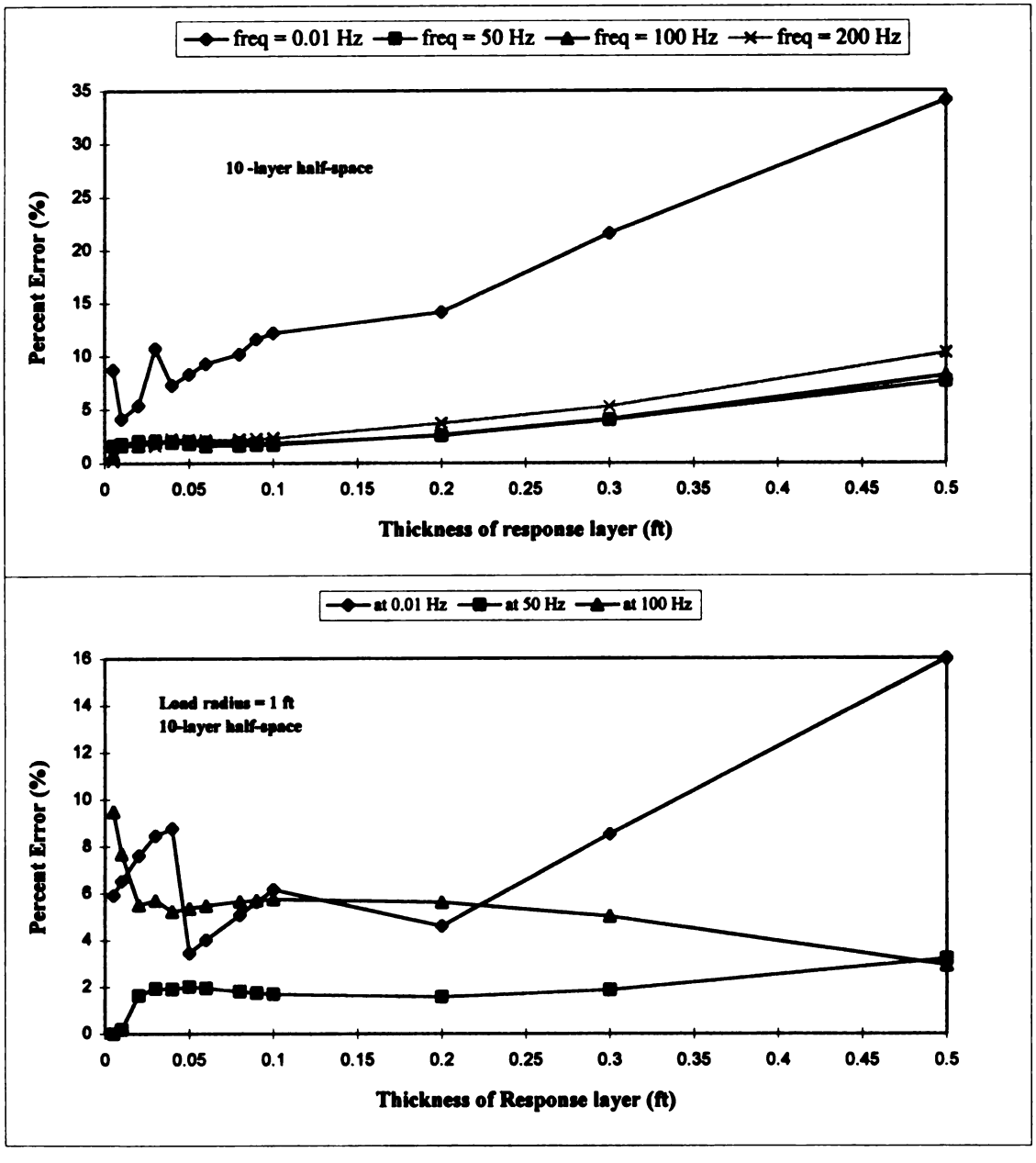

Figure A-1 Effect of the Thickness of the Response Layer and the Number of Layers for Half-space Simulation

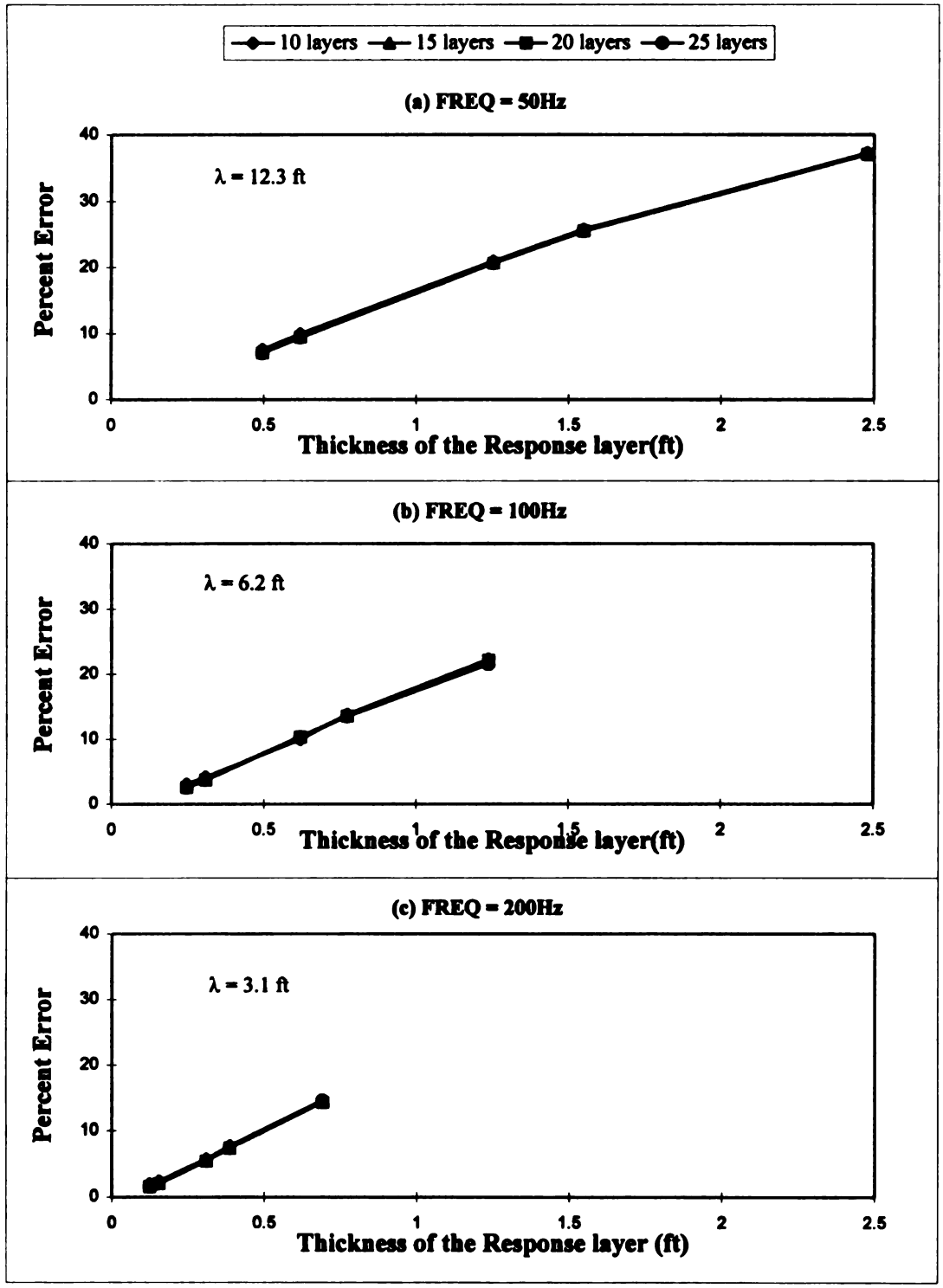

Figure A-2 Effect of the Thickness of the Response Layer and the Number of Layers Simulating for Half-space

the circular load was assumed to be $109in^2$. This translates into a radius of the loaded area being equal to 0.49 ft and an applied pressure equal to 4217 psf.

A.3.1 MATERIAL PROPERTIES

The first step is to find the cutoff frequency beyond which the response does not need to be calculated. The determination of f_{cutoff} is based on the input load and the response. The cutoff frequency is the maximum frequency (f_{max}) at which the load or the response dies out. Therefore no analysis is needed beyond the cutoff frequency. The corresponding time step was calculated as $dt = 1/(2 \cdot f_{max})$ and the frequency step as $df = 1/(N \cdot dt)$. The dynamic analysis within SAPSI-M is performed in the frequency domain and transient loadings are handled by the Fourier transform technique, as mentioned before.

For each layer, the shear modulus, G, and the shear wave velocity, V_s, were calculated from the given values of Young's Modulus, Poisson's ratio and mass density using elasticity equations:

$$G = \frac{E}{2(1+\mu)} \qquad \text{(A-1)}$$

$$V_s = \sqrt{\frac{G}{\rho}} \qquad \text{(A-2)}$$

The maximum wavelength corresponding to the cutoff frequency is: $\lambda = V_s/f$

A.3.2 PROCEDURE

The procedure outlined below was used to design the best profile for Axial Core No. 1. The same number of layers for asphalt concrete, base and subgrade, were used for the other axial cores (3, 4 and 5).

A.3.2.1 Maximum allowable thickness of the response layer:

For a particular profile, the thicknesses of base, subgrade and epoxy were kept constant while varying the thickness of the response layer in the asphalt concrete. The response layer was varied from 0.003ft to 0.2ft. The response was calculated for each of these at different frequencies. A plot of $\varepsilon_z/\varepsilon_H$ versus h/H is shown in Figure A-3 (where

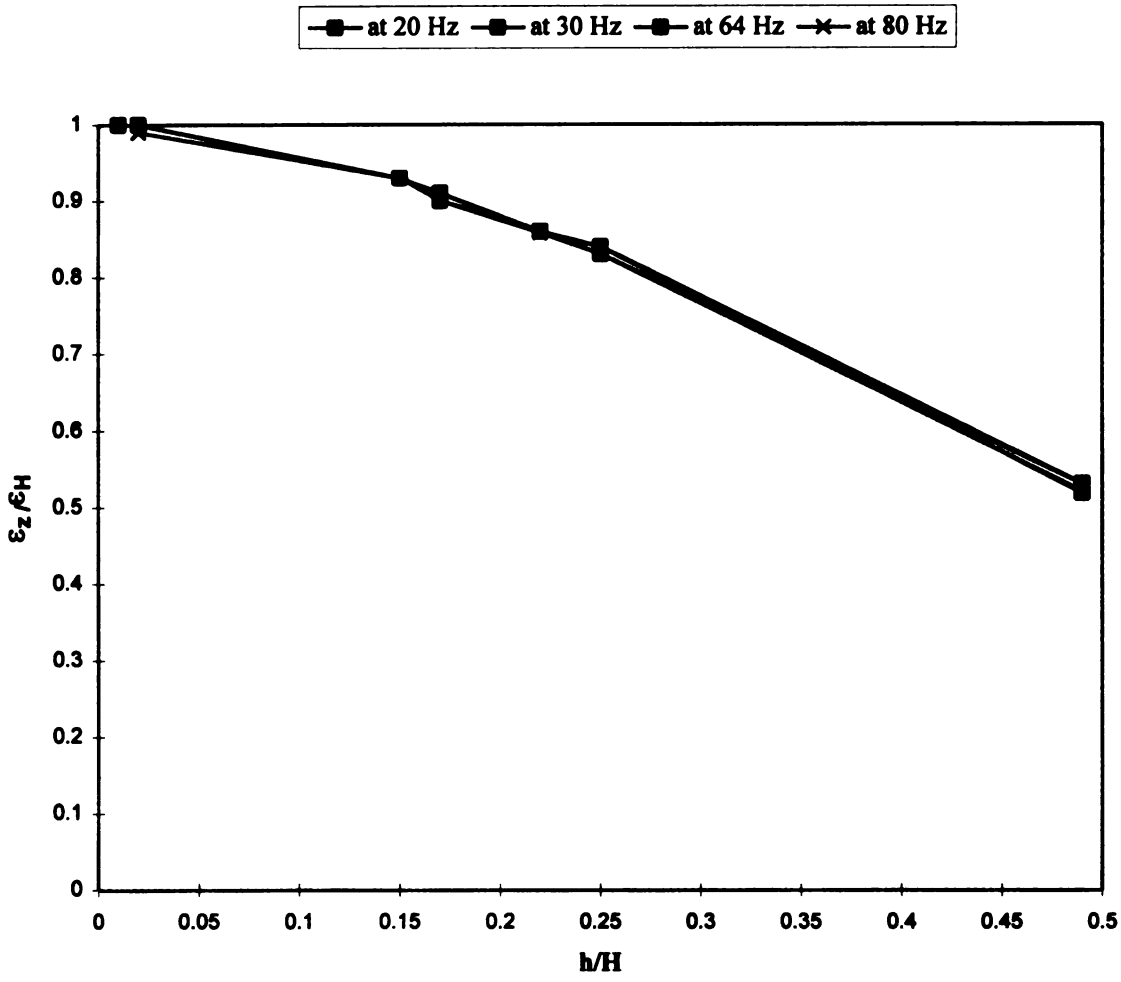

Figure A-3 Normalized Strain Versus Thickness of Response Layer in AC

H is the total thickness of the AC layer, h is the response layer thickness, and z is the depth at which the response is sought). It can be seen that the ratio of $\varepsilon_z/\varepsilon_H$ approaches unity when the response layer thickness is less than about 0.02ft. To get better than 10% accuracy, the thickness should be less than H/6. A thickness equal to 0.01ft was chosen for the AC layer, and the subsequent analyses were performed using this value.

A.3.2.2 Maximum allowable sublayer thickness for pavement layers:

For each material type (AC, Base, Subgrade), the minimum number of sublayers required for an accurate response was determined. One constraint had to be imposed: The total number of layers was limited to 16 in SAPSI-M.

(a) Asphalt Concrete

The profile was started with 3 layers, having response layers of 0.005ft as the top and bottom layers. In the consecutive runs the thickness of the layers other than the response layers were equally subdivided until a convergent response (ε_x) was reached. The response was sought at the bottom of AC and therefore the depth at which the response was sought did not change for the different profiles. It was found that the response converged when the number of sublayers were $12\lambda/dh = 1000$. (see Figure A-4.)

From Figure A-4, it can be seen that an AC profile with four layers ($\lambda/dh = 200$) is sufficient. One can reasonably choose the 4 layer profile, since the percent error for this profile is only about 2 percent.

(b) Base

The profile was started with 3 layers, with equal thicknesses and the response (ε_x) was sought at mid-depth. The response approximately converged at 14 layers. A plot of λ/dh versus percent error is shown in Figure A-4. It can be seen that a 3-layer base $\lambda/dh = 20$ gives an error of 9%, and a 5-layer base ($\lambda/dh = 30$) gives an error of 3%. Therefore a 4-layer base of equal thicknesses was chosen ($\lambda/dh = 25$. A graph of λ/dh versus percent error was plotted including this 4-layer profile. The percent error was within 5%. Hence the 4-layer profile was selected.

(c) Subgrade

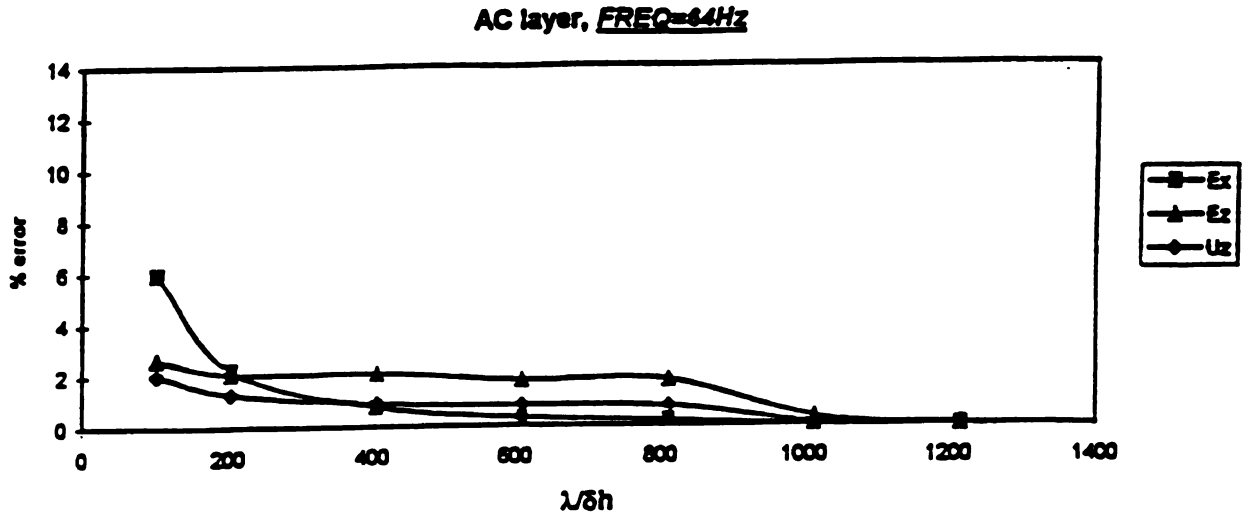

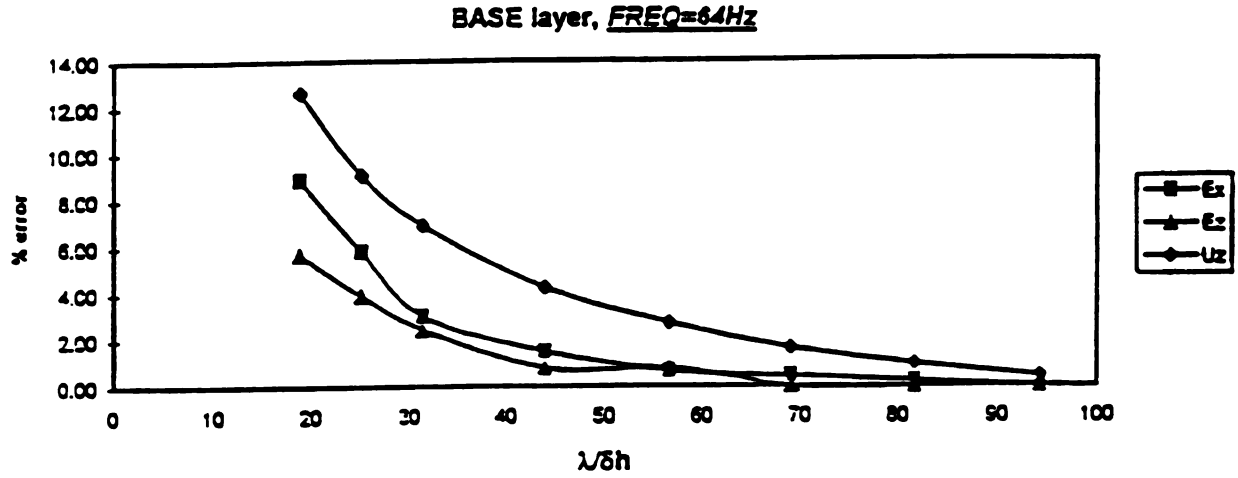

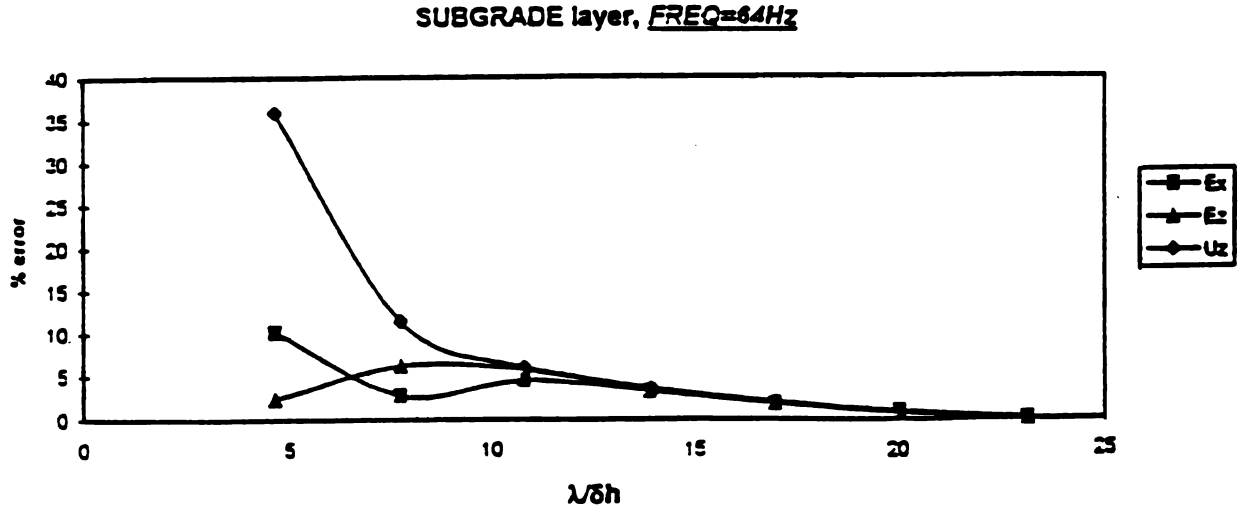

Figure A-4 Effect of Sublayer Thickness

The profile was started with 3 layers of equal thickness and the response (ε_x) was sought at the center of the total subgrade thickness. (similar procedure to that performed for the base). It was found that the response (ε_x) approximately converged at 15 layers. Therefore the percent error was calculated with respect to the 15-layer profile. A plot for λ/dh versus percent error (ε_x) is shown in Figure A-4. It can be seen from the figure that the percent error is 11% for the 3-layer profile $\lambda/dh = 5$ and is 3% for the 7-layer profile ($\lambda/dh = 7$). The figure shows that a 5-layer profile is quite appropriate since it approximately produces a 5% error in the tensile strain response.

A.3.2.3 Accuracy of selected profiles (AC, Base, Subgrade) at different frequencies:

The accuracy of the profiles for AC, base and subgrade as decided upon was checked at different frequencies. Comparing the converging response (ε_x, ε_z, u_z) to that obtained using the selected profiles at different frequencies, a plot of percent error versus frequency was plotted in Figure A-5. The graphs show that the percent error remained less than 10% at different frequencies. Therefore the selected sublayer thicknesses were justified.

A.3.3 PROFILE EFFECTS ON PAVEMENT DYNAMIC RESPONSE

A.3.3.1 The Effect of Stiff Layer

There was evidence from the back-calculation analysis, using the computer program EVERCALC and FWD deflection data, that the subgrade soil was saturated at a relatively shallow depth. The shallow water table translates into the saturated subgrade soil behaving as a "stiff" layer. EVERCALC was used to back-calculate an appropriate value for the stiff layer modulus by an iteration process.

Figure 5-9 shows the model for the soil profiles of the three cores. The layer thicknesses were obtained by coring and layer properties were obtained from back-calculation analysis as described in Chapter 5.

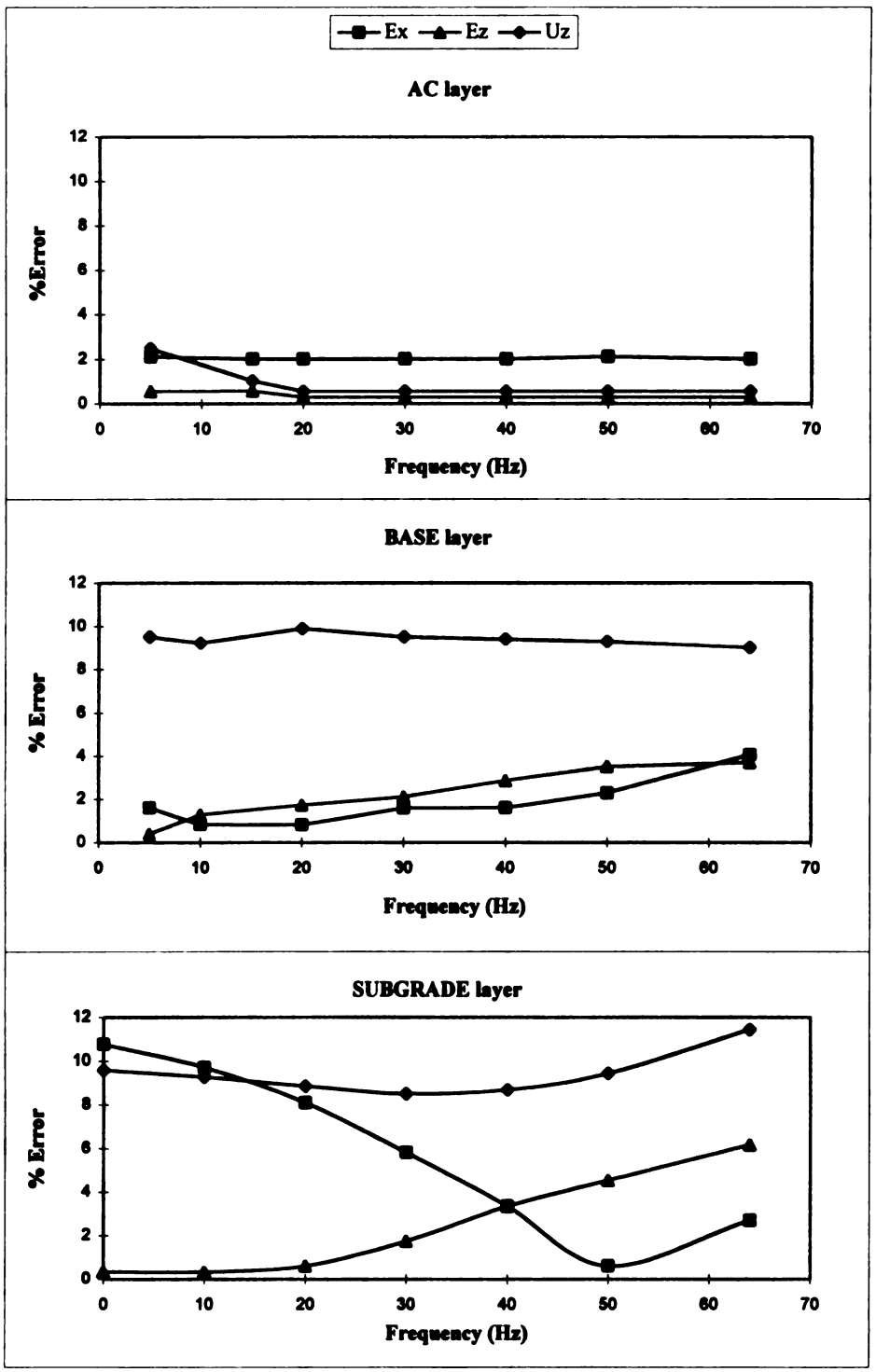

Figure A-5 Accuracy of the Decided Profiles at Different Frequencies

3.3.1.1 Effect of Depth to Stiff Layer

To investigate the effect of the depth to stiff layer on the vertical deflection and longitudinal strain, the thickness of subgrade layer was varied from 2 ft to 20 ft. The profile used was that of Core 1. Transient analysis in SAPSI was performed at the three speeds, 1.7 mph, 20 mph and 40 mph, and using frequency-independent as well as frequency-dependent profiles. Figure A-6 shows the results of the analysis. The figure indicates that the tensile strain at the bottom of the asphalt concrete layer is independent of the depth of the stiff layer for all three speeds and for both frequency-dependent and frequency-independent profiles. The vertical deflection is affected by the depth of the stiff layer only at very low speed, with the deflection decreasing with decreasing depth to stiff layer. This is expected since at very low speed, the behavior approaches static conditions where the shallower the stiff layer the stiffer the foundation soils get and the lower the vertical deflection becomes. Note that for the PACCAR site the depth to stiff layer is about 5 feet. It is interesting to note that at this depth, the displacement curves for creep speed and 20 mph intersect. Since a truck speed of 20 mph is basically equivalent to an FWD pulse, this could explain the finding that the results of static and dynamic analyses were practically identical in the FWD analysis. If the stiff layer were deeper, the back-calculated moduli could have been stiffer, which could result in lower dynamic strains.

3.3.1.2 Effect of Stiff Layer Modulus

To investigate the effect of the stiff layer modulus on the pavement response, the above analysis was repeated with the modulus of the stiff layer being that of rock. The rock layer was assumed to have a Young's modulus of 1,000 ksi (versus 40 ksi for PACCAR site) and a Poisson's ratio of 0.25. Figure A-7 shows the results. Again, only the vertical deflection at very low speed is affected by the modulus (stiffness) of stiff layer, with the rock layer causing smaller deflections than in the PACCAR case for both frequency-dependent and frequency-independent profiles.

3.3.2 The Effect of Base Layer

The effect of the base layer on the vertical deflection and the tensile strain at the bottom of the asphalt concrete layer was investigated. The exercise consisted of calculating the response with and without a base layer. In addition, the response was sought at the bottom of the AC layer and at the bottom of the epoxy. This lead to four cases, (A) through (D) as shown in Figure A-8. The profile of Core 1 (except for base and subbase thick-

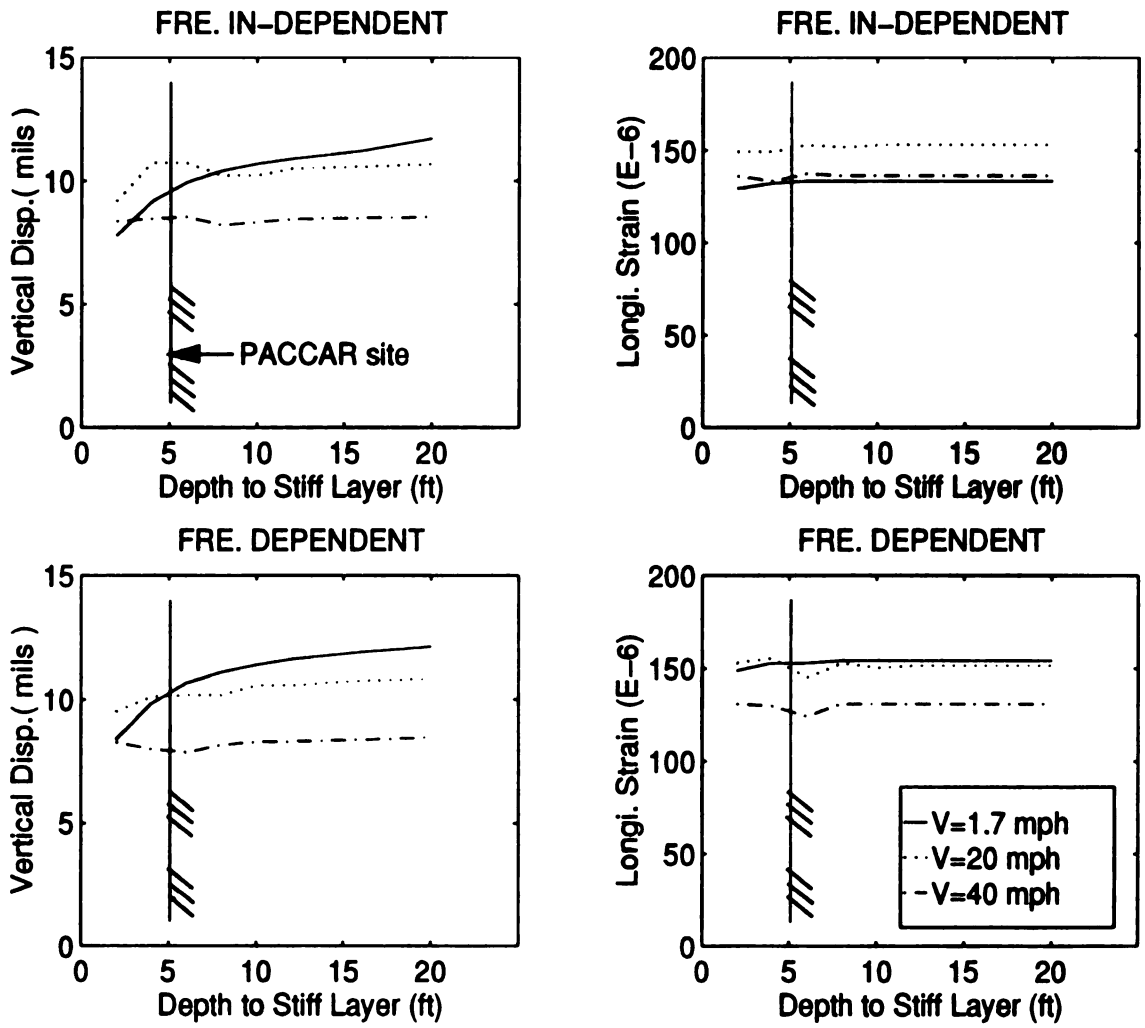

Figure A-6 Effect of Depth to Stiff Layer on Longitudinal Strain and Vertical Displacement

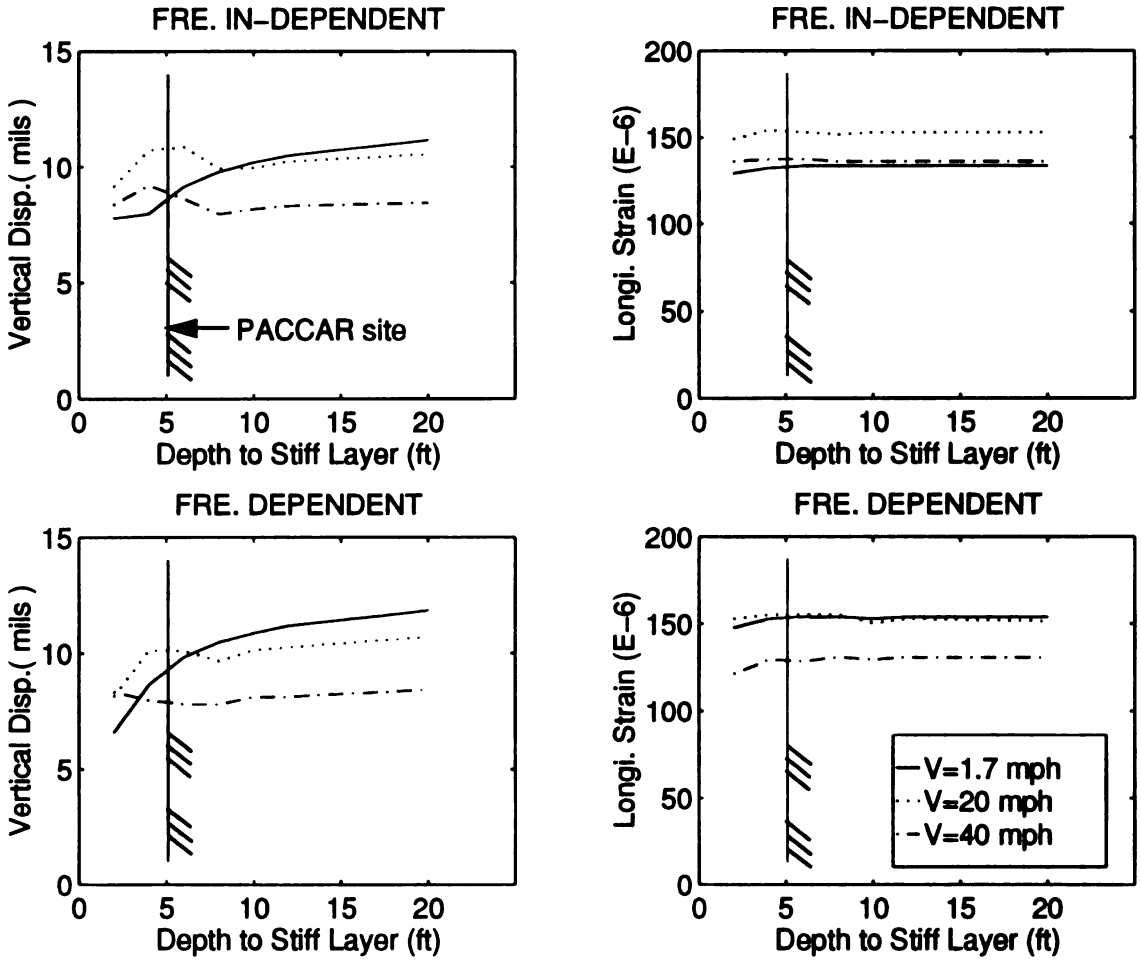

Figure A-7 Effect of Stiff Layer Modulus on Longitudinal Strain and Vertical Displacement

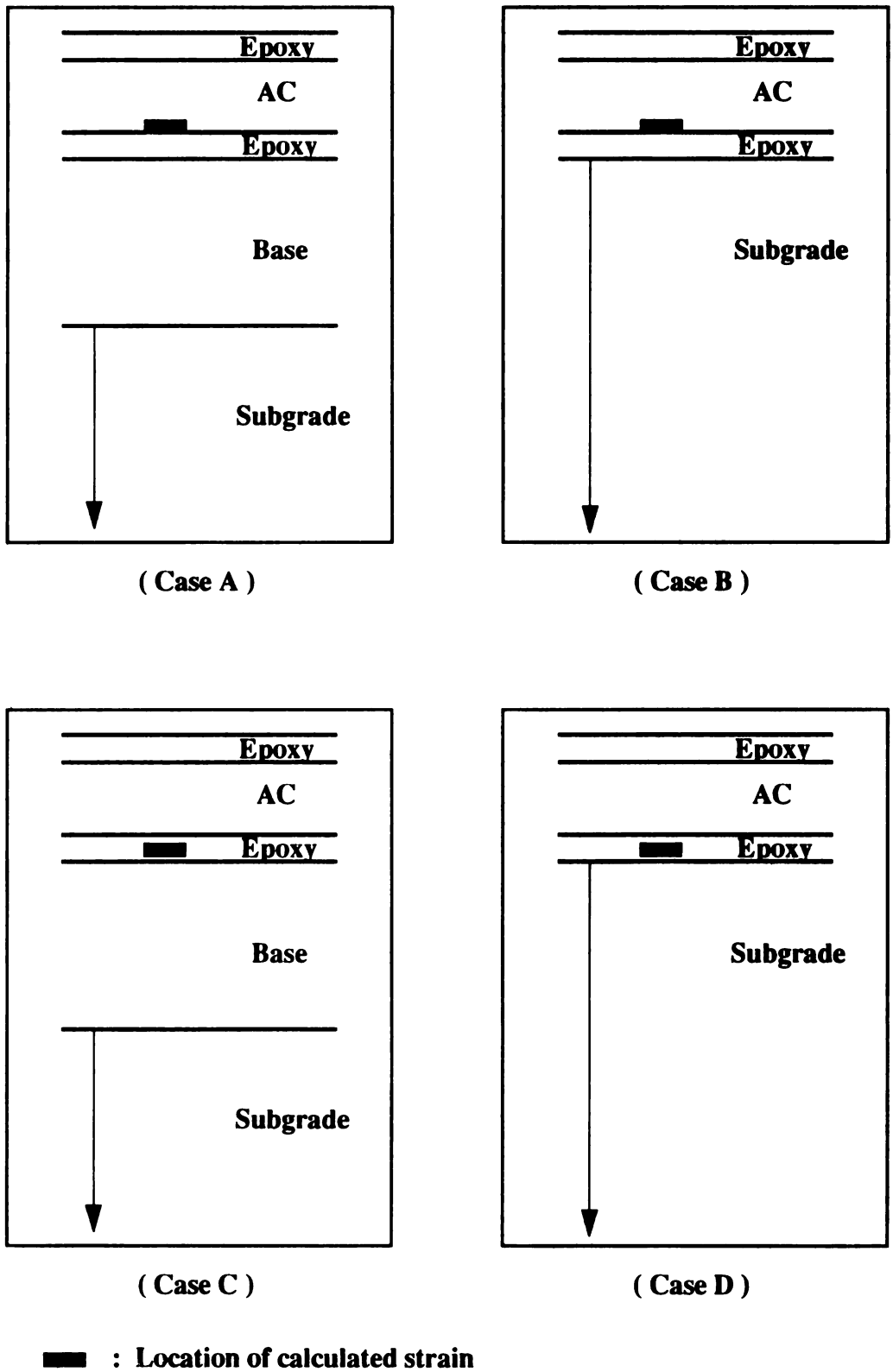

Figure A-8 Pavement Models to Investigate the Effect of Base Layer

nesses) was used with frequency-dependent AC properties. The epoxy was assumed to have the same properties as the asphalt concrete. Figure A-9 shows the results. As expected, removing the base layer increases the tensile strains (B versus A and D versus C.) Also, the tensile strain at the bottom of the epoxy is higher than at the bottom of the asphalt concrete (C versus A and D versus B,) since the response point is farther from the neutral axis. However the speed effect is not affected: The normalized strain with respect to creep speed shows the same trend with speed for all cases. It decreases by 28% as the speed increases from creep to 60 mph.

As expected, the vertical deflections of Cases (A) and (C), and Cases (B) and (D) are exactly the same because they have the same profile and the location of the response is close enough not to cause any additional deflection. The deflection in (A) and (C) are slightly lower than in (B) and (D) because of the absence of the base. The normalized deflection relative to the deflection at creep speed shows the same trend for all the cases at all speeds. They decrease by as much as 50% as the speed increases from creep to 60 mph. Therefore the speed effect on longitudinal strain and vertical deflection is the same with or without the base and regardless of the tensile strain location in the asphalt concrete.

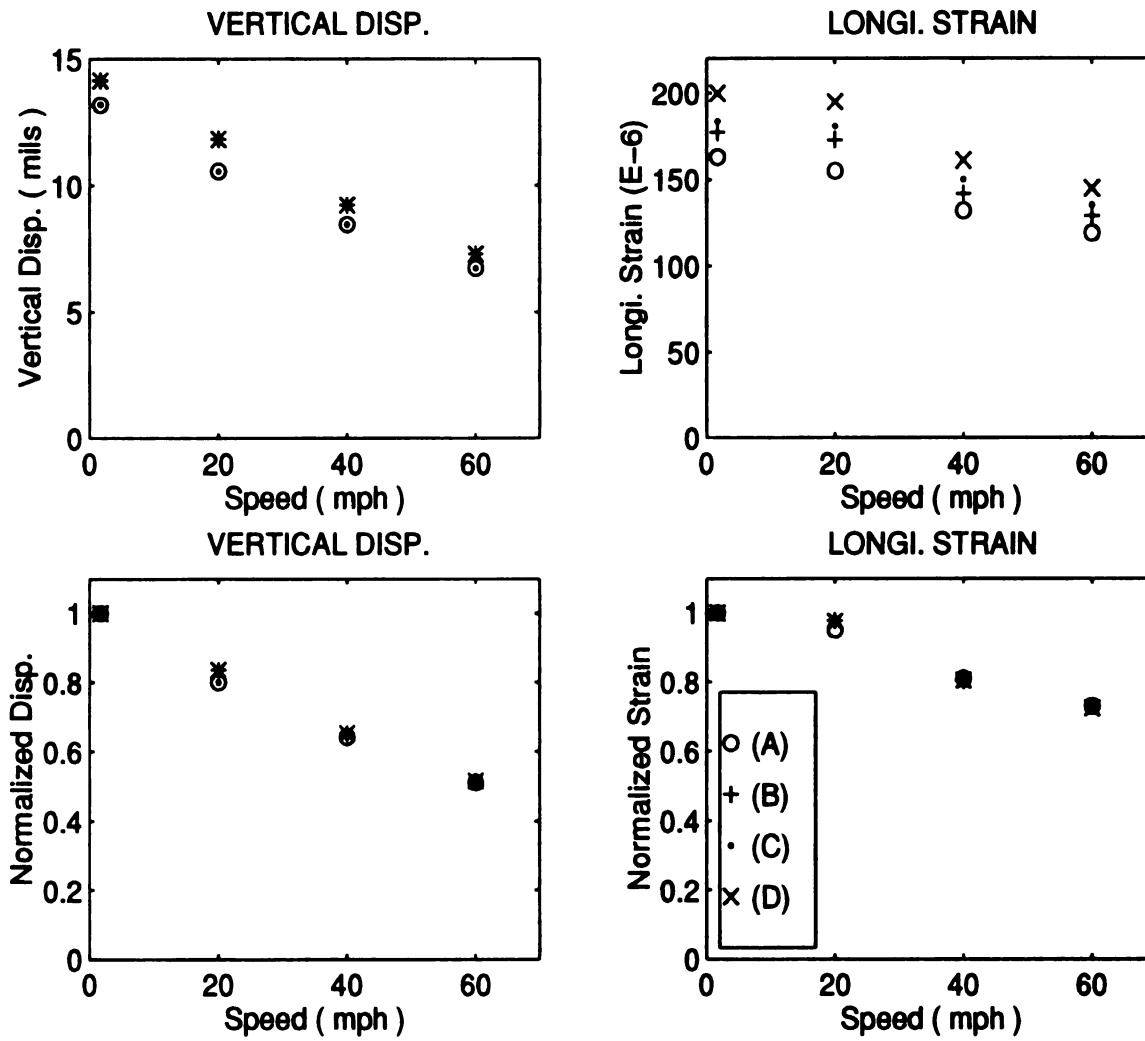

Figure A-9 Effect of Base Layer on Longitudinal Strain and Vertical Displacement

APPENDIX B

SAPSI-M USER GUIDE

B.1 INTRODUCTION

SAPSI-M stands for a System for Analysis of Pavement - Soil Interaction for Moving Loads. The SAPSI-M code is programmed in FORTRAN 77 language. It can be used to calculate the response of a visco-elastic layered system subjected to surface uniformly moving loads.

This computer program is based on the theory of linear visco-elastic layer theory in horizontally and finite element method in vertically. This program was developed on the axisymmetric coordinate, which reduces the 3-dimensional problems into 2-dimensional one. The half space underlying the layered system can be simulated by vertically extending layers and a series of dashpots attached to the bottom of the extended layers.

B.1.1 CAPABILITIES AND LIMITATIONS

B.1.1.1 Capabilities

The computer program SAPSI-M has the following capabilities and limitations:

(1) A steady-state solutions for fixed frequencies can be obtained.

(2) A stationary dynamic solution of transient analysis can be obtained and stored from the steady-state solution and interpolation scheme.

(3) The solution of multiple moving arbitrary loads can be calculated.

(4) The shear modulus, damping ratio, and Poisson's ratio for each layer may be varied with the excitation frequency of the loads.

(5) Multiple loadings are acceptable for both harmonic and transient cases and each loading may have a different radius and time history.

(6) A static load can be simulated by specifying a harmonic load with zero excitation frequency.

B.1.1.2 Limitations

(1) SAPSI-M deals only with a layered system subjected to uniformly distributed circular loads.

(2) It does not calculate the response at zero frequency when using the half space simulation but does the analysis at near zero frequency (0.001 Hz).

(3) It does not use a cutoff frequency after which the response would be set to zero. This concept is very useful when we know that the response is essentially zero after a certain frequency (i.e contained within a certain frequency range). Had SAPSI-M have this option, the user would be able to use small frequency steps (for accurate interpolation in the frequency domain) with a limited number of frequencies, while keeping the time step small enough for a smooth response in the time domain.

(4) The interpolation scheme in SAPSI-M needs a minimum of five frequencies in a particular frequency range and a maximum of 64 frequencies.

(5) Often SAPSI-M would give an error message ("Real indefinite...") which halts the execution. This is due to the fact that the solution is pseudo-exact and may "blow-up" at certain frequencies. All that one needs to do is to shift the frequency at which the response is being computed by one or a few frequency steps. In the case of transient loading, this can occur at different frequencies.

B.1.2 ORGANIZATION OF THE MANUAL

An introduction to the SAPSI-M computer program was given in Section 1. This section also lists the capabilities and limitations of the SAPSI-M program. Section 2 is an application guide to SAPSI-M analysis. The guide explains the logical approach in SAPSI-M analysis, and consideration prior to SAPSI-M analysis. Section 3 explains how to run SAPSI-M job, and shows input format with examples. This contains numerous comments which are helpful to the user in the day-to-day use of the program.

B.2 APPLICATION GUIDE

B.2.1 INTRODUCTION

It is important that the program users understand how to effectively utilize the capabilities of the program in order to efficiently perform the SAPSI-M analysis. This requires knowledge of the analytical procedures used in this computer program. A set of guidelines describing procedures for the SAPSI-M analysis is considered to be very helpful for the users to utilize the program capabilities. It is therefore the purpose of this section to provide such guidelines.

B.2.2 SAPSI-M ANALYSIS PROCEDURE

B.2.2.1 Steps Involved in SAPSI-M Moving Load Analysis

Step1. Select the time history of load (pulse) and compute its harmonic components to highlight the dominant frequencies contained.

Step 2. Determine the possible important frequency range by examining the dominant frequencies of the pavement structure.

Step 3. Based on results of Steps 1 and 2, determine the cut-off frequency of the analysis.

Step 4. Based on laboratory tests, determine the shear modulus, Poisson's ratio and damping ratio at the different frequencies, for use in the frequency dependent profile.

Step 5. Select the frequencies at which the steady-state pavement responses are to be solved. A minimum of 5 frequencies should be selected. These frequencies are selected from Steps 1 and 2. The number of frequencies can be increased, if necessary, to improve the accuracy of the interpolated transfer functions.

Step 6. Perform the moving load analysis in SAPSI-M.

Note: Static analysis is performed at near zero frequency, (0.001Hz), and steady state analysis is done at selected frequencies. The pavement layer properties are independent of frequency for the static analysis, but they can be either one of frequency dependent properties or frequency independent for the steady state analysis.

B.2.2.2 Considerations Prior to SAPSI-M Analysis

A. Rigid Base vs. Half-space

SAPSI-M has the capability to simulate the existence of a uniformly damped or undamped, half-space below the top pavement layers. Therefore, it can avoid using very deep soil models with many sublayers, which leads to additional savings when the soft soil extends to a relatively large depth or when the bed rock boundary cannot be established.

In the case of half-space simulation, the program adds (with the given option) an additional soil layer below the top layers with the thickness of (1.5*Vs)/f, where Vs. is the shear wave velocity of the half space and f is the frequency of analysis because of this modeling, we can not obtain the static response at zero frequency for half-space simulation. In addition to this, the viscous dashpots are added to the base of the new soil.

B. Cutoff Frequency (fcuttoff)

The cutoff frequency is an important parameter since it not only sets an upper limit on the number of frequencies to be analyzed but also controls the maximum allowable element (layer) sizes, and thus, the dimension of the stiffness and mass matrix of the problem. The factors governing the choice of the cutoff frequency are:

a. The frequency content of the input load.

b. The dominant frequencies of the entire pavement system.

c. The time increment of the input time history.

C. Selection of Frequency Points

The frequencies to be selected for the SAPSI-M analysis depend on the number of peaks in the transfer function and how close these peaks are located relative to each other. Since an efficient interpolation scheme on complex response functions has been incorporated into SAPSI-M, it is usually sufficient to solve for 7 to 8 frequencies and intermediate solutions can then be obtained by interpolation.

D. Input of Frequency Points

In the SAPSI-M program, the transfer functions are computed at discrete frequency points which are integer multiples of the frequency step, df. The frequency step is calculated from

$$dt = (1/dt)NFFT \qquad \text{(A-1)}$$

where, the input parameters dt and NFFT are the time step and number of points to be used in the Fourier Transform of the time history, respectively.

Once the frequency step is defined, frequency points, f_i, are input through the use of integer frequency numbers, NFREQi, defined as follows:

$$NFREQ_i = f_i/df \qquad i = 1, 2 \ldots\ldots NF \qquad \text{(A-2)}$$

where, NF is the total number of frequency points selected for the analysis. The maximum frequency number to be specified in the SAPSI-M program is controlled by the cutoff frequency and can be obtained as follows:

$$NFREQ_{NF} = f_{NF}/df \qquad \text{(A-3)}$$

where, f_{NF} is the cutoff frequency.

At present the SAPSI-M computer program can treat the load as a vertically vibrating pressure which is moving or stationary in space, or as a static pressure. However, the movement of the load in the horizontal direction can be approximated by using the concept of influence line. This concept is useful in determining the general shape of the response of a fixed point in the pavement as the truck passes by it. The influence line determines the static effect of a point for a unit load, acting at various positions, on the magnitude and sign of the primary response of the pavement structure (stresses, strains and deflections).

B.2.3 NUMERICAL MODELING CRITERIA

B.2.3.1 Finite Element Meshing

In order to accurately transmit the waves, the finite element model should be discretized so that the thickness of each element (layer) does not exceed $\lambda/8$; where λ is the shortest wave length of interest in the analysis. The wavelength criteria can be relaxed to $\lambda/5$ if the mass matrix used in the analysis is constructed from the combination of consistent and lump mass matrices (usually 50% each). Since the mass matrix computation in SAPSI-M is automated to consist of 50% lump mass and 50% consistent mass, the $\lambda/5$ criteria can be used in constructing pavement models.

B.2.3.2 Half-space Simulation

In order to simulate the half-space condition at the bottom boundary, two techniques of variable depth method and viscous boundary at the base are used. In variable depth method, n extra layers with total thickness of 1.5λ and with the properties of half-space are added to those pavement profile. The wavelength, λ, is the shear wave length in the half space and is a function of frequency. The choice of 1.5λ arose from the observation that fundamental modes of Rayleigh wave in half-space decay with depth and essentially vanish at a depth corresponding to 1.5λ. Furthermore, the 1.5λ layer thickness is subdivided into n layers with increasing thickness with depth. The choice of $n = 10$ is sufficient for many practical problems. With this technique, the layer thickness will increase with depth and decreasing frequency. This is the desired characteristic of the model since surface wave mode shapes decrease exponentially with depth and since their depth of penetration increase with decreasing frequency. The model with extra added layers is further improved by replacing the rigid boundary at the base of the extended layer with viscous dashpots in horizontal and vertical directions.

B.3 INPUT GUIDE

B.3.1 HOW TO RUN A SAPSI-M JOB

SAPSI-M can be run interactively or using batch files. An example of a batch file is given below (for static and dynamic case respectively). To run SAPSI-M using a batch file (file name: CORE1.RUN) the redirection command SAPSIM < CORE1.RUN should be given at the DOS prompt. The input data may be created directly from the keyboard or read from the existing files and they can be modified and saved in either the old file or a new file. The extension *.RUN for a batch file is suggested for convenience.

B.3.1.1 Input Files

All file names for input and output are designated by the user. For convenience, the input and output files should use an extension which designates the type of information contained within for SAPSI-M input files.

The following are suggested extensions:

1. *.PRO - Profile of layered system.
2. *.LOD - Wheel load geometry, configuration and magnitude.

3. *.REQ - Output request points.

4. *.TIM - Time history of the load.

5. *.FRE - Frequency spectrum of the load for transient analysis.

The files are explained in detail later in this Section and an examples for each file are also provided.

B.3.1.2 Output Files

The program SAPSI-M is designed in such a way that the results obtained in each phase of the execution can be saved for later use. The following are suggested extensions:

1. *.BIN - Binary output file for the responses.

2. *.RES - The Output file which saves the global strains and stresses and global responses.

3. *.FOU- This output file contains the fourier transform points of load or response in the frequency domain.

B.3.2 EXAMPLES OF BATCH FILE

The program SAPSI-M can be run interactively with the aid of menus on the screen or using a batch file as shown below. This batch file to run SAPSI-M may have extension of *.RUN.

B.3.2.1 An Example of Static Analysis Batch File

This example shows the case of frequency independent properties and static solution with steady state solution by defining near zero frequency.

I .....Flag for Input parameters
HARMONIC .....Comments
C .....Flag for controlling parameters
F .....Flag for Frequency dependent properties
0 .....Frequency independent property (0: fre. independent, 1: frequency dependent)
H .....Flag for Half-space simulation
10 .....10 layers for half-space (0: no simulation, N: number of layers for half space)
V .....Flag for Viscous dashpot at lower boundary
1 .....Attach a viscous dashpot (0: no dashpot, 1: attach viscous dashpot)
E .....Flag for Eigenvalue solution
0 .....Solves eigen value problem without saving the solution
1 .....This option avoids printing the eigenvalue solution
X .....Exit to previous screen
P .....Flag for Profile
R .....Read the input profile
CORE1.PRO .....Filename of the input profile, being frequency independent
X .....Exit to previous screen
L .....Flag for Load file
R .....Read the load file
0 .....(0: harmonic, 1: transient in time domain, -1: transient in frequency domain)
1 .....Number of frequencies to be analyzed
0.001 .....Near zero frequency for static solution
TIRE31.LOD .....Load input filename
X .....Exits to the previous screen
O .....Flag to Define the output request point
R .....Read the output request file
STATIC.REQ .....Output request filename
1 .....Strain output requested (1: the strains, 0: stresses)
S .....To save the output responses
STATIC1.BIN .....Binary output filename (This file may be used for post analysis)
X .....Exit to the previous screen
X .....Exit to the previous screen
E .....Flag for Program execution
STATIC.RES .....Results are saved in this output filename

B.3.2.2 An Example of Steady State Analysis Batch File

This example shows the case of frequency dependent properties and steady-state solution at 4 frequencies. The same explanations hold true as for the static analysis except for a few as shown below.

I .....Flag for Input parameters
TRANSIENT SOL. .....Comments
C .....Flag for controlling parameters
F .....Flag for Frequency dependent properties
1 .....Frequency dependent property (0: fre. independent, 1: frequency dependent)
H .....Flag for Half-space simulation
10 .....10 layers for half-space (0: no simulation, N: number of layers for half space)
V .....Flag for Viscous dashpot at lower boundary
1 .....Attach a viscous dashpot (0: no dashpot, 1: attach viscous dashpot)
E .....Flag for Eigenvalue solution
0 .....Solves eigen value problem without saving the solution
1 .....This option avoids printing the eigenvalue solution
X .....Exit to previous screen
P .....Flag for Profile
R .....Read the input profile
CORE1F.PRO .....Filename of the input profile, being frequency dependent
X .....Exit to previous screen
L .....Flag for Load file
R .....Read the load file
0 .....(0: harmonic, 1: transient in time domain, -1: transient in frequency domain)
4 .....Number of frequencies to be analyzed
2 .....Frequency at which the steady state solution be obtained
16 .....Same as above
90 .....Same as above
112 .....Same as above
HARMO.LOD .....Load input filename fro Harmonic loads
X .....Exits to the previous screen
O .....Flag for Define the output request file
R .....Read the output request file
HARMO.REQ .....Output request filename
1 .....Strain output requested (1: the strains, 0: stresses)
S .....To save the output responses
STEADF.BIN .....Binary output filename (This file may be used for post analysis)
X .....Exit to the previous screen
X .....Exit to the previous screen
E .....Flag for Program execution
STEADF.RES .....Results are saved in this output filename

B.3.2.3 An Example of Moving Load Analysis Batch File

This example show the case of frequency dependent properties and transient solution at time domain. The same explanations hold true as for the steady state analysis except for a few as shown below.

I .....Flag for Input parameters
TRANSIENT SOL. .....Comments
C.....Flag for controlling parameters
F .....Flag for Frequency dependent properties
1 .....Frequency dependent property (0: fre. independent, 1: frequency dependent)
H .....Flag for Half-space simulation
10 .....10 layers for half-space (0: no simulation, N: number of layers for half space)
V .....Flag for Viscous dashpot at lower boundary
1 .....Attach a viscous dashpot (0: no dashpot, 1: attach viscous dashpot)
E .....Flag for Eigen solution
0 .....Solves eigen value problem without saving the solution
1 .....This option avoids printing the eigenvalue solution
X .....Exit to previous screen
P .....Flag for Profile
R .....Read the input profile
CORE1F.PRO .....Filename of the input profile, being frequency dependent
X .....Exit to previous screen
L .....Flag for Load file
R .....Read the load file
1 .....(0: harmonic, 1: transient in time domain, -1: transient in frequency domain)
512 .....Number of discretized points in time domain
512 .....Number of discretized points in frequency domain
.....A blanks is needed to skip when the input is in time domain
5.....Number of frequencies to be analyzed.
4.....The steady state solution will be obtained at this point
55.....The steady state solution will be obtained at this point
112.....The steady state solution will be obtained at this point
168.....The steady state solution will be obtained at this point
256.....512/2 (N/2 or close number is recommended for good interpolation)
(F15.5) .....Format of input loading
0.0023..... .....Time step of input loading at file PULSE1.TIM
144 .....Multiplier of input loading (for conversion purpose, e.g. from psi to psf)
PULSE1.TIM .....Filename of load-time history
Y .....Yes, to create a Fourier Transform file
TRANS.FOU .....Filename to save Fourier Transform results
PULSE1.LOD .....Load input filename for Transient loads
X .....Exits to the previous screen
O .....Flag for Define the output request file
R .....Read the output request file
TRANS.REQ .....Output request filename
1.....Strain output requested (1: the strains, 0: stresses)
S .....To save the output responses
TRANS.BIN .....Binary output filename for using at post analysis
X .....Exit to the previous screen
X .....Exit to the previous screen
E .....Flag for Program execution
TRANS.RES .....Results are saved in this output filename
1.....Flag for moving load solution

B.3.3 PROFILE FILE

There are two types of profiles, depending on the material properties being either frequency- independent or frequency-dependent. The format of each file has to comply with the following. These profiles may have extension *.PRO for convenience.

B.3.3.1 Format

A. Frequency Independent Properties

Card set 1:

Columns	Variable	Format	Notes	Entry
1-5	NLAY	I5		Number of layers

Card set 2:

Columns	Variable	Format	Notes	Entry
1-5	LAY(I)	I5		Layer identification number
6-17	RO(I)	E12.4		Mass density of this layer (lb.sec^2/ft^4)
18-29	GR(I)	E12.4		Real part of the shear modulus of this layer (psf)
30-41	GI(I)	E12.4		Imaginary part of shear modulus (psf)
42-53	VUR(I)	E12.4		Real part of the Poisson's ratio of this layer
54-65	VUI(I)	E12.4		Imaginary part of the Poisson's ratio of this layer
66-77	TH(I)	E12.4		Thickness of this layer (ft)

Provide NLAY cards for card set 2

B. Frequency Dependent Properties

Card set :1

Columns	Variable	Format	Notes	Entry
1-5	NLAY	I5		Number of layers Card set 2:

Card set 2:

Columns	Variable	Format	Notes	Entry
1-5	LAY(I)	I5		Layer identification number
6-17	RO(I)	E12.4		Mass density of this layer (lb.sec^2/ft^4)
18-29	TH(I)	E12.4		Thickness of this layer (ft)

Card set 3:

Columns	Variable	Format	Notes	Entry
1-5	NG(I)	I5		Total number of shear moduli for this layer
6-10	INTG(I)	I5		Interpolation flag of shear moduli for this layer
				1- Linear/Linear interpolation
				2- Linear/Log (freq.) interpolation
				3- Log/Log interpolation
				4- Log/Linear (freq.) interpolation

Card set 4:

Columns	Variable	Format	Notes	Entry
1-12	FG(1)	E12.4	(1)	The first frequency of the shear modulus curve (Hz)
13-24	GR(1)	E12.4	(1)	The first shear modulus of the shear modulus curve (psf)
25-36	FG(2)	E12.4		The second frequency of the shear modulus curve (Hz)

37-48	GR(2)	E12.4		The second shear modulus of shear modulus curve (psf)

Provide [NG(I)/+2]/3 cards for card set 4

Note(1): Input in Ascending order

Card set 5:

Columns	Variable	Format	Notes	Entry
1-5	NB(I)	I5		Total number of damping ratio for this layer
6-10	INTB(I)	I5		Interpolation flag of damping ratios for this layer
				1- Linear/Linear interpolation
				2- Linear/Log (freq.) interpolation
				3- Log/Log interpolation
				4- Log/Linear (freq.) interpolation

Card set 6:

Columns	Variable	Format	Notes	Entry
1-12	FB(1)	E12.4	(2)	The first frequency of the damping ratio curve (Hz)
13-24	BR(1)	E12.4	(2)	The first damping ratio of the damping ratio curve
25-36	FB(2)	E12.4		The second frequency of the damping ratio curve (Hz)
37-48	BR(2)	E12.4		The second damping ratio of the damping ratio curve

Provide [NB(I)/+2]/3 cards for card set 6

Card set 7:

Columns	Variable	Format	Notes	Entry
1-5	NU(I)	I5		Total number of Poisson's ratio for this layer
6-10	INTN(I)	I5		Interpolation flag of damping ratios for this layer
				1- Linear/Linear interpolation
				2- Linear/Log (freq.) interpolation
				3- Log/Log interpolation
				4- Log/Linear (freq.) interpolation

Card set 8:

Columns	Variable	Format	Notes	Entry
1-12	FN(1)	E12.4	(3)	The first frequency of the Poisson's ratio curve (Hz)
13-24	VU(1)	E12.4	(3)	The first Poisson's ratio of the Poisson's ratio curve
25-36	FN(2)	E12.4		The second frequency of the Poisson's ratio curve (Hz)
37-48	VU(2)	E12.4		The second Poisson's ratio of Poisson's ratio curve

Provide [NB(I)/+2]/3 cards for card set 8

Repeat card set 2 through 8 for NLAY times

Note(2): Input in Ascending order

Note(3): Input in Ascending order

B.3.3.2 Examples of Profile

A. An Example of Frequency Independent Profile (undamped case)

16

1	.4505E+01	.2670E+08	.0000E+00	.3500E+00	.0000E+00	.0333E+00
2	.4505E+01	.3000E+08	.0000E+00	.3500E+00	.0000E+00	.0100E+00
3	.4505E+01	.3000E+08	.0000E+00	.3500E+00	.0000E+00	.1942E+00
4	.4505E+01	.3000E+08	.0000E+00	.3500E+00	.0000E+00	.1942E+00
5	.4505E+01	.3000E+08	.0000E+00	.3500E+00	.0000E+00	.0100E+00
6	.4505E+01	.2670E+08	.0000E+00	.3500E+00	.0000E+00	.0333E+00
7	.4200E+01	.7600E+06	.0000E+00	.4000E+00	.0000E+00	.2650E+00
8	.4200E+01	.7600E+06	.0000E+00	.4000E+00	.0000E+00	.2650E+00
9	.4200E+01	.7600E+06	.0000E+00	.4000E+00	.0000E+00	.2650E+00
10	.4200E+01	.7600E+06	.0000E+00	.4000E+00	.0000E+00	.2650E+00
11	.4039E+01	.5060E+06	.0000E+00	.4500E+00	.0000E+00	.7116E+00
12	.4039E+01	.5060E+06	.0000E+00	.4500E+00	.0000E+00	.7116E+00
13	.4039E+01	.5060E+06	.0000E+00	.4500E+00	.0000E+00	.7116E+00
14	.4039E+01	.5060E+06	.0000E+00	.4500E+00	.0000E+00	.7116E+00
15	.4039E+01	.5060E+06	.0000E+00	.4500E+00	.0000E+00	.7116E+00
16	.4349E+01	2.1333E+06	.0000E+00	.3500E+00	.0000E+00	.1000E+01

B. An Example of a Frequency Independent Profile (damped case)

16

1	.4505E+01	.2670E+08	5.3334E+06	.3500E+00	.0000E+00	.0333E+00
2	.4505E+01	.3000E+08	6.0000E+06	.3500E+00	.0000E+00	.0100E+00
3	.4505E+01	.3000E+08	6.0000E+06	.3500E+00	.0000E+00	.1942E+00
4	.4505E+01	.3000E+08	6.0000E+06	.3500E+00	.0000E+00	.1942E+00
5	.4505E+01	.3000E+08	6.0000E+06	.3500E+00	.0000E+00	.0100E+00
6	.4505E+01	.2670E+08	5.3334E+06	.3500E+00	.0000E+00	.0333E+00
7	.4200E+01	.7600E+06	7.6000E+04	.4000E+00	.0000E+00	.2650E+00
8	.4200E+01	.7600E+06	7.6000E+04	.4000E+00	.0000E+00	.2650E+00
9	.4200E+01	.7600E+06	7.6000E+04	.4000E+00	.0000E+00	.2650E+00
10	.4200E+01	.7600E+06	7.6000E+04	.4000E+00	.0000E+00	.2650E+00
11	.4039E+01	.5060E+06	3.0360E+04	.4500E+00	.0000E+00	.7116E+00
12	.4039E+01	.5060E+06	3.0360E+04	.4500E+00	.0000E+00	.7116E+00
13	.4039E+01	.5060E+06	3.0360E+04	.4500E+00	.0000E+00	.7116E+00
14	.4039E+01	.5060E+06	3.0360E+04	.4500E+00	.0000E+00	.7116E+00
15	.4039E+01	.5060E+06	3.0360E+04	.4500E+00	.0000E+00	.7116E+00
16	.4349E+01	2.1333E+06	1.2798E+05	.3500E+00	.0000E+00	.1000E+01

C. An Example of Frequency Dependent Profile

```
10
 1 4.5050E+00 4.6500E-01
 2  3
0.1000E+00 1.3129E+07 3.2500E+02 7.1001E+07
 2  4
0.1000E+00 2.2500E-01 3.2500E+02 7.8900E-15
 2  2
0.1000E+00 4.9990E-01 3.2500E+02 -7.6600E-02
 2 4.505E+00  1.0000E-02
 2  3
0.1000E+00 1.3129E+07 3.2500E+02 7.1001E+07
 2  4
0.1000E+00 2.2500E-01 3.2500E+02 7.8900E-15
 2  2
0.1000E+00 4.9990E-01 3.2500E+02 -7.6600E-02
 3 4.2000E+00 3.5333E-01
 2  1
0.1000E+00 7.6114E+05 3.2500E+02 7.6114E+05
 2  1
0.1000E+00 5.0000E-02 3.2500E+02 5.0000E-02
 2  1
0.1000E+00 4.0000E-01 3.2500E+02 4.0000E-01
 4 4.2000E+00 3.5333E-01
 2  1
0.1000E+00 7.6114E+05 3.2500E+02 7.6114E+05
 2  1
0.1000E+00 5.0000E-02 3.2500E+02 5.0000E-02
 2  1
0.1000E+00 4.0000E-01 3.2500E+02 4.0000E-01
 5 4.2000E+00 3.5333E-01
 2  1
0.1000E+00 7.6114E+05 3.2500E+02 7.6114E+05
 2  1
0.1000E+00 5.0000E-02 3.2500E+02 5.0000E-02
 2  1
0.1000E+00 4.0000E-01 3.2500E+02 4.0000E-01
 6 4.0390E+00 8.8950E-01
 2  1
0.1000E+00 5.0648E+05 3.2500E+02 5.0648E+05
 2  1
0.1000E+00 3.0000E-02 3.2500E+02 3.0000E-02
 2  1
0.1000E+00 4.5000E-01 3.2500E+02 4.5000E-01
 7 4.0390E+00 8.8950E-01
 2  1
0.1000E+00 5.0648E+05 3.2500E+02 5.0648E+05
 2  1
0.1000E+00 3.0000E-02 3.2500E+02 3.0000E-02
 2  1
0.1000E+00 4.5000E-01 3.2500E+02 4.5000E-01
 8 4.0390E+00 8.8950E-01
 2  1
0.1000E+00 5.0648E+05 3.2500E+02 5.0648E+05
 2  1
0.1000E+00 3.0000E-02 3.2500E+02 3.0000E-02
 2  1
0.1000E+00 4.5000E-01 3.2500E+02 4.5000E-01
 9 4.0390E+00 8.8950E-01
 2  1
0.1000E+00 5.0648E+05 3.2500E+02 5.0648E+05
 2  1
0.1000E+00 3.0000E-02 3.2500E+02 3.0000E-02
 2  1
0.1000E+00 4.5000E-01 3.2500E+02 4.5000E-01
 10 4.3490E+00 1.0000E+00
 2  1
0.1000E+00 2.1333E+06 3.2500E+02 2.1333E+06
 2  1
0.1000E+00 3.0000E-02 3.2500E+02 3.0000E-02
 2  1
0.1000E+00 3.5000E-01 3.2500E+02 3.5000E-01
```

B.3.4 LOAD FILE

There are two types of load file, one is Harmonic loads for steady state solution and the other is pulse loads for transient solution. These load files may have extension *.LOD for convenience. The format of each file has to comply with the following:

B.3.4.1 Format

A. Harmonic Loading

Card set 1:

Columns	Variable	Format	Notes	Entry
1-5	NLOAD	I5		Total number of loads

Card set 2:

Columns	Variable	Format	Notes	Entry
1-5	LOAD(I)	I5		Load identification number
6-18	RL(I)	E13.4		Radius of this load (ft)
19-31	X(I)	E12.4		X-coordinate of this load (ft)
32-44	Y(I)	E12.4		Y-coordinate of this load (ft)

Provide NLOAD cards for card set 2

Card set 3:

Columns	Variable	Format	Notes	Entry
1-12	SL(1)	E12.4		The magnitude of the first load (psf)
13-24	SL(2)	E12.4		The magnitude of the second load (psf)
32-44	SL(3)	E12.4		Y-The magnitude of the third load (psf)

Provide (NLOAD+5)/6 cards for card set 3

A. Transient Loading

Card set 1:

Columns	Variable	Format	Notes	Entry
1-5	NLOAD	I5		Total number of loads

Card set 2:

Columns	Variable	Format	Notes	Entry
1-5	LOAD(I)	I5		Load identification number
6-18	RL(I)	E13.4		Radius of this load (ft)
19-31	X(I)	E12.4		X-coordinate of this load (ft)
32-44	Y(I)	E12.4		Y-coordinate of this load (ft)

Provide NLOAD cards for card set 2

Note: The user may choose to provide the magnitudes of load in either the time-history input file (*.TIM) or in magnitude at batch file.

B.3.4.2 Examples of Load File

A. An Example of Harmonic Loading

```
10
  1  .3042E+00  .0000E+00  .0000E+00
  2  .3150E+00  .4333E+01  .0000E+00
  3  .3042E+00  .0000E+00  .1125E+01
  4  .3150E+00  .4333E+01  .1125E+01
  5  .3117E+00  .0000E+00 6.0625E+00
  6  .3075E+00  .4333E+01 6.0625E+00
  7  .3117E+00  .0000E+00 7.1875E+00
  8  .3075E+00  .4333E+01 7.1875E+00
  9  .3692E+00  .2092E+02  .2500E+00
 10  .3645E+00 .2092E+02  6.9375E+00
 .1297E+05  .1296E+05  .1297E+05  .1296E+05  .1293E+05  .1296E+05
 .1293E+05  .1296E+05  .1280E+05  .1296E+05
```

Note: The first column (from 1 to 5) in row 2 is the load number, the second column (from 6 to 18) gives the radius of the load in feet, the third column (from 19 to 31) specifies the x coordinate of the load in feet, and the fourth column (from 32 to 44) specifies the y coordinate of the load in feet. This is repeated as many times as the number of loads specified.
The last two rows are the magnitudes of the 10 loads in psf.

B. An Example of Transient Loading

```
5
  1  .3042E+00  .0000E+00  .0000E+00
  2  .3150E+00  .4333E+01  .0000E+00
  3  .3042E+00  .0000E+00  .1125E+01
  4  .3150E+00  .4333E+01  .1125E+01
  5  .3693E+00  .2092E+02  .2500E+00
```

Note: The magnitude of the loads is given in the time history of the load either in the time domain or the frequency domain.

B.3.5 OUTPUT REQUEST FILE

This file define the request point by defining layer number and x & y-coordinates at which the response is sought. This output request file may have extension *.REQ for convenience. The format of each file has to comply with the following:

B.3.5.1 Format

Card set 1:

Columns	Variable	Format	Notes	Entry
1-5	NOUT	I5		Total number of points where outputs are requested

Card set 2:

Columns	Variable	Format	Notes	Entry
1-5	LOAD(I)	I5		Layer number where this output point is located
6-15	XO(I)	F10.4		X-coordinate of this output point (ft)
16-25	YO(I)	F10.4		Y-coordinate of this output point (ft)

Provide NOUT cards for card set 2

B.3.5.2 Example of Output Request File

```
6
  4   .0001   .2083
  4  4.3333   .2083
  4 20.9167   .2083
  1   .0001   .2083
  1  4.3333   .2083
  1 20.9167   .2083
```

Note: The first column (1 to 5) gives the layer number at which the response is sought. The second column (6 to 15) is the x coordinate and the third column (16 to 25) is the y coordinate of that particular response point.